

INFORMATION TO USERS

This manuscript has been reproduced from the microfilm master. UMI films the text directly from the original or copy submitted. Thus, some thesis and dissertation copies are in typewriter face, while others may be from any type of computer printer.

The quality of this reproduction is dependent upon the quality of the copy submitted. Broken or indistinct print, colored or poor quality illustrations and photographs, print bleedthrough, substandard margins, and improper alignment can adversely affect reproduction.

In the unlikely event that the author did not send UMI a complete manuscript and there are missing pages, these will be noted. Also, if unauthorized copyright material had to be removed, a note will indicate the deletion.

Oversize materials (e.g., maps, drawings, charts) are reproduced by sectioning the original, beginning at the upper left-hand corner and continuing from left to right in equal sections with small overlaps.

Photographs included in the original manuscript have been reproduced xerographically in this copy. Higher quality 6" x 9" black and white photographic prints are available for any photographs or illustrations appearing in this copy for an additional charge. Contact UMI directly to order.

**ProQuest Information and Learning
300 North Zeeb Road, Ann Arbor, MI 48106-1346 USA
800-521-0600**

UMI[®]

NOTE TO USERS

This reproduction is the best copy available.

UMI

University of Alberta

**Sedimentology and stratigraphy for Quaternary deposits of the Russian
Plain**

by

Edward Charles Little



**A Dissertation submitted to the Faculty of Graduate Studies and
Research in partial fulfillment of the requirements for the degree of
Doctor of Philosophy**

Department of Earth and Atmospheric Sciences

Edmonton, Alberta

Spring 2002



**National Library
of Canada**

**Acquisitions and
Bibliographic Services**

**395 Wellington Street
Ottawa ON K1A 0N4
Canada**

**Bibliothèque nationale
du Canada**

**Acquisitions et
services bibliographiques**

**395, rue Wellington
Ottawa ON K1A 0N4
Canada**

Your file Votre référence

Our file Notre référence

The author has granted a non-exclusive licence allowing the National Library of Canada to reproduce, loan, distribute or sell copies of this thesis in microform, paper or electronic formats.

L'auteur a accordé une licence non exclusive permettant à la Bibliothèque nationale du Canada de reproduire, prêter, distribuer ou vendre des copies de cette thèse sous la forme de microfiche/film, de reproduction sur papier ou sur format électronique.

The author retains ownership of the copyright in this thesis. Neither the thesis nor substantial extracts from it may be printed or otherwise reproduced without the author's permission.

L'auteur conserve la propriété du droit d'auteur qui protège cette thèse. Ni la thèse ni des extraits substantiels de celle-ci ne doivent être imprimés ou autrement reproduits sans son autorisation.

0-612-68597-7

Canada

University of Alberta

Library Release Form

Name of Author: Edward Charles Little

Title of Dissertation: Sedimentology and stratigraphy for Quaternary deposits of the Russian Plain

Degree: Doctor of Philosophy

Year this Degree Granted: 2002

Permission is hereby granted to the University of Alberta Library to reproduce single copies of this dissertation and to lend or sell such copies for private, scholarly or scientific purposes only.

The author reserves all other publication and other rights in association with the copyright in the dissertation, and except as herein before provided, neither the dissertation nor any substantial portion thereof may be printed or otherwise reproduced in any material from whatever without the author's prior written permission.



Edward C. Little
P.O. Box 1842
Iqaluit, Nunavut
X0A 0H0

Dated April 16, 2002


University of Alberta

Faculty of Graduate Studies and Research

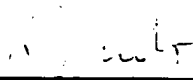
The undersigned certify that they have read, and recommend to the Faculty of Graduate Studies and Research for acceptance, a dissertation entitled *Sedimentology and stratigraphy for Quaternary deposits of the Russian Plain* submitted by Edward C. Little in partial fulfillment of the requirements for the degree of Doctor of Philosophy.




Dr. N.W. Rutter



Dr. M. Sharp



Dr. R. J. Fulton



Dr. M.J. Dudas



Dr. M. E. Evans

April 12th, 2002

Date Approved

“To overturn orthodoxy is no easier in science than in philosophy, religion, economics or any of the other disciplines through which we try to comprehend the world and society in which we live.”

--Ruth Hubbard (b. 1924) U.S. Biologist.

To all those who have helped me to persevere in this endeavour...

ABSTRACT

Composite stratigraphic sequences from four localities along a *ca.* 700 km long north-south transect between Moscow and Volgograd, Russia have yielded new information as to the timing and history of Quaternary events over the last *ca.* 800 ka. Lithostratigraphic and pedostratigraphic analyses, supported by physical data, geochemical data, and micromorphological investigations allowed for the development of an allostratigraphic scheme that was used as a tool for correlations spanning significant distances. Optical dating techniques were used to temporally constrain that portion of the allostratigraphic framework younger than *ca.* 150 ka, whereas the identification of the Brunhes/Matuyama boundary (*ca.* 780 ka) constrains the oldest portion of the observed loess-paleosol record. The resulting chronostratigraphy (*sensu lato*) and geochronology allow reinterpretations of the Quaternary evolution of the Russian Plain. Major advantages of the newly proposed stratigraphy include: 1) correlation of the Likhvin Interglacial soil to MIS 9; 2) correlation of the Muchkap Interglacial to MIS 11, and; 3) association of the Don Glacial to MIS 12 rather than its generally accepted association with MIS 16. The latter is a major change to the chronostratigraphic record that significantly alters Middle Pleistocene geologic history and climatic interpretations.

Pedogenic events identified from field observations, laboratory data and micromorphological investigations have yielded evidence of latitudinal bioclimatic shifts. The most auspicious of the warm periods during the last *ca.* 400 ka was the Muchkap (Holsteinian) Interglacial during which forest-influenced pedogenesis was interpreted at Sebyakova-Mikhailovka (*ca.* 50° N), where arid steppe currently prevails. Furthermore, based on pedogenic evidence, most major interglacial events (MIS 11, 9, and 5.5) of the last *ca.* 400 ka appear to have been warmer and possibly more moist than the present-day climate.

Paleosols present within the studied composite sections represent periods of attenuated sedimentation and hence, define seven depositional megacycles (glacial-interglacial periods) over the past *ca.* 800 ka. A major unconformity below the Don Till (MIS 12) within the fourth megacycle (from the present day) suggests a *ca.* 180 ka hiatus. Of these seven glacial-interglacial events, only three glaciations produced ice sheets large enough to cover parts of the Russian Plain south of Moscow: Don Glacial (MIS 12) representing the all-time Pleistocene maximum glacial advance; the Oka Glaciation (MIS 10), inferred from previous work, and; the Dnieper Glaciation which exhibits a limited earlier ice-sheet advance (MIS 8) and a more extensive later advance (MIS 6) separated by a period of climatic fluctuation (MIS 7). The climatic fluctuations associated with MIS 7 are characterized by two minor paleosols and an intervening loess. The remaining glacial periods resulted in cold steppe conditions that were (generally) dominated by loess deposition in a continuous permafrost environment (north) or loess deposition in a discontinuous permafrost environment (south).

Correlations of these results to other records within and outside the Russian Plain help corroborate the newly developed stratigraphy. The teleconnection between magnetic susceptibility at Sebyakova-Mikhailovka and the orbitally tuned grain-size ratios of the Baoji section (China) suggest that the all-time Pleistocene European glacial maximum and Asian maximum desert expansion are isochronous. Eurasian-scale relationships such as this will provide new insight to climate modellers in order to understand climate forcing mechanisms at hemispheric scales.

ACKNOWLEDGEMENTS

I would like to thank Dr. N.W. Rutter for giving me the opportunity to work on this project, and having the faith in me to conduct this research to the best of my abilities. To Elaine, my loving wife: thank-you for being there for me from the very start of this taxing endeavour; without your patience, understanding and support, I would not have been able to complete this task that has so profoundly affected the both of us over the years. Special thanks go out to Dean Rokosh and Olav Lian for their invaluable support and advise throughout the course of my research. I would also like to take this time to thank all those that helped me to develop philosophically, scientifically and socially: Lionel Jackson, Charlie Schweger, Ted Evans, Loren Davis and Paul Blancheon. Last but not least, I would like to thank all those friends, colleagues and especially family who have made every effort to make my Ph.D. studies as comfortable as possible.

To my friends and colleagues at the Russia Academy of Science: Andrei Velichko, Kostia Dlussky, Vladimir Nechayev, Tatyana Morozova and Victor Semenov. Without you my friends, I would not have experienced a new culture or realized the potential that I have to offer to our discipline. I am truly grateful that our paths have crossed, and hope they will again some day.

Finally, financial support for this undertaking was generously provided by the National Science and Engineering Research Council research grant to Nat Rutter as part of Canada's contribution to the Global Climate Program, Climate Systems History and Dynamics (CSHD).

Table of Contents

CHAPTER 1 - INTRODUCTION	1
General Introduction	1
Research Objectives	2
Study Area	3
Physiography of Section Sites	3
<i>Present-day Climate and Soils</i>	3
<i>Geomorphology</i>	6
Bedrock Geology	7
<i>East-European Platform Basement</i>	7
<i>Regional Bedrock Geology</i>	9
<i>Paleozoic</i>	9
<i>Mesozoic</i>	11
<i>Cenozoic</i>	12
Quaternary Research	12
<i>Previous Work</i>	12
<i>Evolution of Quaternary Stratigraphy for European Russia</i>	12
<i>Last Twenty Years of Quaternary Stratigraphic Research for the Russian Plain</i>	16
<i>Contemporary Russian Plain Quaternary Geology: Discussion</i>	20
<i>European Ice-Sheets and Their Relationship to the Quaternary Sedimentation on the East European Plain</i>	20
<i>Enigmatic Early and Middle Pleistocene Records: Case Studies</i>	24
<i>Evolution of Russian Plain Paleosol Research</i>	25
<i>Dissertation Organization</i>	27
CHAPTER 2 - GENERAL METHODS	29
Introduction	29
Field Methods	29
<i>Sample Collection and Preparation</i>	29
Laboratory Methods	30
<i>Textural (Grain Size) Analysis</i>	30
<i>Pretreatment - Removal of Carbonates</i>	30
<i>Pretreatment - Removal of Organic Matter</i>	30
<i>Separation of Fine (<250 μm) and Coarse (>250 μm) Fractions</i>	31
<i>Fine Fraction Analysis</i>	31
<i>Coarse Fraction Analysis</i>	32
Loss-On-Ignition (LOI)	32
<i>Organic Determination</i>	32
<i>Carbonate Determination</i>	32
Rock Magnetic Parameters	33
<i>Magnetic Susceptibility</i>	33
<i>Frequency Dependence of Magnetic Susceptibility (FD)</i>	34

Geochemistry	35
Optical Dating	35
<i>OSL Sample Collection and Preparation</i>	35
Micromorphology	37
<i>Sample Collection and Preparation for Micromorphology</i>	37
CHAPTER 3 - STRATIGRAPHY AND SEDIMENTOLOGY	39
Introduction	39
<i>Lithostratigraphy</i>	39
<i>Pedostratigraphy</i>	41
<i>Allostratigraphy</i>	42
<i>Optical Age Constraints</i>	42
Likhvin Sections	43
<i>Likhvin Section No. 1: Lithostratigraphy and basic paleosol description</i>	43
<i>LS1-1: 0 - 216 cm (LC-1: 0 - 216 cm)</i>	<i>43</i>
<i>LS1-2: 216 - 716 cm (LC-2: 216 - 716 cm)</i>	<i>44</i>
<i>LS1-3: 716 - 824 cm (LC-3: 716 - 824 cm)</i>	<i>47</i>
<i>LS1-4: 824 - 992 cm (LC-4: 824 - 992 cm)</i>	<i>50</i>
<i>LS1-5: 992 - 1290 cm (LC-5: 992 - 1290 cm)</i>	<i>50</i>
<i>LS1-6: 1290 cm - (LC-6: 1290 - 2290 cm)</i>	<i>51</i>
<i>Likhvin Section No. 2: Lithostratigraphy and basic paleosol description</i>	51
<i>LS2-1: 0 - 31 cm (LC-6: 1290 - 2290 cm)</i>	<i>51</i>
<i>LS2-2: 31 - 118 cm (LC-7: 2290 - 2377 cm)</i>	<i>51</i>
<i>LS2-3: 118 - 240 cm (LC-8: 2377 - 2499cm)</i>	<i>53</i>
<i>LS2-4: 240 - 263 cm (LC-9: 2499 - 2633 cm)</i>	<i>53</i>
<i>LS2-5: 263 - 313 cm (LC-10: 2522 - 2572 cm)</i>	<i>53</i>
<i>LS2-6: 313 - 518 cm (LC-11: 2572 - 2777 cm)</i>	<i>54</i>
<i>LS2-7: 518 cm - (LC-12: 2777 cm -)</i>	<i>57</i>
<i>Likhvin Composite Section</i>	57
<i>Likhvin Site Depositional Environment: overview</i>	<i>59</i>
Gololobovo Sections	63
<i>Gololobovo Section No. 1: Lithostratigraphy and basic paleosol description</i> ..	63
<i>GS1-1: 0 - 205 cm (GC-1: 0 - 205 cm)</i>	<i>63</i>
<i>GS1-2: 205 - 225 cm (GC-2: 205 - 225 cm)</i>	<i>65</i>
<i>GS1-3: 225 - 463 cm (GC-3: 225 - 463 cm)</i>	<i>65</i>
<i>GS1-4: 463 - 610 cm (GC-4: 463 - 646 cm)</i>	<i>67</i>
<i>Gololobovo Section No. 2: Lithostratigraphy and basic paleosol description</i> ..	68
<i>GS2-1: 0 - 120 cm (GC-4: 490 - 610 cm)</i>	<i>68</i>
<i>Gololobovo Section No. 3: Lithostratigraphy and basic paleosol description</i> ..	69
<i>GS3-1: 0 - 90 cm (GC-4: 463 - 646 cm)</i>	<i>69</i>
<i>GS3-2: 90 - 170 cm (GC-5: 646 - 726 cm)</i>	<i>71</i>
<i>GS3-3: 170 - 338 cm (GC-6: 726 - cm)</i>	<i>72</i>
<i>GS3-4: 338 - 450 cm (GC-7)</i>	<i>72</i>
<i>GS3-5: 450 cm - (GC-8)</i>	<i>72</i>

Gololobovo Section No. 4: Lithostratigraphy and basic paleosol description ..	73
<i>GS4-1: 0 - 140 cm (GC-7: 798 - 938 cm)</i>	73
<i>GS4-2: 140 - 249 cm (GC-8: 938 - 1047 cm)</i>	73
<i>GS4-3: 249 - 381 cm (GC-9: 1047 - 1179 cm)</i>	76
<i>GS4-4: 381 cm - (GC-10: 1179 cm -)</i>	76
Gololobovo Composite Section	79
<i>Gololobovo Site: relative data interpretations</i>	79
<i>Gololobovo Site Depositional Environment: overview</i>	81
Korostylievo Sections	85
Korostylievo Composite Section: Lithostratigraphy and basic paleosol description	86
<i>KC-1: 0 - 205 cm</i>	86
<i>KC-2: 205 - 426 cm</i>	89
<i>KC-3: 426 - 700 cm</i>	92
<i>KC-4: 700 - 1017 cm</i>	95
<i>KC-5: 1017 - 1448 cm</i>	98
<i>KC-6: 1448 - 1452 cm</i>	102
<i>KC-7: 1452 - 1478 cm</i>	102
<i>KC-8: 1478 cm -</i>	102
Korostylievo Composite Section	103
<i>Korostylievo Site: relative data interpretations</i>	103
<i>Korostylievo Site Depositional Environment: overview</i>	106
Mikhailovka Sections	111
Mikhailovka Sections Nos. 1 and 2: Lithostratigraphy and paleosol description	112
<i>MS1-1: 0 - 145 cm (MC-1: 0 - 145 cm)</i>	112
<i>MS1-2: 145 - 409 cm (MC-2: 145 - 409 cm)</i>	116
<i>MS1-3: 409 - 748 cm (MC-3: 409 - 748 cm)</i>	118
<i>MS1-4: 748 cm - 1005 cm (MC-4: 748 - 1005 cm)</i>	120
<i>MS1-5: 1005 cm - (MC-5: 1005 - 1263 cm)</i>	121
Mikhailovka Section No. 3: Lithostratigraphy and basic paleosol description	121
<i>MS3-1: 0 - 110 cm (MC-3: 409 - 748 cm)</i>	124
<i>MS3-2: 110 - 335 cm (MC-4: 748 - 1005 cm)</i>	124
<i>MS3-3: 335 - 593 cm (MC-5: 1005 - 1263 cm)</i>	125
<i>MS3-4: 593 - 656 cm (MC-6: 1263 - 1326 cm)</i>	126
<i>MS3-5: 656 cm - (MC-7: 1326 - 2326 cm)</i>	126
Mikhailovka Section No. 5: Lithostratigraphy and basic paleosol description	127
<i>MS5-1: 0 - 20 cm (not used in composite section)</i>	130
<i>MS5-2: 20 - 103 cm (MC-7: 1326 - 2326 cm)</i>	130
<i>MS5-3: 103 - 148 cm (MC-8: 2326 - 2371 cm)</i>	130
<i>MS5-4: 148 - 265 cm (MC-9: 2371 - 2488 cm)</i>	131
<i>MS5-5: 265 - 330 cm (MC-10: 2488 - 2533 cm)</i>	131
<i>MS5-6: 330 - 353 cm (MC-11: 2553 - 2576 cm)</i>	131
<i>MS5-7: 353 - 489 cm (MC-12: 2576 - 2712 cm)</i>	132
<i>MS5-8: 489 - 555 cm (MC-13: 2712 - 2778 cm)</i>	132
<i>MS5-9: 555 - cm (MC-14: 2778 cm -)</i>	133
Mikhailovka Composite Section	134

<i>Mikhailovka Site: relative data interpretations</i>	134
<i>Mikhailovka Site Depositional Environment: overview</i>	138
Distal Section Correlation	143
<i>Allostratigraphic Framework: introduction</i>	143
<i>Allostratigraphic Framework: discussion</i>	144
Chapter Summary	146
CHAPTER 4 - CHRONOSTRATIGRAPHY	147
Introduction	147
<i>Organization</i>	147
<i>Construction of SPECMAP Correlations</i>	147
<i>Stratigraphic Time Scale Development</i>	148
<i>Stratigraphic Implications: Discussion</i>	151
<i>Brunhes/Matuyama Boundary within MC-12</i>	151
<i>Proposed Ages Units A-7 Through A-5</i>	151
<i>Reassessment of the Age of the Don Till on the Russian Plain</i>	151
<i>Age Associations for units overlying KC-8 and MC-7</i>	152
Chapter Summary	157
CHAPTER 5 - RUSSIAN PLAIN QUATERNARY HISTORY	159
Introduction	159
Quaternary History of the Study Area	159
<i>Allunits A-7 through A-5 (pre-Don sediments): MIS 21-17</i>	160
<i>Allunit A-4 (Don-Muchkap cycle): MIS 12-11</i>	160
<i>Allunit A-3 (Oka-Likhvin cycle): MIS 10-9</i>	162
<i>Allunit A-2 (Dnieper-Mikulino): MIS 8-5.5</i>	164
<i>Allunit A-1 (Valdai-Holocene): MIS 5.4-1</i>	166
Chapter Summary	169
CHAPTER 6 - EURASIAN CORRELATION: APPLICATION OF PROPOSED RUSSIAN PLAIN ALLOSTRATIGRAPHY	171
Correlation to other research within the Russian Plain	171
Correlation of the Russian Plain Quaternary Sequence to Siberian and Chinese Records	174
<i>Russian Plain Correlation to Siberian Records</i>	174
<i>Russian Plain Correlation to Chinese Records</i>	177
Chapter Summary	180

CHAPTER 7 - SUMMARIES, CONCLUSIONS AND FUTURE RESEARCH	181
Composite Type-Sections: the 700 km north-south transect revisited	181
<i>Summary of Likhvin Site</i>	<i>181</i>
<i>Summary of Gololobovo Site</i>	<i>181</i>
<i>Summary of the Korostylievo Site</i>	<i>182</i>
<i>Summary of the Mikhailovka site</i>	<i>182</i>
Allostratigraphy and Chronostratigraphy: review	183
<i>Allostratigraphy</i>	<i>183</i>
<i>Chronostratigraphy</i>	<i>184</i>
Correlation to other Quaternary Research: Regional and Eurasian-wide scales	184
Conclusions	185
Recommendations for Future Research	187
REFERENCES.....	189
APPENDIX A: MODERN CLIMATE DATA.....	203
APPENDIX B: OSL DATING METHODS	207
Manuscript Acceptance Letter.....	208
Quaternary stratigraphy and optical dating of loess from the east European Plain (Russia).....	209
<i>Abstract</i>	<i>210</i>
<i>1. Introduction</i>	<i>210</i>
<i>2. Recent stratigraphic schemes for the east European Plain region</i>	<i>213</i>
<i>3. Physical setting, stratigraphy, and sample locations</i>	<i>214</i>
<i>3.1. Likhvin Composite Section</i>	<i>215</i>
<i>3.2. Gololobovo Composite Section</i>	<i>218</i>
<i>4. Optical dating</i>	<i>220</i>
<i>4.1 Sample collection and laboratory preparation.....</i>	<i>221</i>
<i>4.2. Determination of the environmental dose rate</i>	<i>221</i>
<i>4.3. Determination of the equivalent dose</i>	<i>222</i>
<i>4.4. Results.....</i>	<i>224</i>
<i>4.5. Optical ages</i>	<i>226</i>
<i>5. Discussion</i>	<i>226</i>
<i>6. Conclusions</i>	<i>228</i>
<i>Acknowledgments</i>	<i>229</i>
<i>References (Optical Dating Manuscript).....</i>	<i>230</i>
<i>Figure Captions (Optical Dating Manuscript)</i>	<i>240</i>
Korostylievo and Mikhailovka optical dating data tables	251

APPENDIX C - STRATIGRAPHY AND SEDIMENTOLOGY	253
Introduction	253
Types of Stratigraphy - a review	254
<i>Lithostratigraphy</i>	254
<i>Pedostratigraphy</i>	254
<i>Allostratigraphy</i>	257
Technique used to construct New Russian Plain Allostratigraphy	259
APPENDIX D: TEXTURAL DATA	261
Sedigraph 5100 Specifications and Standard Run Results	269

List of Tables

Table 1.1. Distances between site locations.	3
Table 1.2. Quaternary stratigraphic scheme and geologic index of Moskvitin. 1950	15
Table 3.1. Lithofacies codes used in stratigraphic section profiles.....	40
Table 3.2. Distances between sections at the Mikhailovka site.	111
Table 5.1. Paleosol summary table outlining the pedofacies changes between sites along the 700 km north-south transect.	160
Table D.1. Grain-size Data: File reference table	261
Table D.2. Non-Russian-Plain grain-size data: File reference table.	261

List of Figures

Figure 1.1. Location of study sites, loess extent and physiographic regions.	4
Figure 1.2. General present-day climate map for European Russia.	5
Figure 1.3. Climatograms for the Moscow, Tambov and Volgograd regions.	5
Figure 1.4. Tectonic and Basement rock map for the East European Platform.	8
Figure 1.5. Generalized bedrock map for study area.	10
Figure 1.6. Comparison of contemporary Russian Plain Stratigraphic Schemes.	18
Figure 1.7. Quaternary stratigraphy comparison.	21
Figure 1.8. Glacial Limits of the East European Plain.	23
Figure 1.9. Loess distribution over the East European Plain.	23
Figure 3.1. Symbols and patterns used to construct section diagrams.	41
Figure 3.2. Stratigraphic column for Likhvin Section No. 1.	45
Figure 3.3. Likhvin loess versus three loess samples from China.	47
Figure 3.4. Highly deformed sub-units comprising Unit L1-3. A.	48
Figure 3.5. Stratigraphic column for Likhvin Section No. 2.	52
Figure 3.6. Likhvin Composite Section.	58
Figure 3.7A. Stratigraphic column for Gololobovo Sections No. 1.	64
Figure 3.7B. Stratigraphic column for Gololobovo Sections No. 2.	64
Figure 3.8. Mezin paleosol at Gololobovo.	69
Figure 3.9. Stratigraphic column for Gololobovo Section No. 3.	70
Figure 3.10. Loess from Gololobovo versus loess from China.	71
Figure 3.11. Stratigraphic column for Gololobovo Section No. 4.	74
Figure 3.12. Paleosol-F at the Gololobovo site.	77
Figure 3.13. Gololobovo Composite Section.	80
Figure 3.14. Photograph showing stratigraphy at Korostylievo.	85
Figure 3.15. Modern-day soil and krotovena of unit KC-1.	86
Figure 3.16. Korostylievo composite section.	87
Figure 3.17. Krotovena within lithostratigraphic unit KC-3 (below paleosol D).	92
Figure 3.18. Rectilinear fissure pattern developed within unit KC-4.	96
Figure 3.19. Large krotovena within unit KC-4.	97
Figure 3.20. The lower portion of the Korostylievo composite section.	99
Figure 3.21. Korostylievo composite section with scaled data.	104
Figure 3.22. Locational relationships between sections and points of interest. ...	111
Figure 3.23. Stratigraphic column for Mikhailovka Section Nos. 1 and 2.	113
Figure 3.24. Photograph and trace of stratigraphy at sections MS1 and MS2. ...	114
Figure 3.25. Photograph of the loess--paleosol sequence at MS1.	117
Figure 3.26. Paleosols E and F at MS-2.	120
Figure 3.27. Stratigraphic column for Mikhailovka Section No. 3.	122
Figure 3.28. Photograph of the loess-paleosol sequence at MS3.	123
Figure 3.29. Stratigraphic column for Mikhailovka Section No. 5.	128
Figure 3.30. Overview photograph and trace of the exposure in the vicinity of MS5.	129

Figure 3.31. Mikhailovka composite section.....	135
Figure 3.32. Frequency histograms for comparison of loess from the Russian Plain and loess from the Chinese Loess Plateau.	137
Figure 3.33. Correlation of sites over 700 km transect.	INSERT
Figure 4.1. Korostylievo and Mikhailovka data correlated to SPECMAP. .	INSERT
Figure 4.2. Photograph and trace of unconformity below the Don Till.....	INSERT
Figure 4.3. The newly proposed geochronologic and chronostratigraphic scheme for the Russian Plain.	149
Figure 5.1. Estimated accumulation rates based on newly proposed chronostratigraphy.....	161
Figure 5.2. Diagrammatic illustrating general bioclimatic shifts and glacial advance relationships.	163
Figure 5.3. Distance-to-source relationships between correlative loess units along the 700 km long north-south transect.	166
Figure 5.4. Modern-day and Mikulino Interglacial soil maps for the Russian Plain Region.	167
Figure 6.1. Allostratigraphic scheme applied to Korostylievo and Strelitsa stratigraphy and magnetic susceptibility.	172
Figure 6.2. Allostratigraphic scheme applied to Korostylievo and Kurtak stratigraphy and magnetic susceptibility.	175
Figure 6.3. Allostratigraphic scheme applied to the stratigraphy and magnetic susceptibility of Mikhailovka, and the orbitally tuned grain-size ratio record at Baoji, China	178
Figure 7.1. Diagrammatic illustrating three possible origins for loess-paleosol genesis.	188
Figure C.1. Diagrammatic examples of lithostratigraphic boundaries and classification.	255
Figure C.2. Diagrammatic example of an allostratigraphic classification applied to contiguous deposits of similar lithology.	258

List of Plates

Plate 3.1. Photomicrograph for paleosol-C.....	46
Plate 3.2. Photomicrographs from paleosols E ₂ , E ₁ and F at Likhvin.....	56
Plate 3.3. Photomicrographs for upper three paleosols at Golobovo.....	66
Plate 3.4. Photomicrographs for paleosols E ₂ and E ₁ at Golobovo.....	75
Plate 3.5. Photomicrographs of soil-A and paleosol-C at Korostylievo.....	88
Plate 3.6. Photomicrographs of paleosols D ₁ and D ₂ at Korostylievo.....	91
Plate 3.7. Photomicrographs of paleosols E ₂ , E ₁ and F ₂ at Korostylievo.....	94
Plate 3.8. Photomicrographs from paleosols F ₁ and G.....	101
Plate 3.9. Photo micrographs of soil-A at Mikhailovka.....	115

List of Abbreviations

GC: Gololobovo Composite Section

GS1: Gololobovo Section No. 1

GS2: Gololobovo Section No. 2

GS3: Gololobovo Section No. 3

GS4: Gololobovo Section No. 4

KC: Korostylievo Composite Section

KS1: Korostylievo Section No. 1

KS2: Korostylievo Section No. 2

LC: Likhvin Composite Section

LC1: Likvin Section No. 1

LC2: Likvin Section No. 2

LGM: Last Glacial Maximum (in North America, *i.e.*, MIS 2)

MC: Mikhailovka Composite Section

MS1: Mikhailovka Section No. 1

MS2: Mikhailovka Section No. 2

MS3: Mikhailovka Section No. 3

MS5: Mikhailovka Section No. 5

MIS: Marine Isotope Stage

MISS: Marine Isotope Sub-stage

n.a.: not available

n.d.: no data

F_D: Frequency dependence of magnetic susceptibility (also as F%)

CHAPTER 1 - INTRODUCTION

General Introduction

Quaternary sedimentary sequences of the Russian Plain record terrestrial paleoclimate signals from the latter portion of the Pleistocene Epoch (Velichko *et al.* 1999). Through detailed examination of four selected type sections that sequentially span the last *ca.* 800 ka of earth history, this dissertation advances the chronostratigraphy of the Russian Plain as well as improving the understanding of paleoclimatic events that form its Quaternary history. These achievements are accomplished by utilizing classical approaches to stratigraphy and sedimentology in conjunction with modern techniques such as the measurement of magnetic susceptibility, frequency dependence of magnetic susceptibility, geochemistry and soil micromorphology.

This dissertation presents the stratigraphic relationships between two classic sites (Likhvin and Korostylievo), a relatively new site (Gololobovo) and a site that has not been formally described by Quaternary scientists (Sebryakova-Mikhailovka). The data from these sites yields information that improves upon the current stratigraphic framework, and allows for the development of an alternative stratigraphic framework to be used as a basis for future local and regional correlation of East European loess-paleosol sequences.

Prior to this research, the examination of Russian Plain loess-paleosol sequences have provided a potentially promising method of addressing regional- to hemispheric-scale climate dynamics. Once beyond *ca.* 150 ka, however, poor stratigraphic control due to a lack of suitable dating techniques has inhibited both large- and small-scale correlations alike (*e.g.*, Holsteinian-Likhvin correlations: *vide post*). Based on sound sedimentologic and stratigraphic principles, optical dating, paleomagnetic analysis and cross-reference to orbitally tuned $\delta^{18}\text{O}$ records, this dissertation presents new solutions to long-standing stratigraphic problems of the East European Plain. Hence, this research will demonstrate that reasonable correlations between sections in China, southeastern Siberia and western Russia are possible - effectively advancing our knowledge of paleoclimatic links at hemispheric and global scales. Furthermore, new field and micromorphologic observations from these four sites are

examined in conjunction with magnetic susceptibility and geochemical data sets enabling improved resolution for interpretations regarding the depositional environments and pedogenic evolution of Russian Plain loess-paleosol sequences.

Research Objectives

This dissertation represents the first attempt to examine, in detail, the Quaternary sedimentary sequences at four key sites on the East European Plain. The primary objectives of this research project are outlined as below:

- 1. correlate sites along a 700 km, north-south transect and tie the units to a temporally constrained stratigraphic framework;**
- 2. interpret depositional environments and paleoclimatic changes through time, and;**
- 3. propose Eurasian-scale correlations that may be used to test future climate models.**

These three objectives will be facilitated through the following endeavours: 1) describe, sample and analyse sediments from selected sample sites; 2) acquire new independent dating control for the sedimentary sequences at each of the study sites; 3) develop a stratigraphic scheme that can be used for long-range correlation; 4) compare and contrast the newly developed stratigraphy with currently accepted stratigraphic schemes, and; 5) where necessary, propose solutions to existing stratigraphic problems.

The overall regional geologic framework resulting from this project will provide the potential for comparisons to be made between loess-paleosol stratigraphy of the Russian Plain with that of Siberia and the Chinese Loess Plateau, thus aiding in Asian-wide to hemispheric-wide paleoclimate (*e.g.*, soil evaporation models) and atmospheric-dust modelling.

Study Area

Four sites were examined during the course of this study (Figure 1.1A): 1) Gololobovo Site (55° 03'N; 38°34'E) located within an active brick-pit approximately 12 km west-southwest of Kolomna; 2) Likhvin Site (54° 06'N; 36° 16'E) located along the banks of the Oka River, approximately 45 km south of Kaluga; 3) Korostylievo Site (51° 51'N; 42° 22'E) located along the banks of the Vorona River approximately 110 km south-southeast of Tambov; and, 4) Sebryakovo-Mikhailovka Site (50° 06'N; 43° 14'E; hereafter referred to as "Mikhailovka") located within a Cretaceous chalk quarry approximately 170 km northwest of Volgograd. The distances between section localities are given in Table 1.1.

Table 1.1. Distances between site locations.

Site Distances and Location	Gololobovo 55°03'N; 38°34'E	Likhvin 54°06'N; 36°16'E	Korostylievo 51° 51'N; 42° 22'E	Sebryakovo-Mikhailovka 50° 06'N; 43° 14'E
Gololobovo	0km	180km	435km	630km
Likhvin	180km	0km	480km	650km
Korostylievo	435km	480km	0km	200km
Sebryakovo-Mikhailovka	630km	650km	200km	0km

Physiography of Section Sites

Present-day Climate and Soils

Between *ca.* 66°N and *ca.* 44°N, European Russia is classified into a temperate, continental climate belt, that can be subdivided into three zonal bio-climatic regions (Gerasimov *et al.* 1996; Shcherbakova 1998; Figure 1.2): taiga with excess moisture, mixed forest and forest-steppe with sufficient moisture, and steppe with a lack of moisture. The prevailing winds in this region alternate; winds are generally from the south during winter, and from the west during summer (Figure 1.2).

Although all the sites fall within a temperate, continental climate belt, temperatures and precipitation are distinctly different between northern (Likhvin and Gololobovo), south-central (Korostylievo) and southern (Mikhailovka) sites (Figure 1.3 A-C; Appendix A). For Likhvin and Gololobovo, the mean July temperature is approximately 18°C,

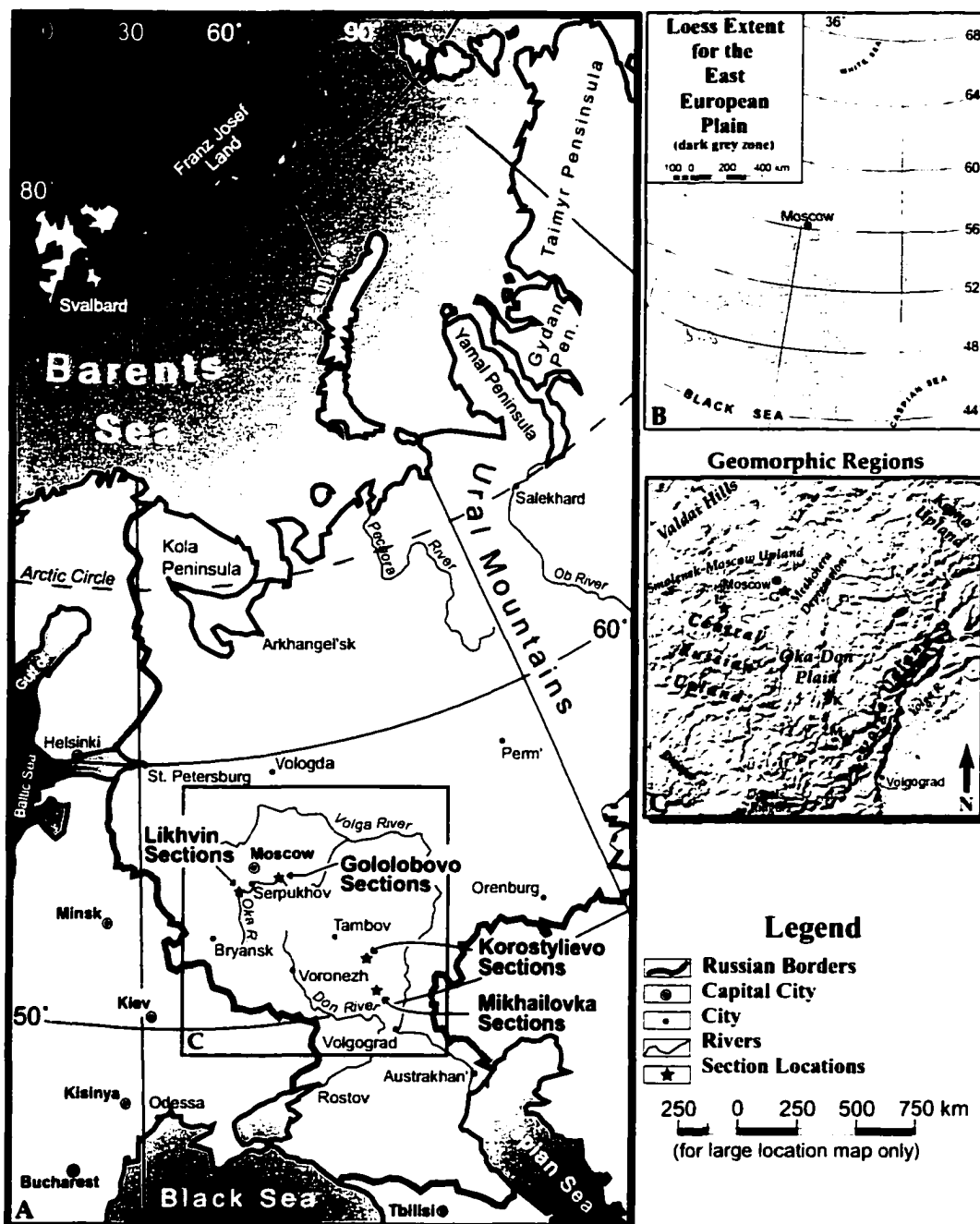


Figure 1.1. A. Location of study sites. B. loess extent in Eurasia (after Velichko 1990). C. physiographic regions (after Anderson and Buckton 1999) within the study area.

with absolute maximum summer temperatures reaching 37°C. Mean January temperature is approximately -10°C, but cold spells during winter months may reach temperatures of -42°C (Lysenko 1971; Lydolph 1977; Shcherbakova 1998). Monthly mean precipitation ranges from 28 mm to 74 mm, peaking in June and July. Mean annual precipitation for the region is 575 mm/year in the northeast, and up to 694 mm/year in

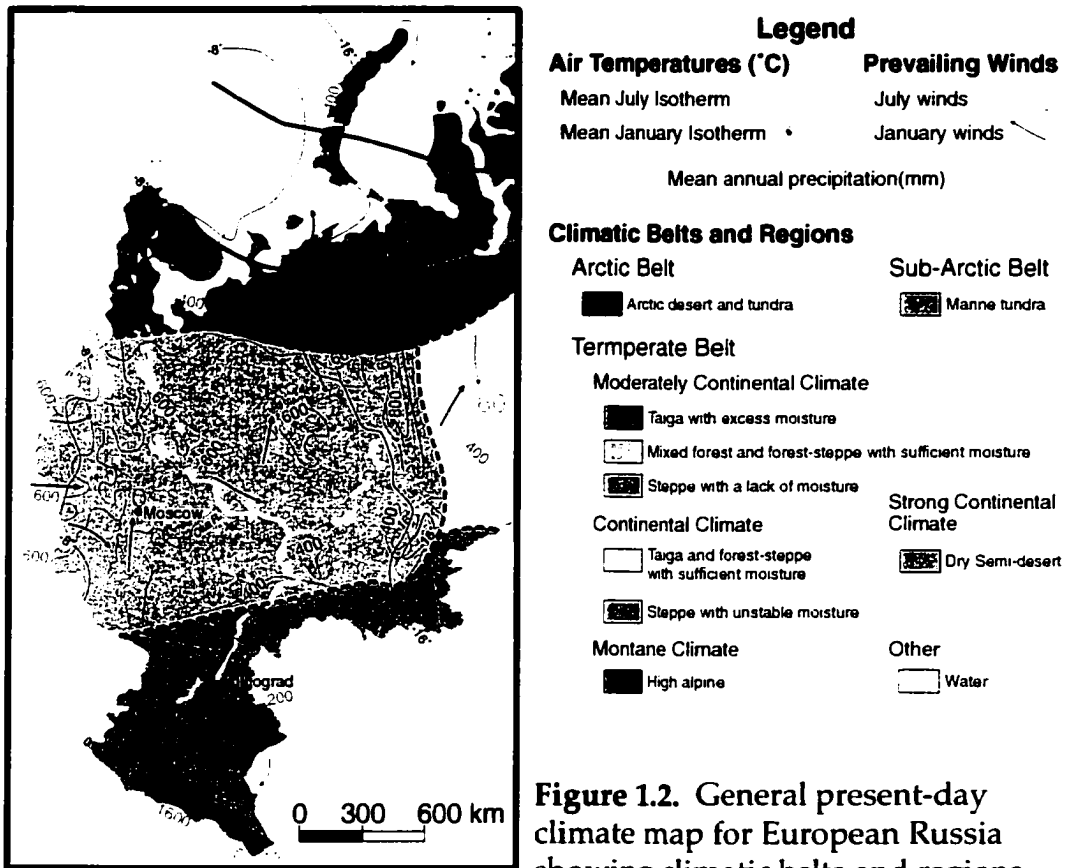


Figure 1.2. General present-day climate map for European Russia showing climatic belts and regions along with mean seasonal air temperature, prevailing winds and mean annual precipitation (modified after Shcherbakova 1998).

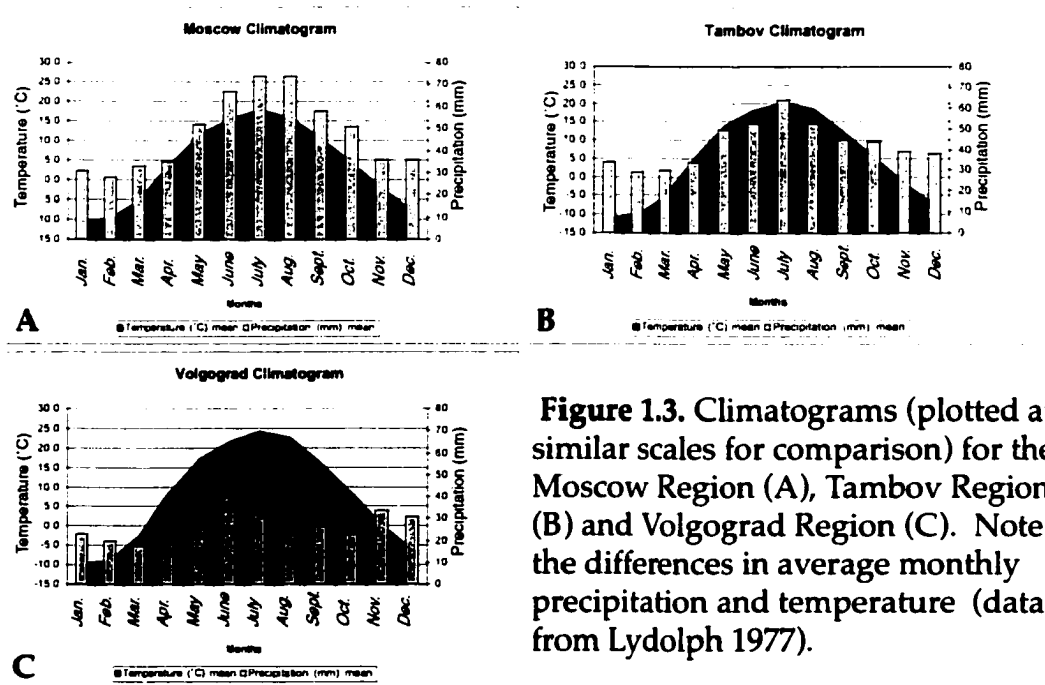


Figure 1.3. Climatograms (plotted at similar scales for comparison) for the Moscow Region (A), Tambov Region (B) and Volgograd Region (C). Note the differences in average monthly precipitation and temperature (data from Lydolph 1977).

the northwest (Lysenko 1971; Lydolph 1977; Shcherbakova 1998). Farther south, in the vicinity of Korostylievo, the mean July temperature is approximately 20°C with an absolute maximum summer temperature of 40°C. Mean January temperature is approximately -11°C with an absolute minimum temperature of -39°C. Monthly mean precipitation ranges from 29 mm to 64 mm, peaking in July. Mean annual precipitation is about 513 mm/year (Lydolph 1977; Shcherbakova 1998). Finally, in the vicinity of Mikhailovka, mean July temperature is approximately 24°C, with absolute maximum summer temperature reaching ~43°C. Mean January temperature is approximately -10°C, with an absolute minimum temperature of -35°C. Monthly mean precipitation ranges from 18 mm to 40 mm, peaking in June. Mean annual precipitation near Mikhailovka is approximately 318 mm/year (Lydolph 1977; Shcherbakova 1998).

Temperature and precipitation characteristics outlined above are partly responsible for the distribution of soils within the study area. From north to south, the soils that currently occupy the study area include the following (Shcherbakova 1998): Mixed-forest luvisols in the vicinity of Golobovo and Likhvin; grey brown luvisols, dark brown chernozems and eluviated brown chernozems between Likhvin and Korostylievo; orthic black chernozems in the vicinity of Korostylievo and Mikhailovka, and; calcic black chernozems south and east of Mikhailovka. Detailed descriptions for these soils and their diagnostic characteristics can be found in "The Canadian System of Soil Classification" (Soil Classification Working Group 1998).

Geomorphology

All sites examined are found on the East-European Plain¹ (Figure 1.1B) -- one of the largest continental plains in the Northern Hemisphere. This geographic region encompasses an area in excess of 5.5 million square kilometres, and has an average elevation of approximately 142 m (Velichko *et al.* 1993).

Relief within the Russian Plain varies from low-contrast basins, plains and rolling hills in the central portions, to high contrast relief in

¹Current literature often refers to this region as the 'Russian Plain'; these two terms are synonymous (Velichko pers. com. 2001).

the borderland plains. Within the central portions of the Russian Plain, topographic undulations have relatively low amplitudes of between 150 m and 250 m. In comparison, the southern borderland plains exhibit elevations that vary from approximately 800 m for the Stavropolskoye Plateau (not shown), down to 350 m for the Don Ridge (not shown); both of these topographic features eventually descend into the Caspian lowland which is near sea-level (Velichko *et al.* 1993).

The Golobovo site is located in the north-central portion of the Russian Plain, in an area referred to as the Oka Basin which lies within the northern extent of the Oka-Don Plain region (Velichko *et al.* 1997; Figure 1.1C). This relatively flat, low lying region is bounded by Smolyenka-Moscow Hills and Meshchera Depression to the north, the Oka-Don Plains to the south, the Kama Uplands and Meshchera Depression to the east, and to the west by the Smolyenka-Moscow Hills, and Central Russian Upland (Figure 1.1C).

The Central Russian Upland (Figure 1.1C) forms the dominant topography in the vicinity of the Likhvin Site. These gently rolling hills trend north-northwest to south-southeast from approximately 54°N, 36°E to approximately 50°N; 38°E, and rise approximately 100 m to 150 m above the Oka-Don Plain. The primary drainage of the hills is taken up by the Oka and Don rivers (Figure 1.1A).

Korostylievo and Mikhailovka sites are both located within the Oka-Don Plain which is characterized as a relatively low-relief region lying approximately 150 m below the bounding Central Russian Upland to the west and the Volga Upland in the east (Figure 1.1C).

Bedrock Geology

East-European Platform Basement

European Russia is situated within the bounds of the East-European Platform (Figure 1.4); an acute-angled continental block spanning *ca.* 3000 km along its greatest axis. It is bound on all sides by thrust fronts of fold belts, except to the southeast, where the Peri-Caspian depression is underlain by Devonian oceanic crust (Zonenshain *et al.* 1990).

The East-European basement consists of three main components: the Baltic Shield, the Ukrainian Shield and Jatulian Proto-platform cover.

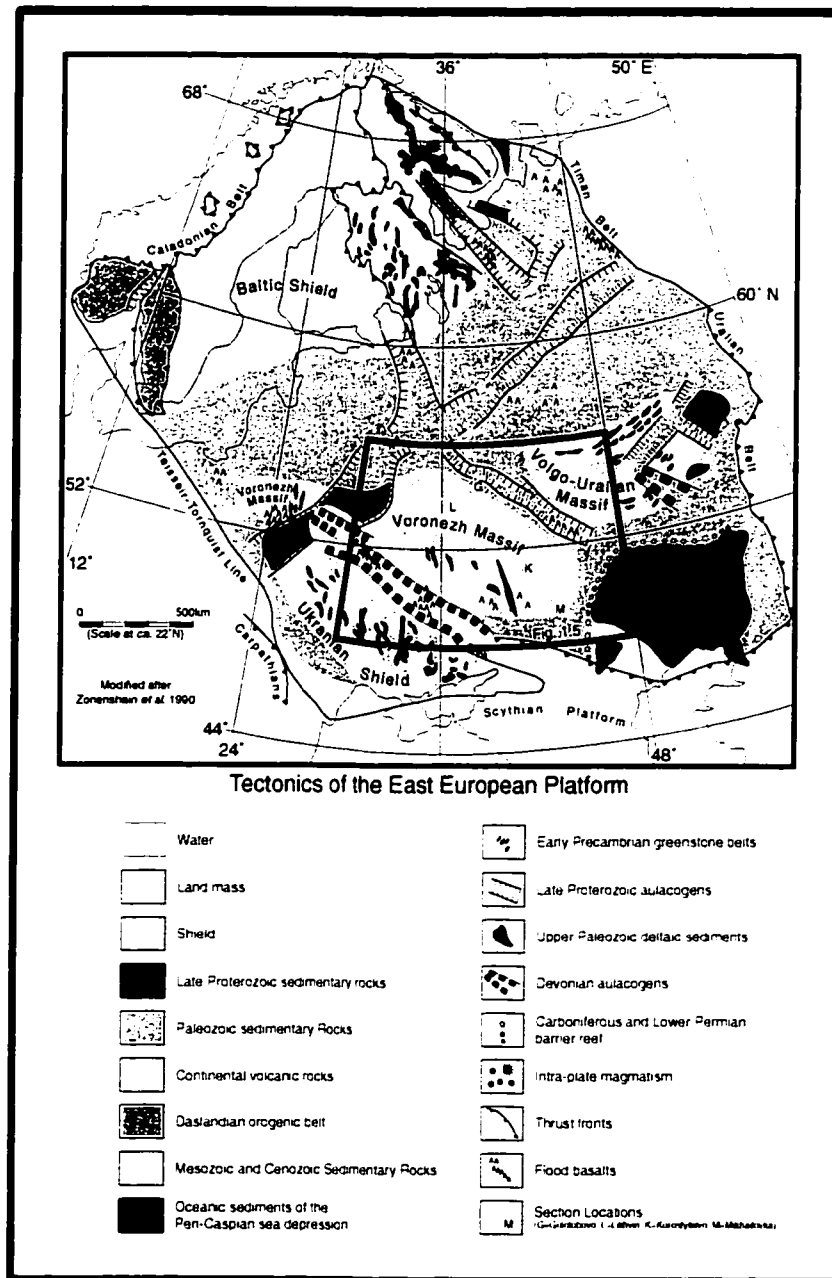


Figure 1.4. Tectonic and basement rock map for the East European Platform. Inset shows area of coverage for Figure 1.5 - Bedrock Map of Study Area.

The two former constituents can be subdivided into an assortment of angular Precambrian blocks 100-300 km wide, separated by suture zones. The blocks consist mainly of Archean² domains of different composition: granite – greenstone (*e.g.*, main portion of Ukrainian

²Geochronometric ages associated with chronostratigraphic strata in the Bedrock Geology section are based on Okulitch (1999).

Shield), granite – gneiss (*e.g.*, north-northeast portion of the Baltic Shield), and schist – gneiss (*e.g.*, main portion of Baltic Shield) (Zonenshain *et al.* 1990). The intra-block suture zones also contain a variety of rock types that include flysch (marine marls, calcareous shales and muds), chert, banded iron stones (jaspillite) and mafic volcanics. The Jatulian Proto-platform formed during the Early Precambrian and is found within the eastern portion of the Baltic Shield and within the bounds of the Ukrainian Shield. It is comprised of two types of cover: 1) clastic sequences of conglomerates, arkoses and quartzites eroded from the shields (not shown in Figure 1.5 due to map scale); and 2) mafic and ultramafic lava flows (Zonenshain *et al.* 1990).

Following the complete formation of the East-European platform (*ca.* 1600 Ma) the Middle Proterozoic Jotnian Platform sedimentary cover was laid down. This consists primarily of sandstones deposited within the limits of the Baltic and Ukrainian shields, and quartzites within the Volga – Uralian area (Zonenshain *et al.* 1990).

Regional Bedrock Geology

Bedrock within the study area consists of a wide variety of types and ages, some of which were briefly mentioned above. The oldest rocks are Archean in age and consist of gneiss, migmatites, phyllites, chloritic and calcareous schists and other highly metamorphosed rocks found in association with the Ukrainian Shield (~49°N, 31°E; Figure 1.5), in addition to some quartzites and jaspilitic iron-ore (Nalivkin 1960, 1973). The youngest deposits are composed of thick (150 - 200 m) Quaternary sediments of the Peri-Caspian sea (~49°N, 47°E; Figure 1.5). The remaining bedrock within the study area is composed primarily of nearly horizontal, marine Paleozoic, Mesozoic and Tertiary sediments (Nalivkin 1960, 1973).

Paleozoic

The earliest major chronostratigraphic period of the Paleozoic that is recognized within the study area is the Devonian. Devonian rocks in the northwest and central portion of Figure 1.5 (~55°N, 49°E and ~53°N, 39°E respectively) consist of marine clays and argillaceous limestones, dolomites, salt-bearing lagoonal deposits and variegated continental red-beds (sandstones).

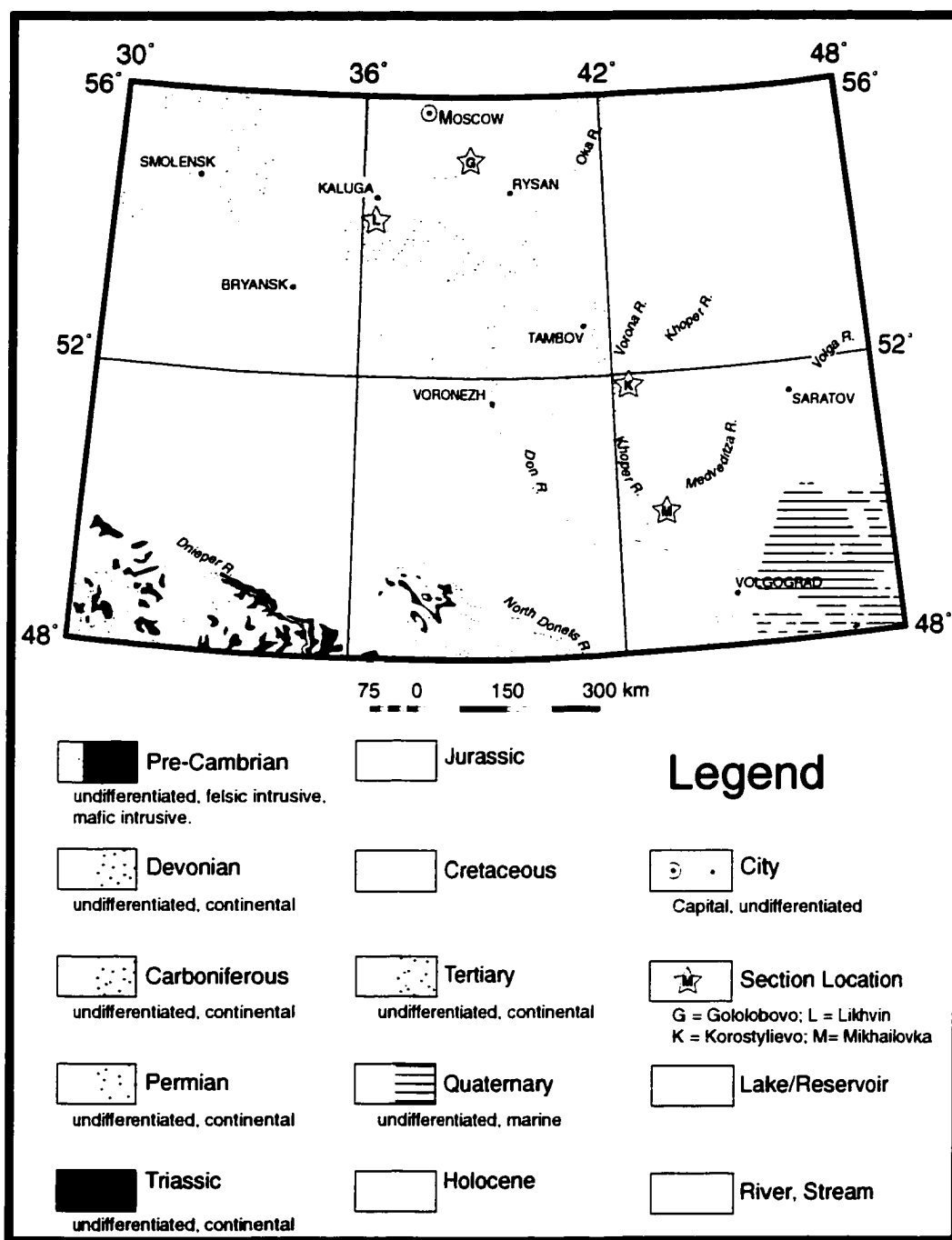


Figure 1.5. Generalized bedrock map for study area. See text for detailed discussion on bedrock types of different age ranges (modified after Nalivkin 1960).

Carboniferous deposits are predominantly observed in the north-central and south-central portions of Figure 1.5 (~55°N, 36°E and 49°N, 39°E respectively). These consist of sandstone, clay with coal seams, and well-bedded limestone that exhibit abundant fossilized marine fauna. Minor occurrences of Carboniferous sediments also occur south of the Medveditza River at approximately 49°30' N, 44°00' E (Figure 1.5); these consist of characteristically light-coloured limestones that also exhibit an abundance of marine fossils.

Permian deposits are found in the northeast and south-central portions of the study area (~55°N, 45°E and 48°30'N, 38°00'E respectively; Figure 1.5). Permian rocks in these areas consist of marine argillaceous shales and sandstones, and continental conglomerates and sandstones, in addition to some red-beds interbedded with minor freshwater calcareous deposits.

Mesozoic

Red-bed formation that began in the Permian continued into the Mesozoic. Continental Permian-Triassic aged red-beds are observed south of the North Donets River at approximately 48°30'N, 38°00'E (Figure 1.5). In the Volga-Emba region (~48°05'N, 47°00'E) the red-beds are overlain by Lower Triassic pale marine clays and marls (Nalivkin 1973).

Middle Triassic and Lower Jurassic successions have not been observed within the study area. Extensive Middle and Upper Jurassic deposits, however, have been observed at numerous locations in the central and eastern portions of the study area; minor occurrences are also observed in the western portions along the Dnieper River (~49°30'N, 32°00'E) and north of Bryansk (53°15'N, 34°25'E). These deposits consist of sands and clays with minor amounts of limestone, glauconite-phosphorite deposits, bituminous shales and minor oolitic sediments.

Closely associated with nearly all Jurassic deposits are the marine Cretaceous strata. In northern portions of the study area near Bryansk, Moscow and west of Tambov, these deposits consist of coarse-grained sandstones and clays. In more southerly locations (*e.g.*, near Mikhailovka at 51°51'N, 43°14'E) the Cretaceous strata are composed of white chalk, marls and argillites.

Cenozoic

Deposition within the Cenozoic was markedly different from previous periods. Lithological and facies characteristics of early Tertiary deposits found within the southwest, south-central and northeast portions of the study area (~50°N, 33°E, 50°N, 39°E, and 53°N, 47°E respectively; Figure 1.5) can be summarized by: 1) having a sharp decrease in carbonate content relative to the chalks and marls of the Cretaceous Period; 2) having a high percentage of siliceous clays, diatomites, and glauconite-phosphorite; 3) having a wide range of marine facies including clays and glauconitic sands, marls, and beach deposits, and; 4) having some near-shore sandy-clayey rocks that contain plant remains and coal seams (Nalivkin 1973). Within the central and southeastern portions of the study area (~52°N, 41°E and 48°N, 44°E respectively; Figure 1.5), Tertiary deposits are chiefly composed of continental sands and clay.

Quaternary deposits are found throughout the area, but are shown in Figure 1.5 only where the underlying bedrock is poorly known (*e.g.*, Caspian Basin east of Volgograd). Detailed discussion of the Quaternary and recent deposits is presented below.

Quaternary Research

Previous Work

This section begins with a general introduction and discussion of events that have contributed to the evolution of Quaternary stratigraphy of the Russian Plain over the last *ca.* 150 years. This is followed by a summary of the European ice-sheets -- timing and extents which, in turn, relates the ice-sheet distributions to the deposition of glaciogenic sediments and loess. A discussion of the lithostratigraphic studies on the Russian Plain ensues, along with a section that highlights some of the problems encountered during the research phase of the dissertation. This section ends with a review of Russian Plain paleosol research.

Evolution of Quaternary Stratigraphy for European Russia

The study of Quaternary geology in Russia began in the C19th with the development of the first hypotheses, theories, methodologies, and partitioning of the surficial sediments. During this period, the devel-

opment of Quaternary stratigraphy was influenced by both Russian and foreign academicians in the fields of geology, paleontology, archaeology, geography and soil science (Gerbova and Krasnov 1982). Researchers who made significant contributions to those fields are considered to be the forefathers of Russian Quaternary geology. The most prestigious of these included: P.A. Kropotkin (1842-1921), S.N. Nikitin (1851-1909), A.P. Pavlov (1854-1929), N.E. Kristoffovich (n.d.), V.A. Obrachev (1863-1956), C.A. Yakolev (1878-1957), V.N. Sukachev (1880-1967), G.F. Mirchink (1889-1942) and V.E. Gromov (1896-1978) (Gerbova and Krasnov 1982). Many have also made major contributions to global geologic problems (*e.g.*, Obrachev 1945) in addition to advancing the understanding of Russian Quaternary geology.

During the late C19th and the beginning of the C20th many Russian researchers were concentrating their studies on the recognition and genesis of glacial sediments. For example, in 1871 P.A. Kropotkin initiated research on ancient glaciations in Finland; his famous monograph “Исследования о Ледниковом Периодии (Research on Glacial Periods)” was published in 1876, whereas in 1885, Nikitin presented his pioneering work on European glacial limits (Nikitin, 1885). Although there was extensive research being done on glacial sediments throughout the world at the close of the C19th, the stratigraphy of Russian glacial sediments was not focused upon until the 1900’s. One of the earliest stratigraphic schemes for the Late Tertiary/Quaternary was developed by N.I Andrusov in 1912 for sediments of the Black and Caspian Sea regions (see Gerbova and Krasnov 1982, pp. 21-2). However, as in most of the stratigraphic schemes of that time, the Quaternary Period was not subdivided. An exception is the work of P.A. Pravoslavlev, who in 1907, studied marine sediments of the Caspian Basin. He was able to compare sediments from that basin with glaciogenic deposits farther north and characterize the climatic conditions for each corresponding epoch (*i.e.*, Würm, Riss, Mindel, Günz).

The period between 1914 and 1928 was one of enormous turmoil and upheaval within Russia/the Soviet Union. With the advent of World War I, the Russian Revolutions of 1917, and the following years of economic hardships and political instability (Dukes 1990), very few scientific advances were accomplished. In 1939, however, I.P.

Gerasimov and K.K. Markov were the first to associate local Russian names with major climatic fluctuations; these included the Valdai and Dnieper glacial periods, and the Moscow Stadial. It is interesting to note that, in the original scheme of Gerasimov and Markov, the name Likhvin (*vide post*) was associated with an Early Pleistocene glaciation. Later, however, the so-called “Likhvin glaciation” (Early Pleistocene) was renamed the Oka glaciation, and the name Likhvin became associated with a Middle Pleistocene pre-Dnieper interglacial period (see Gerbova and Krasnov 1982, p. 24). Following the development of this stratigraphic scheme, World War II (1939-1945) hindered Soviet earth science research.

It was not until 1948 that any further significant advances were made in Quaternary Stratigraphy. At this time, V.I. Gromov proposed a single-glaciation scheme, in which there was only “one great glaciation” within the Pleistocene. He explained the notions put forth in the pre-World War II multi-glaciation schemes by subdividing the “great glaciation” into stadials and interstadials.

While Gromov was advancing his “single-glaciation” hypothesis, one of his contemporaries, A.I. Moskvitin was also working intensively on Russian Plain stratigraphy. In his stratigraphic scheme (Table 1.2) the multi-glaciation hypothesis was reconciled and terms such as Valdai Glaciation (Weichsalian³), Dnieper Glaciation (Saalian³), and Likhvin Interglacial (Holsteinian³) were re-utilized while others, such as the Mikulino Interglacial (Eemian³) and Oka Glaciation (Elsterian³) were introduced; all of these terms are still commonly used in modern-day Quaternary stratigraphic analyses. In addition, a standardized geologic index commonly used by Russian and some Chinese researchers to denote major units (*e.g.*, Q_{II,d}) was also introduced by Moskvitin in 1950 (Table 1.2).

Between 1950 and 1980, the only major changes to occur in the east European Quaternary stratigraphy were the ranking and group status

³ Accepted correlative terms from Northern Europe and The Netherlands Quaternary stratigraphic schemes (Velichko 1990; Zubakov 1993; Sudakova and Faustova 1995; Velichko 1995; Velichko *et al.* 1995; Zagwijn 1992, 1996; Lowe and Walker 1997, Velichko *et al.*, 1999).

Table 1.2. Quaternary stratigraphic scheme and geologic index of Moskvitin, 1950 (modified from Gerbova and Krasnov 1982; their table 7, pg 26). Italicized names indicate current common usage.

Primary Divisions	Epoch	Geologic Index	Glacial	Inter-glacial	Horizon or Phase
Q _{IV}		Q _{IV}		Post Glacial	Sub-atlantic Sub-boreal Atlantic Boreal Sub-arctic
Q _{III}	Neopleistocene (Würm Epoch)	Q _{III, wt}	<i>Ostashkovo</i>		<i>Valdai</i> phase (late glacial)
		Q _{III, mol}		Molovo-shekninskii	Numerous warm/cool phases
		Q _{III, k}	<i>Kalinin</i>		Kalinin phase (early glacial)
		Q _{III, mk}		<i>Mikulino</i> (Riss-Würm)	End phase- warm Middle phase - cool Start phase - warm
Q _{II}	Mesopleistocene (Riss Epoch)	Q _{II, m}	<i>Moscow</i>		Max. phase of penultimate glacial
		Q _{II, od}		<i>Odnatovo</i>	End: forest-tundra Middle: taiga Start: forest-tundra
		Q _{II, d}	<i>Dnieper</i>		Initial phase of penultimate glacial
		Q _{II, l}		<i>Likhvin</i>	
Q _I	Eopleistocene (Mindel Epoch)		Upper Mindel		
		Q _{I, ok}		1 st interglacial	
			<i>Oka</i>		

of the names given in Moskvitin's 1950 stratigraphic scheme. The driving force behind the constant adaptation of Quaternary stratigraphic schemes was the application of thermoluminescence, radiocarbon dating, magnetostratigraphy and biostratigraphy during the 1960's and 1970's (e.g., Shelkopyas and Morozov 1965; Chichagova 1972; Faustova *et al.* 1974; Shevirev *et al.* 1979). Zubakov (1974) and Gerasimov *et al.* (1980) each presented new stratigraphic variants summarizing the Quaternary stratigraphic research completed in the preceding decades (Gerbova and Krasnov 1982). Zubakov (1974) was one of the first to compile a preliminary climatostratigraphic framework based on east European bio-, magneto-, and climato- stratigraphic data together with the existing chronostratigraphy for the last *ca.* 60 ka and

pre-60 ka thermoluminescence (TL) ages. His research attempted to constrain the absolute timing of Quaternary stratigraphic units; this advanced the previous relative stratigraphic chronologies (*e.g.*, Moskvitin 1950; *vide ante*). Gerasimov *et al.* (1980) took the existing stratigraphic schemes one step further; their work was based primarily on earlier research by Velichko and Morozova (1972) and compared the stratigraphic terminology and ages from different regions and compiled them into a comprehensive stratigraphic scheme for the glacial, proximal glacial and coastal regions of eastern Europe.

The evolution of the Quaternary stratigraphy of European Russia is an ongoing endeavour. Research between 1950 and 1980 has played a crucial part in its development, and is the essential framework on which contemporary Quaternary stratigraphic schemes are based. Although some aspects of the early schemes (*e.g.*, Moskvitin 1950; Zubakov 1974; Gerasimov 1980) can be identified in modern versions, many significant modifications and new interpretations have influenced the contemporary Quaternary stratigraphy of European Russia.

Last Twenty Years of Quaternary Stratigraphic Research for the Russian Plain

Developments in Quaternary stratigraphy of the Russian Plain during the 1980's and 1990's followed through from preceding decades which focused on attempts to refine the chronology of glacial / interglacial events (*e.g.*, Velichko *et al.* 1986; Velichko 1990; Velichko *et al.* 1995; Bolikhovskaya and Sudakova 1996). This was done primarily through the correlation of land-mammal fossil assemblages (*e.g.*, Agadjanyan and Glushankova 1987), the use of new dating techniques such as optical dating (*e.g.*, Yakimenko 1995), and other less direct methods such as estimating mean January or July temperatures from paleosols and pollen records and then correlating these results to marine isotope records (MIS; *e.g.*, Velichko 1990). These attempts met with varying degrees of success, and in most cases only served to increase the uncertainty of Russian Plain stratigraphy and chronology.

During the early 80's, the stratigraphic scheme presented in the work of Krasnov and Shantser (1982; their Table 19) was one of the most widely accepted, comprehensive, stratigraphic schemes for the Quater-

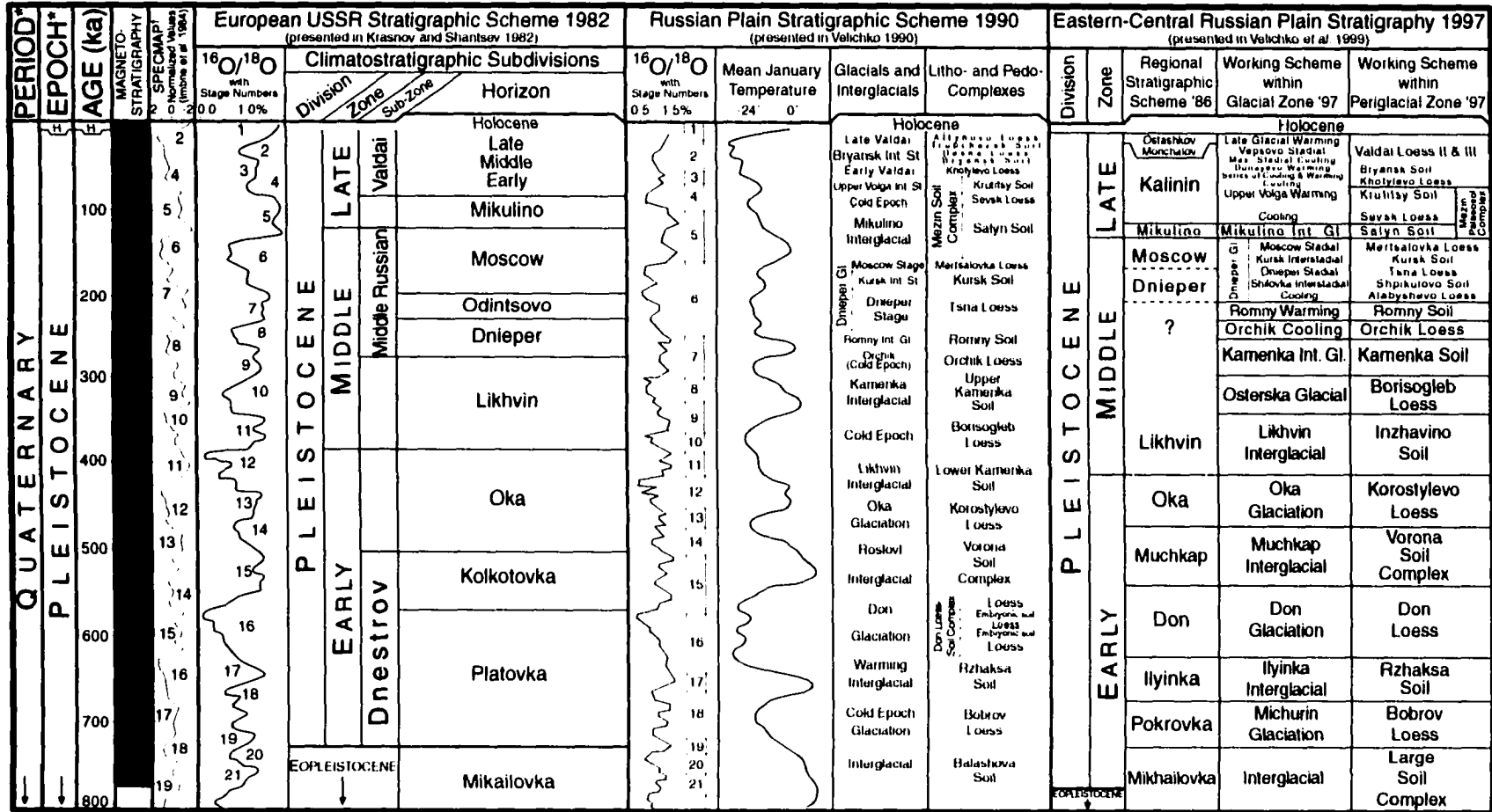
nary of European USSR and western Europe. This compilation⁴ presented magnetostratigraphic, biostratigraphic, climatostratigraphic units spanning the last *ca.* 3.5 Ma and correlated these units to archaeological records and oceanic data (*i.e.*, marine planktonic and benthic foraminifera and MIS). Essentially, this stratigraphic scheme used the regional correlations and terminology of Gerasimov *et al.* (1980) and the chronology of Zubakov (1974). The chronology of the latter was improved by the correlation of the terrestrial and coastal records to archaeological stages and oceanic records. The result was a highly refined Quaternary (and Neogene) stratigraphic scheme (Figure 1.6) that correlated different regions of European Russia to each other and to oceanic records, thereby giving this scheme the potential to compare Russian Plain records at a global scale.

Velichko (1990) used the stratigraphic scheme presented in Krasnov and Shantser (1982; their Table 19) as a basis for his work, but retained the stratigraphic subdivision detail of Gerasimov *et al.* (1980). In his stratigraphic scheme, rather than correlating terrestrial records to oceanic records *via* coastal sections, he used a more direct method; terrestrial climate proxies from paleosols and cryogenic features yielded estimates of mean January temperatures through time (Figure 1.6). These data produced a curve that he was able to compare to the MIS curve of Shackleton and Opdyke (1976). This enabled him to refine the chronostratigraphy using only terrestrial data (*i.e.*, no link through coastal sections) and again allowed global correlation of Russian Plain sections to other terrestrial and oceanic records.

Although a tremendous effort has been made to solve many of the Russian Plain stratigraphic problems that have evolved over the decades, many of these so-called “advances” have only added to the confusion. Due to the limitations of contemporary dating methods, correlation with the marine record without the necessary absolute dating control makes such correlations highly subjective. Thus, many contradictory Quaternary stratigraphic schemes for the East European Plain

⁴The comprehensive stratigraphic scheme presented in Krasnov and Shantser (1982) was compiled by K.V. Nikiforova, I.I. Krasnov, L.P. Aleksandrova, Yu. M. Rasilev, N.A. Konstantinova, and A.L. Chepalyga.

Figure 1.6. Comparison of contemporary Russian Plain Stratigraphic Schemes. Each scheme shown here is a summary of the original (as presented therein). In each of these schemes, the Brunhes/Matuyama boundary is presented at 730 ka (black bar); for reference, the corrected date of 780 ka (Cande and Kent 1995) is shown in darkgrey. Medium grey zones within the sub-zone category of the 1982 scheme are un-named time intervals. The SPECMAP data (Imbrie *et al.* 1984) is supplied as an accepted standard on which to compare the Russian records. ' = N.A. usage (Okulitch 1999); † = modified as per Bassinot *et al.* 1994; H = Holocene.



have been correlated to other stratigraphic schemes, thereby compounding the problems (*cf.* Chapter 3). This is especially true for those portions of the stratigraphy that are beyond *ca.* 150 ka (*cf.* Velichko 1990; Zagwijn 1992; van Kolfschoten *et al.* 1993; Sanko 1995; Sudakova and Faustova 1995; Zagwijn 1996; Turner 1996; Lowe and Walker 1997).

Despite these problems, the stratigraphic framework currently accepted by the Russian Academy of Sciences was first developed in 1997 and is presented in Velichko *et al.* (1999; presented herein with a slight modification as per the author's request -- Velichko pers. com. 2001). This stratigraphic scheme is a compilation of the past *ca.* 30 years of research and includes: an absolute time scale, magnetostratigraphy, stratigraphic units in both glacial and periglacial zones, faunal complexes with their corresponding land mammal assemblages, supporting strip logs of type sections, regional landscape and climatic characteristics, and semi-quantitative paleoclimatic curves; a summary of the original 1999 scheme is presented in figure 1.6.

Upon inspection of the 1997 version of the Russian Stratigraphic scheme (Figure 1.6), one can identify many changes from the 1982, 1986 and 1990 versions. The most significant of these involve timing changes of upper and lower zone boundaries. For instance, the last interglacial period, the "Mikulino Interglaciation", was originally shown as an early to middle MIS 5 event (Figure 1.6, 1982 scheme). Later, however, it encompassed the whole of MIS 5 and at present it is considered to correspond to the MIS 5 climatic optimum (MISS 5.5 - *ca.* 129-122; Martinson *et al.* 1987; *cf.* Figure 1.7). Changes such as this occur throughout the schemes of the 1980's and 1990's while others involve stratigraphic nomenclature (*cf.* Odinstovo Interstadial with Kurska Interstadial; 1982 and 1990 schemes respectively) or subdivision of established units (*cf.* Likhvin Interglacial; 1997 scheme).

Although the above examples are problems that make comparisons to other schemes exceedingly enigmatic, one problem stands out above all others. In each of the schemes presented in Figure 1.6 (including the most recent), the Brunhes-Matuyama paleomagnetic boundary is placed at 730 ka. The age for the Brunhes-Matuyama boundary was revised in the mid-90's (Cande and Kent 1995) and is now widely accepted to be

780 ka. The placement of the boundary at 730 ka instead of the revised 780 ka age has significant repercussions for the application of a time scale to the stratigraphy, especially when this is the primary method used to constrain the chronology of the lower portion of the stratigraphic scheme. Consequently, many uncertainties are introduced when attempting to correlate to non-Russian stratigraphic schemes (Figure 1.7). An attempt is made to rectify this problem later in the dissertation (*vide* Chapter 4). However, until this problem is corrected, the ages presented in Figure 1.7 (Russian Terrestrial Stratigraphy) will suffice in the following discussion.

Contemporary Russian Plain Quaternary Geology: Discussion

The following subsections outline some of the current controversies and inconsistencies that are encountered when attempting to understand and correlate Russian Plain stratigraphy both internally and with other Quaternary stratigraphic records (*e.g.*, China, Western Europe). These problems are primarily associated with events older 100 ka and are the result of “fundamental difficulties in the studies of the Middle (and Lower) Pleistocene cycle stemming from the different understandings of its (their) chronological position by different researchers” (Velichko 1995, p. 12).

The presentation of this information, and the discussion of its implications are crucial towards understanding the reasons and motives for research and interpretations presented in ensuing chapters.

European Ice-Sheets and Their Relationship to the Quaternary Sedimentation on the East European Plain

Before contemporary stratigraphic and paleoclimate research can be evaluated and fully understood, a basic understanding of the timing and extents of related ice masses must first be reviewed (Rutter 1995, p. 19). The timing and extent of the European ice sheets have influenced the distribution and preservation of the Quaternary sedimentary sequences deposited on the East European Plain. These sequences consist not only of loess, but also of secondary loess, colluvium, till, glaciofluvial and glaciolacustrine sediments. Ice-sheet proximity was a primary factor contributing to the distribution of this wide variety of sediments.

The proximity to ice sheets plays a particularly important role in Quaternary sedimentation throughout the East European Plain. Figure

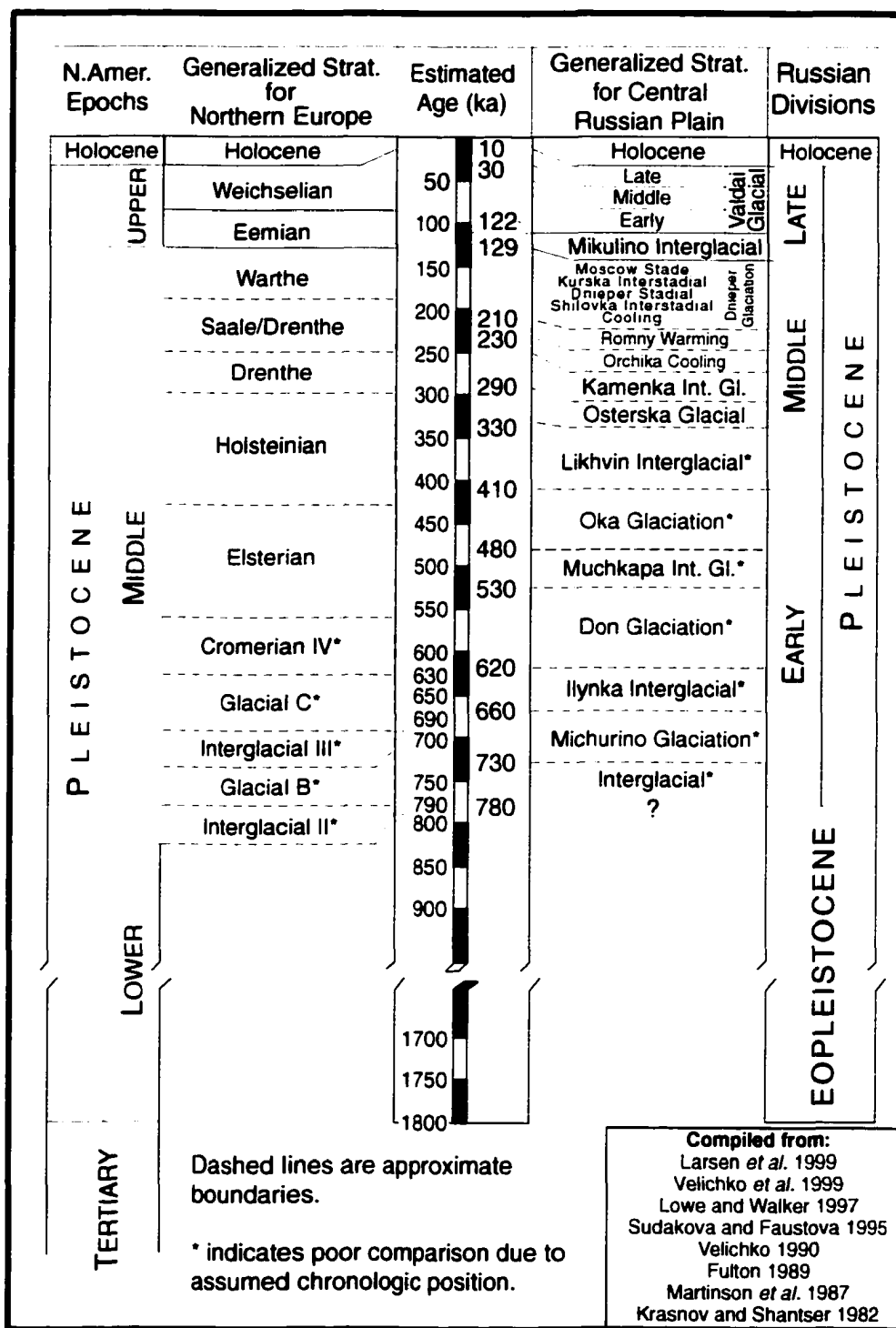


Figure 1.7. Quaternary stratigraphy of The Netherlands and Europe compared to the currently accepted stratigraphic scheme for the Russian Plain. The Late Pleistocene scheme presented here is generalized due to space requirements; for the detailed 1997 Late Pleistocene scheme for the Russian Plain refer to Figure 1.6.

1.8 depicts accepted limits of past ice sheet advances onto the East European Plain; generally, the older glaciations are the most extensive. Figure 1.9 depicts the spatial distribution and age ranges for sediments of the East European Plain. A similarity is clearly observed between the extent and timing of the ice margins and Quaternary sediment spatial and temporal distributions. Most of the relationships have been widely accepted by contemporary researchers, save those pertaining to the Valdai glacial limits, and Valdai ice-sheet genesis which have been intensively debated for the last three decades (*e.g.*, Grosswald 1980; Arkhipov *et al.* 1986; Svendsen *et al.* 1999).

The last glacial period (*i.e.*, Valdai Glacial) is the most intensively studied and critically evaluated and therefore many aspects of that glacial period (*e.g.*, ice cover, limits, genesis *etc.*) have been scrutinized by various researchers (*vide* Rutter 1995 and references therein). Recently, however, controversies surrounding certain aspects of the last glacial cycle in Russia have been resolved. Moraine-mapping by Astakhov *et al.* (1999) revealed the Markhida Line, which represents a zone of hummocky tills marking the last major stationary position between the Barents and Kara ice-sheet margins. Furthermore, Astakhov *et al.* (1999) were able to elucidate early-middle Weichselian (Valdai) ice domes that were situated on the shelves of the present-day Barents and Kara seas. Detailed examination of ice-dammed lakes and spatial distribution patterns of moraine and ice-marginal deposits enabled Mangerud *et al.* (1999) to conclude that the late Weichselian (Valdai) Barents-Kara ice-sheet limit occurred in a region presently offshore of mainland Russia. Their work implies a late Weichselian maximum glacial limit that was much farther north than classical late glacial limits (*e.g.*, Velichko 1990) or those proposed by Grosswald (1993). Svendsen *et al.* (1999) expanded upon the work of both Astakhov *et al.* (1999) and Mangerud *et al.* (1999), and mapped the extent of Barents and Kara ice-sheets of the early-middle Weichselian, which advanced farther south onto mainland Russia than did the late Weichselian Barents-Kara ice sheets.

Previous research has also focused on dating the prevalent Bryansk paleosol; a marker horizon within the last glacial cycle. Currently the accepted age for this warming event is 30 ± 1 ka to 23 ± 1 ka ^{14}C years

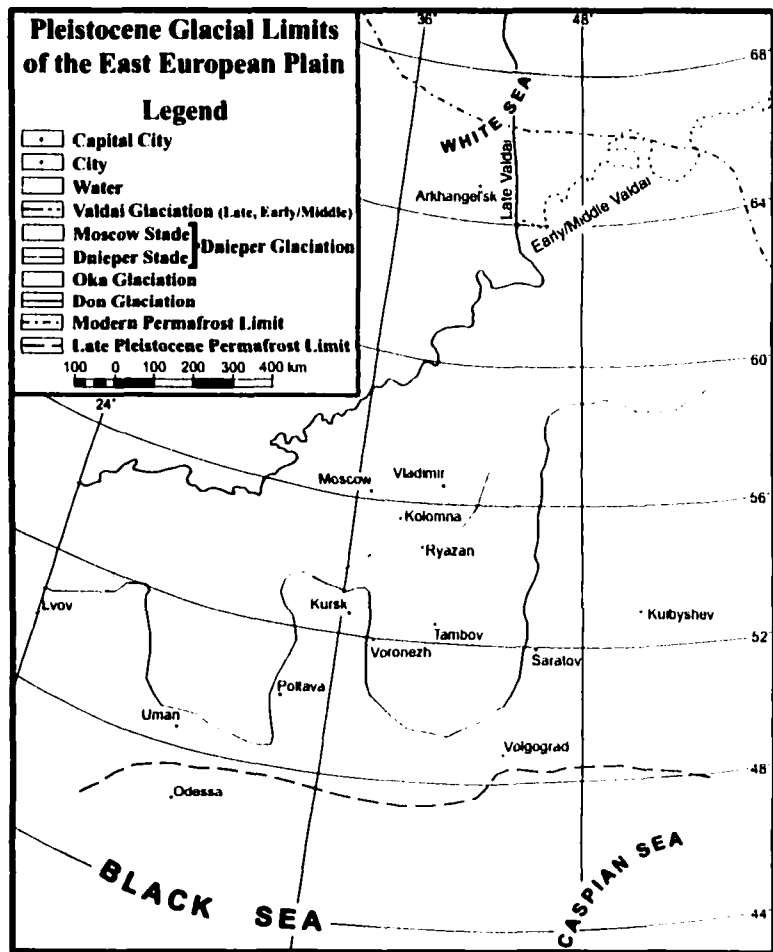


Figure 1.8. Glacial Limits of the East European Plain (modified after Velichko 1990 and Svendsen *et al.* 1999).

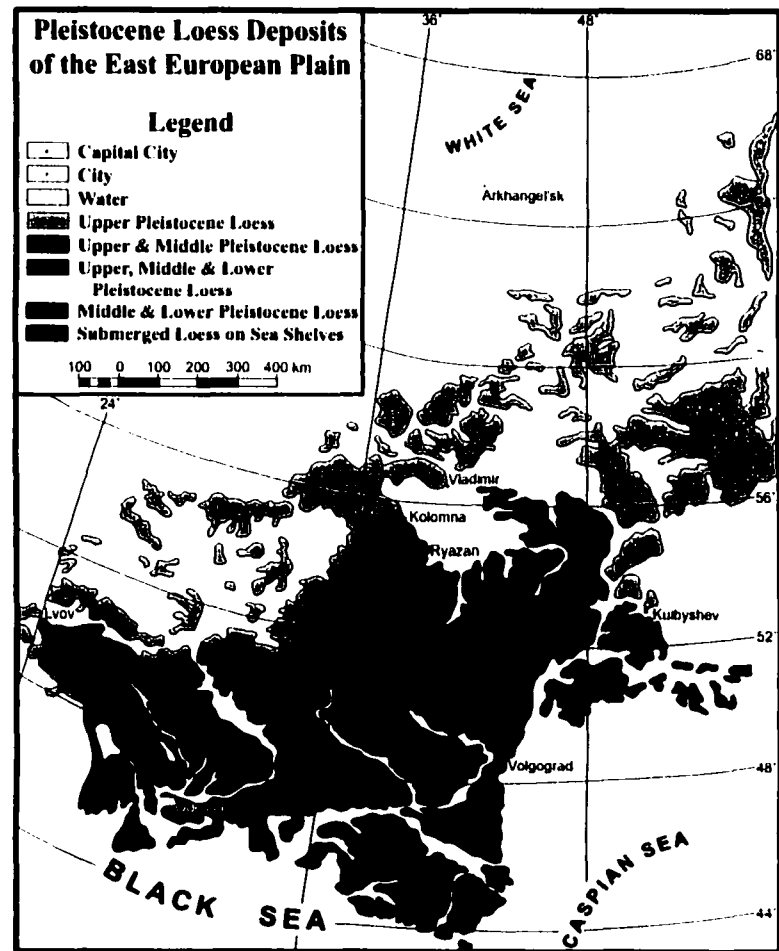


Figure 1.9. Loess distribution over the East European Plain (modified after Velichko 1990).

(e.g., Velichko *et al.* 1964; Velichko and Morozova 1972, 1987; Dobrodeyev and Parunin 1973; Chichagova 1972, 1985; Velichko *et al.* 1992; Tsatskin 1997), or between 34 ± 1 ka and 27 ± 1 ka calendar years, using the calibration data of Bard *et al.* (1998) and Kitagawa and van der Plicht (1998).

The timing and distributions of glacial extents that predate the last interglacial are more problematic (e.g., Fig. 1.7 & 1.8; e.g., *vide* Velichko 1995). Typically, these problems are avoided by presenting an asynchronous Quaternary glacial-maximum limit (*cf.* Svendsen *et al.* 1999). Clearly, much work is needed to elucidate the timing and distribution of Early and Middle Pleistocene glacial intervals and warm interglacial periods that punctuate them.

Enigmatic Early and Middle Pleistocene Records: Case Studies

The chronology of Russian Plain loess-paleosol sequences beyond *ca.* 150 ka is presently under considerable discussion (*cf.* Velichko 1990; Zubakov 1993; Sudakova and Faustova 1995; Velichko 1995; Velichko *et al.* 1995; Lowe and Walker 1997). The Middle Pleistocene sequence itself has three different interpretations which are summarized in Velichko (1995):

1. **The Middle Pleistocene (in Russian Division; *cf.* Figure 1.7) includes the Likhvin (Holsteinian) interglacial and the Dnieper (Saalian) glaciation. In this interpretation, the Moscow event (no Western European equivalent) is classified as a stadial within the Dnieper glaciation.**
2. **Subsequently, some researchers concluded that interglacial "layers" existed between the Dnieper glaciation and the Moscow "glaciation".**
3. **The most recent interpretation is based on integrated multidisciplinary studies. It does not find any paleosols separating the Dnieper glaciation and the Moscow event, reinforcing interpretation "1" above. However, they do find two paleosols between the Likhvin (Holsteinian) Interglacial and Dnieper (Saalian) Glaciation (Velichko, 1995).**

Contributing to the enigmatic nature of the Early and Middle Pleistocene Russian Plain stratigraphy is the timing and associations of the Likhvin Interglacial (*vide ante*), which is often referred to as a Russian equivalent to the Holsteinian Interglacial of Western Europe (currently accepted as MIS 11; *e.g.*, Turner 1996, Poorc *et al.* 1998). However, in Russian Quaternary schemes for the East European Plain, it is also commonly correlated to MIS 9 (*e.g.*, Zagwijn 1992, 1996). To further complicate this particular issue, Velichko (*per. com.* 2001) stated that he associates the Likhvin Interglacial with MIS 9, but this does not support the time limits Velichko *et al.* (1999) assign to the Likhvin Interglacial, where it tentatively spans MIS 7 through MIS 11 (Figure 1.6).

Finally, problems with stratigraphic nomenclature are prevalent throughout Russian Plain stratigraphy (*cf.* Zubakov 1993, Velichko 1990; *e.g.*, the Likhvin Interglacial, Figure 1.6). Furthermore, figure 35 of Velichko *et al.* (1999, p. 71) clearly shows a sequence of Early and Middle Pleistocene paleosols (listed here from oldest to youngest): Vorona, Lower Kamenka, Upper Kamenka and Romny. In their figure 37 the sequence is: Vorona, Inzhavino, Kamenka, Romny. Comparing the two figures reveals that the terminology for paleosols within a single article is not consistent inducing potential problems for future correlations. Together, the above examples alone have significant negative implications towards the advancement of precise Russian Plain stratigraphy.

Despite inconsistencies such as those presented above, researchers continue to focus on Pleistocene climate interpretations of Russian Plain sediments, and attempt to correlate these interpretations to other parts of the world (*e.g.*, Likhvin interglacial of Russia = Holsteinian interglacial of Europe) without adequately addressing the problems (*vide ante*). For the reasons stated above and in the foregoing paragraph, a rigorous evaluation of East European Quaternary Stratigraphy is imperative, hence an independent chronology is developed herein to further test the Russian Plain stratigraphic *status quo*.

Evolution of Russian Plain Paleosol Research

The first climate-soil relationships for the Russian Plain were reported by Dokuchayev (1883) who stated “the Russian Chernozem serves as a living link with the climate and natural vegetation of the

country... forests do not produce Chernozems" (p. 375-6 as referenced in Alexandrova 1983). This profound statement outlines a basic principle that has been a keystone in soil studies around the world, and continues to be used in modern-day research. The concept that soils and climate are linked allows us to interpret past climates from paleosols identified in the geologic record. However, in the initial stages of paleosol research, even Dokuchayev interpreted the humic-rich horizons buried in loess sections as glacial mud (Dokuchayev 1893 as referenced in Tsatskin 1997); it was Glinka (1904) who first interpreted the humic horizon in loess sections as paleosols (Tsatskin 1997⁵).

Paleosol research has evolved significantly over the decades since Glinka's (1904) pioneering research and now encompasses studies that include the examination of Holocene and modern-day soils being used as analogs. Continued examination of loess-paleosol sequences has also yielded relationships between paleosol horizons and cryomorphologic features such as ground wedges, solifluction features and involutions (Velichko 1973; Moskvitin 1976; Tsatskin 1997). In some cases, aspects of these cryogenic features were found to be associated with particular paleosols and thus together these could be used as relative dating techniques (*e.g.*, Velichko 1990). Advances in stratigraphic time-series analysis were enhanced by the application of ¹⁴C-dating (dating soil humus), paleomagnetic analysis and luminescence dating techniques. These contributed to the understanding of time-stratigraphic relationships. However, the latter of the three techniques, which was thought to fill the Middle Pleistocene 'dating gap', has not been verified by geological evidence prior to the empirical correlations to SPECMAP presented herein (*i.e.*, Imbrie *et al.* 1984). Hence, luminescence dating has not, and is still not, considered to be a reliable technique on which to base time-stratigraphic relationships for sediments older than approximately 150 ka (Zubakov 1976; Dremanis *et al.* 1978; Wintle and Huntley 1982; Prescott and Robertson 1997; Tsatskin 1997; Little *et al.* in press). This matter unfortunately did not retard time-stratigraphic investigations between 1970 and the present-day; over zealous correlations during this period have inevitably led to convoluted Russian Plain stratigraphy and correlation to other records (Figure 1.6).

⁵A thorough summary of Russian Plain paleosol research is presented in Tsatskin (1997).

Although prior stratigraphic studies utilize questionable absolute-time stratigraphic relationships (*cf.* Figure 1.6), excellent paleoclimatic interpretations based on individual soil horizons and relative time scales have been produced from Russian Plain research (*e.g.*, Figure 4.1 - Morozova 1995). In order to achieve such results, however, only the best-suited paleoclimatic parameters obtained from paleosols can be used. Suitable pedogenic features are those that exhibit little diagenetic change after burial (Yaalon 1971; Gerasimov 1971; Sokolov and Targulian 1976; Tsatskin 1997); parameters such as clay and carbonate eluviation/illuviation, carbonate nodule formation and gleyzation, are generally accepted as being relatively stable soil constituents (Catt 1990; Tsatskin 1997). Methods used to evaluate these types of parameters and interpret paleoclimates include descriptive field observations, laboratory analyses (*e.g.*, geochemistry), micromorphology, and stratigraphic/geographic context (*vide* Chapter 3). Thus, paleosol data together with lithostratigraphy and chronostratigraphy allow paleoenvironmental conditions to be compared over significant distances and periods of time.

Dissertation Organization

The following chapters begin with an outline of the methods and procedures used to obtain the data presented throughout the dissertation. This is followed by a stratigraphy chapter that describes and constructs basic and composite litho- and pedo- stratigraphic columns that represent the units observed at each site. From these constructs, allostratigraphic units are defined based on optical dating (younger sediments), marker bed association, and paleosol counting. The allostratigraphic units are then correlated over distances >100 km. Chapter 4 examines the interpreted stratigraphy for Korostylievo and Mikhailovka and proposes new correlations between the empirical section data (*e.g.*, magnetic susceptibility) and the SPECMAP record of Imbrie *et al.* (1984).

Once the stratigraphic correlations are complete and a new chronostratigraphy is proposed, depositional environments and pedogenic horizons are compared and contrasted over the 700 km transect. This allows further evaluation and development of the Quaternary history

for the region, which is presented in the latter portions of Chapter 5 along with its climatic implications. Chapter 6 proposes preliminary correlations to other records in Russia, and records in Siberia and China. The final chapter summarizes the major results of the thesis, and presents research proposals that need to be addressed in order to further advance our understanding of East European paleoclimate dynamics, as well as hemispheric and global climate dynamics.

Supplementary data used throughout the dissertation are presented in the appendices.

CHAPTER 2 - GENERAL METHODS

Introduction

Detailed field investigations of Russian Plain loess-paleosol-cryogenic sequences were undertaken during the summers of 1996 (north-central) and 1998 (central). Sections were chosen by Russian colleagues at the Russian Academy of Science based on research experiences and each section's regional and temporal context.

This chapter outlines the methods, and conventions used throughout the course of this dissertation with the following sections being broken down into field methods and laboratory methods. Each section begins with a short explanation of why the given technique was used and to what ends the results were to be used. Only a brief explanation of the optical dating technique is provided in this chapter; a more detailed description can be found in Appendix B.

Field Methods

Section descriptions focused on physical characteristics of the sediments and the physical relationships between juxtaposed units. Once descriptions were completed and sample locations were marked, the section was photographed and sampled. Thin section sampling was completed prior to bulk sampling in order to ensure thin-section-sample precision.

Sample Collection and Preparation

General purpose sediment samples were collected from each site with a knife and shovel; care was taken to minimize contamination of the samples. Each sediment sample was stored in plastic sample bags for transport. Once in the lab, the samples were transferred into resealable plastic containers. The average sample size was approximately 250 g which yielded enough sediment to run grain-size and loss-on-ignition (LOI) analyses. Sampling methods for optical dating and micromorphology are presented later in this chapter as they require special field and laboratory treatments.

Laboratory Methods

Textural (Grain Size) Analysis

Textural analysis of samples was undertaken in order to ascertain the physical properties of the sedimentary units. Physical properties such as sorting and median grain size diameter enable textural classification and aid in genetic depositional environment interpretations for each sample and unit/facies. Textural characteristics from other “known” deposits are also processed using techniques outlined below in order to compare and contrast Russian Plain samples thereby aiding in the interpretive process.

For each sample selected for textural analysis, approximately 45-50 g of sediment was sub-sampled into a 250 ml beaker. To ensure that the sub-sample was representative, small scoops of sediment were taken from 8 locations around the edges of the container, and one from the middle (Hicock, pers. com. 1994). Distilled (or filtered de-ionized – hereafter referred to as DI) water was then added until the entire sub-sample was submerged.

Pretreatment - Removal of Carbonates

The technique from Barrett and Brooker (1989) was utilized to remove carbonates: Once weighed and wetted, 20 ml of 10% HCl was added to each sample submerged in distilled (or DI) water. In order to speed up the reaction, samples were placed under 250 W heat lamps and stirred occasionally until the reaction ceased. Once the reactions ceased, approximately 5 ml of 10% HCl was added to test for complete carbonate removal. If the reaction continued, the process was repeated until no reaction was observed. The samples were then transferred into a 250 ml centrifuge bottle and rinsed 3 times with distilled (or DI) water using a large capacity centrifuge at a rotation speed of 4000 rpm for 10 minutes.

Pretreatment - Removal of Organic Matter

Following carbonate removal, samples were placed into 600 ml beakers. Approximately 10 ml of 30% H₂O₂ (hydrogen peroxide) and distilled (or DI) water were added to each sample (Sheldrick and Wang, 1993). The samples were placed under 250 W heat lamps and left to stand, stirring occasionally, until all reactions ceased. Once the reac-

tions ceased, approximately 5 ml of 30% H_2O_2 was added to test for complete removal of organic matter. If a reaction was observed, the organic removal procedure was repeated until no reactions were observed. When reactions were no longer observed, the samples were transferred into 250 ml centrifuge bottles and rinsed 3 times with distilled (or DI) water using a large capacity centrifuge at rotation speeds of 4000 rpm for 20 minutes. Once rinsing was completed, the sediments were carefully transferred into 200 ml beakers for sonication and mechanical agitation.

Separation of Fine (<250 μm) and Coarse (>250 μm) Fractions

Dispersion of the samples were accomplished by mechanical mixing (with just enough power to keep the stirrer in motion), and ultrasonic vibration for a minimum of 5 minutes. Once completed, each sample was wet sieved through a 250 μm sieve, retaining the < 250 μm sediment in a tared 600 ml beaker; the >250 μm particles were washed into tared petri dishes or 60 ml beakers. Both particle fractions were dried in an oven at 120°C to obtain dry weights.

Fine Fraction Analysis

In order to disperse the sample, 50 ml of 0.1% NaPO_3 (sodium metaphosphate) solution was added to 4.0-4.5 g of the dried <250 μm sediment fraction. The sample was then initially stirred by hand to mobilize all particles in the sample. To ensure adequate dispersion, the samples were mechanically mixed (with just enough power to keep the stirrer in motion), while sitting in an ultrasonic bath for 5 to 15 minutes, depending on the clay content of the sample.

Following sediment dispersion, the sample was loaded into a SediGraph 5100 Particle Size Analysis System. Manufacturer's specifications of this apparatus outline an error of $\pm 5\%$ for the >63 μm fraction and $\pm 2\%$ error for the >2 μm fraction. Periodically, standards were run to ascertain if the apparatus was operating normally; all such tests indicated no problems (Appendix C). Mechanical mixing of the sediment was used rather than the typical magnetic mixing (standard sedigraph procedure) to prevent separation of magnetic particles within the sample.

Coarse Fraction Analysis

The majority of samples contained only a small proportion (<1g per 40g) of particles >250 μm . In these situations, only qualitative visual description of the coarse fraction was noted; no further analysis was undertaken. Results were classified as ">250 μm fraction".

Loss-On-Ignition (LOI)

Loss-on-Ignition (LOI) was used to quantify the weight percent of bulk organic carbon and calcium carbonate within each sample. The quantification of these parameters is useful in interpreting deposition and post-depositional environments by aiding in the identification of pedogenic horizons high in organic content (*e.g.*, Ah-horizons) or CaCO_3 (*e.g.*, Cca-horizons), and loess horizons that typically exhibit higher CaCO_3 content. LOI results can also be used as a correlation tool by comparing these lithic parameters and their associated units between sequential sections at distances <1 km (*e.g.*, Gololobovo composite section).

LOI sub-samples consisted of 1-2 g aliquots obtained from the general sample lot. Any roots and rootlets observed within the sub-sample were removed with tweezers prior to drying. Each of these aliquots was then placed in a crucible, dried in an oven at $\sim 105^\circ\text{C}$ for at least 8 hours and weighed to 4 decimal places to obtain a dry weight.

Organic Determination

Once dried, the sample was placed in a muffle-furnace at 550°C for one hour (Dean 1974). After cooling to room temperature, the sample was weighed; the difference between this weight and the dried weight is a measure of the amount of organic carbon that was burned off (Dean 1974).

Carbonate Determination

After obtaining the 550°C burn weights, the sample was placed into the muffle furnace and heated to 1000°C for one hour. The difference in weight between 550°C and 1000°C burns is the amount of CO_2 that has evolved from carbonate minerals. This value was then divided by 0.44 which represents the fraction of CO_2 in CaCO_3 ; the result represents the percentage of CaCO_3 lost during the 550-1000 $^\circ\text{C}$ burn.

Rock Magnetic Parameters

Two different but related rock magnetic parameters were used as an aid for identifying, interpreting and correlating discrete lithic and pedogenic units in stratigraphic sequences. For Russian Plain loess examined herein, magnetic susceptibility and frequency dependence of magnetic susceptibility are generally greater in pedogenic units than in loess units, thereby allowing local correlation of units (*e.g.*, Korostylievo composite section - Chapter 3). Where the magnetic susceptibility signal tracks marine isotope stages (*e.g.*, SPECMAP) and independent chronologic constraints are recognized, correlations to oceanic records and the development of an orbitally tuned age model can be established. The frequency dependence of magnetic susceptibility often corroborates interpretations of soil development based on section descriptions and micromorphology, and thereby aids in the identification and interpretation of pedogenic units. A brief discussion explaining the use and methods of each of these rock magnetic parameters is presented below.

Magnetic Susceptibility

The rock magnetic parameters of clastic sediments, in particular of loess and overprinting soils and paleosols, often reflect paleoenvironmental processes such as transport, deposition or transformation of magnetic grains (Verosub and Roberts 1995, Evans 1999) and organic/inorganic *in situ* formation of magnetic grains (Evans *et al.* 1997, p. 183). Given the depositional setting and accepted paleosol genesis for sediments of the Russian Plain, magnetic susceptibility (χ), a measure of the magnetizability of a sediment, were taken to help interpret those paleoenvironmental conditions that lead to the development of the Russian Plain stratigraphy. Also, in some cases, the magnetic susceptibility data track marine isotope stratigraphy (*e.g.*, Korostylievo and Mikhailovka - Chapter 4), thus allowing orbitally-tuned MIS records to be used as a time scales for correlative terrestrial Quaternary stratigraphic sequences. For these reasons, magnetic susceptibility measurements were conducted at all of the study sites.

Magnetic susceptibility data were collected both in field and laboratory settings. As it is the trends in magnetic susceptibility that are the

focus of this research, both field and laboratory analyses are used, depending on the conditions-of-sampling and the resolution of the final data set. At the Likhvin and Gololobovo sites, *in situ* field measurements and cube samples for laboratory analyses were obtained. In both cases a Bartington MS-2 Susceptibility meter was used and calibrated with a series of pure chemical compounds. However, the sensor used to detect the magnetic susceptibility in the field differs from that used in the laboratory setting: for the field, a Bartington MS2F configuration was utilized; in the laboratory, a MS2B configuration was utilized. Samples obtained for laboratory analyses were collected in 2 cm³ plastic cubes for transportation and analysis in the Bartington MS2B Susceptibility meter. At Korostylievo, incomplete *in situ* measurements required the use and presentation of only the laboratory data. At Mikhailovka, high-resolution *in situ* magnetic susceptibility data collect by V.V. Semenov (1996 and 1998 field-team participant) were used.

Frequency Dependence of Magnetic Susceptibility (F_D)

The magnetic response of sub-micron particles near the superparamagnetic / single-domain grain (SP/SD) boundary is dependent on the frequency of the applied field. Changing the frequency of the applied magnetic field will detect the presence of the aforementioned grains, with lower frequencies producing higher susceptibilities (Stephenson 1971).

In practice, the instrument used in this work (Bartington MS2B Susceptibility meter) utilizes two applied fields (~0.5 kHz to ~5 kHz). If the low frequency magnetic susceptibility minus the high frequency susceptibility ($x_{LF} - x_{HF}$) is large, then there are many grains near the SP/SD boundary (*i.e.*, finer-grained magnetic particles). If $x_{LF} - x_{HF}$ is relatively small, then the magnetic particles are mostly larger SD grains. Higher percent decreases (*i.e.*, more magnetic grains close to the SP/SD boundary) tend to be present in soils / paleosols (Heller and Evans 1995). The genesis of the magnetic grains that produce these observed F_D data trends is a function (theoretically) of the soils' productivity (Evans, pers. com 2000; *e.g.*, Heller and Evans 1995).

Geochemistry

Geochemical analyses yielding Fe_2O_3 , Al_2O_3 and SiO_2 were obtained from selected loess and paleosol samples at each of the four sites. The data are used (where applicable) to aid in the soil horizon identification (e.g., aluminium depletion in an Ah-horizon and corresponding enrichment in a B-horizon). Identification of such processes aids in the classification of soil types and their associated paleoclimates.

Geochemistry was completed at Moscow State University under the direction of the Russian Academy of Sciences. The techniques used are described in Arinushchikina (1970).

Optical Dating

Optical dating was first proposed by Huntley *et al.* (1985), and differs from thermoluminescence and electron spin resonance, in that it utilizes light to induce luminescence in samples. In all of these techniques, the basic principle is a time-dependent, cumulative response of naturally-occurring minerals to environmental radiation (Huntley *et al.* 1985). There are essentially two methods of optically stimulated luminescence (OSL): green light stimulated luminescence (GRSL), and infrared stimulated luminescence (IRSL). In the literature, the former is also often simply referred to as OSL, even though both methods are strictly "optical" (Prescott and Robertson 1997).

Optical dating techniques presented in Appendix B utilize IRSL and are used in this research to help constrain and temporally correlate units across distances >100 km.

OSL Sample Collection and Preparation

Samples were collected in normal daylight from freshly exposed sediment in a vertical face. Each sample was obtained by carefully pushing a copper cylinder (10 cm diameter and 7 cm high) into the exposure while removing the surrounding material. Once the entire volume of the cylinder was filled, the sample was removed from the section. Excess sediment protruding from the ends of the cylinder was carved off, and the sample was wrapped in heavy-duty aluminium foil and duct tape.

Once in the lab, the samples were prepared under subdued lighting conditions; all lab light was filtered through a Lee 158 “deep orange” optical filter. Foil and duct tape were removed on one side of the copper cylinder, and the surficial 1 cm to 1.5 cm of sediment in contact with the foil was discarded. Approximately 12 g of sediment was removed from the centre of the cylinder for water content experiments, along with approximately 150 g of sediment. A sub-sample (~30 g) was obtained from the 150 g sample for dosimetry. The remainder was treated in 40% HCl until reactions ceased in order to remove all carbonates, followed by a treatment of 27% H₂O₂ for 24 hours to remove any organic material present within the sample. The sample was then rinsed in distilled water 3 times, and treated with CBD solution (71 g sodium citrate, 8.5 g sodium bicarbonate, and 2 g sodium dithionate per litre of distilled water) for 12 hours to remove any iron oxide coatings that may block the luminescence (Lian *et al.* 1995). Finally, 1% calgon solution (sodium hexametaphosphate) was added until a thick, 1:1 (sediment:calgon solution) slurry was produced. The sample was then placed into an ultra-sonic bath and mechanically stirred for one hour in order to deflocculate clays and clean individual grains (Norrish and Tiller 1976).

In order to obtain the desired grain size (4-11 µm), the samples were transferred into 1 litre graduated cylinders and settled out in distilled water according to Stokes Law. First, the >11 µm particles were separated out by settling for 30 minutes in a 20 cm water column. The remaining sediment was then settled for 4 hours in a 20 cm water column, and several 2 hour settlings in a 10 cm water column in order to remove the <4 µm particles. Once the 10 cm water column was clear (sediment free) after 2 hours, the settled sediment at the bottom of the graduated cylinder (4-11 µm) was rinsed several times in distilled water. Methanol was then added to remove all water from the fraction and 1 mg aliquots were settled in acetone onto 1 cm sterile aluminium disks (disks were pretreated with 47% hydrofluoric acid for ~10 min.). A minimum of 60 disks were required for standard optical dating measurements, however, 240 disks were made for LCSL1 and GCSL1 for additional tests. For a more detailed account of the laboratory procedures used in this dissertation, see Little *et al.* (in press). A copy of this manuscript is presented in Appendix B.

Micromorphology

Through the study of soil microfeatures, evidence of soil development such as particle/void distributions, direct evidence of clay illuviation and distinctive fabrics could be easily ascertained. Data collected from this type of research are then used to classify soil types and infer climatic condition(s) in which the paleosol had formed (Morozova 1972; Múcher and Morozova 1983; Gerasimova *et al.* 1992, 1996; Morozova 1995; Tsatskin 1997). Such studies have identified peculiar micromorphological features that characterize interstadial vs interglacial soils, or differentiate between forest, forest-steppe, and steppe bio-climatic conditions (*e.g.*, Velichko *et al.* 1992; Morozova 1995; Morozova and Nechaev 1997).

Basic micromorphology presented herein is used as an aid in paleosol description, pedogenic process recognition and classification. Procedures and terminology are based on the methods proposed in Bullock *et al.* (1985); the interpretation of micromorphologic features are based both Bullock *et al.* 1985 and Gerasimova *et al.* (1996). As micromorphology is a jargon-intensive field of study, the author assumes familiarity with micromorphological terms and concepts; it is beyond the scope of this dissertation to familiarize readers with such material and therefore readers are referred to the aforementioned texts.

In order to obtain a thin section to examine under transmitted and reflected light, blocks of sediment were first cut from the sections. These blocks were oriented and therefore, the utmost care had to be used during their collection.

Sample Collection and Preparation for Micromorphology

The collection of these samples followed description and photography of the section. Where a sample was marked to be collected, a 10 cm x 10 cm area was cleaned and the local wall cut to a vertical plane. After being cleaned and cut to a vertical plane, the blocks were cut out using a sharp, flat edged knife. Sides and tops were also cut to vertical planes and horizontal planes respectively. Once removed, the samples were cleaned, trimmed and an up-arrow was scratched into the outer vertical surface.

Once in the lab, soil thin sections were examined under reflected, normal-transmitted and polarized-transmitted light.

CHAPTER 3 - STRATIGRAPHY AND SEDIMENTOLOGY

Introduction

This chapter presents field and laboratory sedimentologic and stratigraphic data in order to develop an allostratigraphic scheme for sedimentary sequences along the *ca.* 700 km long north-south transect. The construction of such a scheme is invaluable as it forms the basis for all time-stratigraphic relationships and spatial interpretations presented in subsequent chapters as well as being used as a tool to explain the geologic and paleoclimate history of the study area.

This chapter begins with a discussion of the different types of stratigraphies and the reasons why they are instrumental towards facilitating the development of the final site-to-site correlation (for more detailed reviews see Appendix C). This discussion is followed by basic lithostratigraphy and descriptive pedostratigraphy along with interpretations for each unit. Once lithological and pedological characteristics have been presented and interpreted, local (intra-site) correlations and composite sections can be constructed. Subsequently, an overview of the interpretations for each of the composite sections is presented in order to convey a relative-time depositional history for each site. Once all composite sections are described and interpreted at local scales, introduction of inter-site correlations based on allostratigraphy follows.

Lithostratigraphy

Lithostratigraphy (North American Commission on Stratigraphic Nomenclature 1983) is used as a descriptive stratigraphic tool to define units and correlate locally at each site. Lithostratigraphic units presented in this chapter were characterized according to texture, sedimentary structure, geometry of the beds (thickness and relative elevation), types of contacts, organic carbon and carbonate contents, magnetic susceptibility and homogeneity/heterogeneity. The initial description of lithostratigraphic units summarizes the major components of each section. This will be immediately followed by subdivision (where necessary) and detailed descriptions of those components. Lithofacies codes used to summarize the lithic character of each unit are presented in table 3.1; symbols and pattern fills used to construct the section diagrams are presented in figure 3.1.

Table 3.1. Lithofacies codes used in stratigraphic section profiles; based on formally defined lithofacies codes presented in (Eyles *et al.* 1983).

Primary Classification

Code	Description
D	Diamicton
G	Gravel
S	Sand
F	Fines (silt, clay or mud)

Secondary Classification

Code	Description
Dmm	matrix-supported, massive diamicton
Gmm	matrix-supported, massive gravel
Gcm	clast-supported, massive gravel
Sm	massive sand
Sh	horizontally stratified sands
Sr/St	rippled (tabular cross-stratified)/trough cross-stratified sands
Sd	deformed/loaded sands
Fm	massive fines
Fl	laminated fines
Fd	deformed fines
Fp	Pedogenic structures

Tertiary Classification (Genetic Interpretation)

Code*	Interpretation
F_(a)	aeolian
F_(r)	reworked
F_(l)	lacustrine/glaciolacustrine
F_(or)	organic (pedogenic)
G_(f)	fluvial/glaciofluvial

* Primary classification for example purposes only.

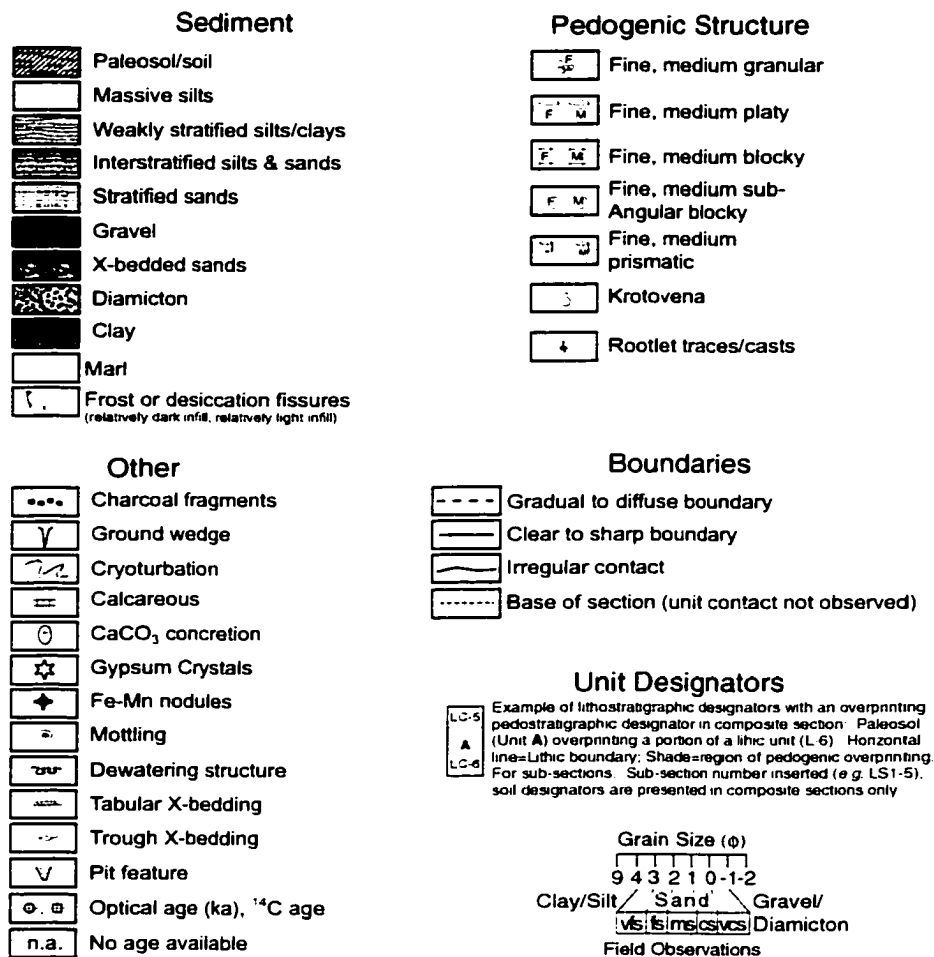


Figure 3.1. Symbols and patterns used to construct section diagrams.

Pedostratigraphy

Pedostratigraphy presented in this dissertation is based on the North American Commission on Stratigraphic Nomenclature (1983) but also follows the recommendations of Morrison (1981). Descriptions of pedogenic features and unit boundaries, as well as interpreted soil classification follow from the Soil Classification Working Group (1998). Pedo-units presented in this chapter were initially recognized in the field based on preliminary observations (*vide* Chapter 2). Subsequent laboratory analyses such as: micromorphological analysis (of selected samples and soil horizons), textural analysis, loss-on-ignition (for bulk organic and carbonate contents), and magnetic susceptibility are used to refine field descriptions and supply complementary lines of evidence for pedogenesis. For simplicity, only the organic-enriched horizons of each paleosol are highlighted in the main stratigraphic columns; more

detailed illustrations of soils / paleosols are presented along with photomicrograph plates.

Allostratigraphy

Allostratigraphy (North American Commission on Stratigraphic Nomenclature 1983) is used here for long-distance correlation between sites. Allostratigraphic units are defined only after intra-site correlations and composite section construction. Details as to the construction of the allostratigraphic scheme are outlined in detail under the sub-heading "*Allostratigraphic Framework: introduction*" presented later in this chapter.

Optical Age Constraints

The locations of optical dating samples are presented within each individual stratigraphic column (where applicable), as well as in the composite sections for each site. However, the ages obtained from these samples are presented only within each composite stratigraphic column (Figures 3.6, 3.13, 3.15 and 3.31 as well as those presented in Appendix B).

Likhvin Sections

The Likhvin site, situated along the Oka River (Figure 1.1), has been the type locality for the study of Middle and Upper Pleistocene sedimentary successions for *ca.* 3 decades (*e.g.*, Faustov *et al.* 1974; Bolikhovskaya and Sudakova 1996). Likhvin sediments reported by other researchers include loess, alluvium, lacustrine silts and clays, and glacial diamictons (*e.g.*, Faustov *et al.* 1974; Bolikhovskaya and Sudakova 1996). Overprinting these parent materials are pedogenic horizons at various intervals.

The Likhvin sections presented below exhibit many similarities to published data, and therefore, correlation is relatively simple. For these reasons, detailed glacial geology of tills and palynology have not been re-evaluated.

Likhvin Section No. 1: Lithostratigraphy and basic paleosol description

There are six primary units comprising Likhvin Section No. 1 (hereafter referred to as LS1). These units are illustrated in figure 3.2 (*e.g.*, LS1-1). Corresponding composite section unit designators and depths are presented in parentheses for convenience. Textural data for those units with more than one sample are presented in Appendix D.

LS1-1: 0 - 216 cm (LC-1: 0 - 216 cm)

Lithic Description: The uppermost unit (LS1-1, Figure 3.2) consists primarily of brown (10 YR 6/4 d) to yellowish brown (10 YR 5/3 d) silty-clay loam to silty loam. The unit is predominantly massive, but does exhibit zones of weak, laterally discontinuous textural banding between approximately 98 - 134 cm. These bands range in thickness from 1 cm to 8 cm and are composed of alternating silt (dark grey-brown 10 YR 4/2 d) and silty-clay (light yellowish-brown 10 YR 6/4 d) strata. No structure is observed from 134 cm to 204 cm. Between 204-211 cm there is charcoal-rich layer that exhibits charcoal clasts up to 3 cm and oxidized granite clasts up to 7 cm. Radiocarbon dating of the charcoal yields an age of 2770 ± 60 ¹⁴C yrs. B.P. (TO-7408). A pit-shaped infill structure crosscuts the charcoal-rich horizons and continues down to a depth of approximately 300 cm (into the next unit). The texture of the infilling sediment is silt to clayey-silt with a moderate, medium angular blocky structure. Organic-rich zones within this unit are easily

identified on median grain size, magnetic susceptibility, and organic content graphs (Figure 3.2) down to a depth of *ca.* 45 cm. The lower contact is sharp and planar.

Soil-A: Relatively high organic content (Figure 3.2) and weak to moderate fine granular structure in the upper 33 cm of the unit represent the Ap horizon of the modern-day soil; this is repeated between 64-98 cm but is solely a function of slope position (*i.e.*, not a true unit). The lack of pedogenic structure below the Ap horizon and the peaks in iron and aluminium oxides at 49 cm suggests the underlying soil horizon is a weak B or B-C horizon. Therefore, soil-A at the Likhvin site is interpreted to be relatively immature, and may in fact represent a brunosolic soil subsequently modified by anthropogenic reworking. This is corroborated by the ^{14}C age (2770 ± 60 ^{14}C yrs. B.P.) at a depth of 204-211 cm.

Interpretation: Oxidized granite clasts and charcoal fragments in a 6 cm thick, localized layer within this unit suggest the presence of a fire pit. The young age of this horizon (see above) and the ~2 m of overlying sediment suggests rapid deposition over the last *ca.* 2 ka. This, in conjunction with the silty, well-sorted matrix, the presence of rare small clasts and discontinuous textural banding all suggest that the parent material was a colluviated loess.

LS1-2: 216 - 716 cm (LC-2: 216 - 716 cm)

Lithic Description: This unit consists primarily of light yellowish-brown (10 YR 6/4 d) silty clay (base) to silty loam (top). Between 237 - 312 cm, the colour darkens to brown (10 YR 5/3 d). From 312 - 538 cm, the colour lightens to light yellowish-brown (10 YR 6/4 d) and the sediment becomes calcareous (Figure 3.2; CaCO_3 content graph) and relatively well sorted (*e.g.*, Figure 3.3). Calcium carbonate concretions up to 2-3 cm in diameter are observed in this interval. The base of this carbonate-rich interval is marked by a peak in carbonate content and a clear, wavy contact. Below this contact, from 538 cm to 628 cm, the colour darkens to brownish-yellow (10 YR 6/6 d) which reflects the decrease in calcium carbonate content and the increase in organic content (Figure 3.2; calcium and organic graphs). At a depth of 628 cm, the colour darkens again to yellowish-brown (10 YR 5/6 d). Downward

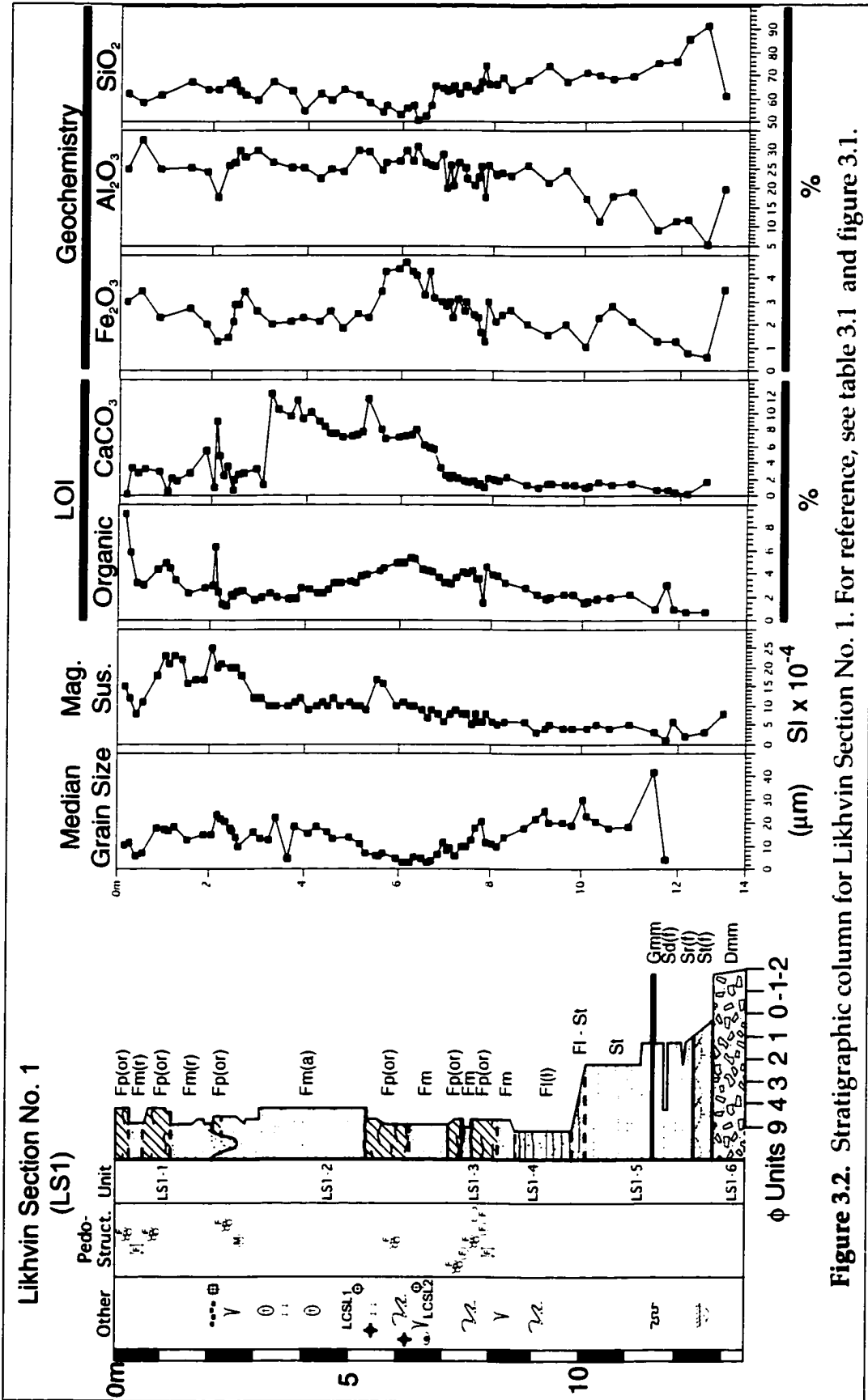


Figure 3.2. Stratigraphic column for Likhvin Section No. 1. For reference, see table 3.1 and figure 3.1.

oriented wedges of darker coloured material are clearly visible; the size of these features is approximately 7 - 10 cm wide and 12 - 20 cm high. Below (641 cm) the sediment lightens to brownish-yellow (10 YR 6/6 d). Irregularly shaped mottles are also observed within and below the wedge features, however, mottles are more abundant (>20%) below the wedge features. Peaks in the iron oxide content of this unit correspond to highs in magnetic susceptibility at 216 - 280 cm and 538 - 600 cm (Figure 3.2, magnetic susceptibility). There is also a weak organic peak below the charcoal spike of unit LS1-1 (Figure 3.2; organics) and a gradual decrease in organic content from approximately 640- 400 cm, peaking at 640 cm. The organic-content highs centred around 266 cm and 640 cm also correspond to peaks in iron oxide and magnetic susceptibility. The lower contact is sharp and planar.

Paleosol-B: Weak, fine granular structure and an increase in organic content (local maximum at 266 cm) mark a weakly developed A-horizon from 216-237 cm. Below 266 cm there is a slight decrease in the organic content which corresponds to a medium sub-angular blocky structure, both of which suggest the presence of an A-B or B-horizon. A sharp increase in calcium carbonate content at 312 cm and the presence of carbonate concretions identify the C-horizon of this paleosol. The weakly developed nature of this paleosol suggests it was an immature soil (regosol) formed under conditions that inhibited soil development.

Paleosol-C: This pedogenic horizon (538-628 cm) has a relatively high organic carbon content (Figure 3.2), darkens in colour and exhibits a moderate, fine granular structure in thin section (Plate 3.1). The thickness of this unit, relative to paleosol-B, and the presence of silty calcareous material above and below suggests it was a cumulic soil in which the continuous accumulation of parent material retarded pedogenic development. These factors suggest that this soil is a cumulic regosol.



Plate 3.1. Photomicrograph (mag. 25x; PPL) of moderate fine granular structure interpreted to be the Ah horizon of paleosol-C.

Interpretation: The massive silty nature of this unit, and the presence of two weakly developed cumulic paleosols suggests that deposition of the sediment was through aeolian processes. This interpretation is corroborated by a comparison of cumulative frequency curves (Figure 3.3) from other well known loess deposits. The two soils represent the Bryansk (see Little *et al.* in press for details) and possibly the Trubchevsk paleosols (paleosols C and B respectively). Both soils appear to be cumulic regosols, although, based on the lack of structure and thickness of paleosol-C, the accumulation rate during its formation was presumably much higher than that for paleosol-B. Also, the

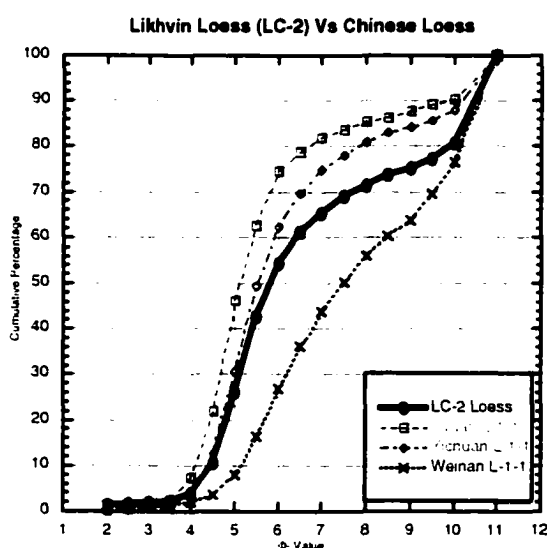


Figure 3.3. Cumulative frequency graphs of three loess samples from the Chinese Loess Plateau, plotted with an example of loess from Unit LS1-2 (LC-2). The Russian Plain example falls between all Chinese end members.

ground-wedges (*cf.* ice-wedge pseudomorphs) observed at the base of paleosol-C are a testament to subsequent cold periods that induced permafrost conditions.

LS1-3: 716 - 824 cm (LC-3: 716 - 824 cm)

This unit is comprised of six sub-units, each having been intensely deformed following initial deposition and pedogenic overprinting (Figure 3.4). Due to the highly deformed nature of the unit, subunits defined by: colour, stratigraphic position, sedimentary structure and pedogenic structure are observed in the field and in thin section. These subunits are cross-referenced in figure 3.4A. The lower contact is diffuse and planar.

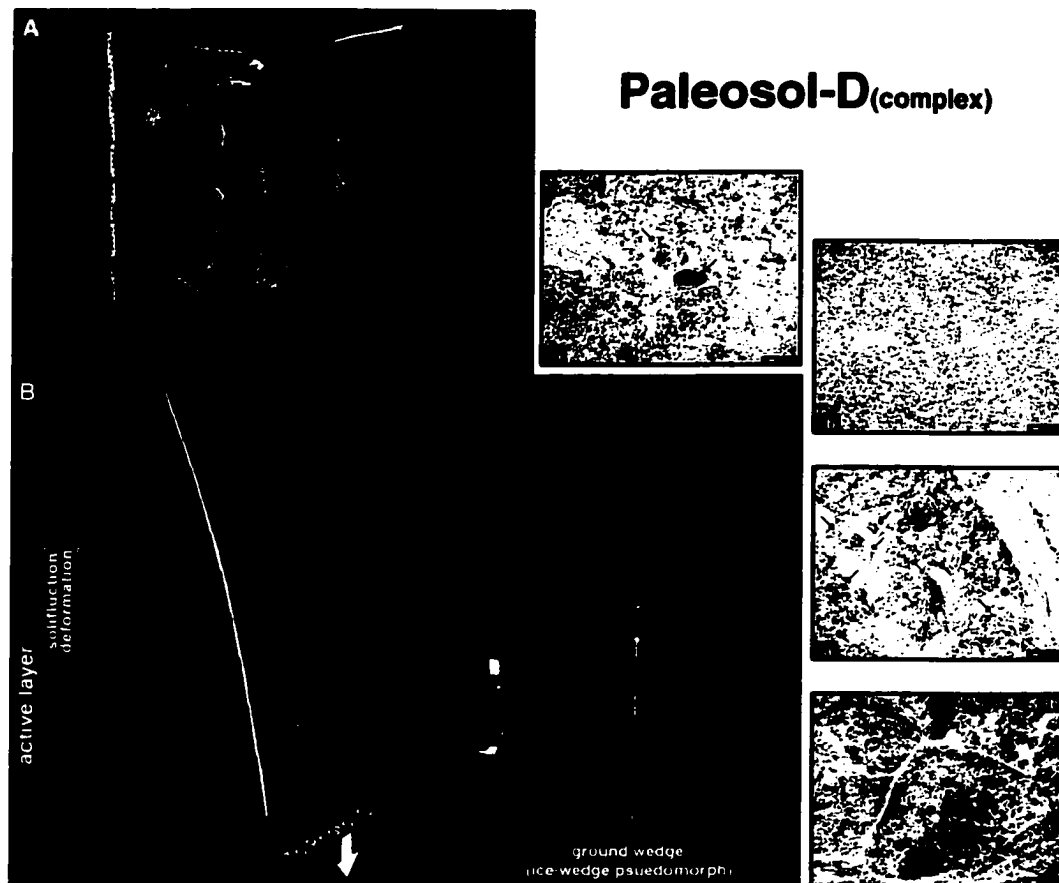


Figure 3.4. Highly deformed sub-units comprising Unit L1-3. **A.** Unit L1-3 as described in text and figure 3.2. **B.** Correlative unit located approximately 200 m upstream (south) of **A**; notice soliflucted upper portion of dark organic-rich sub-unit (active layer). **C.** Ground wedge observed below **B** -- evidence of cryogenic deformation of Unit L1-3. Sub-units (*i.e.*, 3a - 3e) correspond to descriptions L1-3a - L1-3e in text. Photo micrographs (mag. 25x; PPL) illustrate structure observed in thin section: **3a** - arrows pointing to weak granular structure; **3b** - partially accommodated weak sub-angular structure; **3a'** - weak to moderate granular structure with partially decayed organic matter (right side in void space); **3b'** - accommodated strong sub-angular blocky structure.

Sub-unit L1-3a (a'): This sub-unit occurs as two vertically separated, horizontally discontinuous intervals (Figure 3.4A; 3a, 3a'). They are characterized by a dark yellowish-brown (10 YR 3/6 m to 10 YR 4/6 m) silty-clay loam. The only structures detected were fine orange mottles in sub-unit 3a. Micromorphological analysis, however, reveals weak granular structure in 3a and weak to moderate granular structure and organic matter in 3a' (Figure 3.4A; 3a, 3a').

Sub-unit L1-3b (b'): This sub-unit occurs immediately beneath each of the aforementioned sub-units (Figure 3.4A). They are characterized by a yellowish-brown (10 YR 5/8 m to 10 YR 5/4 m) silty-clay loam to silty loam. Sub-angular structure was identified in thin section for both sub-unit 3b and 3b', however, much stronger ped development is observed in the latter (*cf.* Figure 3.4A; 3b and 3b'). Only sub-unit 3b' exhibits mottling.

Sub-unit L1-3c: This sub-unit is highly deformed (Figure 3.4A; 3c) and consists of light yellowish-brown (10 YR 6/4 d) to very pale brown (10 YR 7/3 d) silty loam to silt. There are intra-stratified sub-parallel bands that dominate this sub-unit in the lower and right-hand portions of figure 3.4A. This sub-unit appears to have been interstratified with sub-units 3a' and 3b' (Figure 3.4A; 3a', 3c, 3b')

Sub-unit L1-3d: This sub-unit is represented as four discrete zones (Figure 3.4A, 3d). They consist of dark brown (7.5 YR 3/3 d), loose friable silty loam to silty clay.

Sub-unit L1-3e: This sub-unit consistently occurs at the base of the unit (Figure 3.4A; 3e). It consists of light olive-brown (2.5 Y 5/6 m) silty loam with a moderate to strong, fine angular blocky structure. Ground wedges originating within this sub-unit penetrate down into sub-unit LS1-3f.

Sub-unit L1-3f (no photo): This sub-unit consists of pale brown (10 YR 6/3 m) to light grey (10 YR 7/2 d) silty-clay loam. A moderate, fine, sub-angular blocky structure is observed within this sub-unit. One of the ground wedges originating in the overlying sub-unit penetrate through this unit into Unit L1-4.

Interpretation: Based on its stratigraphic position and physical character this unit is interpreted to represent the Mezin pedocomplex consisting of two paleosols. The lower of the two exhibits an Ae horizon (LC-3c) and a Bt horizon (LC-3f) suggesting a strong pedogenic influence under forested conditions (luvisol). The upper paleosol in this pedocomplex also exhibits Ah- and B-horizons, but the lack of an Ae- or Bt-horizon suggests that it may have formed in a cooler and drier climate, with less forest influence on its genesis (grey brown chernozem). The highly deformed nature of the sub-units and presence of ice-wedge

pseudomorphs in the base of the unit suggests subsequent cold conditions resulting in the development of permafrost.

LS1-4: 824 - 992 cm (LC-4: 824 - 992 cm)

Lithic Description: This unit consists of pale brown (10 YR 6/3 m) to light grey (10 YR 7/2 d) silty-clay loam to silty loam. The upper 30 cm of this unit are massive. At 854 cm, very weak, highly deformed silt laminae are discernible and gradually increase in strength to 891 cm. Below 891 cm, strongly deformed, discontinuous laminae of silty-clay loam and silty loam are clearly observed. The deformation weakens with depth to weakly deformed laminae near the base of the unit which is marked by a concentration of heavy clay. The lower contact is gradual and planar.

Interpretation: This unit is interpreted to have been deposited in standing water, perhaps a glacial lacustrine environment following the deglaciation of the region (Little *et al.* in press). Cryoturbation of this unit followed the formation of LS1-3 and deformed the fine silt and clay laminae as the permafrost developed.

LS1-5: 992 - 1290 cm (LC-5: 992 - 1290 cm)

Lithic Description: The upper 169 cm of this unit consists of parallel stratified fine-medium sands, silt and clay (*vide* Appendix D for details on the texture of the fine grained components). Underlying these strata is a relatively thin (4 cm) layer of highly oxidized, poorly sorted pebble gravel with a medium sand matrix; clasts are weathered and range in size up to 2 cm. This layer is underlain by a 35 cm thick horizon of load structures consisting of clays, silts and fine to medium sands. The lower 90 cm of this unit are composed of tabular- and cross-stratified medium to well sorted, fine to medium sand. Some portions of this interval exhibit clay and silt drapes over ripples. The lower contact is sharp and planar.

Interpretation: The sharp basal contact with the underlying diamicton of unit LS1-6 (LC-6) and stratified sands suggest current flow in a glaciofluvial setting. The generally fining upward sequence and the change from sigmoidal cross stratification to planar-tabular beds suggests that flow over this site waned over time. However, at approxi-

mately 1100 cm load structures consisting of clay and silt within these sands, and overlain by pebble-gravel strata suggest that flow was highly variable at times.

LS1-6: 1290 cm - (LC-6: 1290 - 2290 cm)

Lithic Description: This unit consists of a light yellowish-brown (10 YR 6/4 d) massive diamicton with a clayey-loam matrix and <5% clasts (visual determination). Clasts within this unit are sub-angular to rounded with the majority being sub-angular; clast size was variable, but ranged from <1 cm up to a maximum (observable) of 8 cm. The lower contact is not observed at this section (*vide post*).

Interpretation: This unit is interpreted as till. A detailed description of the till from the Likhvin site can be found in Bolikhovskaya and Sudakova (1996).

Likhvin Section No. 2: Lithostratigraphy and basic paleosol description

There are six main units comprising Likhvin Section No. 2 (hereafter referred to as LS2). As above, complete unit descriptions are presented below; the units are illustrated in figure 3.5 (*e.g.*, LS2-1). Corresponding composite section unit designators and correlative depths are presented in parentheses (*e.g.*, LC-6 1290 - 2290 cm). Munsell colours are not available for this section.

LS2-1: 0 - 31 cm (LC-6: 1290 - 2290 cm)

Lithic Description: This unit consists of medium brown diamicton with a clayey-loam matrix and <5% clasts (visual determination). Clasts within this unit are sub-angular to rounded with the majority being sub-angular and range in size up to 8 cm. As above (*i.e.*, LS1-6), a detailed description of the diamicton can be found in Bolikhovskaya and Sudakova (1996). The lower contact is gradational and planar.

Interpretation: See unit LS1-6 (LC-6) above.

LS2-2: 31 - 118 cm (LC-7: 2290 - 2377 cm)

Lithic Description: This unit exhibits wavy bands of diamicton (deformed intraclasts derived from LS2-1) within a greenish-grey clayey loam matrix. The diamicton bands vary from 3 cm to 10 cm in thickness. The spacing between the bands increases in thickness with depth until the deposit appears to be massive (*i.e.*, no diamicton banding) at

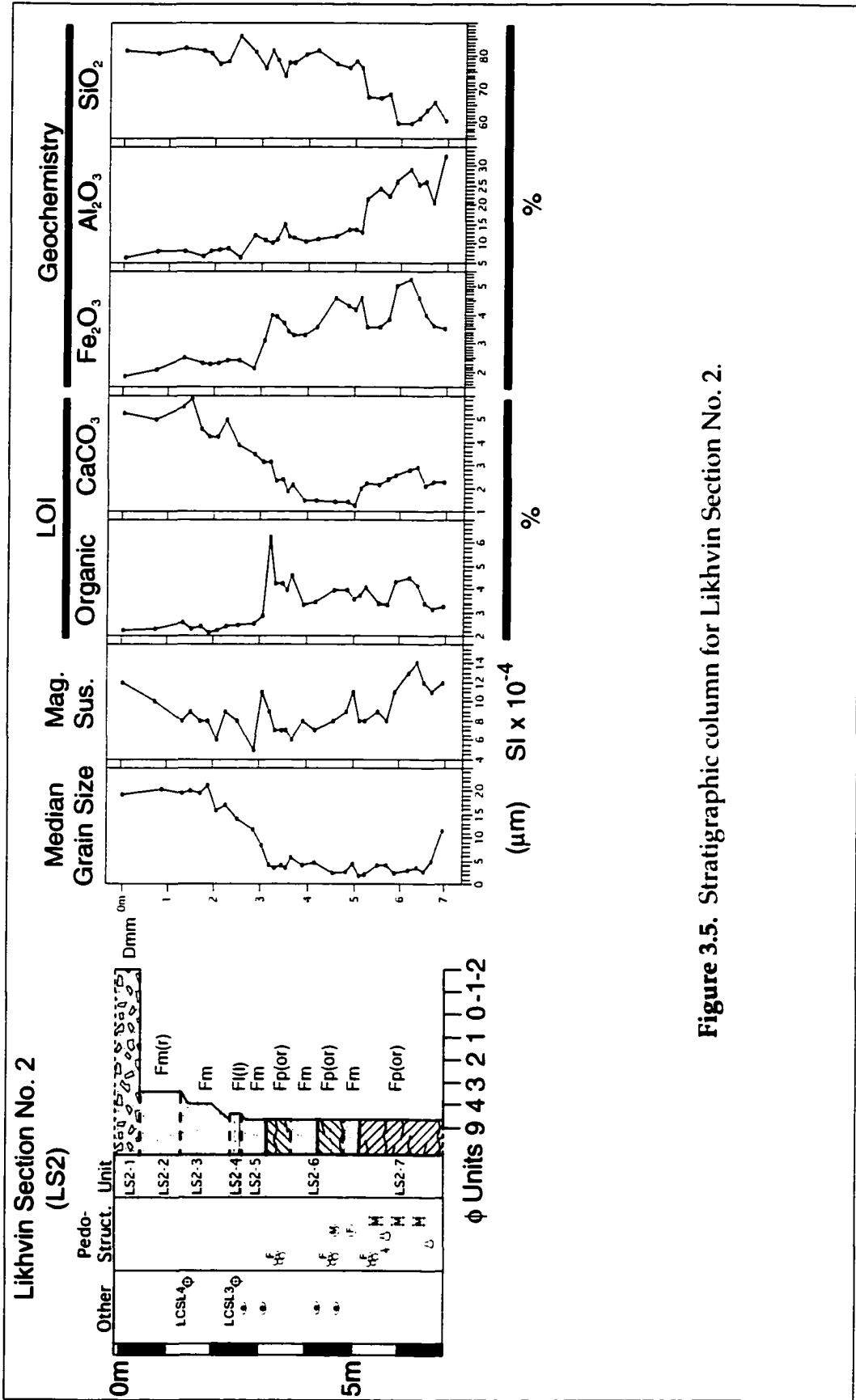


Figure 3.5. Stratigraphic column for Likhvin Section No. 2.

the base of the unit. Interspersed within the upper portions of the unit are banding-parallel sand lenses approximately <2 cm x 5 cm in size. The lower contact is gradational and planar.

Interpretation: Deformed intraclasts of the overlying diamicton in the upper portions of this unit suggest it is a transitional (reworked) horizon between the diamicton above, and underlying silty unit (*vide post*).

LS2-3: 118 - 240 cm (LC-8: 2377 - 2499cm)

Lithic Description: This unit consists primarily of greenish-grey silty-clay loam to silty loam that exhibits rust coloured banding. These rust-coloured bands range in thickness from 1 cm to 8 cm. Occasional banding-parallel sand lenses up to 2 cm x 5 cm occur in the upper 80 cm of the unit. The lower contact is gradual and planar.

Interpretation: This unit is interpreted to be loess based on textural analyses and a massive structure below 198 cm (2457 cm) with occasional aeolian sand lenses being deposited during the latter stages of the unit formation. The inverse grading (Figure 3.5; Grain Size) of this unit suggests that the depositional energy increased with time resulting in an increase in the median grain size.

LS2-4: 240 - 263 cm (LC-9: 2499 - 2633 cm)

Lithic Description: This unit consists primarily of greyish silty-clay loam interstratified with greenish-grey silty-clay. Together these produce a diffuse parallel bedding with each bed ranging from 1 cm to 4 cm thick. The lower contact of this unit is gradational and planar.

Interpretation: A silty-clay loam texture combined with parallel stratification suggest quiet-water deposition within a lacustrine environment.

LS2-5: 263 - 313 cm (LC-10: 2522 - 2572 cm)

Lithic Description: This unit consists of massive silty-clay loam. At 284 cm (2543 cm) however, the clay content increases (but is still classified as silty-clay loam; *vide Appendix D*) and zones of oxidation are observed down to 302 cm (2561 cm). The oxidization occurs as mottles that are either blotchy or form stringers typically less than 20 cm in length and 1 cm to 4 cm in thickness. The lower contact is gradual and planar.

Interpretation: The massive nature of this silt-clay loam (bordering on silty loam) in the lower portions of the unit suggests that the base of the unit is loess. The loessic sediment grades into a finer silty-clay loam (Appendix D) with mottled stringers, and the gradational contact with the lacustrine unit above. Therefore, this unit is interpreted to be a fine-grained loess with an increasing lacustrine influence as the site was gradually flooded, ultimately giving rise to the lacustrine deposits of the overlying unit.

LS2-6: 313 - 518 cm (LC-11: 2572 - 2777 cm)

Lithic Description: From a depth of 313 cm to 374 cm (2572-2633 cm) the unit exhibits 2 sets of alternating dark and light bands consisting of silty clay to silty-clay loam. The upper dark band is approximately 10 cm thick while the lower dark band is approximately 13 cm thick. Both of these darker bands correspond to increases in organic content (Figure 3.6; Organic). Mottles within the upper 50 cm of the unit range from 2-5 cm and are spread ubiquitously throughout the interval. Below 313 cm, however, blotchy mottles (up to 1 cm) and sub-horizontally oriented discontinuous mottled stringers (0.5 cm to 1 cm thick) are present in both the dark and light bands. Based primarily on colour, the lower contact of this interval is sharp and planar.

Below 374 cm, the primary constituent of this unit is a grey silty-clay, however, portions of the unit exhibit various secondary (overprinted) features. For example, from 374 cm to 401 cm (2633 - 2660 cm) the unit exhibits rust-coloured bands from 0.5 to 1 cm in thickness; these bands make up close to 25% of the interval. From 401 cm to 429 cm (2660 - 2688 cm) the rust coloured bands increase in concentration, making up 75% of the unit. This structure development and size decrease to a weak, fine sub-angular blocky structure from 485 cm to 518 cm (2744 - 2377 cm) At 518 cm there is a sharp inclined (17° from horizontal) planar contact.

Paleosol-E₂: Granular structure identified in thin section (Plate 3.2 A) and a sharp increase in organic content and magnetic susceptibility (Figure 3.5) clearly identify a pedogenic horizon. At the top of the paleosol, the abrupt decrease in organic content and magnetic susceptibility denote the termination of soil formation as the unit gave way to

increased aeolian deposition (*cf.* increase in grain size, Figure 3.5) of unit LS2-5 (LC-10). Evidence of clay illuviation in the form of clay cutans (Plate 3.2 B) is observed from thin section and denotes a Bt₁-horizon located below the horizon of granular structure. The peak in Fe₂O₃ and the presence of mottles suggest that sufficient water was available to mobilize iron. This is corroborated by the larger median grain size relative to the horizon that immediately underlies paleosol-E₂ (*i.e.*, lessivage) and the formation of medium sub-angular blocky structure overprinting paleosol E₁. These data suggest that paleosol E₂ was formed under relatively moist soil-forming conditions conducive to translocation processes and therefore it is interpreted to be a luvisolic soil.

Paleosol-E₁: This horizon exhibits moderately developed, medium sub-angular blocky structure from 429 cm to 485 cm (2688 - 2744 cm) that overprints the rust-coloured bands. A relatively broad, low-magnitude organic peak, a sharp Fe₂O₃ peak, and a local low in the median grain size (Figure 3.5) support field observations (*vide ante*). The identified pedogenic horizons include: an A-horizon denoted by a relative increase in organic content and granular structure (Plate 3.2 C, E) overprinted by translocation of iron-oxides and clay lessivage of a Bt₂-horizon (Plate 3.2 D, E) related to the formation of paleosol E₂. Based on the above evidence, this soil is tentatively interpreted to be a weak grassland soil (*i.e.*, very-weak eluviated brown chernozem).

Interpretation: The original parent material of this unit is tentatively interpreted as aeolian. However, the pervasive overprinting by subsequent paleosol formation (E₂ and E₁) makes elucidation of either a primary or colluviated loess tenuous.

Considering both paleosols, it appears that during the formation of this unit, the climate was progressing from dryer steppe (E₁) conditions into more moist, forested conditions (E₂). However, the punctuation of pedogenesis by an intervening non-soil-forming horizon (Figure 3.5) suggests an inherent instability superimposed on the general climatic-amelioration trend.

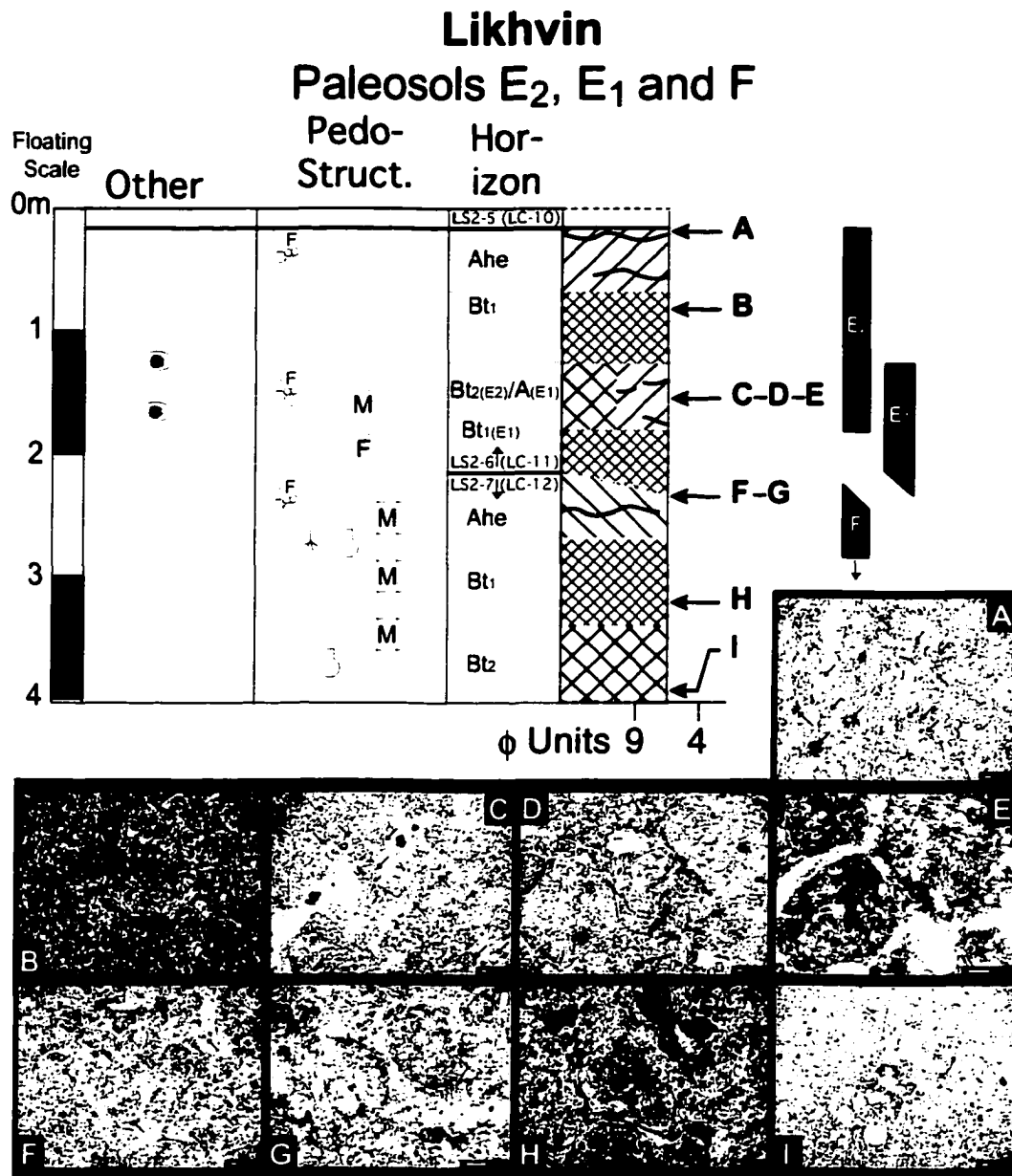


Plate 3.2. Photomicrographs from paleosols E₂, E₁ and F at Likhvin. **A.** Arrows point to granular structure that denotes the A-horizon of paleosol-E₂; mag. 25x; PPL. **B.** Clay cutan in the Bt₁-horizon of paleosol-E₂; mag. 25x; XPL. **C.** Arrows point to weak granular structure of denoting the A-horizon of paleosol-E₁; mag. 25x; PPL. **D.** Sub-angular blocky structure illustrating the Bt₂-horizon of paleosol-E₂ at the same elevation as "Plate C"; mag. 25x; PPL. **E.** Close-up of granular structure associated with paleosol-E₁ being cross-cut by accumulations of clay (arrows) translocated during paleosol-E₂ formation; mag. 100x; PPL. **F.** Arrows point to tightly packed granular structure that denotes the A-horizon of paleosol-F; mag. 25x; PPL. **G.** Close-up of A-horizon granular structure in paleosol-F; mag. 100x; PPL. **H.** Strong sub-angular blocky structure with clay cutans coating peds within the Bt₁ horizon of paleosol-F; mag. 25x; XPL. **I.** Clay coating and infilling voids in the Bt₂-horizon of paleosol-F; mag. 25x; PPL.

LS2-7: 518 cm - (LC-12: 2777 cm -)

This unit consists of massive silty-clay to silty-clay loam with well developed medium angular blocky and granular structures. The upper 20 cm of the unit is predominantly greyish-red in colour with some iron nodules. The redness of the unit increases to a rust colour from 538 cm to 660 cm (2797 - 2919 cm). Below 660 cm (2919 cm) the character of the unit gradually changes back to a grey silty clay. The lower contact of the unit was not observed. The base of the cleared section occurs at 691 cm (2950 cm).

Paleosol-F: This horizon exhibits granular structure (Plate 3.2 F, G) of an A-horizon, well developed medium angular blocky and fine sub-angular blocky structure (Plate 3.2 H) of a Bt₁-horizon, clay cutans and clay infillings within a Bt₂-horizon, sub-vertical divergent rust-coloured bands (root traces), and greyish oval-shaped krotovena. The major-axis diameter of these krotovena range from 10 cm to 20 cm. Laboratory data for this pedon illustrate corresponding double-peaks in magnetic susceptibility, organic matter, and Fe₂O₃ which suggests a paleosol complex or two different zones of translocated material (*i.e.*, Bt₁ and Bt₂). Given the development of the structure, the thickness of the unit and presence of krotovena, this pedogenic horizon is interpreted to have experienced a relatively higher degree of development than paleosols E₁ or E₂. Based on the above evidence which suggests that strong translocative processes contributed to the development of this soil (*cf.* Plates 3.2 H, I and Figure 3.5: Al₂O₃, Fe₂O₃, CaCO₃), paleosol-F is interpreted as an undifferentiated luvisol that formed in a moist forest environment.

Interpretation: Given the grain size and apparent massive structure, the parent material of this unit is tentatively interpreted as aeolian in origin. As is the case in LS2-6 (LC-11), discerning whether this loess is primary or secondary (*i.e.*, colluviated) is problematic given the degree of pedogenic overprinting.

Likhvin Composite Section

The thickness of the composite section (Figure 3.6) is based on the observed average thickness of the diamicton unit. Correlative depths for LS2 were simply calculated by assuming an average thickness of

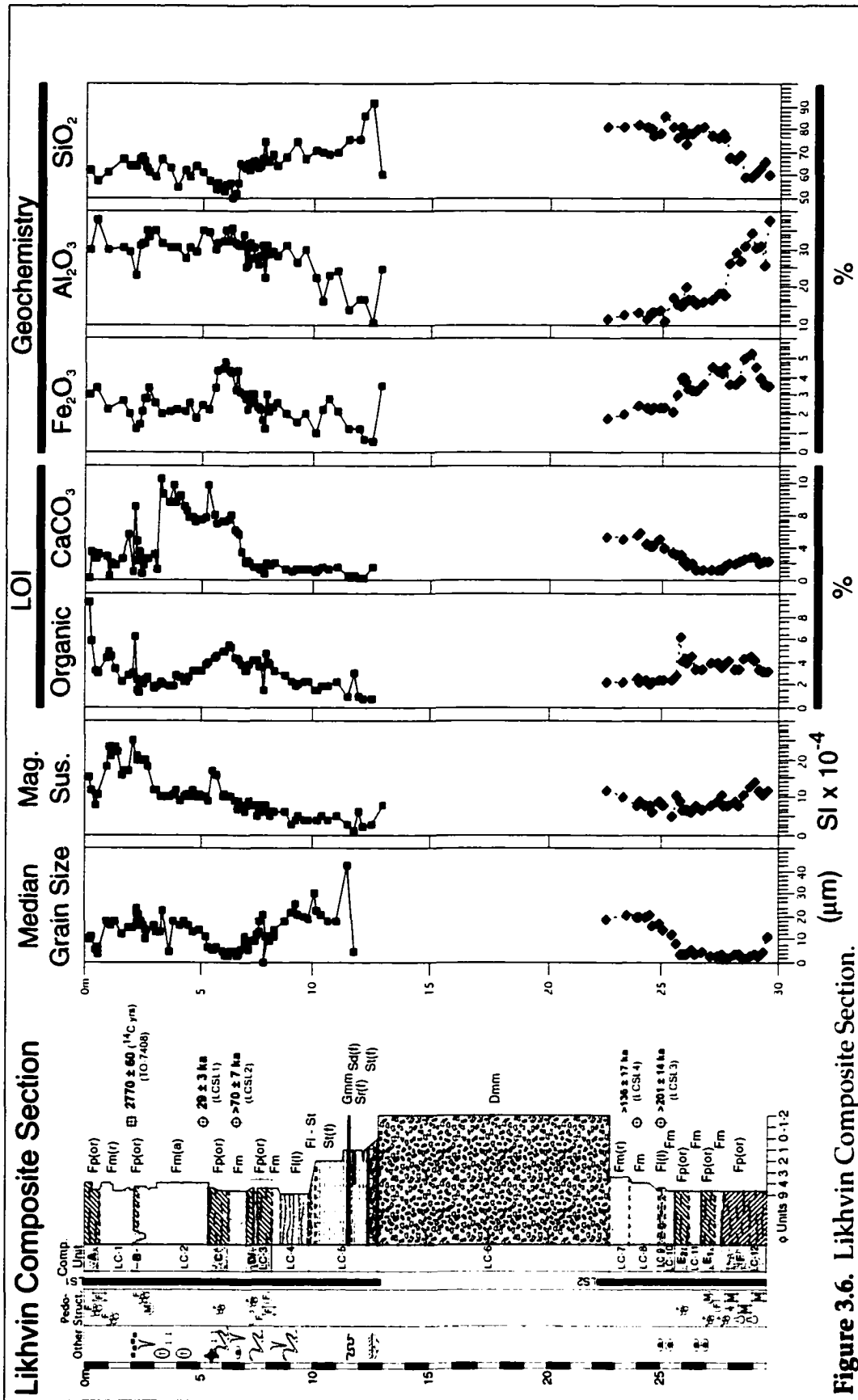


Figure 3.6. Likhvin Composite Section.

10 m for the till unit. According to Bolikhovskaya and Sudakova (1996) the till at the Likhvin site varies in thickness from approximately 7 m to 15 m (data extrapolated from their Figure 1, p. 295).

In all, 7 soil/paleosol horizons were identified at the Likhvin site (Figure 3.6; A-F). Due to the simple compilation of this composite section, the data-lithostratigraphy relationships and interpretations presented for LS1 (Figure 3.4) and LS2 (Figure 3.6) still apply. Therefore, they will not be reiterated here.

Four optical luminescence dating samples were collected at the Likhvin site. The stratigraphic position of each of the optical dating samples is presented in the corresponding stratigraphic column, and the ages are presented in Figure 3.6. For a detailed discussion on the procedures and interpretation of these ages see Little *et al.* (in press) which is presented in Appendix B.

Likhvin Site Depositional Environment: overview

Many researchers have conducted research on the Likhvin type section (*e.g.*, Dremanis *et al.* 1978, Bolikhovskaya and Sudakova 1996; Velichko *et al.* 1999) resulting in a fairly well accepted stratigraphy and chronostratigraphy of the sediments observed at this site. Interpretations presented herein regarding the environments in which these sediments were deposited (primary sedimentologic environment and lithostratigraphic descriptions) generally agree with those reported by Bolikhovskaya and Sudakova (1996). The timing and age relationships, however, are modified in the light of the new stratigraphic data. For these reasons, only a summary of genesis of the units is presented here with brief discussion on soil formation.

The sedimentary sequence observed at the Likhvin site records both pre- syn- and post- glacial environments. The weakly to non-stratified silty-clay to silty-loam sediments that comprise the lower-most units (LC-7 through LC-12) most likely represent aeolian deposition (LC-8, -10, -11 and -12), reworked loess (LC-7) and shallow localized ponding of water (LC-9). Oxidation banding and mottling that accentuate stratified grain size changes suggest periodic saturation and drying possibly due to flooding events or a fluctuating ground-water table. Three soil forming intervals are identified within these units, paleosols F, E, and

E_2 . Of these overprinting horizons, paleosol-F is the best developed, exhibiting numerous rootlet traces, krotovena and well developed medium angular blocky structures (*cf.* Plate 3.2 H, I and Figure 3.5; magnetic susceptibility, organic matter, Fe_2O_3). These data represent a paleosol with at least two zones of translocation (*i.e.*, Bt_1 and Bt_2). The upper contact of this paleosol is sharp, planar and inclined; this, in conjunction with weak granular structure and the presence of well developed Bt horizons suggests that an erosive event removed portions of the A-horizon (*e.g.*, Ahe or Ae that would coincide with B-horizon development). Burial of the horizon by aeolian sediments preserved the sharp contact. The genesis of units LC-11 and LC-10 was a continuation of processes similar to those that produced LC-12. The soil genesis, however, that produced paleosols E_1 and E_2 resulted in less developed soils relative to paleosol F, given the pedogenic structures observed within these horizons (Figure 3.6).

Given the relative soil development and evidence for varying degrees of translocation and pedogenesis (*vide ante*), the initial climate appears to be one during which a forest-environment dominated the site (paleosol-F: luvisol). This is followed by a climatic deterioration resulting in drying and erosion of the Ahe or Ae horizons leaving only a weak (and possibly reworked) A-horizon and well developed Bt_1 and Bt_2 horizons of paleosol-F. A subsequent period of weak climatic amelioration resulted in the formation of paleosol- E_1 , a weak chernozem or cumulic regosol. The general trend towards climatic amelioration was punctuated resulting in the cessation of paleosol- E_1 . This was followed by a return to forest or forest-steppe conditions during the formation of paleosol- E_2 (Luvisol).

The fine-grained, stratified sediments of Unit LC-9 represents a period of quiet-water deposition, thus allowing relatively well developed beds of silty-clay-loam and silty-clay to settle; given the thickness of the unit, it most likely represents a localized ponding of water. With the advent of the glaciation that produced units LC-6 and LC-7, katabatic wind strength would have increased and the intensity of loess deposition in the Russian Plain region followed accordingly. This is reflected in the increasing grain size trends (Figure 3.6) and the pres-

ence of sandy lenses in the upper portion of LC-8, as the distance to the glacier margin decreased. Changes in lithic content from LC-8 to LC-7 provide evidence of a reworking of the primary loess deposit. During the reworking process, diamicton clasts are incorporated into the substrate giving rise to the intraclasts of till and sand lenses within LC-7. With decreasing distance to the upper contact of LC-7, these intraclasts increase in frequency and size supporting the notion of a glaciogenic reworking of a primary loess which was deposited prior to ice advance and deposition of unit LC-6.

Following the loess accumulation, the area was glaciated (LC-6); approximately 10 m of diamicton separate units LC-5 and LC-7. Bolikhovskaya and Sudakova (1996) classified the diamicton observed at the Likhvin site as the Dnieper Till based on clast provenance, heavy mineral suites, and ice-movement directions determined from clast a-axis trends. No evidence to contradict Bolikhovskaya and Sudakova (1996) was identified and therefore this unit is classified herein as the Dnieper Till.

Above the Dnieper Till there is a typical deglacial sequence beginning with well sorted, cross-stratified, medium to coarse grain sands (LC-5) that were, based on the nature and scale of the cross-stratification, deposited within a glaciofluvial environment. As the distance-to-source increased (*i.e.*, retreating glacial margin by association with underlying Dnieper Till), a fining-upward trend of these glaciofluvial sediments resulted (Figure 3.6). Occasional fluctuations in discharge produced both coarse grained gravel deposition and rapid fine-grained sedimentation; the latter resulted in well-developed load structures.

Following glaciofluvial deposition, local changes in the drainage networks caused ponding of water and consequent deposition of laminated silty-clay and silt that constitute LC-4. Stratification within this unit is evident in the lower portions of the unit because these areas were well below the active layer observed in LC-3 (*vide post*). Much of the primary structure in the upper portions of the unit were destroyed during the cryoturbic phase that followed the development of paleosol-D in the overlying unit.

The depositional setting of unit LC-3 is enigmatic due to the pedogenic and pervasive cryogenic overprinting (Figures 3.2 and 3.4). However, given the fine median grain size and presence of paleosols, it appears that the local ponding that produced LC-4 ceased and was replaced by fine-grained deposits reworked by aeolian processes. This interpretation is based primarily on the increase in median grain size but is, nonetheless, purely a speculative one as there is a lack of primary sedimentary structures on which to base a well-founded interpretation.

The degree of pedogenic overprinting in unit LC-3 is comparable to both the modern soil and paleosol-F observed below the Dnieper Till. At least 2 phases of soil development are evident as there are 2 Ah-horizons and 2 Bt-horizons (Figure 3.4A; Little *et al.* in press). The presence of an eluviated horizon below the lower Ah-horizon suggests that the paleosol associated with these horizons may have developed under forested conditions rather than the forest-steppe conditions interpreted for the overlying paleosol. This is consistent with observations in similar sequences overlying the Dnieper Till (Velichko and Morozova 1987) and therefore the paleosols developed within this interval are interpreted as the last interglacial pedocomplex (*cf.* Figure 1.6, p. 18).

Based on the sharp upper contact of unit LC-3, it appears as though there was a relative increase in aeolian deposition following the upper soil-forming interval. The result was unit LC-2 deposition. Grain size trends suggest that deposition was initially very slow which is corroborated by the relatively thin (178 cm) package of loess between the top of paleosol-D and paleosol-C. Stratigraphic position and relative pedogenic development of paleosol-C suggests that it represents a major interstadial within the last glacial period. A thick loess package above paleosol-C suggests aggressive loess deposition during the latter stages of the glacial event. A fire pit (charcoal rich horizon) with an age of 2770 ± 60 ^{14}C years (TO-7408) or 2870 ± 120 calendar years (*vide ante* for method) and an anthropogenically excavated pit that crosscuts both the charcoal horizon and paleosol-B suggests the presence of an anthropogenically induced unconformity, above which are *ca.* 200 cm of potentially reworked sediments (LC-1) deposited during the latter portions of Holocene.

Gololobovo Sections

The Gololobovo site lies to the southeast of the Kolomyenka River, at the Gololobovo Quarry Brick Factory (Figure 1.1). Four sequential sections make up the Gololobovo composite section. Each of these four sections will be presented individually with construction of the composite section to follow. The maximum distance between the sections is approximately 800 m (GS1 and GS4) while the minimum distance is 75 m (GS2 and GS3).

Due to the complicated procedure for constructing the Gololobovo composite section (compared to Likhvin) and the presence of overlapping lithologic units, all data-trends and lithostratigraphic relationships are discussed after the composite section presentation. Lithic data (*e.g.*, median grain size, magnetic susceptibility, LOI, geochemistry) are presented for each lithostratigraphic section.

Gololobovo Section No. 1: Lithostratigraphy and basic paleosol description

Four lithic units comprise Gololobovo Section No. 1 (hereafter referred to as GS1). These are illustrated in figure 3.7A.

GS1-1: 0 - 205 cm (GC-1: 0 - 205 cm)

Lithic Description: The surface of this section has been disturbed by pit operations. The upper 112 cm of this unit consists primarily of light yellowish-brown (10 YR 6/4 d) to brownish yellow (10 YR 6/6 d) clayey-silt. The lower 93 cm of the unit consists primarily of massive darker coloured clayey-silt sediments (dark yellowish brown, 10 YR 4/4 m). The lower contact is gradational and planar.

Soil-A: A number of different (albeit related) pedogenic characteristics are present within the upper 112 cm of the unit: from 0 - 9 cm a moderately developed, fine blocky structure is observed; from 9 - 30 cm the sediment exhibits a moderately developed sub-angular blocky structure superimposed on a weakly developed, fine prismatic structure; from 30 - 63 cm there is evidence of weak ash-grey (no Munsell colour) gley and weak sub-angular to angular blocky structure; from 63 - 112 cm the sediment exhibits a weak, fine granular microstructure, a moderately developed fine sub-angular blocky mesostructure, and a

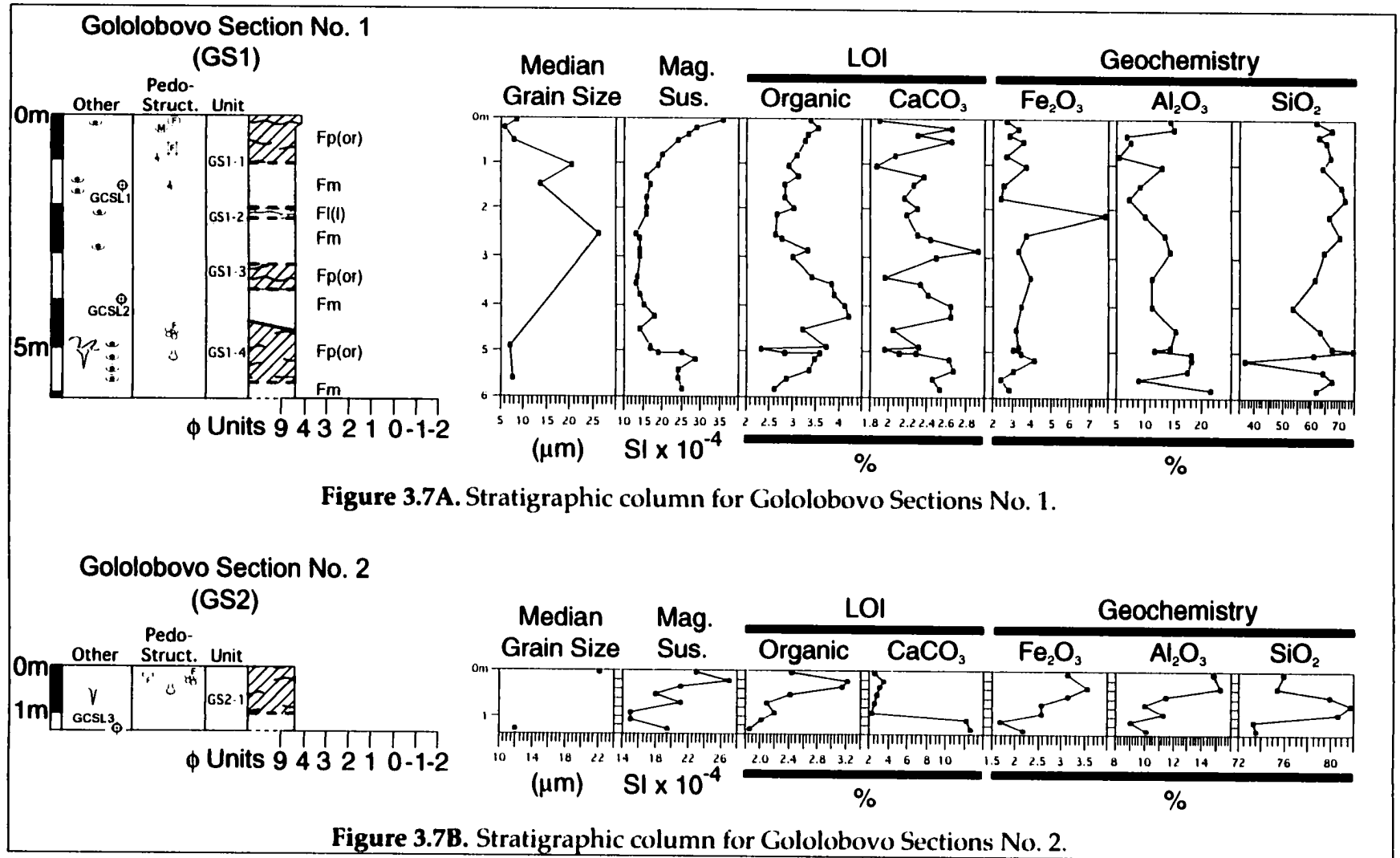


Figure 3.7A. Stratigraphic column for Gololobovo Sections No. 1.

Figure 3.7B. Stratigraphic column for Gololobovo Sections No. 2.

weak fine prismatic structure. Between 112 cm and 146 cm, clay cutans have developed on peds and within voids (Plate 3.3, A-E).

Interpretation: Based on the grain size and the massive nature below the pedogenically altered sediments (*i.e.*, from 146 - 205 cm) the parent material of this unit is interpreted to be primary loess. Paleosol-A, being the modern-day soil, is observed to be within a forest zone. Unfortunately, the A-horizon has been removed, but the degree of translocated clays in the Bt₁ (0 - 63 cm) and Bt₂ (63 - 146 cm) suggests that there may have been Ahe and/or Ae horizons above thereby allowing inference that this soil belongs to the Luvisolic Order. Furthermore, the presence of weak Ah-horizon development from 63-112 (evident from fine-granular structure) suggests that the initial stages of soil-A development may have been cumulic (regosolic), forming in tandem with aeolian deposition.

GS1-2: 205 - 225 cm (GC-2: 205 - 225 cm)

Lithic Description: This unit consists of weakly stratified brownish-yellow (10 YR 6/6 d) silty-clay. The stratification fades below 220 cm and is not observable at 225 cm. The lower contact is diffuse and planar.

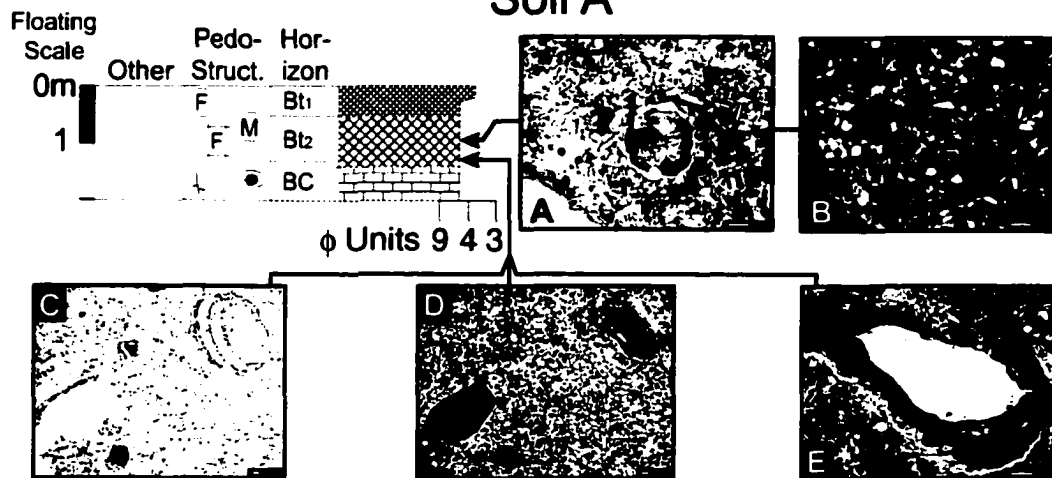
Interpretation: Based on the grain size and stratification, the unit is interpreted to have formed in a quiet-water setting. Given the thickness and context of the unit relative to bounding units, the general setting is one in which loess was deposited into a localized lacustrine environment.

GS1-3: 225 - 463 cm (GC-3: 225 - 463 cm)

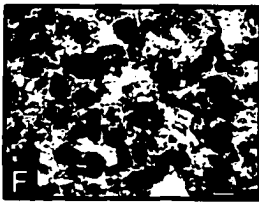
Lithic Description: This unit consists entirely of massive silty-clay. Dark yellowish-brown (10 YR 4/4 m) sediments occur between 310 cm and 380 cm; above and below this horizon, colour is slightly lighter (*i.e.*, yellowish brown, 10 YR 5/4 m). Weak orange-brown (no Munsell colour) mottles up to 0.25 cm in diameter, and separated by 1 - 10 cm, are present between 304 cm and 349 cm. The lower contact is clear and irregular.

Paleosol-C: The only field indication of a paleosol within this unit comes from the darker colour between 310 cm and 380 cm, however, organic and CaCO₃ profiles (Figure 3.7A), and micromorphological

Gololobovo Soil A



Paleosol C



Paleosol D

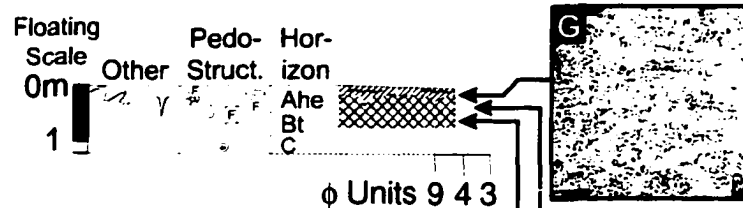


Plate 3.3. Photomicrographs for the upper three paleosols at Gololobovo. **A and B.** Clay infilling illustrating clay translocation into this horizon; mag. 100x; A, PPL; B, XPL. **C and D.** Multiple clay cutans surrounding void spaces

suggesting episodic clay translocation to this horizon; mag. 25x; C, PPL; D, XPL. **E.** 100-200 μm clay cutan surrounding void space; mag. 100x; PPL. **F.** Compacted granular structure of paleo-Ah horizon; mag. 100x; PPL. **G.** Platy structure in Ahe horizon of paleosol-D; mag. 25x; PPL. **H.** Accomodated sub-angular blocky structure; mag. 25x; PPL. **I.** Arrows point to illuviated clay infillings; mag. 100x; PPL.

observations corroborate field evidence. Both organic content and CaCO_3 content increase at approximately 310 cm and peak at approximately 420 cm. The observation that these curves track one another suggests that there may have been post-pedogenic translocation processes acting on these materials. Very-fine, granular structure (Plate 3.3, F), in addition to increases in organic matter and CaCO_3 content, suggest this pedogenic horizon is a weak paleo-Ah horizon.

Interpretation: The massive nature, (limited) grain size data and relatively high CaCO₃ content suggest this unit is comprised of fine-grained loess. The gradational contacts and relatively weak development of paleosol-C suggest that perhaps this paleosol is a cumulic soil that formed contemporaneously with aeolian deposition. Based on the very-fine granular structure identified from micromorphological investigations, organic and CaCO₃ values and relative context, paleosol-C is interpreted to be a cumulic regosol that developed in a steppe to forest-steppe environment.

GS1-4: 463 - 610 cm (GC-4: 463 - 646* cm)

Lithic Description: This unit consists of massive silty-clay. From 463 cm to 520 cm the dominant colour was dark brown (10 YR 3/3 m). This colour lightened below 520 cm to brownish-yellow (10 YR 6/6 m) with occasional (<5%) very pale brown patches. Gley and mottling were pervasive throughout the unit. At 593 cm the colour changes to yellowish brown (10 YR 5/8 d) and the grain size changes from clay to clayey-silt. The base of the unit exhibits irregular shaped fissure-like infill structures. These structures are infilled with sediments similar to that observed in the upper 57 cm of the unit. They are typically <4 cm at their tops (*i.e.*, start at approximately 520 cm) and pinch out in the underlying unit (*i.e.*, GS1-5). The tail ends of fissure-like structures (*vide ante*) originating in the overlying horizon (463-593 cm) are visible in the upper part of the unit. The lower contact is not observed at this section.

Paleosol-D: Fine granular structure, platey structure and krotovena are the only pedogenic structures observed between 463 cm and 593 cm; from 593 cm to 610 cm no pedogenic structures are identified from field observations. However, LOI and geochemical data provide important evidence as to the origin of this paleosol. Between 487 cm and 504 cm, organic matter, CaCO₃, Fe₂O₃ and Al₂O₃ all exhibit sharp decreases whereas an associated peak in SiO₂ is present within the same interval. These data, in conjunction with platey structure (Plate 3.3, G) suggest the presence of an eluviated horizon (*e.g.*, Ahe) within paleosol-D. Peaks in CaCO₃, Fe₂O₃ and Al₂O₃ in addition to sub-angular blocky

* Depths from corresponding units in GS4 are used to for the composite section depths.

structure (Plate 3.3, H) and illuviated clay infillings (Plate 3.3, I) suggest a Bt horizon is located immediately below the Ahe horizon.

Interpretation: This unit continues down into Gololobovo Section No. 2. The data are interpreted after considering observations from unit GS2-1 (*vide post*).

Gololobovo Section No. 2: Lithostratigraphy and basic paleosol description

This section is relatively thin, consisting of 120 cm of *in situ* sediments which exhibit overprinting pedogenic and cryogenic features. There is only one lithologic unit that comprises Gololobovo Section No. 2 (hereafter referred to as GS2); this unit is described in detail below, illustrated in figure 3.7B and depicted in figure 3.8. Correlated composite section depths are presented in parentheses.

GS2-1: 0 - 120 cm (GC-4: 490 - 610 cm)

Lithic Description: The upper 12 cm of this unit consists of brownish-yellow (10 YR 6/6 d) clayey-silt. From 12 cm to 27 cm (502 - 517 cm) the colour changes to strong brown (7.5 YR 5/8 d) but the grain size remains unchanged. Below 27 cm (517 cm) this unit exhibits ground wedges infilled with sediments from the 12 cm to 27 cm (502 - 517 cm) interval. These wedges penetrate down to 62 cm (552 cm) through yellow (10 YR 7/6 d) massive silt which extends to a depth of 120 cm (610 cm). The lower portion of the unit exhibits rare (<2%) CaCO₃ nodules ranging in size from 1-3 cm. The lower contact is not observed in this section. Optical dating sample GSCL 3 was obtained from this unit at a depth of 108 cm (598 cm); ages are reported on the composite section diagram (*vide* Figure 3.13).

Paleosol-D: The paleosol presented here is the lateral equivalent of the paleosol identified in LS1-4; evidence for this correlation is presented under the subsection entitled: *Gololobovo Composite Section*. The upper 27 cm exhibit moderate to strong fine granular structure. This structure corresponds to peaks in magnetic susceptibility, organic matter content, Fe₂O₃ and Al₂O₃ (Figure 3.7B). Colour changes denote the B-horizon in the field (Figure 3.8), and are corroborated by LOI data. The B-horizon represents the zone bounded by peaks in organic matter (above) and CaCO₃ (below; Figure 3.7B). Other features include krotovena up to 6 cm x 4 cm and occasional (<5%) CaCO₃ rootlet casts.

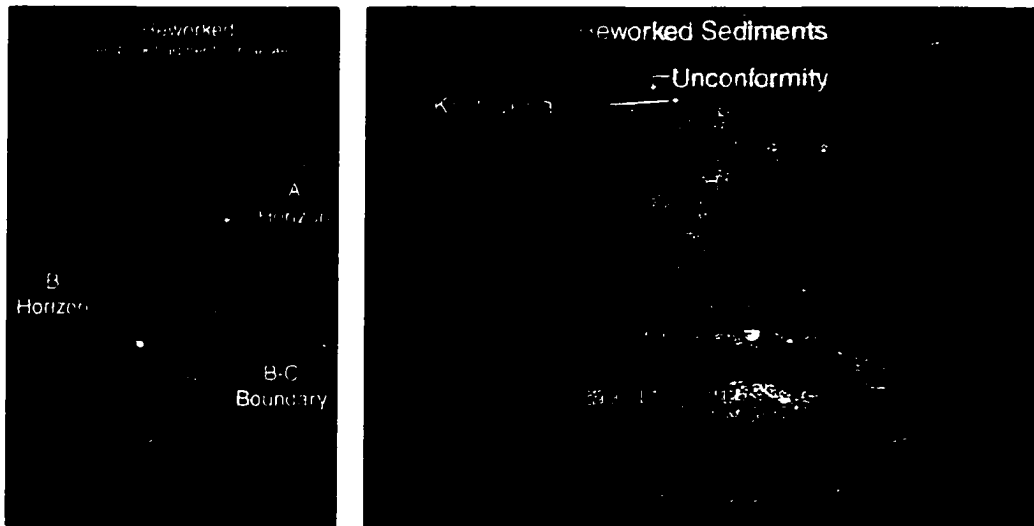


Figure 3.8. Mezin paleosol at Gololobovo. Ground wedges infilled with organic rich sediment penetrate into underlying parent material (loess).

Interpretation: The parent material of this unit is interpreted as loess based on the grain size data and massive structure. Increasing median grain-size up through the section supports the notion of increasing aridity and winds as the climate deteriorates. Subsequent warming and reduction of accumulation rates allowed pedogenic processes to produce paleosol-D which, based on LOI, geochemical and micromorphological evidence, is interpreted as a luvisol forming under moist forested conditions. Cryoturbation in the form of ground wedges infilled with A-horizon material suggests climatic deterioration towards permafrost conditions followed the climatic optimum represented by paleosol D.

Gololobovo Section No. 3: Lithostratigraphy and basic paleosol description

Gololobovo Section No. 3 (hereafter referred to as GS3) is located approximately 75 m from GS2. Five primary units make up GS3 (Figure 3.9); the upper most unit is visually correlative with the base of unit GS2-1.

GS3-1: 0 - 90 cm (GC-4: 463 - 646 cm)

Lithic Description: This unit consists of yellowish-brown (10 YR 5/8 m) to brownish-yellow (10 YR 6/6 m) massive silty-clay loam to silty loam. The unit exhibits a weak fine granular structure and rare (<2 %) CaCO₃ nodules up to 3 cm. The lower contact is diffuse.

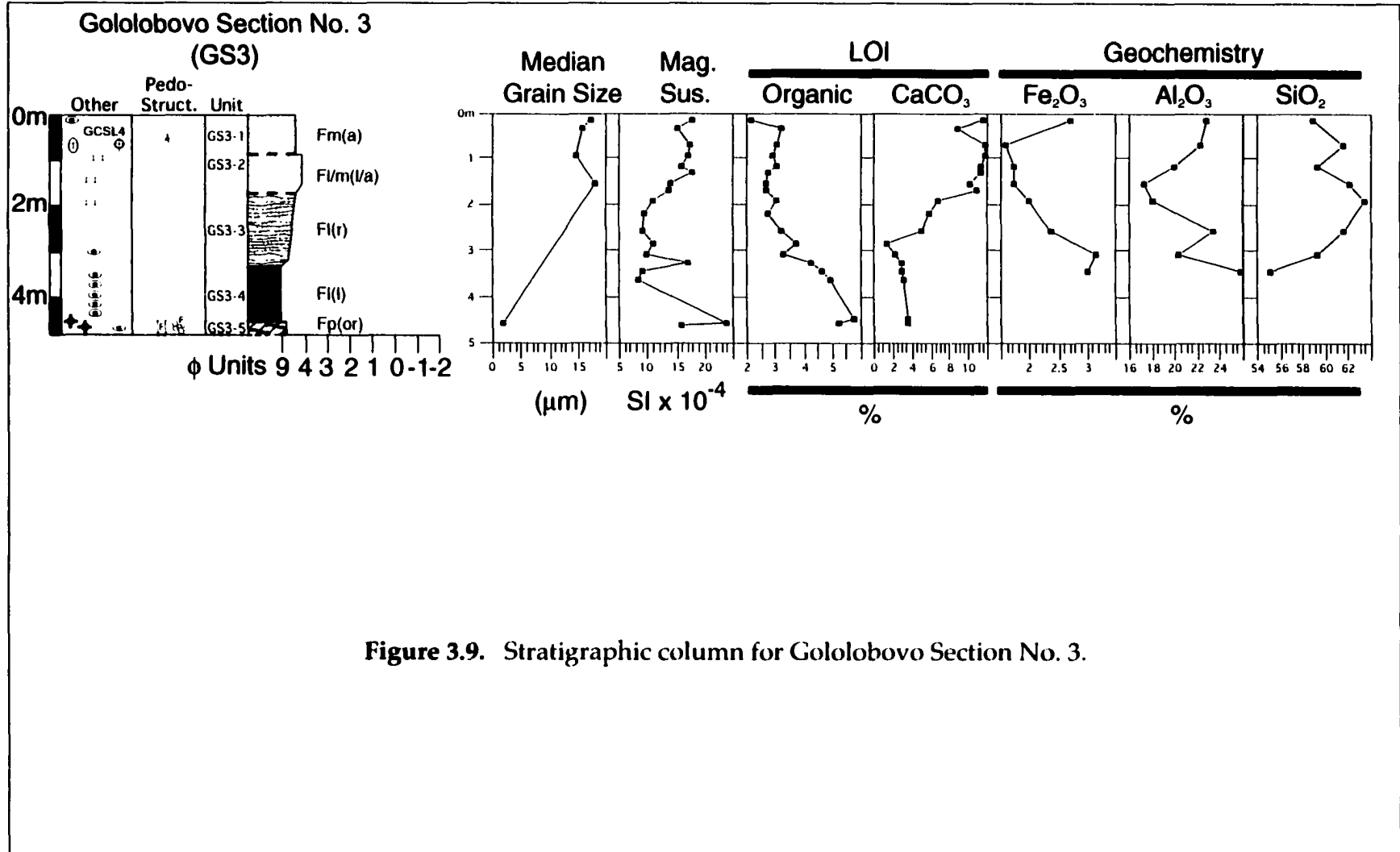


Figure 3.9. Stratigraphic column for Gololobovo Section No. 3.

Interpretation: This unit is interpreted as loess. The weak fine granular structure is interpreted to represent weak pedogenic processes acting on an aggrading paleosurface and the immediately underlying parent material. As loess accumulated, the inferred weak pedogenic processes were not sufficient to produce a significant pedostratigraphic horizon.

GS3-2: 90 - 170 cm (GC-5: 646 - 726 cm)

Lithic Description: This unit consists of yellowish-brown (10 YR 5/6 m) silty loam. In contrast to the overlying unit, this unit is slightly coarser and exhibits sub-horizontal oxidized bands from 0.5 - 2 cm thick and 6 - 7 cm wide; the frequency of these bands decreases with depth. Below 136 cm (692 cm), the colour changes to brownish-yellow (10 YR 6/6 m). Rare (<2%) CaCO₃ nodules up to 3 cm are also present within this unit. The lower contact is planar and gradational.

Interpretation: This unit is interpreted as loess based on the context of the unit relative to bounding units and grain size data characteristics (Figure 3.9 and Appendix D). Further corroboration of this interpretation is presented in figure 3.10 where a sample from GC-5 is compared to the grain-size frequency distribution of loess samples from the Chinese Loess Plateau. Oxidation banding may have been developed by slightly coarser strata deposited under higher energy conditions. The

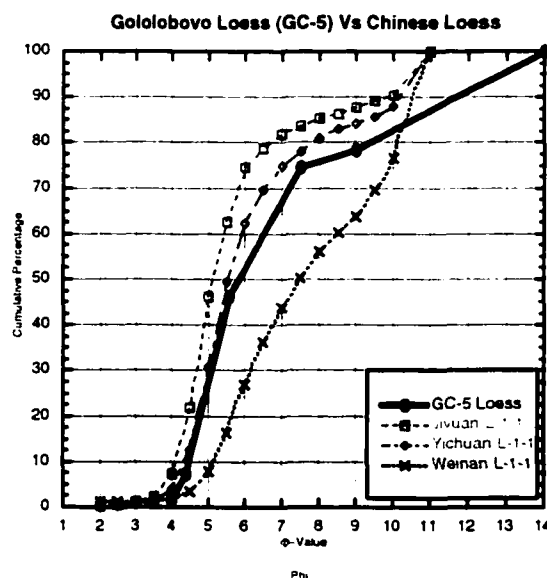


Figure 3.10. Cumulative frequency graphs of three loess samples from the Chinese Loess Plateau, plotted with an example of loess from Unit GS3-2 (GC-5). The Russian Plain example falls between all Chinese-loess members. Difference in the fine and coarse tails are due to different laboratory procedures - nevertheless, the samples are comparative.

oxidation banding is interpreted to be the result of porosity and/or permeability differences from the contrasting grain-size strata. The grain-size-controlled difference in the amount of water and/or air permeating the sediments has resulted in differential oxidation states and the observed oxidation banding.

GS3-3: 170 - 338 cm (GC-6: 726 - * cm)

Lithic Description: This unit consists of yellowish-brown (10 YR 5/6 m) high-angle, weakly stratified clayey-silt. The stratification also exhibits alternating oxidation/reduction bands overprinting the primary stratification. The lower contact is sharp and planar.

Interpretation: Based on grain size and stratification, this unit is interpreted as a colluviated loess.

GS3-4: 338 - 450 cm (GC-7: * cm)

Lithic Description: This unit consists of strongly mottled/gleyed light grey (10 YR 7/2 m) to greyish-brown (10 YR 5/2 m) massive clay. Mottles present within this unit are yellow (10 YR 7/6 m) to dark yellowish-brown (10 YR 4/6 m) and range in size from 3 cm to 4 cm. The lower contact is marked by a 3 cm thick strongly oxidized zone containing iron nodules; the contact is abrupt and planar.

Interpretation: The well sorted, extremely fine grain size of this unit suggests sub-aqueous deposition in a lacustrine or glaciolacustrine setting. Variations in magnetic susceptibility (Figure 3.9) are most likely due to the influence of the iron mottles within this unit.

GS3-5: 450 cm - (GC-8: * cm -)

Lithic Description: This unit consists of brown (10 YR 4/3 m) to dark yellowish-brown (10 YR 4/6 m) silty-clay. Occasional (<5%) mottles present within this unit are brownish-yellow (10 YR 6/8 m) and have a diameter of less than 0.5 cm. The lower contact is not observed.

Paleosol-E₂: The dominant characteristics of this unit are the moderately to strongly developed fine sub-angular blocky structure that overprints a weak fine granular structure (e.g., Plate 3.4 A,B). Clay cutans were observed during field investigations and in thin section (Plate 3.4,

* Depths from corresponding units in GS4 are used to for the composite section depths.

C, D). Given moderate to strongly developed structure in this paleosol and the nature of the upper contact (*i.e.*, erosive), it is possible that Ahe and/or Ae horizons have been removed. There remains, however, a relative abundance of organic matter (Figure 3.9, Organic) within this horizon. Given the evidence presented above, paleosol-E₂ is interpreted to be a luvisol that formed under moist forest conditions.

Interpretation: The parent material is interpreted to be a secondary (pedogenically altered) loess. This is based on the lack of primary bedding and the silty nature of the sediment (similar to other fine-grained loess interpreted at this site). The high-degree of pedogenic alteration, however, makes this interpretation tenuous.

Gololobovo Section No. 4: Lithostratigraphy and basic paleosol description

Gololobovo Section No. 4 (hereafter referred to as GS4) is located approximately 450 m from G3. Four primary units comprise GS4 (Figure 3.11). Correlated depths are presented in parentheses.

GS4-1: 0 - 140 cm (GC-7: 798 - 938 cm)

This unit consists of light brownish-grey (10 YR 6/2 m) to greyish-brown (2.5 Y 5/2 m) massive clay. Mottles present within this unit are brownish-yellow (10 YR 6/8 m) to olive-yellow (2.5 Y 6/8 m) and range in size from 1 cm x 1 cm up to 12 cm x 19 cm; some of the mottles contain hard iron/manganese cores. The mottle size and abundance decrease with depth below 90 cm (888 cm) from many (>20%) to common (2-20%). The lower contact is clear and wavy.

Interpretation: See unit GS3- 4 above.

GS4-2: 140 - 249 cm (GC-8: 938 - 1047 cm)

This unit consists of brown (10 YR 4/6 m) to yellowish-brown (10 YR 5/4 m) silty-clay. The upper 43 cm exhibits vertical to sub-vertical dark grey fissure-like infill structures. These structures are irregularly spaced with horizontal distances between stripes of 6 cm to 17 cm. The lower contact is diffuse and planar.

Paleosol-E₂: The upper 43 cm of this unit consists of strong, fine sub-angular blocky structure overprinting a moderately developed fine granular structure (Plate 3.4, A, B) and is therefore interpreted as an AB-horizon. Below 183 cm (981 cm), only a fine, angular blocky structure is

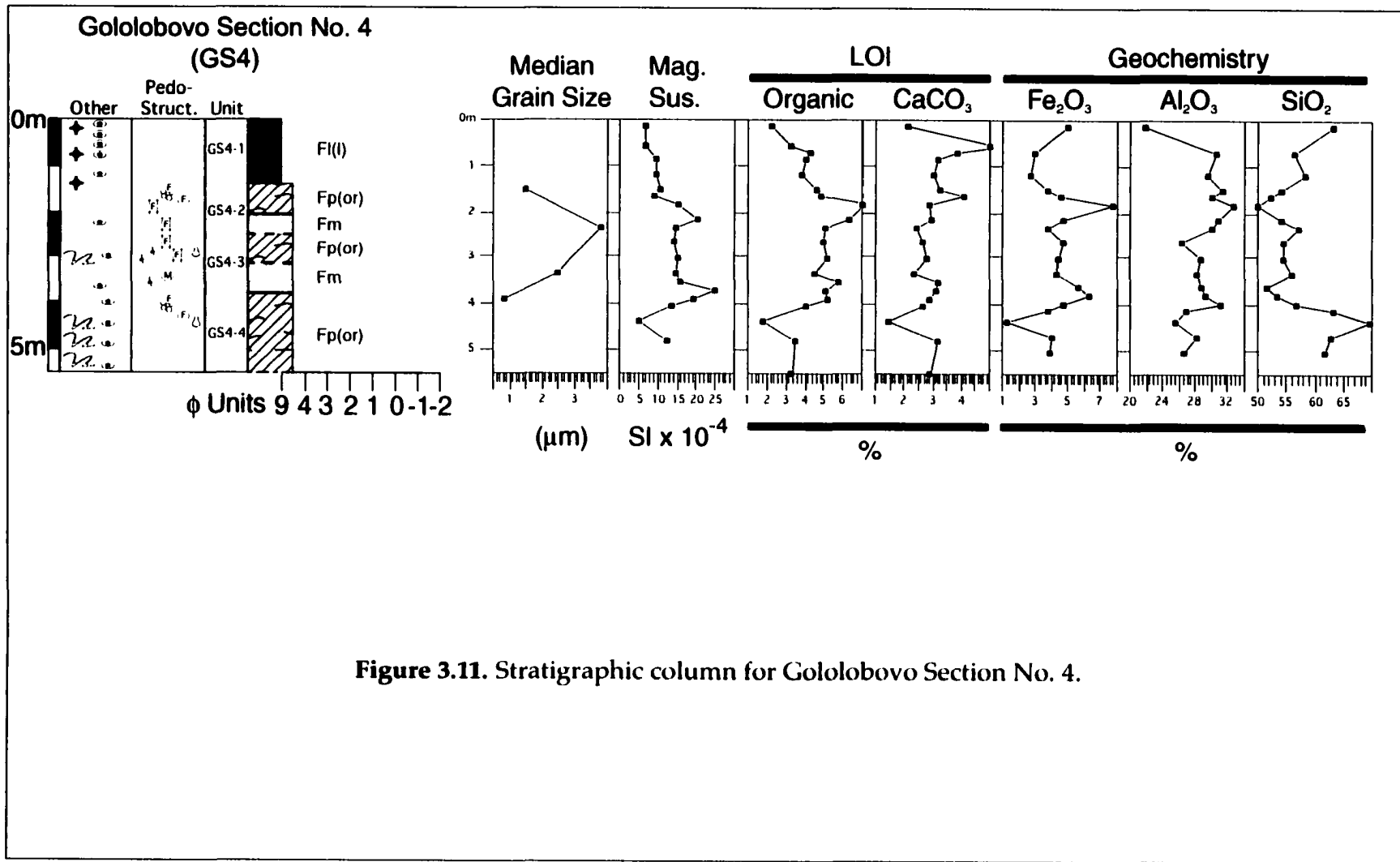


Figure 3.11. Stratigraphic column for Gololobovo Section No. 4.

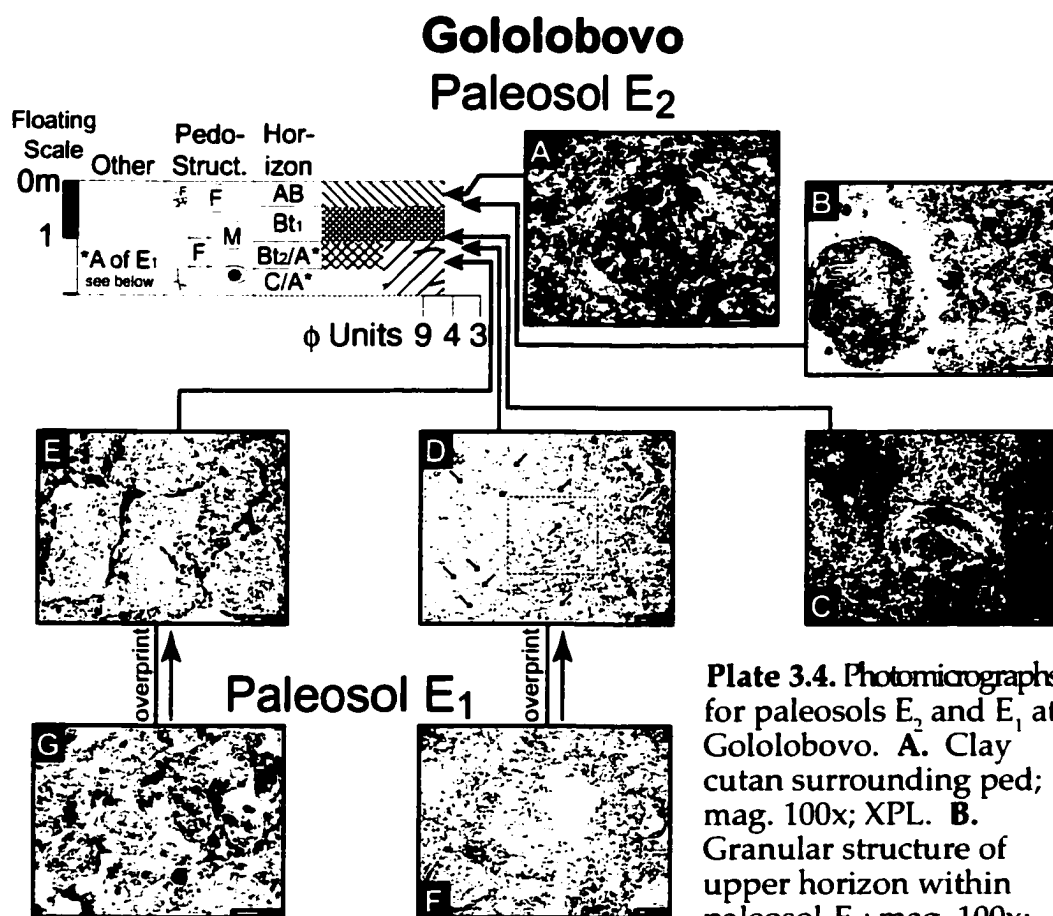


Plate 3.4. Photomicrographs for paleosols E₂ and E₁ at Gololobovo. **A.** Clay cutan surrounding ped; mag. 100x; XPL. **B.** Granular structure of upper horizon within paleosol-E₂; mag. 100x; PPL. **C.** Multiple clay cutans forming around ped within Bt₁-horizon; mag. 25x; XPL. **D.** Arrows point to granular peds (see also below) whereas the dashed box draws attention to a sub-angular ped with a thin cutan. Note the presence of a granular ped within the upper-right corner of the larger blocky ped suggesting a Bt-horizon overprints an Ah-horizon; mag. 25x; PPL. **E.** Unaccommodated to partially accommodated, strong sub-angular blocky structure; mag. 25x, PPL. **F and G.** Examples of granular structure from paleosol E₁ that were subsequently overprinted by the formation of sub-angular blocky structure during the E₂ soil-forming event (presented in **D** and **E** respectively); **F**, mag. 25x; PPL; **G**, mag. 100x; PPL.

identified from field investigations, however, micromorphological analyses suggest the presence of sub-angular blocky structure and clay cutans (Plate 3.4, C-E). These structures are interpreted to result from Bt (Bt₁ and Bt₂; Plate 3.4) horizon formation which, in its upper portions, overprints a previous Ah horizon (fine-granular structure). Also within this unit are krotovena up to 10 cm x 20 cm. Given the stratigraphic position below the massive clay unit (i.e., GS3-4 and GS4-1) and the similarity in pedogenic structures, this unit is the lateral equivalent of GS3-5.

Interpretation: See unit GS3-5 above.

GS4-3: 249 - 381 cm (GC-9: 1047 - 1179 cm)

Lithic Description: This unit consists of silty-clay sediment. The colour of this unit lightens with depth from dark yellowish-brown (10 YR /6 m) at 249 - 314 cm (1047 - 1112 cm) through brownish yellow (10 YR 6/6 d) between 314 - 339 cm (1112 - 1137 cm). At 339 cm (1137 cm) a gradual contact is observed between the brownish yellow (10 YR 6/6 d) clayey-silts and the underlying brown (10 YR 4/3 m) massive clayey-silt; the colour of this massive clayey-silt lightens to brownish-yellow (10 YR 6/6 m) with depth. The lower contact is abrupt and planar.

Paleosol-E₁: This paleosol horizon exhibits moderate, medium sub-angular blocky structure (from E₂) that overprints a weak, fine granular structure (E₁) from 249 - 314 cm (1047 - 1112 cm). Below 314 cm (1112 cm), a weakly developed sub-angular blocky structure related to E₁ pedogenesis dominates. The weak, fine granular structure and weakly developed, fine sub-angular blocky structure are attributed to weak eluviated brown chernozemic or brunosolic soil formation. Therefore, paleosol-E₁ is interpreted to have formed under steppe to forest-steppe conditions. Evidence of pervasive clay translocation during the subsequent soil-forming event (paleosol-E₂, *vide ante*), would have overprinted the granular structure of paleosol-E₁, giving rise to the moderately developed, medium, sub-angular blocky structure (Bt₂ of paleosol-E₂) observed in the upper portions of this interval.

Interpretation: Pervasive pedogenic overprinting of this unit makes parent material interpretation problematic. Based on comparative grain sizes in other problematic units and the relative context of bounding horizons, a speculative interpretation of secondary (pedogenically altered) loess is given to this unit.

GS4-4: 381 cm - (GC-10: 1179 cm -)

This unit consists of silty-clay intensely overprinted by pedogenic horizons and intense cryoturbation (Figure 3.12). In order to simplify the following, descriptions are subdivided into discrete packages (*e.g.*, Sub-unit GS4-4a, Figure 3.12, A, B) that include both lithic and pedogenic components. The lower contact of the unit is not observed within this section. There are six sub-horizons observed within this unit:

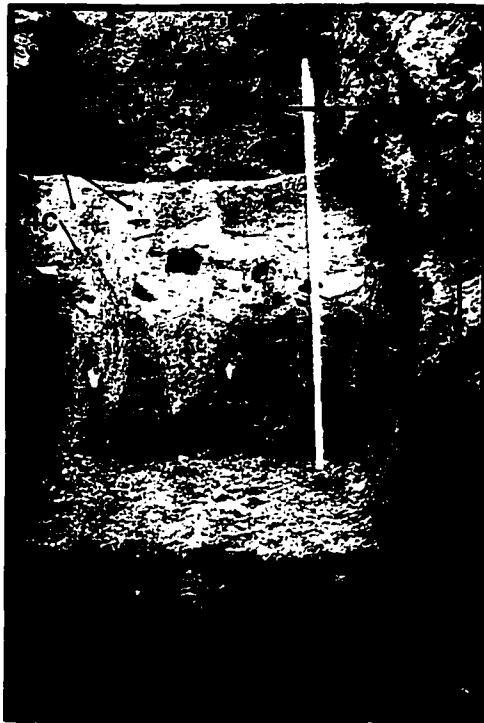
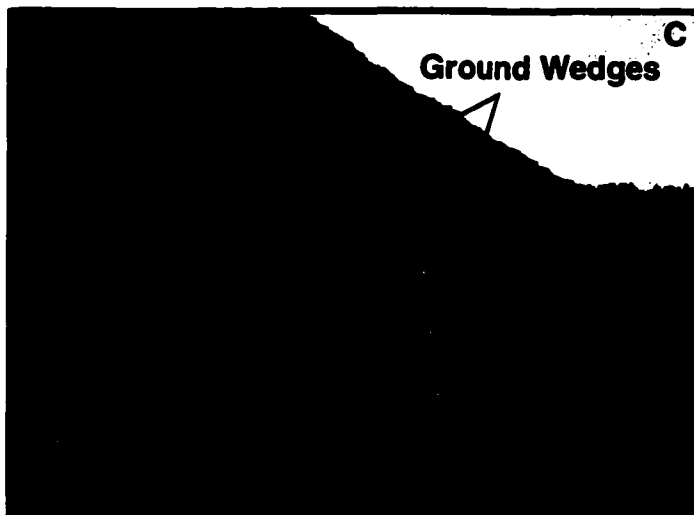
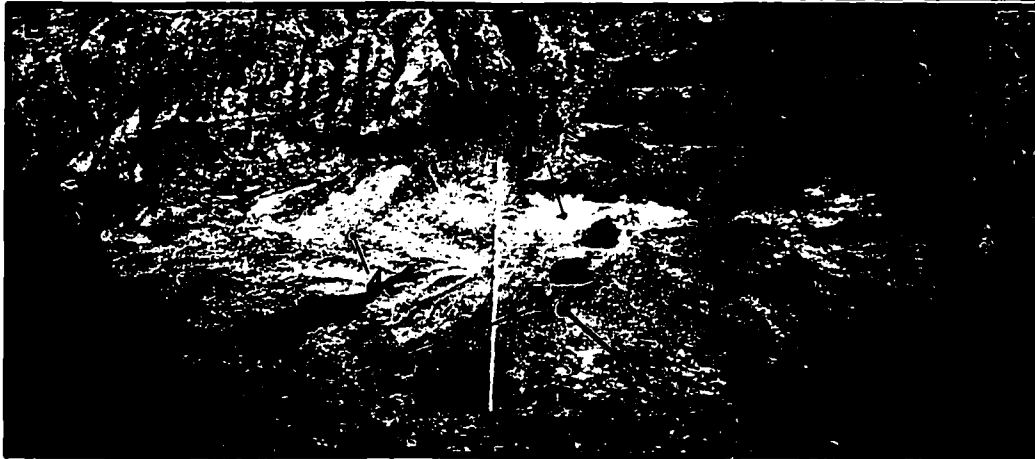
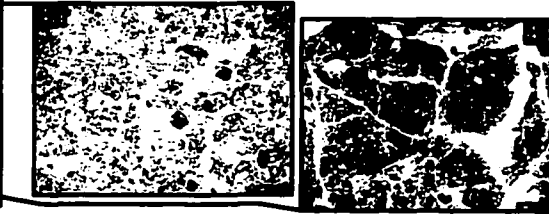


Figure 3.12. A. Photo of unit GS4-4 depicting the chaotic distribution of sub-units (4a to 4f). **B.** Unit GS4-4 located approximately 50 m northeast of section GS4. This exposure depicts the horizontal extent and relationships of paleosol horizons that were not discernable at section GS4 due to limited exposure. Clearly visible (from top to bottom) are horizons (units) 4a, 4b, 4c and 4e. Sub-units 4d and 4f are not discernable at this scale of observation. **C.** Ground wedges penetrating into GS4-4 (GC-10).



Photomicrographs (PPL) depicting various structures observed in sub-units: 4a, granular structure (mag. 25x); 4d, sub-angular blocky structure (mag. 25x); 4e, clay cutans (mag. 100x).

Sub-unit GS4-4a consists of yellowish-brown (10 YR 5/4 m) silty-clay. Weak sub-angular blocky to weak fine granular structures are present within this unit in addition to krotovena up to 7 cm x 10 cm and infilled with what appears to be sub-unit GS4-4e (*vide post*). Extremely small (<1 mm) organic pellets are also present throughout this unit and comprise <2% of the observed area. The colour gradually lightens to light yellowish-brown (10 YR 6/4 m) at 432 cm (1230 cm). The lower contact of this sub-unit is clear and irregular.

Sub-unit GS4-4b consists of highly deformed, structureless, very pale brown (10 YR 8/3 d) silt.

Sub-unit GS4-4c consists of weakly oxidized, highly deformed, discontinuous olive-yellow (2.5 Y 6/6 m) silt. Weak fine granular structure is discernable within this sub-unit.

Sub-unit GS4-4d consists of dark yellowish-brown (10 YR 4/6 m) silty-clay. Moderate fine sub-angular blocky and weak fine granular structures are present within this sub-unit; clay cutans are also observed. This sub-unit exhibits a strong fissility.

Sub-unit GS4-4e consists of strong brown (7.5 YR 5/8 m) silty-clay. Moderate to strong medium sub-angular blocky structure is present in addition to well developed clay cutans and moderate oxidation. Strong fissility is also present in this sub-unit.

Sub-unit GS4-4f consists of gleyed zones of yellowish-brown (10 YR 5/6 m) silty clay. This sub-unit exhibits moderate to strong medium sub-angular blocky structure and a strong fissility.

In addition to the involuted nature of this unit, large ground wedges have been observed crosscutting the various sub-units described above. These wedges can reach 50 cm - 75 cm in maximum width and 150 cm - 175 cm in height, with a spacing between wedges of up to 200 cm.

Interpretation: This unit exhibits an extremely well developed paleosol that exhibits the following horizons: Ah (GS4-4a), Ae (GS4-4b), Bt₁ (GS4-4c) and Bt₂ (GS4-4d). The overall thickness exceeds two metres. From these observations, this paleosol is interpreted to be a Grey-brown luvisol that developed under forested conditions. Given the thickness of the soil, it is reasonable to infer a relatively long period of soil devel-

opment. The well-developed ground wedges that crosscut the paleosol are testament to the subsequent cold conditions that lead to the formation of permafrost.

Gololobovo Composite Section

The Gololobovo composite section was compiled originally by comparing similar lithologic units from sequential sedimentary sections. Fine-tuning of the lithostratigraphic correlation was accomplished by comparing overlapping laboratory data plotted *versus* section depth (Figure 3.13). The result is a well constrained composite section that outlines the general stratigraphic relationships observed at the Gololobovo site. The stratigraphic relationship between units GC-6 and GC-7 is clear at GS4, therefore the composite section depths for these units correspond to those observed in GS4.

Four optical luminescence dating samples were collected at the Gololobovo site. The stratigraphic position of each of the optical dating samples is presented in the corresponding stratigraphic column, and the ages are presented in figure 3.13.

Gololobovo Site: relative data interpretations

In all, six soil / paleosol horizons were identified in the field; the organic enriched horizons are clearly highlighted on the stratigraphic column in figure 3.13 (shaded portion of composite units). Unfortunately, the grain size data obtained from this section are too sparse to relate to the lithostratigraphy. However, other data do illustrate reasonable correlation to soils.

The magnetic susceptibility in the Gololobovo stratigraphic record (Figure 3.13) shows strong peaks in each of the strongly developed pedogenic horizons (A, D, F) as well as peaking in other less well developed pedogenic horizons (*i.e.*, E₂). A peak is also observed within Gololobovo composite unit GC-7 (equivalent to GC3-4 and GC4-1 in figures 3.9 and 3.11 respectively). This peak is, in all likelihood, a function of the mottling and oxidation within that unit. The magnetic susceptibility sample in this case was located close to, or within a mottle or oxidized zone.

Relative organic highs are found to be associated with soil / paleosol horizons A, C, D, E₂ and F. Paleosol-C exhibits a gradual increase in

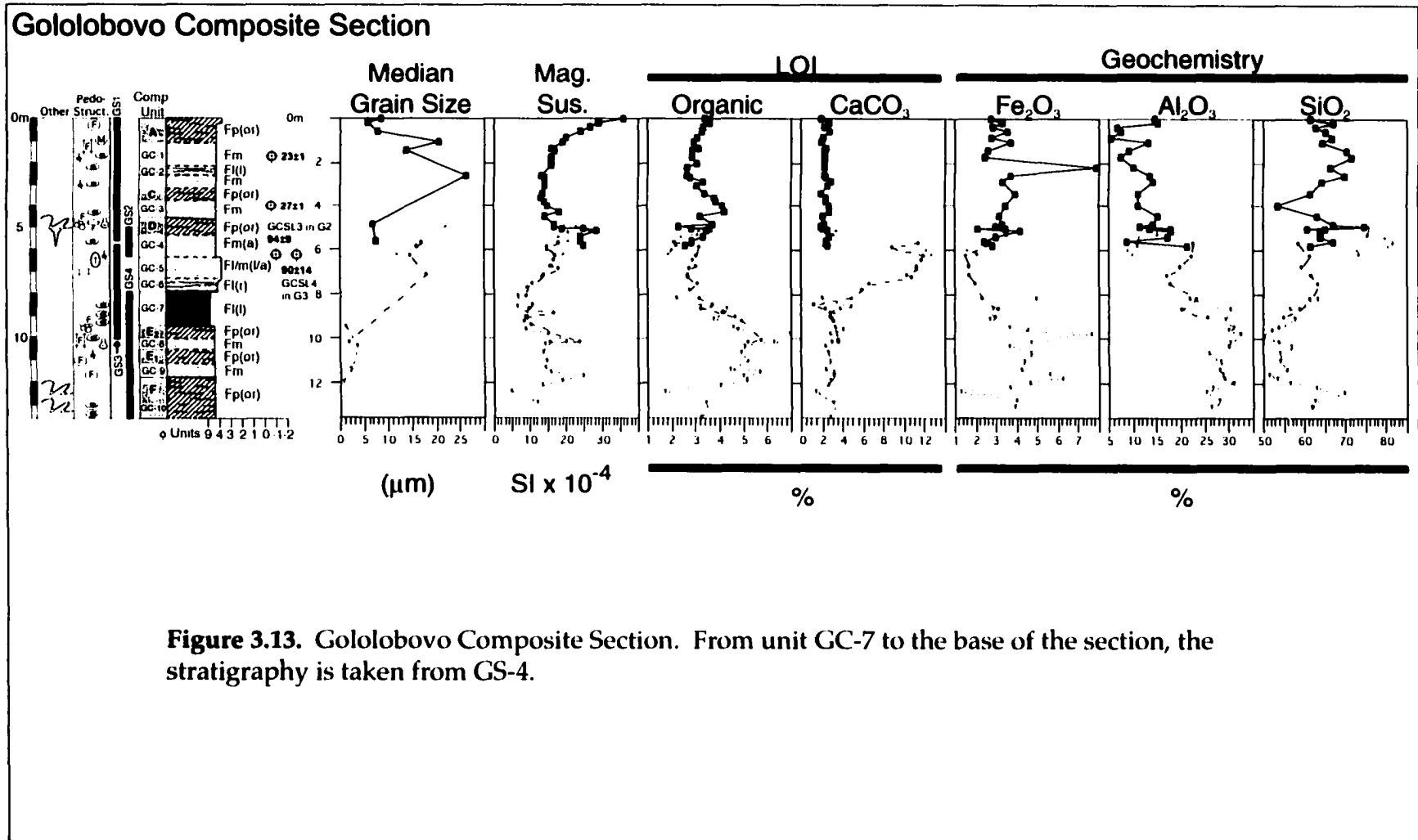


Figure 3.13. Gololobovo Composite Section. From unit GC-7 to the base of the section, the stratigraphy is taken from GS-4.

organic content from approximately 310 cm to 430 cm, but the lower limit of the observed pedogenic horizon (from field observations) occurs at approximately 380 cm. Further investigations into the vertical extent of paleosol-C at the Gololobovo site may be required. Other paleosols, specifically paleosol E₁, exhibit organic peaks (Figure 3.13; depth of approximately 1100 cm), however, this peak consists of only one datum point and is only greater than the adjacent data points by a fraction of a percent. Therefore, this may be an artifact of insufficient data resolution.

The main feature observed in the CaCO₃ data set (Figure 3.13) is the large broad peak that dominates the profile from approximately 580 cm to 730 cm, and to a lesser extent from approximately 730 cm to 800 cm. The upper portion (Figure 3.13; GC-4) corresponds to a massive silty horizon interpreted to be primary loess. The lower portions (Figure 3.13; GC-5 and GC-6) correspond to weakly stratified silty horizons interpreted to be secondary (colluviated) loess. The high calcium carbonate percentages characterizing sediments between 580 cm and 730 cm are interpreted to be the result of post-depositional “loessification” - type processes (*cf.* Pécsi 1990, 1995).

Both Fe₂O₃ and Al₂O₃ data have good correspondence with soil/paleosol horizons. Weak peaks in Fe₂O₃ data are observed for paleosols C and E₁, while relatively strong Fe₂O₃ data peaks correspond to paleosols D, E₂ and F. With regards to Al₂O₃ data, relatively moderate to strong peaks correspond to soil-A, and paleosols D, E₂ and F. In some cases the Al₂O₃ data peak is slightly offset or spread out from the correlative Fe₂O₃ peak (*e.g.*, E₂ and F) suggesting that post-depositional processes were active, giving rise to accumulations of these materials in different parts of the paleo-soil solum.

Gololobovo Site Depositional Environment: overview

Similar to Likhvin, the Gololobovo site consists of material representing deposition in at least two different sedimentary environments: aeolian and lacustrine/glaciolacustrine; due to difficult exposure and/or working conditions (*i.e.*, excessive moisture) interpretation of some units is problematic and therefore any interpretation associated with these units is purely speculative. Despite its location behind several

published glacial limits (*cf.* Figure 1.8), no diamicton units are observed at the Gololobovo site. This suggests that the observed sedimentary sequence at this site was deposited beyond the regional glacial limits.

The sequence of events at Gololobovo starts with the deposition of unit GC-10. Any diagnostic primary structures and textures of this unit have been completely destroyed during subsequent pedogenesis and cryoturbation, making the interpretation of a depositional environment difficult. However, the degree of pedogenesis within this unit (*i.e.*, paleosol-F) is unequalled at this site, even considering the modern-day soil. The unit exhibits at least three different pedogenic horizons which include: an Ah overprinted by subsequent illuviation structures (sub-unit GS4-4a and GS4-4d); an Ahe-Ae (sub-unit GS4-4b) stripped of organics, CaCO_3 , Fe_2O_3 , and to some degree Al_2O_3 . (Figure 3.11: 450 - 480 cm or Figure 3.13: 1248 - 1278 cm); and an illuviated horizon that can be subdivided into Bt1 (GS4-4d) and a Bt2 (GS4-4e, f). The thickness of the unit reaches *ca.* 200 cm suggesting a significant period of soil development; clearly a major paleosol solum (grey-brown luvisol) formed during forested interglacial climate conditions. The overprinting cryogenic involutions and ground wedges that disrupt the soil horizon stratification suggest extremely cold conditions following the development of paleosol-F.

The upward coarsening of units GC-9 and GC-8 (Figure 3.13 - Grain Size/GC-9) and a lack of primary structure in weakly organic horizons suggests that perhaps these fine-grained sediments were genetically related, being deposited in similar aeolian environments. Although the entirety of these units has been pedogenically altered, the organic content and structure in unit GC-9 (paleosol-E₁) is much less pronounced than that in unit GC-8 (paleosol-E₂). The weakly formed granular structure forming in loessic sediments, suggests that paleosol E₁ may have been a weak eluviated brown chernozem or brunosol forming in a steppe to forest-steppe environment, whereas pervasive translocation processes within paleosol-E₂ (luvisol) represent a period of more significant pedogenic development in a forest environment.

Overlying GC-8 and paleosol-E₂ are the gleyed, heavy clays of unit GC-7. These extremely well-sorted very fine-grained sediments are

interpreted to have been deposited in a lacustrine environment. As described earlier, the Gololobovo site is located within the Oka Basin at the southern edge of the Meshchera Depression and thus, any change in local drainage could create a depositional basin within which these clays have accumulated. The texture of the unit GC-7 clays is testament to the extremely low energy conditions present at the time of deposition.

Gradually, the quiet-water conditions during the deposition of unit GC-7 slowed or ceased. With the subsequent onset of glaciation (*cf.* Dnieper Till at Likhvin), drier and cooler climatic conditions gave rise to increased wind strength (katabatic winds) and associated deposition of wind-blown dust in the region. The increase in wind strength and excess of material being deposited, produced conditions ideal for colluviation. Being located in a basin, much of this colluviated loess was deposited along slopes which resulted in the weak stratification of unit GC-6. Eventually, these weakly stratified sediments gave way to the silty sediments of unit GC-5 which are interpreted as primary loess. Strata of loess that vary slightly in grain size and packing density (from differential oxidation bands) suggest varying wind strengths during the Dnieper glacial maximum (*cf.* Dnieper Till at Likhvin). Subsequent retreat gave way to reduced katabatic winds evident from increased pedogenesis that produced weak, fine granular structure in the upper portions of unit GC-4 (paleosol-D).

Paleosol-D, although not exhibiting the degree of development experienced by paleosol-F, does exhibit well developed Ah and Bt horizons. Subsequent cryoturbation and ground wedge formation suggest re-working during a post-pedogenic cold interval. Only one pedogenic event is detected within unit GC-4.

Unit GC-3, composed of massive silty-clay, was excavated under extremely wet conditions; this sullegic factor hampered identification of any primary structure that may have been present in the exposed sections and therefore the following interpretation for this unit is speculative. The (apparent) massive, fine-grained nature of this unit may suggest either rapid sedimentation in a lacustrine environment, or extremely slow deposition in an aeolian environment. Given that there

is only *ca.* 153 cm between the top of paleosol-C and the top of paleosol-D, and the sediments between were deposited between post *ca.* 94 ka and *ca.* 27 ka (*i.e.*, *ca.* 2.28 cm per 1000 years) the latter "slow aeolian" interpretation is favoured. In this scenario, the initiation of aeolian deposition would have buried paleosol-D which formed during the preceding interglacial period. This aeolian sedimentation would have continued throughout the early last glacial period until aeolian sedimentation was attenuated enough to allow paleosol-C to develop. Subsequent climatic deterioration once again increased the sedimentation rate and buried paleosol-C.

With the advance of late glacial ice to the northwest of the Golobovo site, water and drainage patterns may have fluctuated causing a minor local ponding of water. Aeolian deposition, and weak fluvial deposition of sediments into this lake contributed to the formation of unit GC-2. However, this body of water was ephemeral and once drained or filled with sediments, aeolian sedimentation buried the unit under GC-1. This final phase of aeolian sedimentation continued until the advent of the Holocene interglacial, in which the modern-day soil formed.

Korostylievo Sections

The Korostylievo site is located on the southwest bank of the Vorona River, approximately 435 km southeast of Gololobovo (Figure 1.1; Table 1.1). The site exhibits 6 well to moderately-well developed pedogenic horizons, and one set of very weakly developed pedogenic horizons. These soil/paleosol horizons overprint 5 of the 8 major lithostratigraphic units observed at the site. Although descriptions presented below corroborate the observations of Krasnenkov *et al.* (1984), this dissertation advances the knowledge of this site by cross-referencing micromorphology, magnetic susceptibility, geochemistry and LOI data with detailed field descriptions.

In order to evaluate all litho- and pedostratigraphic units/horizons present at the Korostylievo site, two sections separated by approximately 70 m were excavated (Figure 3.14). The 'layer-cake' litho- and pedostratigraphy coupled with continuous exposure between these two sections allowed a simple visual correlation (elevation correlated using a Suunto level) in order to produce a composite section spanning the entire exposure. For this reason, individual sections are not presented, but rather the compiled composite stratigraphy is presented to avoid repetition of results. Differentiation of sections is not considered when

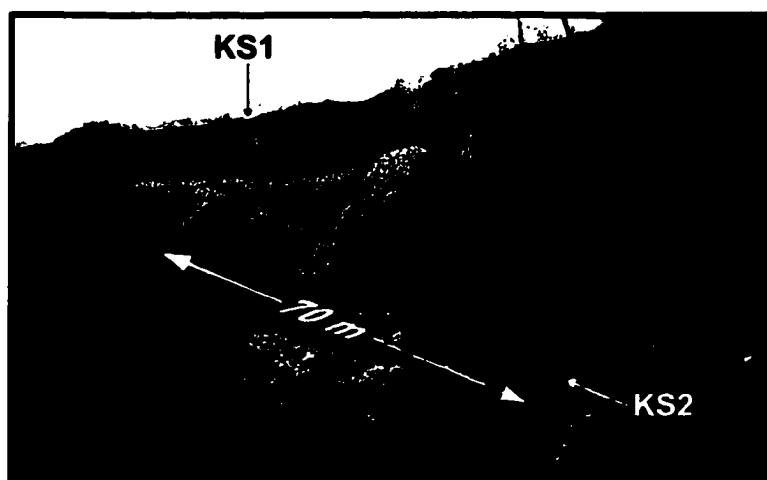


Figure 3.14. Exposure of 'layer-cake' lithologic and pedogenic units/horizons at the Korostylievo site along the west bank of the Vorona River southeast of Uvarovo, Russia. KS1 terminates just below dark grey-brown pedogenic horizon (vertically centred in exposure); KS2 starts in lighter band immediately below aforementioned dark grey-brown horizon (just above person at right-hand side of photo). Together, these comprise the Korostylievo Composite section (KC).

applying unit labels, hence, units within the Korostylievo Composite section are designated by 'KC-#'. Also, the modern soil (orthic black chernozem) has produced data-trends that transcend data-trends from the paleosol horizons. Therefore, to highlight paleosol-related data trends (e.g., magnetic susceptibility, F_D (F%), organics, carbonate, Fe_2O_3 , Al_2O_3), a second Korostylievo stratigraphic column is also presented with the appropriate re-scaled data.

Korostylievo Composite Section: Lithostratigraphy and basic paleosol description

KC-1: 0 - 205 cm

Lithic Description: This unit consists of massive, black (5 YR 2/1 d) clayey silt that exhibits a weak vertical joint pattern from 6 cm to 70 cm. At 70 cm the aforementioned characteristics gradually (5-15 cm) change to a friable, dark-reddish brown (5 YR 3/2 d) silty-clay. From 92 cm through 168 cm the colour lightens to brown (7.5 YR 5/4 d) and exhibits common (2-20%) $CaCO_3$ tubules and stringers. From 168 cm to the

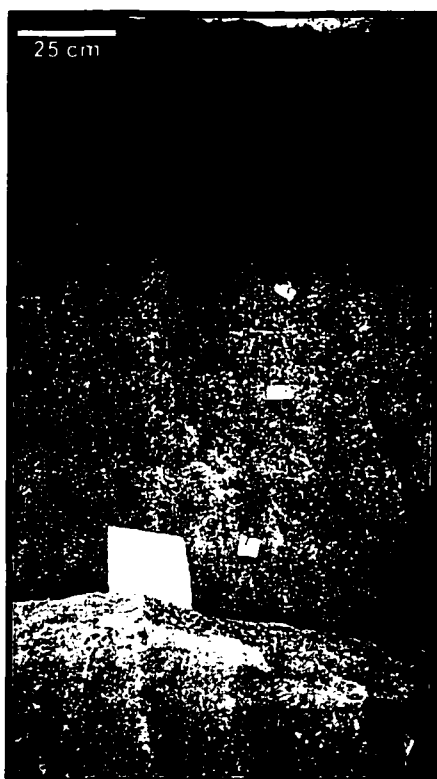


Figure 3.15. Modern-day soil (pedostratigraphic unit A) and krotovena that overprint lithostratigraphic unit KC-1.

base of the unit the sediments consist of yellowish-brown (10 YR 5/8 d) clay to silty-clay. Carbonate tubules and stringers are still present, although slightly less common relative to the overlying horizon (92 - 168 cm). The lower contact is defined by tonguelike structures with wavelengths of 2 cm to 4 cm and amplitudes up to 8 cm; the contact is clear and irregular.

Soil A: This unit (Figures 3.15 and 3.16) consists of massive silty-clay which is overprinted by the modern-day soil (Figure 3.15). The upper 6 cm of unit KC-1 consists of fibric and mesic organic matter. From 6 cm to 70 cm the unit exhibits a well developed fine granular structure (Plate 3.5 A) with abundant (>100/square decimetre) fine to very

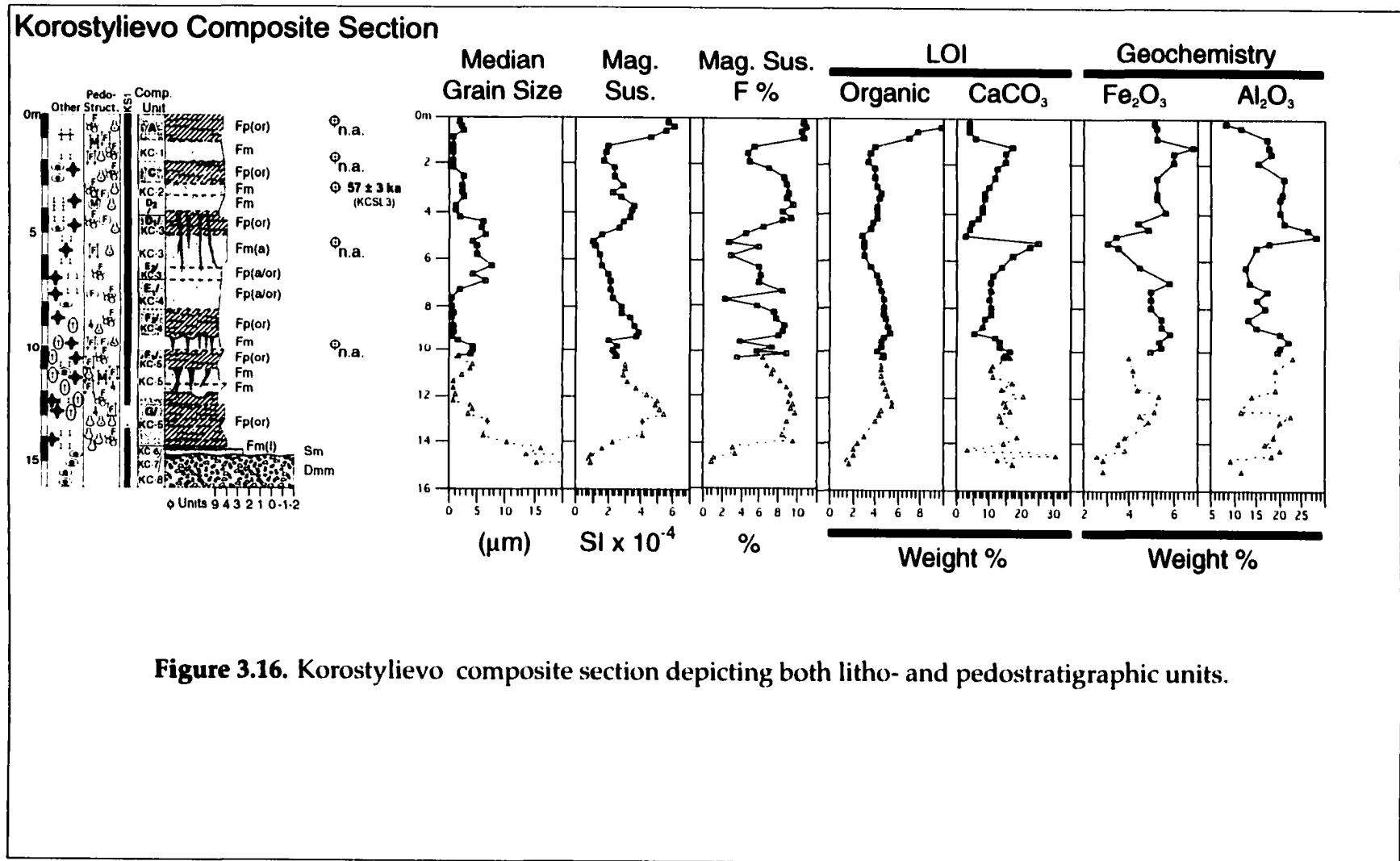
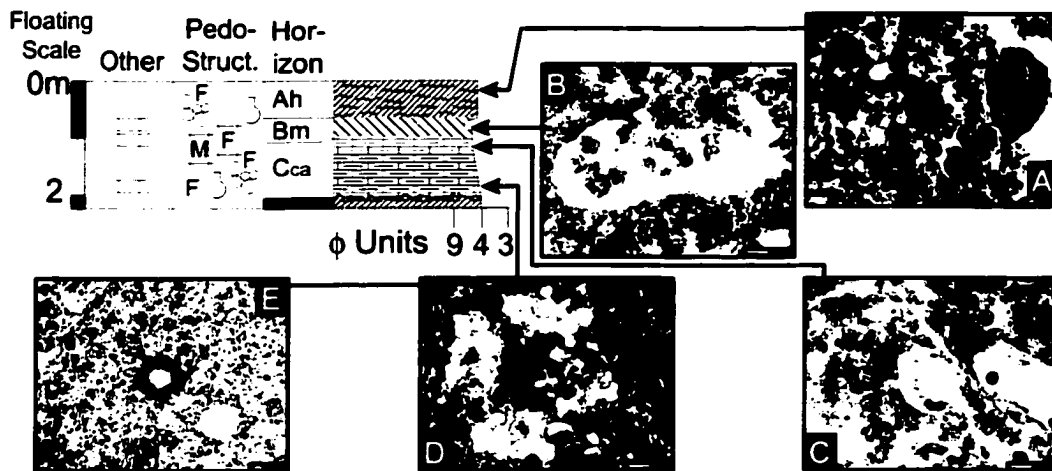


Figure 3.16. Korostylievo composite section depicting both litho- and pedostratigraphic units.

Korostylievo Soil A



Paleosol C

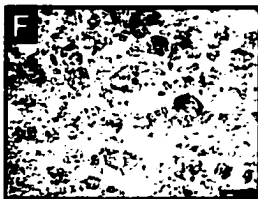


Plate 3.5. Photomicrographs of pedogenic features associated with soil-A and paleosol-C at Korostylievo. **A.** Well developed granular structure; mag. 25x; PPL, B&W. **B.** Mite excrement observed in a void space within the Ah-horizon; mag. 100x; PPL. **C.** CaCO₃ cast of rootlet, mag. 100x; PPL. **D.** Coarse-grained calcium carbonate nodule; mag. 100x; PPL. **E.** CaCO₃ hypocoating around void space; mag. 25x; PPL. **F.** Granular structure of the Ah-horizon of paleosol-C; mag. 25x; PPL.

fine rootlets. At 70 cm this structure gradually (5-15 cm) changes to a moderately developed fine granular structure that is observable to a depth of 92 cm; within this zone there is evidence of microbial activity (Plate 3.5 B). From 92 cm through 168 cm there is a clear (2- 5 cm) change to a moderately developed, fine to medium angular blocky structure and evidence of weak CaCO₃ precipitation (Plate 3.5 C). This horizon also exhibits common (2-20%), circular and elongate krotovena (Figure 3.15) which range in size from 4 cm x 7 cm to 7 cm x 10 cm and are infilled with either material from the 6-70 cm interval (*i.e.*, black: 5 YR 2/1 d) or material brought up from below (*i.e.*, 168 - 205 cm interval). The basal portion of the unit (168 - 205 cm) exhibits weakly developed, fine angular blocky to fine granular structure and elevated CaCO₃ content which is corroborated from LOI data (Figure 3.16, CaCO₃) and micromorphological evidence (Plate 3.5 D, E).

Interpretation: The parent material of this unit is interpreted as loess based on the lack of primary structure, grain size and vertical jointing. The character of the soil pedon described above suggests that this soil is an orthic black chernozem forming within the present-day forest-steppe environment.

KC-2: 205 - 426 cm

Lithic Description: The upper and lower contacts of this unit are inferred primarily from changes in the median grain size (Figure 3.16). The unit consists primarily of a silty-clay, but does contain some finer zones of clay (Appendix D). From 205 cm to 297 cm the sediment exhibits a brown (7.5 YR 5/4 m) to dark reddish-brown (5 YR 3/3 m) colour which reflects a slight increase in organic matter (Figure 3.16). Vertically oriented, irregularly spaced bifurcating fissures with widths ranging from 1 mm to 12 mm are present within this interval and underlying intervals down to a depth of 370 cm. These structures are infilled with yellow (10 YR 7/6 m) silty-loam material and have sharp irregular contacts with the surrounding material. From 297 cm to a depth of approximately 341 cm the average colour of the unit lightens to reddish-brown (5 YR 5/4 m). From 341 cm to 406 cm the colour gradually changes to brown (10 YR 4/3 m) and becomes slightly more indurated relative to the upper portions of the unit. The lower-most portion of the unit (406 - 426 cm) is characterized by dark-brown (10 YR 3/3 m) silty-clay. Near the base of this interval are irregularly shaped and distributed fissures that extend downwards into unit KC-3 to a depth of 625 cm. The width of these features decreases with depth from 20 cm at approximately 426 cm, through 10 - 15 cm at a depth of 505 cm, to <1 cm between 600 cm and 650 cm. The lower contact of the unit is gradational and planar.

Oval to circular krotovena (Figure 3.16) ranging in size from approximately 6 cm x 8 cm to 8 cm x 12 cm are present throughout this unit and are infilled with sediments similar to the 6 cm to 70 cm and 70 cm to 92 cm intervals of unit KC-1 (*i.e.*, recent to modern animal activity). Fe-Mn nodules <3 mm in size are present between 205 cm and 406 cm; the concentration of these nodules decreases from approximately 1% near the top of the unit to <<1% from 297 cm to 406 cm. Within this

unit, CaCO_3 precipitate is present, but decreases with depth until 406 cm; from 406 cm to 426 cm carbonate nodules are present. These nodules range in size from 2 cm x 4 cm to 2 cm x 6 cm. Despite the field observations of these carbonate nodules, laboratory results exhibit minor percentages of CaCO_3 (Figure 3.16, CaCO_3). This may be due to sample location (*i.e.*, localized CaCO_3 concentrations) or low concentrations of CaCO_3 in the matrix, as it has migrated to the nodule sites.

Paleosol-C: This paleosol exhibits a very weak, fine granular structure from 205 cm to 297 cm and a weak, fine granular structure from 297 cm to 341 cm (*e.g.*, Plate 3.5 F). From 341 cm to 406 cm the unit exhibits a moderately developed fine to medium sub-angular blocky structure.

Paleosol-D₂: This paleosol is recognized primarily by the presence of the following: granular (Plate 3.6 A) and sub-angular blocky (Plate 3.6 C) structure; a drastic change to a darker colour corresponding to elevated organic content (Figure 3.16); local highs in magnetic susceptibility and frequency dependence, and; a significant grain-size reduction. The latter denotes the base of paleosol-D₂ and is interpreted as a hiatus in deposition. Furthermore, structures in the Bmk horizon overprint a granular structure associated with the previous pedogenic event (*cf.* Plate 3.6 C and D) Together, these data suggest paleosol-D₂ had formed during a pedogenic event temporally separated from paleosol-D₁ formation (see below).

Interpretation: The sharp reduction in median grain size marks the transition between this unit and KC-3 below. The changes in median grain size represent a depositional hiatus that allowed the formation of paleosol-D₂ which is interpreted to have been a calcic dark-brown chernozem based primarily on micromorphological evidence, frequency dependence, CaCO_3 enrichment in lower horizon and the relatively dark coloured Ah-horizon. Above paleosol-D₂, the fine granular structure (upper 62% of unit) and sub-angular blocky structure (29% of unit) suggests pedogenic processes were active throughout formation of the unit. The presence of these structures suggests steady, cumelic formation of a regosol which also resulted in CaCO_3 precipitation in the Ah-horizon of paleosol-D₁ (Plate 3.6 B). This weak regosolic soil formation eventually evolved into an eluviated brown chernozem (paleosol-C)

Korostylievo - Paleosol D_(complex)

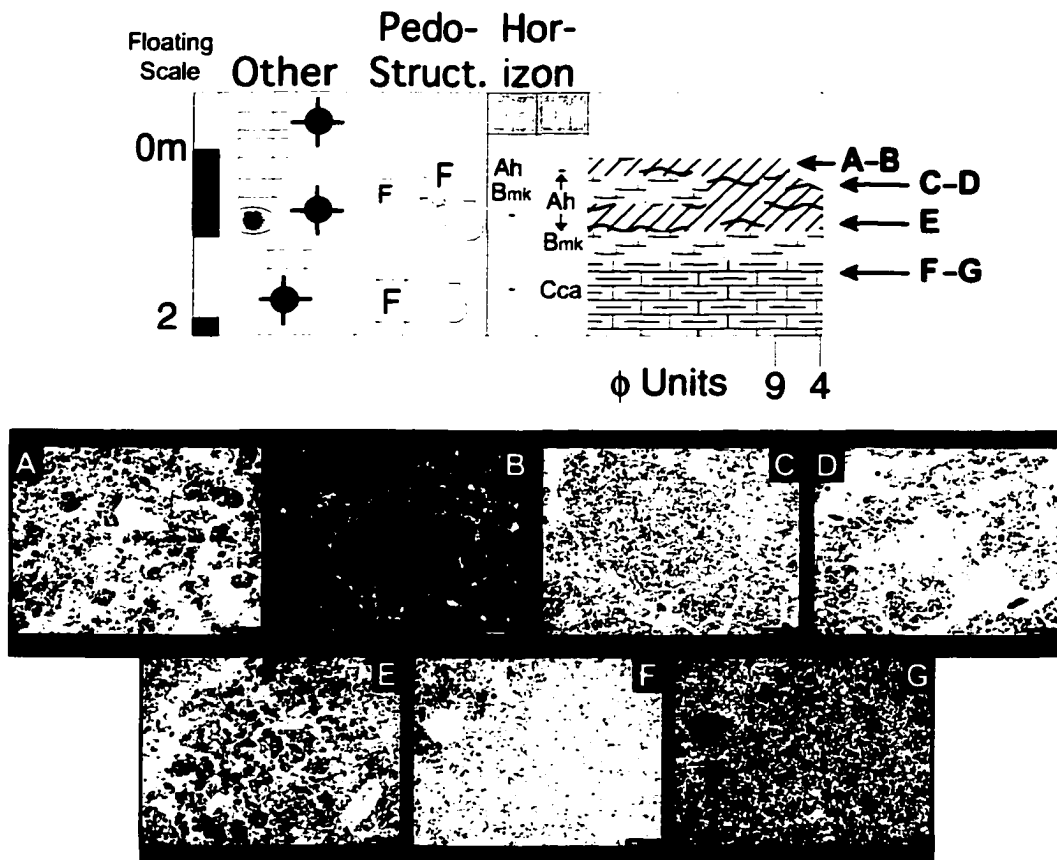


Plate 3.6. Photomicrographs of paleosols D₁ and D₂. **A.** Granular structure that exemplifies the Ah-horizon of paleosol-D₂; mag. 25x; PPL. **B.** CaCO₃ hypocoating that reflects overprinting CaCO₃ precipitation caused by subsequent regosol pedogenesis; mag. 100x; XPL. **C.** Sub-angular blocky ped associated with the Bmk-horizon of paleosol-D₂; mag. 100x; PPL. **D.** Coarser granular structure of paleosol-D₁ that is overprinted by the structure observed in "Plate C"; mag. 25x; PPL. **E.** Paleosol D₁ granular structure near the base of its Ah-horizon; mag. 25x; PPL. **F and G.** CaCO₃ hypocoating around void (greyish-zone in upper left of Plate F) and structureless parent material that represents the Cca horizon of paleosol D₁; mag. 25x; F, PPL; G, XPL.

due to changing soil forming parameters (*e.g.*, climatic changes). Given the soil types for paleosols C and D₂ that are suggested from field, laboratory and micromorphology data, paleosol-D₂ is associated with a mesophytic steppe environment within a semiarid climate whereas paleosol-C is a product of a xerophytic steppe environment. The parent material of this unit is interpreted to be fine-grained loess based on the lack of primary structure, grain-size and pedogenic structures observed

throughout the upper 91 cm of this unit (*i.e.*, subaerial deposition allowing pedogenesis).

KC-3: 426 - 700 cm

Lithic Description: This unit consists primarily of silty-clay loam, but does have end-members classified as silty clay and silty loam. The colour of the upper 30 cm of this unit (426 - 456 cm) is brown (10 YR 5/3 m); below 456 cm through 506 cm the colour gradually changes to light yellowish-brown (2.5 YR 6/4 m). Below 506 cm the colour lightens to yellowish-brown (10 YR 5/4 m) down to 580 cm, then darkens slightly



Figure 3.17. Krotovena within lithostratigraphic unit KC-3 (below paleosol D). Calcium carbonate precipitation crosscuts the contact between the parent material (brownish-yellow) and the krotovena (dark brown) suggesting the krotovena are not associated with recent animal activity, and may be related to paleosol D.

to brown (10 YR 5/3 m) towards the base of the unit. Very rare ($<<1\%$) Fe-Mn nodules up to 2 mm in diameter are present down to 506 cm below which, they increase in size to approximately 3 mm. The lower contact of this unit, inferred from changes in median grain size, is identified as gradational and planar.

Paleosol-D₁: A fine granular structure from 426 cm to 510 cm suggests the presence of an Ah-horizon. This horizon is also evident in thin section (Plate 3.6 D, E), magnetic susceptibility and frequency dependence of magnetic susceptibility (F_D). From 510 cm to 580 cm there is a fine, weak angular blocky structure that is apparent in addition to relatively high CaCO_3 content (Figure 3.16). Oval to irregular-shaped krotovena (Figure 3.17) ranging in size from 6 cm x 10 cm up to 10 cm x 30 cm are infilled with brown (10 YR 5/3 m) silty-clay-loam material similar to that observed in the upper most portion (426 -456 cm) of unit KC-3. Krotovena present between 540 cm through 650 cm exhibited calcium carbonate precipitation that often crosscuts krotovena/matrix boundaries (Figure 3.17).

Paleosol-E₂: Unlike other paleosols described herein, paleosol-E₂ (and E₁ - *vide post*) were detected only through laboratory analyses (Figure 3.16) and micromorphological investigations. Between 700 cm and 650 cm, there is a plateau in both magnetic susceptibility and frequency dependence of susceptibility suggesting that pedogenic processes had acted on the parent material. These both correspond to slight decreases in organic material (up section), and peaks in Fe₂O₃ and Al₂O₃ within that same interval. Together with weak granular structure (Plate 3.7 A, B) and moderately developed sub-angular blocky structure (Plate 3.7 C), this paleosol is interpreted as an orthic brown chernozem developing in a steppe environment.

Interpretation: The increase in median grain-size at the base of the unit is interpreted as an increase in depositional energy thereby allowing larger grain sizes to be entrained. During this period, there is also a decrease in organic matter, and corresponding plateaus (that decrease above 650 cm) in magnetic susceptibility and frequency dependence curves. The relative magnitude of the frequency dependence curve, suggests paleosols D₁ and D₂ are better developed than paleosols E₁ and E₂. Therefore, the following is proposed: Paleosol-E₂ represents an orthic brown chernozem forming in a relatively dry steppe environment dominated by aeolian deposition. The higher soil productivity inferred from the higher frequency dependence of magnetic susceptibility and thicker soil horizons suggests paleosol-D₁ was an orthic dark-brown chernozem forming under more moist steppe conditions whereas paleosol-D₂ is interpreted as an calcic dark-brown chernozem with thinner horizons and less-developed structures forming in dryer climatic conditions.

The parent material of this unit is interpreted to be a primary loess given the above interpretations, the nature of the grain size characteristics (*i.e.*, relatively coarse) and the lack of primary structures. Characteristics and context of paleosol-D₁ suggests aeolian deposition would have terminated or been greatly reduced relative to preceding and subsequent accumulation rates.

Korostylievo - Paleosols E₂, E₁ and F₂

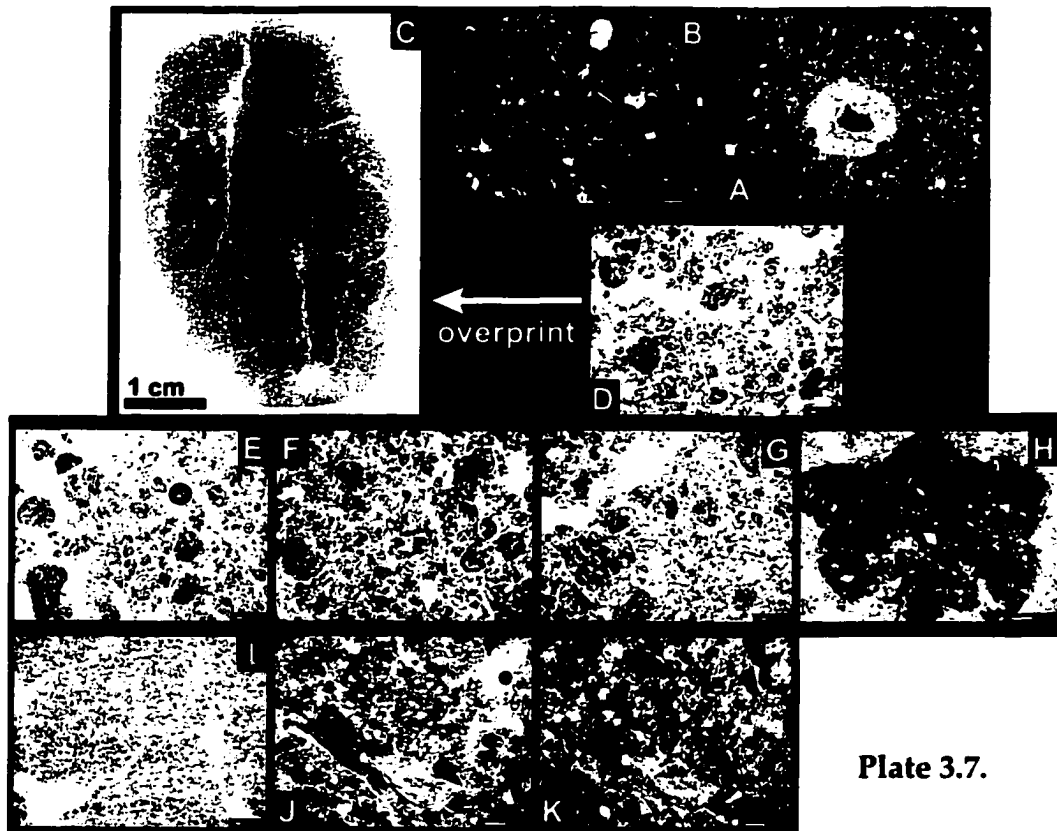
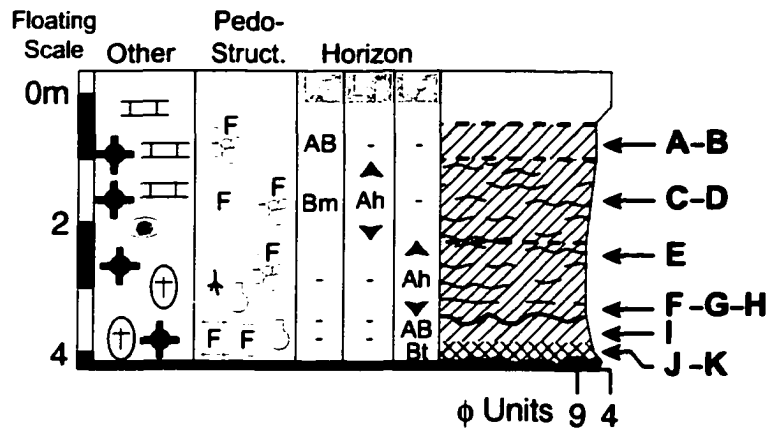


Plate 3.7.

Photomicrographs of paleosols E₂, E₁ and F₂. A. Granular structure and overprinting CaCO₃ hypocoating around void in paleosol-E₂; mag 25x; XPL. B. Iron nodule and thin clay cutan surrounded by granular structure; mag. 100x; XPL. C. Sub-angular blocky structure of Bmk horizon. D. Granular structure of paleosol-E₁ which is overprinted by the Bmk horizon of paleosol-E₂; mag. 25x, PPL. E, F and G. Well-developed granular structure of paleosol-F₂; mag. 25x; PPL. G. Impregnative Fe-Mn nodule; mag. 100x; PPL. I. Sub-angular blocky peds within the AB-horizon of paleosol F₂; mag. 25x; PPL. J and K. Clay infillings representing the last event of significant clay translocation at Korostylievo; mag. 100x; J, PPL; K, XPL.

KC-4: 700 - 1017 cm

Lithic Description: The materials comprising the upper portion (700 - 830 cm) of the unit consist of massive brown (10 YR 5/3 m) silty-clay with a weak brownish-grey gley (2.5 Y 6/2 m) and corresponding mottling (no Munsell colour); elliptical mottles typically exhibit a vertical major axis of 5 cm to 7 cm and a minor axis of 1 cm to 2 cm. CaCO₃ and Fe-Mn precipitation are present within this interval. From 830 cm to 855 cm the colour darkens to brown by a value of 1 (*i.e.*, 10 YR 4/3 m) and fines to a structureless clay. Fissures infilled with lighter material (yellowish brown: 10 YR 5/8 m) from above are evident when in contrast with the darker matrix of this unit. Below 855 cm, the unit's colour further darkens to dark brown (10 YR 3/3 m) near a local high in organic content at 902 cm (Figure 3.16). From 940 cm to 980 cm Fe-Mn nodules up to 2 mm and CaCO₃ nodules <4 cm are present. Finally, the interval below 940 cm exhibits a well developed rectilinear fracture pattern (Figure 3.18) which penetrates 10 cm to 50 cm into the underlying unit. The spacing between the darker tongues of sediment is 30 cm to 40 cm by 15 cm to 20 cm, and the majority of fissures exhibit orthogonal intersection. Upon closer inspection, there is also a smaller quasi-rectilinear pattern with dimensions ranging up to 8 cm x 10 cm; this set appears to crosscut the larger set. The upper contact of this unit is denoted primarily by the relatively sharp decrease in median grain size, while the lower contact is identified by a corresponding increase in the median grain size; the unit itself, being characterized by a consistently fine median grain size (Figure 3.16)

Paleosol-E₁: Similar to paleosol-E₂, this paleosol is recognized through the following: elevated organic matter content, peaks in frequency dependence (F_p), a plateau in magnetic susceptibility, and pedogenic structure identified through thin section. Moderately developed granular structure (Plate 3.7D) supports the interpretations of Ah-horizon formation. As this is the only identified horizon associated with this paleosol, it is interpreted to be a cumulic regosol.

Paleosol-F₂: A local high in organic matter between 830 cm and 855 cm (Figure 3.16), supported by strongly developed granular structure (Plate 3.7 E, F and G) suggests the presence of the Ah-horizon. Below 855 cm, this granular structure is also recognized in field descriptions



Figure 3.18. Rectilinear fissure pattern developed within lithostratigraphic unit KC-4 and beneath paleosol F_2 . **A.** Relationship between paleosol F_2 , lithostratigraphic unit KC-4 and fissures; the contact between F_2 /KC-4 and KC-4 is an average of the actual contact which is irregular and abrupt. **B.** Close-up of rectilinear pattern (plan view). **C.** Close-up of fissure tails.

along with manganese coated root casts and krotovena down to a depth of 940 cm. Krotovena are infilled with a yellowish-brown (10 YR 5/6 m) silty-loam exhibiting a high carbonate content relative to the surrounding material. One such krotovena (Figure 3.19) at a depth of approximately 875 cm, consists of an infilled chamber and connecting tunnel which spans 66 cm in overall length and 50 cm in overall height. The modal krotovena shape in this unit, however, was oval and ranged in size from 3 cm to 11 cm by 10 cm to 12 cm. Some fine fissures infilled with dark material crosscut the smaller krotovena. At a depth of 940 cm there is a sharp intra-unit pedogenic contact, below which weak sub-angular blocky structure (Plate 3.7 I) and a decreasing organic matter trend are observed, suggesting the presence of an AB-transitional horizon. At 990 cm, a Bt-horizon is interpreted from the presence of translocated clay (Plate 3.7 J and K). The presence of CaCO_3 precipitate in void spaces (Plate 3.7 K) and an associated increase in CaCO_3 wt. percent (Figure 3.16) is attributed to subsequent leaching of carbonates



Figure 3.19. Large krotovena with connected chamber and tunnel within unit KC-4 and paleosol-F₂ (Figure 3.16) at a depth of ~875 cm. Infilling sediment has been brought down from overlying sediments.

after Bt-horizon formation. These data suggest paleosol-F₂ was an eluviated brown chernozem.

Interpretation: The basal portion of this unit comprising the Bt and AB horizons of paleosol-F₂ is interpreted as fine-grained primary loess based on relative grain size and massive primary structure. The overlying clay can be interpreted as a lacustrine deposit composed of aeolian-transported fines. However, the lack of primary stratification allows an alternative interpretation: grain size pretreatments may have broken down fine silt-sized aggregates entrained and deposited by aeolian processes. From this, paleosol-F₂ is interpreted to have been an aggrading eluviated brown chernozem that formed as climate deteriorated from the preceding soil forming interval. The addition of new parent material through aeolian processes provided an abundant calcium supply for subsequent translocation out of the Ah horizon thereby overprinting the Bt horizon. Continued climatic deterioration produced exceedingly dry and cold conditions that resulted in the seasonal frost/desiccation fissures that crosscut krotovena within unit KC-4.

Following the formation of paleosol-F₂, pedogenesis was greatly reduced, but was still enough to allow the granular structure of paleosol-E₁ to form in a cumulic environment. Based on the granular structure, and on relative peaks in magnetic susceptibility and frequency dependence (F_D), this paleosol is interpreted to be a cumulic regosol which is overprinted by the sub-angular blocky structure of the Bm-horizon associated with paleosol-E₂.

KC-5: 1017 - 1448 cm

Relative to the overlying units, unit KC-5 is characterized primarily by its lithologic heterogeneity; consisting of silty-loam, silty-clay loam, silty-clay, clay and heavy clay. Overprinting the highly variable lithic component are two paleosols (F₁ and G). Given this situation, a slightly different approach is used to describe this unit (*vide post*).

Descriptions: The upper contact of the unit is identified by a change from the consistently fine-grained material of unit KC-4, to a coarser and variable median grain size; results for unit KC-5 also exhibit an overall coarsening trend that increases with depth (Figure 3.16). The following paragraphs describe how individual characteristics vary with depth.

Colouration of this unit varies greatly (Figure 3.20): from 1017 cm to 1032 cm the unit is brown (10 YR 5/3 m) which darkens slightly to brown (10 YR 4/3 m) from 1032 cm to 1098 cm; from 1098 cm to 1170 cm the unit consists of several colours that include the colour of the low-carbonate matrix (brown - 10 YR 5/3 m), the carbonate rich matrix (yellowish-brown - 10 YR 5/4 m), iron staining (brown - 7.5 YR 5/4 m), gley (light yellowish-brown - 2.5 Y 6/4 m), and krotovena (brown - 10 YR 4/2 m and very dark greyish-brown - 2.5 Y 3/2 m).

Two sets of fissure-infill structures were observed in this unit: a darker set (10 YR 4/3) penetrating approximately 3 cm to 4 cm into the top of the unit, and a lighter set originating from the base of paleosol-F. The latter set of fissure-infill structures are light yellowish-brown (10 YR 6/4 m) and are approximately 4 cm in width at their origins, bifurcating midway through the fissures and pinching out at a maximum depth of approximately 1220 cm. Some of these fissure-infill structures crosscut the krotovena present within this interval (1098 - 1170 cm).

Pedogenic structure is strongest in the upper two metres of the unit. From 1017 cm to 1027 cm a weak fine granular structure is present and is overprinted by a moderately developed, fine angular blocky structure that continues down to a depth of 1290 cm. Between 1098 cm and 1170 cm, this fine angular blocky structure is attenuated by a moderate to well developed medium angular blocky structure; clay cutans are observed within this interval. From 1290 cm to 1315 cm only a very weak



Figure 3.20. The lower portion of the Korostylievo composite section. Three paleosols are observed: F_2 (top of photo), F_1 (upper portion of photo) and G (lower half of photo) Lithostratigraphic unit KC-5 is characterized by heterogeneity that is unique to the unit.

fine angular blocky structure is present. A fine granular structure dominates the unit from 1414 cm to 1448 cm.

The average CaCO_3 content is moderate relative to the other units, but also exhibits a relatively high degree of variability (Figure 3.16, CaCO_3). Calcium carbonate concretions are present only from 1098 cm to 1170 cm; within this interval they are vertically oriented and range in size from 2 cm x 4 cm up to 3 cm x 4 cm. Zones of relatively enhanced CaCO_3 precipitation, however, are observed between: 1017 cm to 1098 cm, 1170 cm to 1212 cm and 1370 cm to 1354 cm. Iron and manganese concentrations are present from

1017 cm to 1170 cm and from 1317 cm to 1414 cm. Manganese nodules are observed within the 1098 cm to 1170 cm interval and range in size up to 3 mm.

Bioturbation and krotovena are prevalent within this unit, with individual krotovena present at 1137 cm, 1400 cm, and 1440 cm ranging in size from 10 cm x 31 cm and 24 cm x 28 cm chambers to 5 cm x 23 cm channels. Between 1317 cm and 1354 cm however, the krotovena are pervasive; krotovena observed within this zone range in size from 7 cm x 10 cm up to 13 cm x 19 cm. Many of the krotovena in this zone overprint one another and are therefore difficult to discern. In addition to

krotovena, there is a zone of concentrated rootlet casts observed in this unit; fine carbonate root tubules are observed between 1170 cm and 1212 cm. The rootlet symbol observed at approximately 1300 cm (Figure 3.16) identifies the interval where modern roots were growing through the colluviated material into the cleaned (*in situ*) face of the described section.

Paleosol-F₁ Interpretation: The granular structure of the Ah-horizon observed in the field between 1017 cm and 1027 cm extends down to approximately 1090 cm based on micromorphological evidence (Plate 3.8 A and B). Immediately below the Ah-horizon, weak granular structure is present within sub-angular blocky structure and in association with clay illuviation (Plate 3.8 C, D, E and G), suggesting that the early phases of this paleosol were cumulic. Given the above characteristics, this paleosol is interpreted to be a dark-grey chernozem that formed in a forest-grassland transition zone.

Paleosol G_(complex) Interpretation: Strong granular structure (Plate 3.8 F, H) marks the location an Ah-horizon associated with paleosol-G formation. Carbonate precipitation within this unit appears to have been followed by clay translocation (Plate 3.8 G, J, L, M and N) as clay cutans are observed coating depleted carbonate nodules (Plate 3.8 G) and void spaces within carbonate nodules (Plate 3.8 K, L and M). Remnant granular structure near the base of unit KC-6 (Plate 3.8 O), in association with thin clay cutans that coat voids (Plate 3.8 P and Q) suggest there may have been an earlier phase of soil formation, however, intensive bioturbation has severely degraded the pedogenic horizons needed to identify a separate paleosol. Given the CaCO₃ and clay cutan associations, this soil is interpreted to be polygenetic. Initial phases of pedogenesis (by association with lower AB-horizon of Plate 3.8 O, P and Q) are difficult to interpret due to intensive bioturbation. The following phase of soil development, however, is interpreted to have occurred in a steppe environment. During this period, a calcareous brown chernozem likely formed, as evident from the strong granular structures and carbonate precipitate. Subsequently, the climatic conditions changed such that an undifferentiated luvisolic soil formed under forest-steppe or forested conditions. When available carbonate was

Korostylievo - Paleosols F₁ and G_(complex)

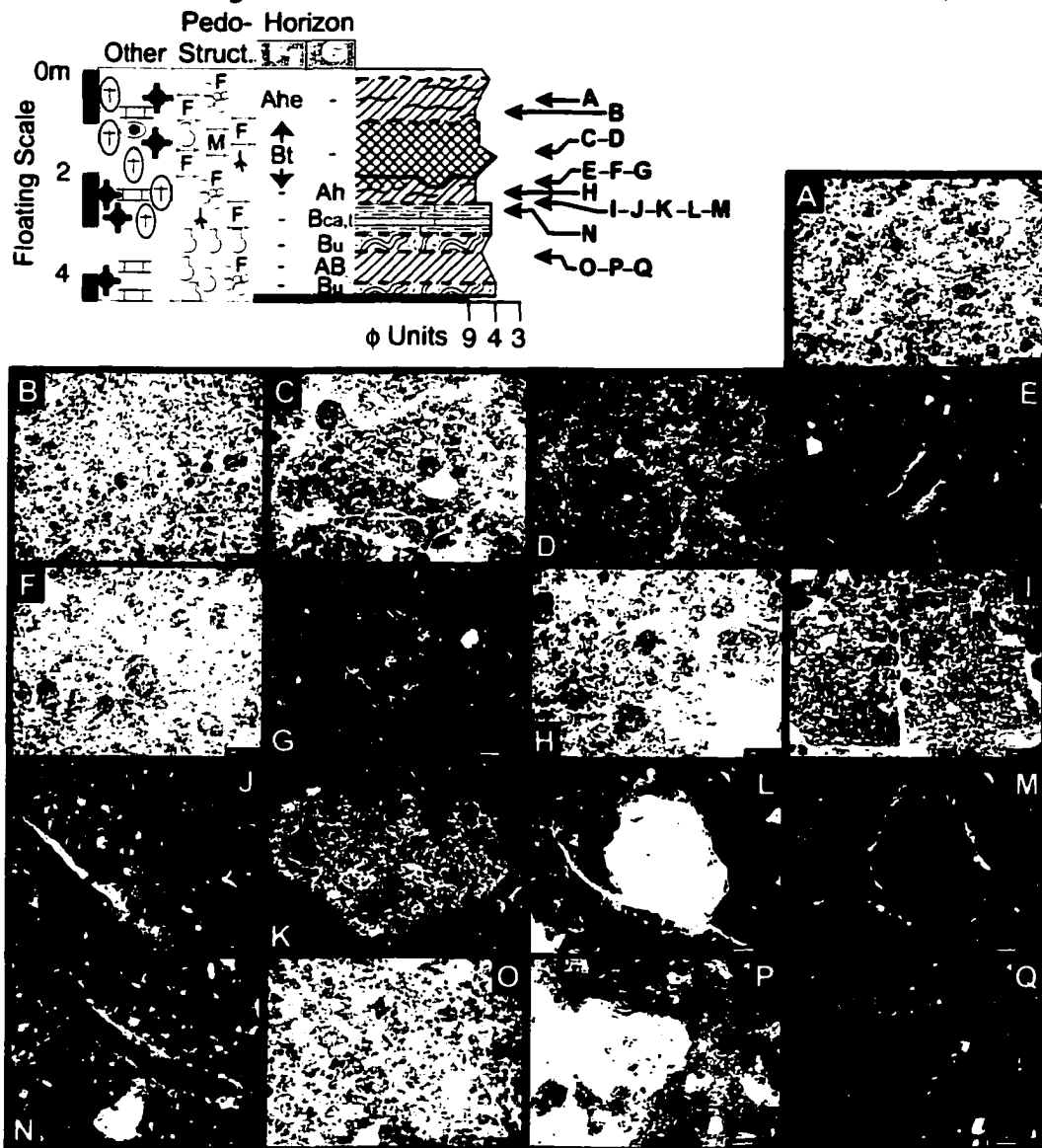


Plate 3.8. Photomicrographs of paleosols F₁ and G. **A and B.** Granular structure and organo-mineral complexes, paleosol-F₁; mag. 25x; PPL. **C and D.** Sub-angular blocky structure and illuviated clay (repectively) that overprint weak granular structure, paleosol-F₁; mag. 25x; C, PPL; D, XPL. **E.** Clay cutans that overpring paleosol-G, mag. 25x; XPL. **F.** Strong granular structure, paleosol-G; **G.** Clay cutans coating depleted carbonate nodule; mag. 100x; XPL. **H.** Strong granular structure, paleosol-G below the influence of paleosol-F₁ overprint; mag. 25x; PPL. **I and J.** Sub angular blocky structure and clay cutan (light zone in J); mag. 25x; I, PPL; J, XPL. **K.** CaCO₃ nodule with clay cutans coating internal voids; mag. 25x; XPL. **L and M.** Close-up of a cutan coating a void within a CaCO₃ nodule (Plate K); mag. 100x; L, PPL; M, XPL. **N.** Thick clay cutans coating void; mag. 25x; XPL. **O.** Granular AB-horizon; mag. 25x; PPL. **P and Q.** Cutans observed in same sample as Plate O; mag. 100x; P, PPL; Q, XPL.

removed from the Ah-horizon, the pH would have been reduced providing conditions more conducive for clay and sesquioxide translocation (Plate 3.8 J-N and Figure 3.16 respectively), thereby overprinting the previously translocated CaCO_3 precipitate.

KC-6: 1448 - 1452 cm

Lithic Description: This unit consists of a pale-yellow (2.5 Y 8/2 m) marl easily identified as a global maximum peak on the CaCO_3 graph, and a sharp decrease in F_D (Figure 3.16). It is laterally discontinuous and has an abrupt planar lower boundary.

Interpretation: Localized ponding resulted from changing drainage networks that immediately followed deglaciation of the local area. The presence of these small, localized ponds facilitated carbonate accumulation and the development of this marl horizon.

KC-7: 1452 - 1478 cm

Lithic Description: This unit consists of a fine sandy-silt that contains some granules. The dominant colour within this unit is yellowish-red (5 YR 5/8 m). The median grain size of this unit is 58.7 microns; due to scaling factors, this data point (sample K-2-98-19) is not plotted in figure 3.16 (Median Grain Size). The lower contact is abrupt and wavy.

Interpretation: The abrupt lower contact with the diamicton, in conjunction with the coarse grain size suggests that this unit was a deglacial glaciofluvial deposit.

KC-8: 1478 cm -

Lithic Description: This unit consists of a strongly gleyed / mottled diamicton with a sandy-matrix. Clasts make up approximately 10 % of the unit; they are well rounded to sub-angular with an average of sub-angular; the clast sizes range from <1 cm to 35 cm with the average being 3 cm. Basic lithologies observed included: sandstone, limestones, and various granitoids; the sedimentary clasts observed within the till are much more abundant than the granitoid clasts.

Interpretation: Given the lithic content, the context in which this deposit is observed (Oka-Don Plain), and the location relative to known ice limits, the current author supports the conclusions of Krasnenkov *et al.* (1984) and interprets this diamicton as the Don Till (*cf.* Figure 1.8).

Korostylievo Composite Section

As previously stated, the Korostylievo Composite section is comprised of two sections (KS1 and KS2) which are correlated through visual levelling techniques based on diagnostic horizons (*vide* Figure 3.14). The composite section (KC) consists of 8 primary lithologic units, 6 primary pedogenic units and one set of pedogenic horizons (*i.e.*, E_2 and E_1). In order to aid in the explanation behind the subdivision of some of these paleosols, another composite section diagram is presented which scales the data-trends to maximize exaggeration of the paleosol data at the expense of the modern-day soil data (Figure 3.21).

Five optical luminescence dating samples were obtained from this section; sullegic and strategic factors dictated that of these five samples, only one sample was processed to obtain burial age (KCSL3). This sample yielded an age of 57 ± 3 ka calendar years. Procedures used to obtain this age follow from Little *et al.* (in press); laboratory results are presented in Appendix B.

Korostylievo Site: relative data interpretations

The complex sediment depositional history and overprinting nature of soil development has made distinguishing different soil forming events difficult. Therefore, when interpreting the depositional history and identifying different soil forming events, reference made to data trends is imperative. Comparison of results between units has yielded several interesting relationships.

Rock magnetic parameters, LOI results and geochemical data from the Korostylievo site have proven to be instrumental in differentiating pedogenic horizons and estimating soil productivity. Although the magnetic susceptibility and F_D trends are in close agreement, there are fundamental differences that allow a more refined interpretation of the pedostratigraphy. In order to do this, the relationships that these data sets have in the modern soil solum (*cf.* Figure 3.16) are used as a model to be compared with paleosol horizons (Figure 3.21).

Above the marl unit (KC-6) both the magnetic susceptibility and frequency dependence of magnetic susceptibility (F_D) increase, however, the rise in the F_D is more abrupt suggesting an increased presence of ultra-fine (sub-micron) grains on the superparamagnetic/single domain boundary (Heller and Evans 1995). When combined with

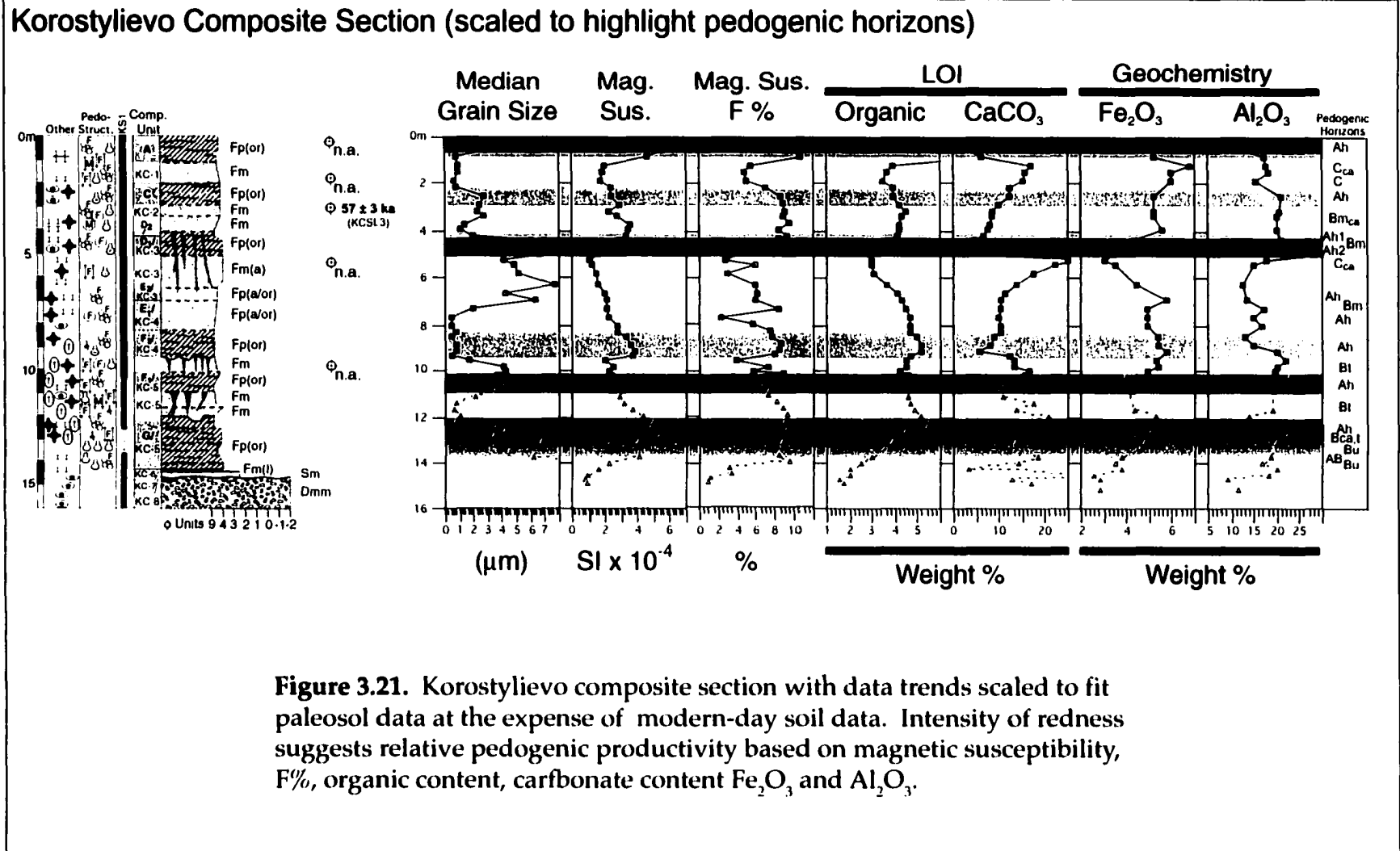


Figure 3.21. Korostylievo composite section with data trends scaled to fit paleosol data at the expense of modern-day soil data. Intensity of redness suggests relative pedogenic productivity based on magnetic susceptibility, F%, organic content, carbonate content Fe₂O₃ and Al₂O₃.

pervasive bioturbation, and the pedogenic structures observed within paleosol-G, the production of such grains is interpreted to have also occurred during pedogenesis. These grains would have been produced in an upper mull-type, soil horizon setting. Then, through translocation (down to the till and marl which act as an aquifuge) and through bioturbation processes, these small grains were dispersed throughout the unit resulting in the "box-shaped" curve represented in figure 3.21 between *ca.* 1200 cm and *ca.* 1400 cm.

Frequency dependence of magnetic susceptibility (F_D) decreases above paleosol-G and does not peak again until the top of paleosol F_1 , which, together with physical evidence, suggests the last pedogenic event to affect the paleosol-G_(complex), *i.e.*, luvisolic (undifferentiated) soil, was the result of an interglacial soil-forming event. The intervening non-soil interval between paleosols G and F_1 would therefore represent deposition during a glacial event followed immediately by another interglacial-type event resulting in paleosol- F_1 (dark-grey chernozem). Both magnetic susceptibility and F_D show relatively strong and abrupt peaks within paleosol- F_2 . This, coupled with the presence of granular structure, root traces and krotovena in the upper F_2 paleo-pedon, and fine blocky structure of a Bt horizon in the lower F_2 paleo-pedon (Plate 3.7), suggest that a relatively pronounced eluviated brown chernozem had developed.

From 810 cm to 780 cm the magnetic susceptibility drops slightly and F_D decreases rapidly suggesting retarded pedogenic processes relative to the preceding interval. Organic matter content, however, does suggest that there is some authigenic organic matter being produced as the sediments accumulate (*i.e.*, paleosol E_1 and E_2 formation). The decrease in magnetic susceptibility changes to a plateau at depths of 750 cm through 650 cm; this magnetic susceptibility plateau corresponds to another peak in F_D suggesting pedogenesis may have increased and stabilized at a higher level of soil productivity during formation of paleosol E_2 . This is corroborated by micromorphological evidence. Above E_2 , magnetic susceptibility, F_D , organics and $Fe_2O_3\%$ all reach local minima within KC-3 suggesting little or no soil formation during deposition. An increase in all of the aforementioned parameters does occur, however, at a depth of approximately 500 cm.

Above *ca.* 500 cm, magnetic susceptibility, F_D and $Fe_2O_3\%$ increase, reaching local maxima between 410 cm and 380 cm; within this interval organic matter also plateaus. All of these support the existence of paleosol-D (consisting of D_1 and D_2 *vide post*). Given the sediment and paleosol characteristics outlined in figure 3.21, it appears that post-paleosol-D soil formation continued, albeit at a reduced rate and culminating between approximately 300 cm and 205 cm (paleosol-C). Pedogenic overprinting from this phase of soil development occurs down to approximately 380 cm.

The final two zones of interest are the local magnetic susceptibility and F_D minima that occur between *ca.* 200 cm and *ca.* 100 cm, and which also correspond to a minimum in percent organic matter. Together, these support a non-soil-forming interval; any pedogenic features present within this zone are attributed to modern-day soil formation and overprinting. These minima in data are promptly followed by sharp increases that are associated with modern-day soil formation.

Korostylievo Site Depositional Environment: overview

The sequence of strata at the Korostylievo site represent the type section for the region (Upper Don Basin). Lithic and pedogenic description of the strata present at the Korostylievo site agree well with previously documented observations (*e.g.*, Krasnenkov *et al.* 1984). The only notable difference between descriptions presented herein, and those presented in previous works are the textural classifications of sediments; the Russian system bases textures on different criteria than the Canadian system that is used in this dissertation (*cf.* Lysenko 1971; his Table 1, pp. 16-17). Despite this apparent difference, Krasnenkov *et al.* (1984) observed several "loamy" units and at least seven humus horizons (lower two are combined), that represent 1 soil and 6 paleosols between the modern day surface and the diamicton. According to their interpretations, the diamicton (KC-8) is a till associated with the Don Glacial maximum; the overlying 2 humus horizons (paleosols G and F_1) represent soils of the Muchkap Interglacial; the next two soils (moving up-section) represent the Likhvin interglacial (paleosols F_2 and $E_{undifferentiated}$); overlying these are deposits are straw-coloured massive "typical" loess inferred to be deposited during the Dnieper Glaciation;

the “Mezin soil complex” comprises two soils (paleosols D and C according to Krasnenkov *et al.* 1984) and is interpreted as a weak steppe-type soil series that overlies the loess of Dnieper Glaciation and; the uppermost soil represents a contemporary orthic black chernozem (soil-A).

To further advance the depositional environment interpretations presented above, without inferring absolute time associations (*vide post* for temporal correlations), a detailed examination of units described herein will be discussed below.

The diamicton (KC-8) present at the base of the section contains not only local sandstone (*cf.* Figure 1.5), but also erratic granitoids suggesting a glacial transport mechanism and till deposition. A lack of significant topography to induce gravity debris flows also supports this interpretation. Overlying sands and coarse grained marl (units KC-7 and -6 respectively) are interpreted as remnants of deglacial glaciofluvial sediments and local ponding of water. The highly gleyed nature of these beds is a post-depositional phenomenon that was imparted to the sediments by nested water table fluctuations; a function of the underlying till acting as an aquifuge.

Unit KC-5 is interpreted as having a predominantly aeolian genesis based on grain size data. Given this interpretation, the fluctuating nature of the grain size data (Figure 3.21: Grain Size) is attributed to changing energy conditions that may reflect deposition during a chaotic deglacial phase following the full glacial phase represented by units KC-7/6 and the underlying till (KC-8). During the KC-5 phase of deposition, pedogenic processes were active. Initially, the proximal deglacial environment gave way to undifferentiated soil-forming conditions as evident from AB- and Bu-horizons comprising the lower paleo-pedon within paleosol-G. The continued deposition and climatic amelioration allowed a steppe environment to follow which resulted in an early phase of the upper paleo-pedon of paleosol-G, *i.e.*, calcareous brown chernozem. Then, given the extremely fine nature of the sediment between 1150 cm and 1210 cm, a period of relatively calm conditions ensued (*e.g.*, distal ice front position). This inferred depositional hiatus and the continued climatic amelioration associated with it, allowed the

formation of an undifferentiated luvisolic soil within a mixed-forest environment (latter phase of the upper paleo-pedon comprising paleosol-G). These calm conditions gradually gave way to increasing depositional energy with the advent of climatic deterioration (upper KC-5) that ceased for a brief period of time (grain size low at *ca.* 1020 cm). The ensuing warm period allowed the forest-grassland transition zone to migrate to the site, resulting in the development of the dark-grey chernozem denoted by paleosol-F₁.

The cessation of F₁ pedogenesis was followed by the continuation of a relatively short-lived cold period that is responsible for the deposition of the parent material in which paleosol-F₂ formed. The consistently fine-grained sediments observed within this unit may represent lacustrine deposition of aeolian-transported fines. The lack of primary structure, however, conflicts with a lacustrine interpretation for its origin. Alternatively, grain size pretreatments may have broken down fine silt-sized aggregates that were transported to the site; consequently, the sediment appears finer than what was actually deposited and hence, is tentatively interpreted to be fine-grained loess; the subaerial depositional environment thereby allowing the formation of paleosol F₂. Because of this ambiguity, however, the interpretation of this fine portion of KC-4 is speculative.

The subsequent attenuation of soil formation inferred from pedogenic characteristics (*i.e.*, magnetic susceptibility plateau, F_D peaks, relatively high organic content and granular structure *etc.*) allowed paleosol-E₁ to be interpreted as a cumulic regosol that formed during a cold and dry period. The increasing grain size (up-section) within this unit lends support to this argument (*i.e.*, increasing deposition energy) and suggests increasing climatic deterioration through time until sedimentation rates decreased thereby allowing an orthic brown chernozem (paleosol-E₂) to develop in a steppe environment.

Fluctuations in sediment texture and changes in character of the sediment (*i.e.*, lightening of sediment due to decreasing organic matter) suggest that the region experienced continued climatic deterioration that eventually resulted in the cessation of E₂-pedogenesis and the continuation of aeolian deposition (above paleosol-E₂).

The KC-3/KC-2 boundary is marked by a sharp decrease in grain size. This is interpreted as a depositional hiatus that allowed the formation of paleosol-D₁. Pedogenic characteristics observed immediately above paleosol-D₁ suggest that slow aeolian deposition was coeval with cumulic-type soil formation which resulted in paleosol-D₂. As accumulation rates increased, attenuation of soil-forming processes followed and imparted a regosolic character between 406 cm and 297 cm.

The presence of paleosol-C at *ca.* 200 cm suggests that the preceding aeolian deposition was reduced or had ceased. The coarser-grained sediments deposited prior to this depositional hiatus were then overprinted by soil-forming processes (paleosol-C). As this interstadial came to an end, loess deposition increased and deposited KC-1. Presumably, the primary grain size of this unit would have gradually increased up-section until its culmination during the last glacial maximum. However magnetic susceptibility, F_D, organic content, carbonate content and Al₂O₃ data all correspond well to the observed grain size change, suggesting that the relatively fine-grained portion of KC-1 is the result of pedogenic overprinting by the translocated fines and sesquioxides from the A-horizon to the B-horizon of soil-A (*i.e.*, post last-deglaciation).

Mikhailovka Sections

The Mikhailovka sections are located within a Cretaceous chalk quarry in the town of Mikhailovka, approximately 200 km southeast of the Korostylievo site (Table 1.1). The town is situated northwest of the Medveditsa River and south of two of its tributary streams (Figure 1.1). Four primary sections at this site exhibit a total of seven well to moderately-well developed pedogenic horizons, and two weakly developed pedogenic horizons. These soil/paleosol horizons overprint 9 of the 14 major lithostratigraphic units observed at the site. None of these sedimentary sequences have been formally described prior to this study.

Although Mikhailovka exhibits successive sections that can be correlated into a composite section, the site does differ significantly from all other study sites. At this site, local unconformities and undulating paleotopography are observed; the construction of the composite section considers these phenomena.

The sections are spread along 1960 m of vertical to near-vertical exposures (Figure 3.22). The minimum and maximum distances between sections used in the construction of the composite section are 40 m and 1680 m respectively (Table 3.2). The correlation of sections separated by relatively large distances (*i.e.*, no direct levelling is possi-

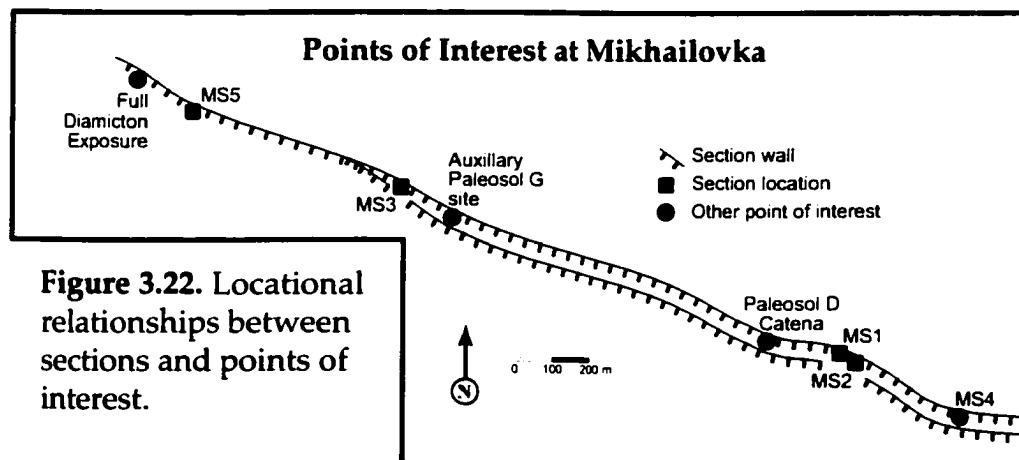


Figure 3.22. Locational relationships between sections and points of interest.

Table 3.2. Distances between sections used to construct the composite section diagram.

Section	MS1	MS2	MS3	MS5
MS1	0 m	40 m	1120 m	1640 m
MS2	40 m	0 m	1160 m	1680 m
MS3	1120 m	1160 m	0 m	520 m
MS5	1640 m	1680 m	520 m	0 m

ble) required the use of multiple criteria in order to fix their stratigraphic position within the composite section.

Mikhailovka Sections No. 1 and No. 2: Lithostratigraphy and basic paleosol description

The upper two sections at the Mikhailovka site (MS1 and MS2) are separated by only 40 m, hence, they can be correlated by visual leveling the base of paleosol-D between MS1 and MS2. For this reason, these two sections are presented in one section diagram (*cf.* KS1 and KS2). For simplicity, all unit names, regardless of section will be denoted as 'MS1' followed by the unit number; black vertical bars on figure 3.23 illustrate the relationship between MS1 and MS2 on the section diagram. With the exception of the upper portion of MS1-1 and pedo-unit A (partially removed by pit machinery), there are no unconformities observed within or between these two sections. There are however, two unconformities within this stratigraphic sequence farther east, in the vicinity of MS4 (Figure 3.22) and hence that section is not discussed herein. Photographs of pedogenic horizon relationships within MS1 and MS2 are presented in figures 3.24 and 3.25. Due to the overlapping nature of MS1-4 (MC-4) and MS1-5 (MC-5) with corresponding units in MS3, the interpretations of these units are presented under the subheading "Mikhailovka Section No. 3: Lithostratigraphy and basic paleosol description".

MS1-1: 0 - 145 cm (MC-1: 0 - 145 cm)

The upper portion of this unit has been removed during pit activity. Judging from field reconnaissance above the section, not more than 1 m of sediment is suspected to have been removed.

Lithic Description: Sediments comprising the upper 35 cm (*in situ* deposits) of this unit consist of very dark grey (10 YR 3/1 d) silty-clay. At 35 cm, the sediment coarsens slightly (Figure 3.23: Median Grain Size), and the colour gradationally changes to dark greyish-brown (10 YR 4/1 d); within this interval 20 cm long subvertical fissures are observed. These fissures are typically 1 cm to 2 cm wide at their origins, and <8 mm wide at a depth of 55 cm. From 55 cm to 80 cm, the sediment fines to clay and the unit colour lightens to dark yellowish-brown (10 YR 4/4 d) -- most likely the result of much higher calcium carbonate

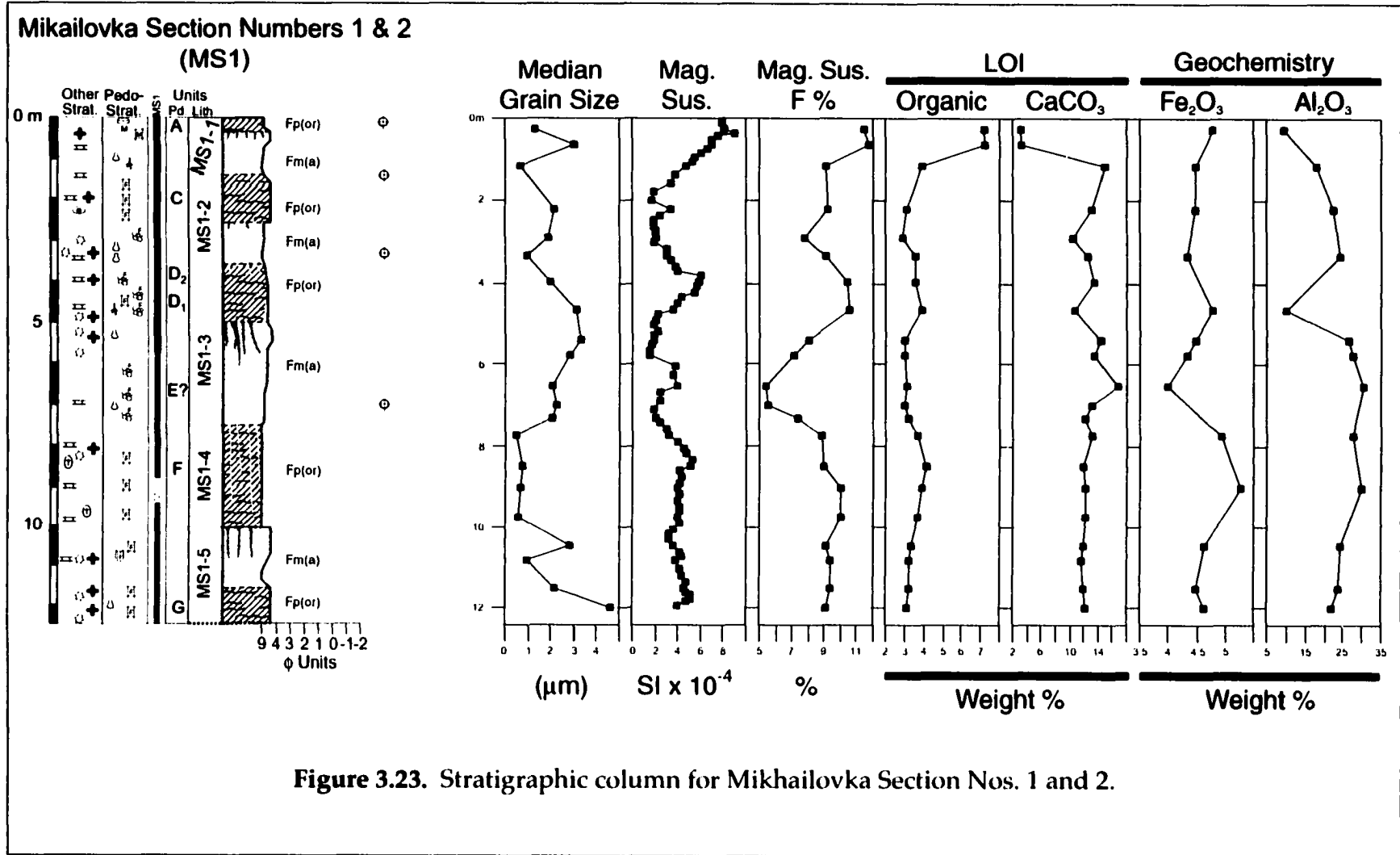


Figure 3.23. Stratigraphic column for Mikhailovka Section Nos. 1 and 2.



Figure 3.24. Photo and trace of stratigraphy at sections MS1 and MS2. The “layer-cake” stratigraphy between the two sections enabled direct visual leveling for correlation. The primary soil horizons (visible in photo) are labeled A, C, D, and F in the underlying trace.

concentrations (Figure 3.23). The basal contact of this unit is gradational and planar.

Soil-A: The upper 35 cm exhibits a moderate, fine platy structure in the upper 5 cm, however, micromorphological analysis of the upper horizon exhibits fine platy structure and partially decomposed organic matter down to a depth of at least 25 cm (Plate 3.9 A and B, respectively). From 5 cm to 80 cm the structure changes to a moderately developed, fine angular blocky structure (*e.g.*, Plate 3.9 C) that exhibits illuviated sediments occupying void spaces (Plate 3.9 D). The interval from 55 cm to 80 cm exhibits carbonate rich zones (Plate 3.9 E, F) comprising approximately 15% of this interval (55-80 cm). From 80 cm to 145 cm the unit colour lightens to yellowish-brown (10 YR 5/6 d), the development of the angular-blocky structure weakens, and the carbonate concentration decreases to <1% (by area). The CaCO₃ is generally in the form of carbonate rootlet casts that are concentrated below 80 cm, suggesting leaching of carbonate from overlying horizons (Figure 3.23). Irregularly shaped krotovena infilled with dark-grey (10 YR 4/1 d)

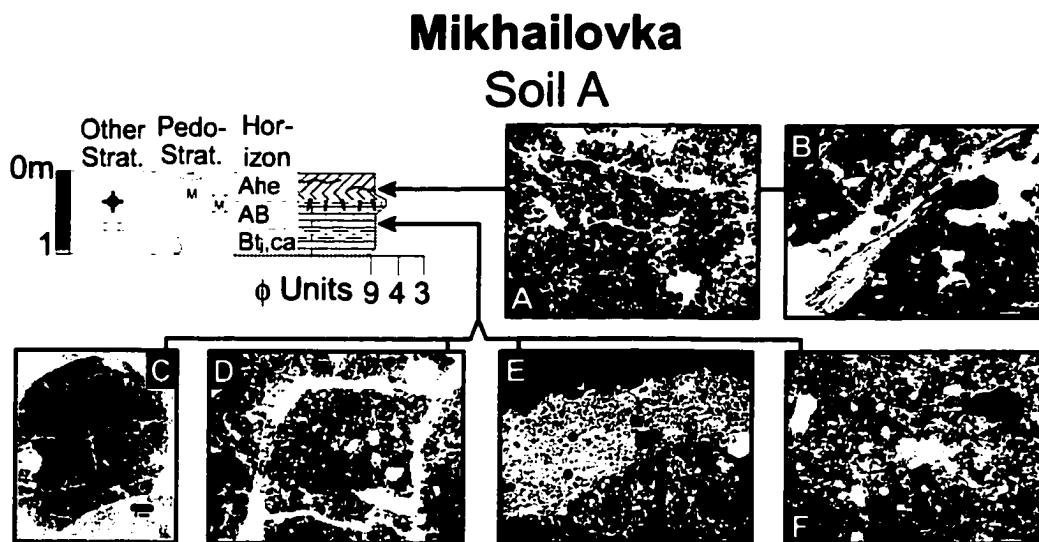


Plate 3.9. Photomicrographs of soil-A at Mikhailovka. **A.** Platy structure of Ahe horizon; mag. 2.5x; PPL. **B.** Partially decayed organic matter within Ahe horizon; mag.10x; PPL. **C.** Medium and fine blocky structure of the Btj horizon; PPL. **D.** Translocated sediment infilling packin-void space between peds; mag. 2.5x; PPL. **E.** Arrow points to carbonate nodule in B-horizon; mag. 2.5x; XPL. **F.** Arrows point to calcium carbonate coatings and micro-nodules/cement; mag. 10x; XPL.

sediment from the overlying A_{he}-horizon are present within the lower portions of the unit; they typically range up to 5 cm x 7 cm. Given the above, soil-A is interpreted as an eluviated brown chernozem.

Interpretation: The lack of primary structure and the 36-48% silt content (Appendix D), suggests that the parent material is loess. Fissures observed between 35 cm and 55 cm are interpreted to be small seasonal frost/desiccation cracks that infill with A-horizon material during episodes of precipitation -- testament to the observed arid-steppe conditions (cf. Figure 1.3).

MS1-2: 145 - 409 cm (MC-2: 145 - 409 cm)

Lithic Description: The upper 110 cm (145 - 255 cm) of this unit exhibit irregular, vertically oriented yellowish-brown (10 YR 5/4 d) silty-clay mottles; the width of these mottles ranges from 6 cm to 8 cm and they make up approximately 60% of the interval (by area), thereby imparting the dominant colour. The remaining 40% of the interval consists of a light yellowish-brown (10 YR 6/4 d) silty-clay. From 255 cm down to approximately 355 cm the dominant colour changes to light yellowish brown (10 YR 6/4) and the sediment fines to silty-clay with zones of very weak, fine granular structure. In addition, this interval (255-233 cm) exhibits fine vertical fissures (<8 mm in diameter) infilled with yellowish brown (10 YR 5/4 d) clayey-silt from the overlying interval (145 - 255 cm). Krotovena within this unit range from 5 cm x 8 cm to 8 cm x 10 cm; they are infilled with dark grey (10 YR 4/1 d) sediments derived from soil-A of MS1-1. From 255 cm to the base of the unit (409 cm) there are small amounts (<1%) of Mn oxide staining, CaCO₃ precipitate and gypsum crystals. From 355 cm to the base of the unit the colour gradually darkens from brown (10 YR 4/3 d) to very dark greyish-brown (10 YR 3/2 d) and the texture fines slightly from silty-clay to clay. Within this interval, yellowish-brown (10 YR 6/4 d) fissures penetrating from the lighter interval (255-355 cm) are contrasted against the darker-coloured background (Figure 3.25b). The lower portions of this unit (i.e., below 355 cm) are composed of the darker silty-clay material and exhibit a moderately well developed, fine granular structure. The lower contact of this unit is diffuse and irregular.

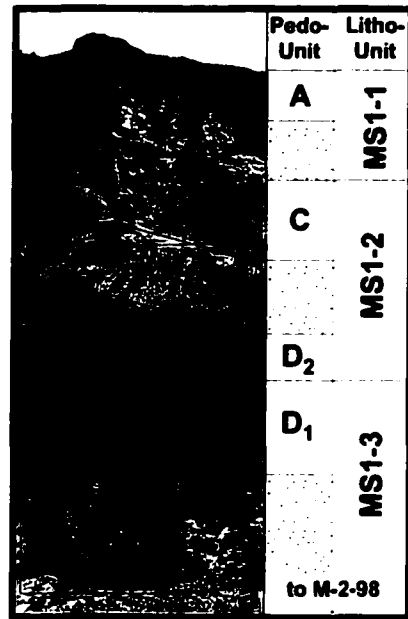
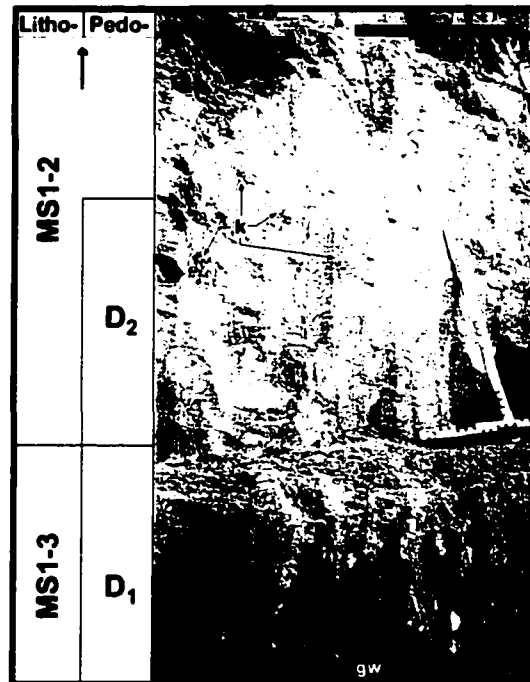


Figure 3.25. a. Upper portions of MS1 depicting litho-units and organic horizons of pedo-units A through D. b. Blow-up of MS1-2, D₂ (above step), and the upper portions of D₁. At the boundary of D₂, krotovena (k) are infilled with sediment from D₁. Also, within D₁, ground-wedges (gw) infilled with lighter material from D₁ and the middle portions of MS1-2 are present. c. Lower portions of D₁ and MS1-3: Dark ground wedges (gw) cross-cutting krotovena (k) are observed.



Paleosol-C: This paleosol is recognized through field and laboratory investigations. Field observations identified a weak, fine angular blocky structure in the upper 110 cm (145 - 255 cm) of unit MS1-2 (MC-2). This interval exhibits a peak in magnetic susceptibility and corresponding plateau in frequency dependence data (Figure 3.23). From 255 cm to 233 cm a weak granular structure is identified from field and micromorphological observations (Figure 3.23). These data suggest that this paleosol was a cumulic regosol.

Paleosol-D₂: This paleosol is recognized by a small increase (down section) in organic matter with a corresponding darker colour (Figure 3.25 a, b), a constant rate of increase in magnetic susceptibility (down section) between approximately 355 cm and 409 cm and weak granular structure. These observations, in addition to the gradational upper contact with the overlying loess suggest this paleosol was a rego brown chernozem or cumulic regosol developing in a steppe environment. Based on the lack of supporting micromorphological data, the latter, more general interpretation is preferred.

Interpretation: Given the cumulic nature of paleosols C and D₂, and the massive structure of the intervening sediments, this unit is interpreted to be a fine-grained primary loess. The gradational contact of paleosol-D₂ and the overlying loess suggests that a deteriorating climate eventually produced an environment non-conducive to soil development (at least at a level detectable by the methods used). The fissures penetrating into paleosol-D₂ that are infilled with material from the overlying loess suggest paleosurfaces were present in which desiccation/season frost cracks had developed. Propagation of these fissures allowed downward movement of the overlying loess into paleosol-D₂. The inference of an aggrading paleosurface on which loess accumulated, and presence of the desiccation/seasonal frost fissures, suggest that during this time interval loess deposition processes dominated in a climatic environment that was dryer and colder than during paleosol-C and -D₂ soil forming intervals.

MS1-3: 409 - 748 cm (MC-3: 409 - 748 cm)

There is a strong contrast between the primary deposit comprising the majority of the unit and the portion of the unit that has been overprinted by pedogenic and cryogenic processes (*vide post*).

Lithic Description: From 409 cm to 500 cm the unit is dominated by very dark greyish-brown (10 YR 3/2 d) silty-clay loam which exhibits reddish-yellow (7.5 YR 6/6 d) mottles that decrease in frequency with depth as the sediment texture coarsens to silty loam (Figure 3.23). Throughout this interval, there is an abundance of gypsum crystals present (<2 mm in size) in addition to traces of Mn oxide nodules and CaCO₃ precipitation. Below 500 cm, the colour lightens to yellowish brown (10 YR 5/4 d) and continues to lighten to light yellowish-brown

(10 YR 6/4 d) at a depth of 700 cm. Just below the 500 cm level, there are well developed ground wedges (Figure 3.25c) infilled with material from the overlying interval (409 - 500 cm). These wedges range in size from 2 cm to 20 cm at their apparent origins and pinch out at a maximum depth of 597 cm. The majority of these wedges bifurcate with depth and in some cases they crosscut large krotovena (Figure 2.25c). From 597 cm to 748 cm the unit consists of a light yellowish-brown silty-clay to clayey-silt. Trace (<1%) CaCO₃ precipitate and Mn oxide nodules are observed within this interval. The basal contact is gradational and planar.

Paleosol D₁: The interval between 400 cm and 409 cm exhibits a moderately developed, fine granular structure overprinted by a moderately developed, angular blocky structure and manganese-stained rootlet traces. Krotovena within this interval are pervasive and range in size from 5 cm x 7 cm up to 25 cm x 30 cm. Although no prismatic structure is observed, the relatively dark colour, granular and angular blocky structures and abundant precipitation of gypsum crystals suggest that this may have been an solonchic dark brown chernozem forming in a mesophytic steppe environment.

Paleosol-E: From 597 cm to 748 cm, a weak, fine granular structure is noted from field observations. Local peaks in the magnetic susceptibility between approximately 597 cm and 680 cm also support the interpretation of a paleosol within this interval. Relative to paleosol-D₁, the amount of krotovena within this pedogenic horizon has decreased. Krotovena observed within the limits of paleosol-E are generally oval to circular in shape, and range in size up to 8 cm x 9 cm. They are infilled with a very dark-grey (10 YR 3/1 d) silty-clay to clay, suggesting that they are related to paleosol-D₁ soil formation. The weak nature of this pedogenic horizon, combined with its relative thickness and gradually increasing grain size suggest that it is a cumulic regosol.

Interpretation: The massive structure and gradually increasing grain size suggest that parent material is fine-grained primary loess. The presence of fissure-infill structures that penetrate down into the underlying paleosol-F are interpreted to be desiccation/seasonal frost structures. These features would have opened at aggrading paleosurfaces below which cumulic paleosol-E was forming. In comparison, ground

wedges observed in association with paleosol-D₁ are generally wider with bifurcating bases - suggesting they are ice-wedge pseudomorphs related to permafrost conditions (Rutter pers. com. 1996).

MS1-4: 748 cm - 1005 cm (MC-4: 748 - 1005 cm)

Lithic Description: This unit consists of brown (10 YR 4/3 d) clay with extremely narrow (typically <1 cm) vertical fissures that are infilled with sediment from the overlying unit (Figure 3.26). These fissures penetrate the entire unit, but the relative frequency of deep penetrating infillings is reduced below 850 cm. Trace (<1%) Mn oxide nodules, CaCO₃ precipitation and gypsum crystals are present within the unit. With the exception of the infilled fissures and a slight darkening to very dark greyish brown (10 YR 3/2 d) below 850 cm, the unit is fairly homogenous. The lower contact is sharp and planar.

Paleosol-F: A local high in magnetic susceptibility and the broad plateau in frequency dependence of magnetic susceptibility (Figure 3.23) that occur in this unit suggest that pedogenic processes had acted on the parent material. This is supported by the weak to moderately developed, fine angular blocky structure present between fissure infill structures (Figure 3.26). The presence of these structures, and the relative lack of any other pedogenic structures, in conjunction with the environmental context in which this paleosol formed (*vide post*) suggest that it was an immature soil and therefore is interpreted to have been a rego brown chernozem.

Interpretation: vide post.

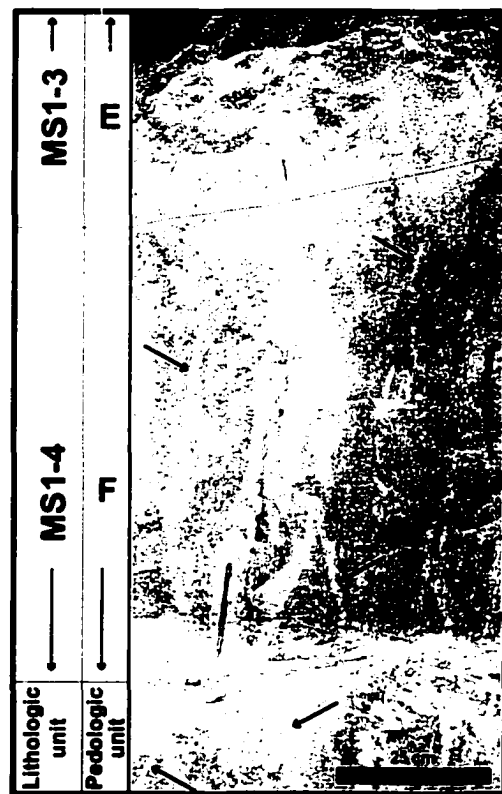


Figure 3.26. Paleosols E and F. Note light-coloured ground wedges (arrows) in paleosol-F infilled from MS1-3.

MS1-5: 1005 cm - (MC-5: 1005 - 1263^f cm)

Lithic Description: The upper 118 cm of this unit consists of yellowish-brown (10 YR 5/4 d) silty-clay that gradually fines to clay at 1088 cm and exhibits numerous intersecting fissures infilled with material from the base of MS1-4. These features are typically 3-4 mm wide and up to 80 cm long. Between these fissure infillings the unit also exhibits weak to moderate, fine prismatic macro structure and a weak, fine angular blocky structure. Below 1123 cm, the sediment coarsens to a dark yellowish brown silty-clay that exhibits only a weak, fine blocky structure and one large (10 cm x 10 cm) krotovena. Throughout the unit, there are trace (<1% area) amounts of gypsum, CaCO₃, and Mn oxide; however, a large (2 cm) gypsum rosette is observed between 1123 cm and the base of the section (1246 cm). The lower contact of MS1-5 is not observed at this location.

Paleosol-G: Because of thick accumulations of colluvium at the base of MS2, resulting in only partial exhumation of unit MS1-5 (MC-5), this pedogenic horizon is not observed at this section.

Interpretation: vide post.

Mikhailovka Section No. 3: Lithostratigraphy and basic paleosol description

This section represents the middle portion of the Mikhailovka stratigraphic record. It is located on a paleotopographic high with an unconformity marking the upper surface (Figures 3.27, 3.28A); the development of the modern soil occurs within MS3-1; a unit that corresponds to MS1-3 below the D₁ paleosol (*cf. ante*). The presence of unit MS3-1 and a complete equivalent unit to MS1-4 (*i.e.*, paleosol-F) allows correlation between MS1 and MS3; the datum for correlation is defined by the correspondence between the MS1-4/MS1-5 contact and the MS3-2/MS3-3 contact (Figure 3.27). The thicknesses of these units vary locally, hence, the thickness of the composite section units and MS3 units do not equate. In these cases (marked with “*”) the thicknesses measured at MS1 are used in the composite section (MC) because priority is given to the most detailed field observations.

*Base of the composite unit MC-5 is based on the depth observed at MS3 (*vide post*).

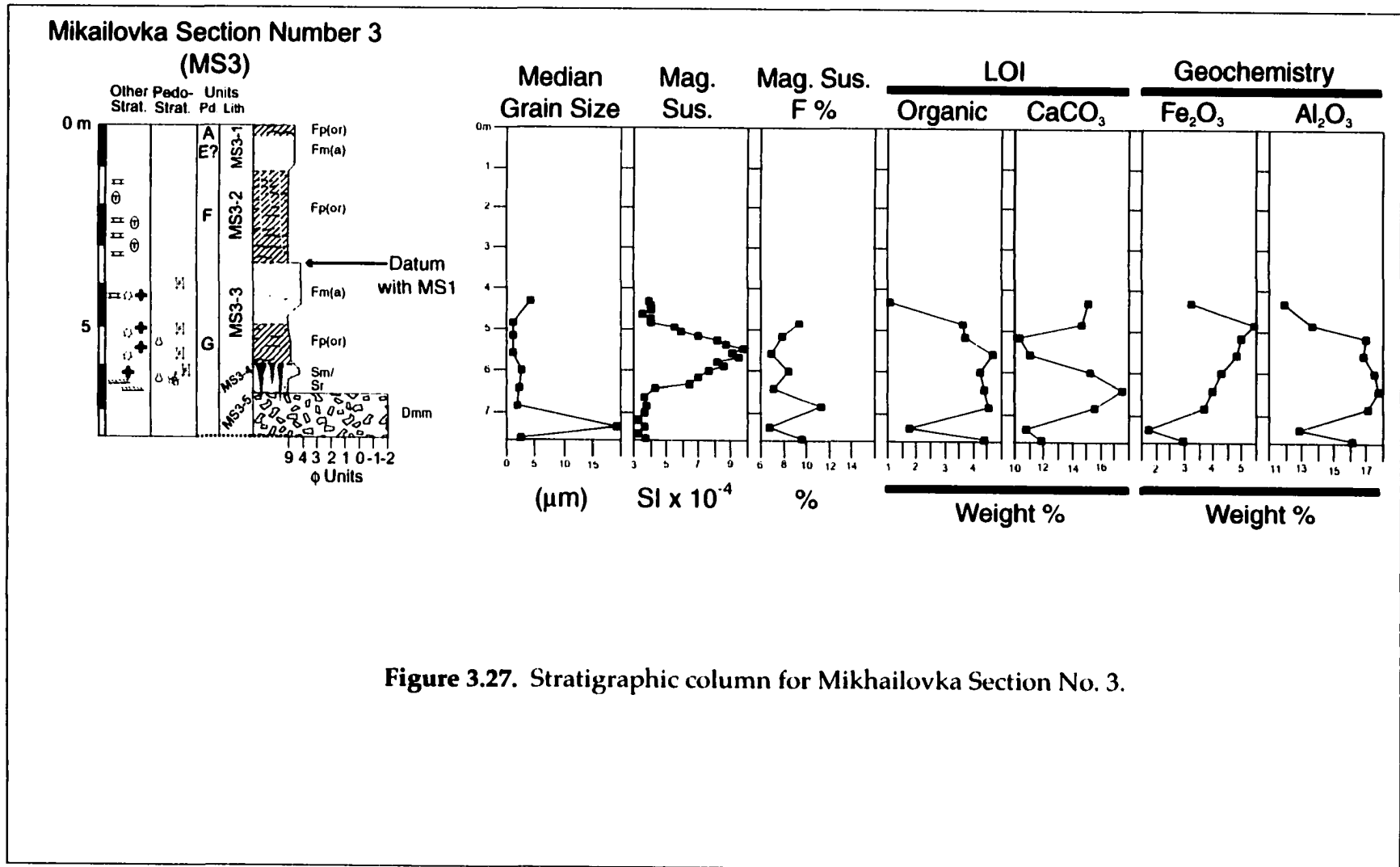


Figure 3.27. Stratigraphic column for Mikhailovka Section No. 3.

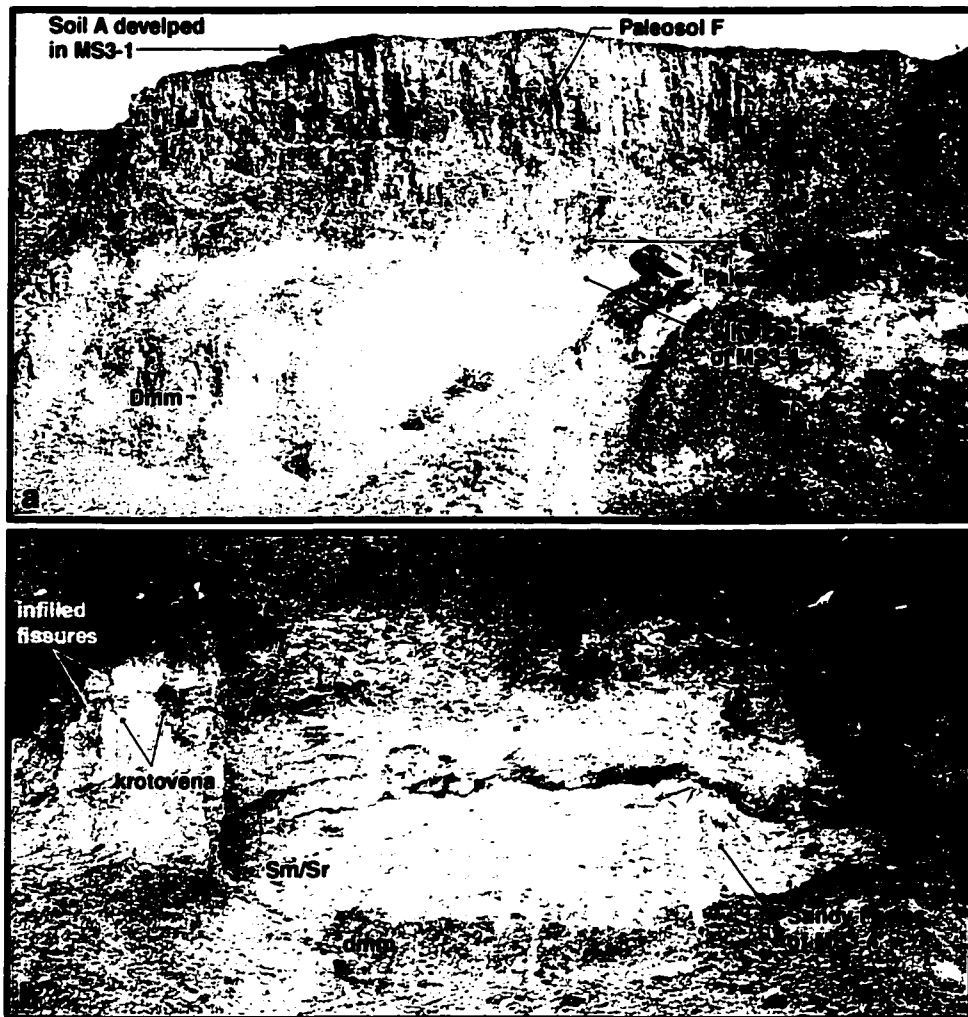


Figure 3.28. a. Overview of MS3. Soil-A has developed in a unit that directly overlies a thicker paleosol (paleosol-F) that correlates to unit MS1-4. This implies that the surface above soil-A is an unconformity. Also visible are paleosol-G, the silty facies of unit MS3-4, and the upper portions of the diamicton unit observed at MS3 and MS5 (*vidi post*). b. Unit MS3-4 and paleosol-G at the MS3 auxiliary site. Here, MS3-4 is sandy and exhibits both massive and cross-stratified lamination. Infilled fissures from paleosol-G are present in the upper portions of this unit in addition to numerous krotovena. For the locational relationship between MS3 and the MS3 auxiliary site, see figure 3.22 and table 3.2.

Due to difficult working conditions (no-access to upper portions), only the lower most portion of MS3 are described in detail. A brief distally observed description will be presented for those sediments occupying the upper 430 cm of the section. From approximately 430 cm to the base of the section at a depth of 761 cm, observations are taken directly from the section. However, unit MS3-4 does exhibit a lateral facies change and so, an auxiliary site (Figures 3.22 and 3.28a) is used to fully describe this unit. Correlated depths used in the Mikhailovka composite section are given in parentheses.

MS3-1: 0 - 110 cm (MC-3: 409 - 748 cm)*

Distal Lithic Description: This unit consists of pale brown (no Munsell colour) fine-grained sediment (Figures 3.25 and 3.26a). The modern soil developed within the upper 30 cm of the unit is very dark grey (no Munsell colour) and exhibits small (<30 cm) infilled fissures at the base of the dark-coloured organic horizon. Below the organic horizon, there is a 40 cm thick zone of concentrated CaCO₃ precipitate which is, in turn, underlain by 40 cm of nondescript pale brown fine-grained material.

Interpretation: The lack of paleosols that are correlative to paleosol C and D, in addition to the close proximity (<1 m) between paleosol-F equivalent (vide post) and the modern-day soil suggest that the upper surface of MS3-1 is unconformable. Therefore, this unit is interpreted to be correlative with the lower portions of MS1-3 and a paleotopographic high is inferred.

MS3-2: 110 - 335 cm (MC-4: 748 - 1005 cm)*

Distal Lithic Description: This unit consists of medium-brown (top: no Munsell colour) to dark-grey-brown (base: no Munsell colour) fine grained sediment (Figures 3.25 and 3.26a). The upper portions exhibit narrow fissures infilled with lighter sediment from the overlying unit. At the top of the unit CaCO₃ precipitation is minor (<1%) but this increases to approximately 5% (by area) at a depth of approximately 250 cm where numerous CaCO₃ stringers and CaCO₃ nodules up to 10 cm by 4 cm are present (Figure 3.26 within paleosol-F). The lower contact is gradational and planar.

*Depths are based on detailed descriptions observed at MS1.

Interpretation: The thickness and general character (outlined in the preceding paragraph) of this unit suggests that it is correlative with MS1-4 and the overprinting paleosol-F. The presence of carbonate nodules within the soil pedon at this locality (*cf.* Figure 3.22) suggests that there was a soil catena that exhibited rego brown to calcareous brown chernozemic pedofacies. These would have formed in an aggrading environment dominated by loess deposition.

MS3-3: 335 - 593 cm (MC-5: 1005 - 1263 cm)

Lithic Description: The upper 140 cm of this unit consist of a yellowish-brown (10 YR 5/4 d) silty-clay that gradually darkens and fines to a dark-brown (10 YR 3/3 d) clay by 583 cm (1253 cm). Within this interval, there is a weak, fine angular blocky structure. CaCO₃ precipitation/nodules (<3 cm), and Mn nodules (<2 mm) are present within this interval. Below 490 cm there is a small amount of scattered granitic granules and pebbles; at least one angular granitic clast (<5 cm) that exhibits striations and facets is present. Also, below 490 cm, the colour darkens to very dark greyish brown (10 YR 3/2 d) and the amount of CaCO₃ precipitation and Mn nodules drops to <1%. Granule to pebble sized clasts are still scattered throughout the unit, but within this interval, the largest observed clast was 8 mm. The lower contact is gradational and planar.

Paleosol-G: From 490 cm to the base of the unit, well developed, fine angular blocky structure is observed along with clay coatings on individual peds. A prominent peak in magnetic susceptibility and organics, in addition to carbonate eluviation and illuviation horizons (Figure 3.27) suggest that paleosol-G was a well-developed soil. Based on these data, this paleosol is interpreted to have been a dark-grey chernozemic soil formed in a forest-steppe environment.

Interpretation: The coarsening-upwards massive silts above paleosol-G are interpreted as loess. Below 490 cm, the presence of granules and pebbles scattered throughout this unit, suggests a non-aeolian origin for the parent material. Although the sediment has undergone turbid events, thereby destroying any primary structure, the parent material is interpreted to be glaciofluvial based on the presence of erratic lithologies and by association with units MS3-4 and MS3-5 (described below).

MS3-4: 593 - 656 cm (MC-6: 1263 - 1326 cm)

This unit exhibits two different lateral facies: a finer facies observed at MS3 (Figure 3.28a) and coarser facies observed at the auxiliary paleosol-G site (Figure 3.28b), approximately 130 m southeast of MS3 (Figure 3.22).

M3-4 -- Fine Facies: This facies consists of a pale brown (10 YR 6/3 d) silty-clay to silty-loam. It exhibits pervasive bioturbation (krotovena) and fissures infilled with material from the overlying unit. It also exhibits a moderate, fine angular blocky structure that overprints a weak granular structure. The lower contact is sharp and wavy.

M3-4 -- Coarse Facies: This facies consists of a pale brown to reddish brown (no Munsell colour) sandy clay to sandy loam. Similar to the finer facies, this coarse facies exhibits pervasive bioturbation (krotovena) and fissures infilled with material from the overlying unit (Figure 3.28b). However, it consists of a single-grain structure that supports both massive and cross-stratified lamination. The lower contact is sharp and wavy.

Interpretation: Both facies of this unit are interpreted to have glaciofluvial origins by association with MS3-5; the finer facies being associated with lower flow regimes. Krotovena are associated with the paleosol-G soil forming event whereas the morphology of the fissures (e.g., Figure 3.28) suggest the presence of permafrost that would have followed the development of paleosol-G.

MS3-5: 656 cm - (MC-7: 1326 - 2326 cm)[†]

This unit consists of a diamicton that can be subdivided into 4 sub-units described below:

Sub-unit 1: Consists of dark yellowish-brown clayey diamicton with fine sand and up to 5% clasts and occupies the upper 50 cm of the unit. Clasts are sub-angular to subrounded (average = subrounded) and range in size from <0.5 cm up to 10 cm (average = 1 cm). Clast lithologies include: granite, gneiss, sandstone (red, green and orange varieties), quartzite, chert and chalk. Manganese oxide staining is prevalent throughout this sub-unit.

[†]Unit depths are based on the average observed thickness of the diamicton unit and the correlated elevations of the upper and lower contacts.

Sub-unit 2: Consists of a 10 cm thick pale green sandy zone (no Munsell colour). This zone is a smeared out lens that originates from a large green sandstone clast approximately 3 m to the northwest at the same stratigraphic level.

Sub-unit 3: Consists of a 30 cm thick red (2.5 YR 5/6 m) silty-clay-loam diamicton. The clast content of this sub-unit is much greater (approximately 25%) than that observed in sub-unit 1. All other characteristics are similar to sub-unit 1.

Sub-unit 4: This sub-unit is the predominant diamicton unit, having a thickness of approximately 8 m to 10 m (only excavated to a depth of 761 cm, but can be traced in outcrop). It consists of a massive yellowish-brown (10 YR 5/6 m) clayey diamicton. Clast characteristics are similar to those noted in sub-unit 1.

Interpretation: This unit is interpreted as till, given the lack of a debris flow source, and the presence of distally transported granitoid erratics. Interpretation of the glacial regime (*e.g.*, supra-, sub-glacial *etc.*) in which this till was emplaced was not focused upon during field investigations and is therefore beyond the scope/purpose of this work. However, the identification of this diamicton as a till deposit, at a latitude of 50° 06' N is of great importance since it can be associated with an all-time Pleistocene maximum advance of the European ice sheets.

Mikhailovka Section No. 5: Lithostratigraphy and basic paleosol description

This section represents the stratigraphically lowest sequence of sediment and paleosols studied at Mikhailovka. They outcrop below the major till unit (*cf. ante*) at the Mikhailovka site. The upper contact of the unit immediately underlying this diamicton is an unconformity which is clearly visible in figures 3.29 and 3.30. At the location of MS5 (Figure 3.22), there are 3 paleosols that overprint a very fine textured sediment. The composite depths (in parentheses) are calculated by estimating an observed thickness of 10 m for the overlying till.

The fine-grained, massive nature of sediments comprising units MS5-3 (MC-8) through MS5-9 (MC-14) make preliminary genetic interpretations difficult. Therefore, the origins of these sediments are discussed in *Mikhailovka Site Depositional Environment: overview* which follows section descriptions and relative data interpretations.

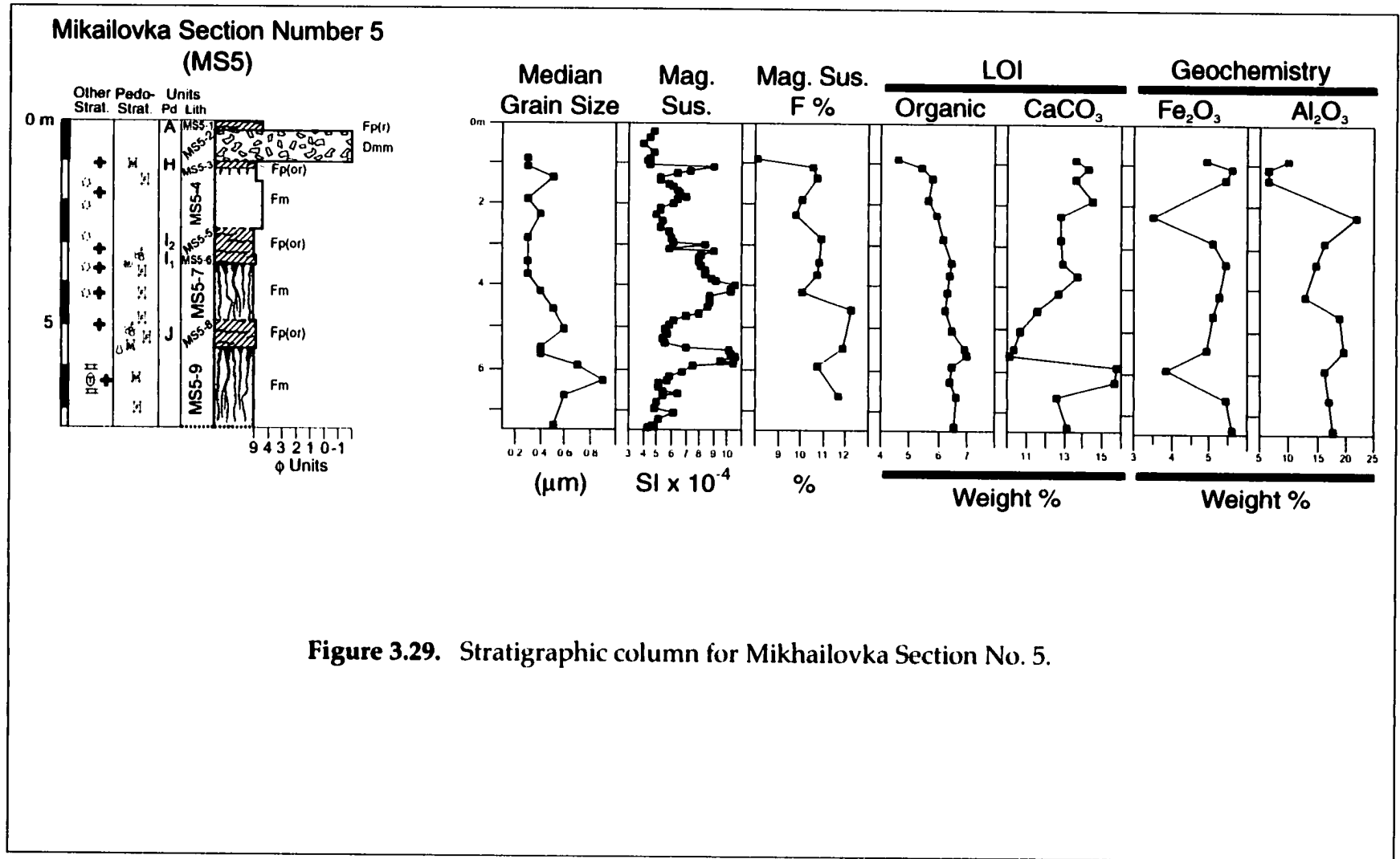


Figure 3.29. Stratigraphic column for Mikhailovka Section No. 5.

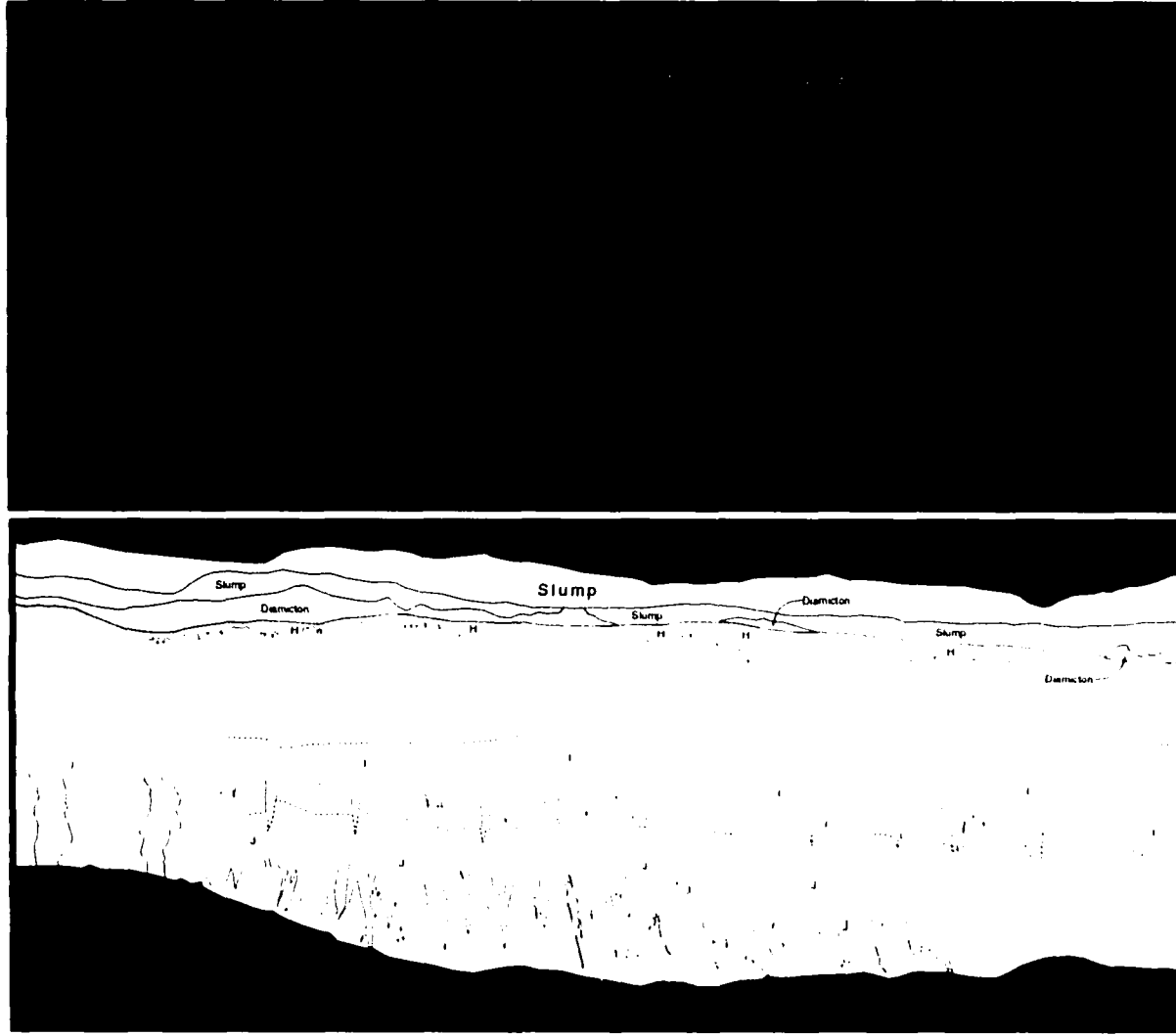


Figure 3.30. Overview photograph and trace of the exposure in the vicinity of MS5. Three distinct organic rich soil horizons are visible along with the basal portion of the diamicton observed at MS3 and MS5; the diamicton clearly truncates the uppermost paleosol-H (below red line in lower trace). Prominent fissures increasing in size with depth in each of the paleosols are also observed.

MS5-1: 0 - 20 cm (not used in composite section)

This unit consists of colluviated, modern-day soil/sediments.

MS5-2: 20 - 103 cm (MC-7: 1326 - 2326 cm)^t

Lithic Description: This unit consists of yellowish-brown (10 YR 5/4 m) massive clayey diamicton. Clast content within this unit is approximately 2-5%; other clast characteristics are similar to MS3-5, sub-unit 4. Trace (<1%) amounts of gypsum crystals and Mn oxide staining are present, in addition to minor (<5%) zones of gleyed sediment. The lower contact is sharp and planar.

Interpretation: This unit the equivalent to unit MS3-5, and hence is interpreted as till.

MS5-3: 103 - 148 cm (MC-8: 2326 - 2371 cm)

Lithic Description: From 103 cm to 118 cm this unit is composed of a brown (10 YR 5/3 m) clay with very dark-grey (10 YR 3/1 m) Mn oxide stains along fracture planes that define a well developed coarse blocky structure. Breaking down the coarse peds yields a weakly developed, fine granular structure. Below 118 cm, the sediment darkens slightly to brown (10 YR 4/3 m). Within this portion of the unit, the structure weakens to a weak, fine angular blocky structure. Also below 118 cm, there are vertical to subvertical infilled fissures approximately 5 cm to 6 cm wide that originate from the overlying interval (103-118 cm) and pinch out at a depth of 145 cm. There are also minor amounts (<5%) of Mn oxide nodules and small nodular gypsum concretions (not rosettes). The lower contact is diffuse and planar.

Paleosol-H: This paleosol is identified in the field from Mn oxide staining along fracture planes that define a well developed coarse blocky structure. These observations are corroborated by prominent peaks in magnetic susceptibility, frequency dependence of magnetic susceptibility and geochemistry (Fe_2O_3) in addition to a correlative (lesser) peak in organic matter (Figure 3.29). The coarse angular blocky structure, Mn oxide stains on individual peds and the peak in Fe_2O_3 suggest a moist environment conducive to illuviation processes. Based on the above, this soil is tentatively interpreted to be luvic gleysol that formed in a relatively moist environment.

^tUnit depths are based on the average observed thickness of the diamicton unit and the correlated elevations of the upper and lower contacts.

Interpretation: vide post.

MS5-4: 148 - 265 cm (MC-9: 2371 - 2488 cm)

Lithic Description: This unit consists of a dark yellowish-brown (10 YR 4/4 m) clay with no apparent primary structures. There is however, a moderately developed, fine angular blocky pedogenic structure present throughout the unit. There are trace (<1%) amounts of Mn oxide nodules, and gypsum concretions up to 4 cm in diameter; gypsum concretions are made up of numerous smaller gypsum crystals up to 1 mm in size. The basal contact is gradational and planar.

Interpretation: vide post.

MS5-5: 265 - 330 cm (MC-10: 2488 - 2533 cm)

Lithic Description: This unit consists of a brown (10 YR 4/3 m) clay. Small Mn flecks (<1 mm) and gypsum crystals (<1 cm) are present within this unit. Also, 20% of the unit exhibits small (<1 cm) zones of lighter-coloured sediment (yellowish-brown: 10 YR 5/4 m). The basal contact is gradational and planar.

Paleosol-I₂: Pedogenic processes related to this paleosol are suggested by this horizon's darker colour relative to the overlying unit and moderate to fine angular blocky structure observed from field investigations. These are in addition to a drastic increase in magnetic susceptibility (Figure 3.29) and corresponding increases (down section) in frequency dependence of magnetic susceptibility and organic matter. These data allow a tentative interpretation to be applied to this paleosol; it is classified as an eluviated brown chernozem formed in a steppe environment. Also, given its thickness, it may have cumulic components.

Interpretation: vide post.

MS5-6: 330 - 353 cm (MC-11: 2553 - 2576 cm)

Lithic Description: This unit consists of a dark-brown (10 YR 3/3 m) clay that exhibits lighter zones of yellowish-brown (10 YR 5/4 m) clay. These lighter zones have diffuse outer boundaries and are typically <1 cm in diameter. There are trace (<1%) amounts of Mn oxide nodules and gypsum concretions within this unit. The basal contact is clear and irregular.

Paleosol-I₁: This pedogenic horizon exhibits well developed, medium sub-angular blocky structure with clay cutans that are visible on the peds. It is differentiated from paleosol-I₂ based on the decrease in colour value, and the presence of well developed structure and clay cutans. Given the above, it is not clear if paleosol-I₁ represents a separate soil-forming event relative to paleosol-I₂ or if both are transitional soils with the former being overprinted by the latter. Regardless, characteristics of paleosol-I₂ suggest that this it was a dark grey chernozem formed in forest-grassland transition zone.

Interpretation: vide post.

MS5-7: 353 - 489 cm (MC-12: 2576 - 2712 cm)

Lithic Description: This unit consists primarily of yellowish-brown (10 YR 5/6 m) clay that exhibits a moderate, fine angular blocky structure. There are numerous irregular, vertically oriented fissure infillings that crosscut the unit. These fissures consist of dark-brown (10 YR 3/3 m) clay material derived from the overlying unit and comprise 80% of this unit at a depth of 353 cm (2576 cm) and only 30% of this unit at 489 cm (2712 cm); their width at the top of the unit ranges between 7 cm and 8 cm.

Interpretation: vide post.

MS5-8: 489 - 555 cm (MC-13: 2712 - 2778 cm)

Lithic Description: This unit consists of dark brown (7.5 YR 3/2 m) clay that exhibits weak, very dark grey (10 YR 3/1 m) Mn-oxide stain on well developed fracture planes. Small Mn nodules are also present, but make up <1% of the unit. The lower contact is gradational and irregular.

Paleosol-J: Other than a colour change, as outlined above, the only indication of this pedogenic horizon in the field was the weak, angular blocky structure. However, magnetic susceptibility, organic matter and an enrichment of calcium carbonate in the underlying unit (vide post) also suggest pedogenesis. Both the angular blocky structure and pervasive CaCO₃ translocation (figures 3.29 and 3.30) suggest that this paleosol was a calcareous brown or dark brown chernozem forming in a xerophytic to mesophytic steppe environment.

Interpretation: vide post.

MS5-9: 555 - cm (MC-14: 2778 cm -)

Lithic Description: The upper 45 cm of this unit consist of clay that gradually lightens with depth from dark brown (10 YR 3/3 m) to yellowish brown (10 YR 5/4 m). Irregular vertical to subvertical fissure infillings make up 80% to 90% of the unit (Figure 3.30). These fissures are infilled with material from the overlying unit. The regions between fissures exhibit moderately developed, fine to medium angular blocky structure; clay cutans are observed on peds. There are Mn nodules (<1%) present throughout the unit and below 590 cm (2813 cm) there is a drastic increase in CaCO₃ precipitate (Figure 3.29, CaCO₃; Figure 3.30 above basal slump) that lightens the unit colour to very pale brown (10 YR 8/2 m). Krotovena are also present within this interval; they are typically infilled with a yellowish-brown (10 YR 5/6 m) clay to silty-clay and range in size from 5 cm x 7 cm to 7 cm x 7 cm. From 600 cm to 695 cm (2823 - 2918 cm) the unit darkens slightly to dark yellowish brown (10 YR 4/4 m) and exhibits fissures infilled with very dark-greyish brown (10 YR 3/2 m) sediment (originating from above) that comprise approximately 30% of this interval. The structure observed within this interval strengthens to a moderately to well developed, medium angular blocky structure and exhibit clay cutans. There are trace (<1%) amounts of gypsum crystals and Mn nodules, but CaCO₃ is still strong. In zones of enhanced CaCO₃ precipitation, the colour of the unit lightens to very pale brown (10 YR 8/4 m) and often CaCO₃ nodules are present up to 1 cm x 1 cm. Krotovena are still present within the cleaned section wall below 600 cm; they are infilled with a very dark brown (10 YR 2/2 m) clay and are typically 5 cm x 6 cm. The basal portion of this unit occurs from 695 cm (2918 cm) down to the base of the exposure at 746 cm (2969 cm). Within this interval of the unit, the structure fines to moderately developed, fine angular blocky structure and the fissures that originated at the top of the unit pinch out at approximately 705 cm (2928 cm). CaCO₃ precipitation drops to approximately 13% (by weight: Figure 3.29, CaCO₃). In all other respects, this interval is similar to the overlying interval. The basal contact of this unit is not observed at this section.

Interpretation: vide post.

Mikhailovka Composite Section

The previous subsections of this chapter describe the sediments observed within four individual sedimentary sections (MS1, MS2, MS3 and MS5) at the Mikhailovka site. These sedimentary sections will now be correlated on the basis of local marker beds (*e.g.*, paleosol-F present in both MS2 and MS3) and the comparison of the data-sets (*e.g.*, magnetic susceptibility, Organic and CaCO₃ wt.% etc...) in the overlapping portions of the sections (Figure 3.31). The resulting composite section exhibits seven moderately to well developed paleosol horizons (A, D, F, G, H, I and J) and two relatively weak paleosols (C and E). Some of these paleosols can be subdivided based on interpreted differences between pedogenesis and inferred accumulation rates (*e.g.*, D_1/D_2 and I_1/I_2), both of which will be discussed below and in the ensuing chapters. The following subsection further describes, discusses and more importantly, interrelates laboratory data collected at Mikhailovka. This is in turn followed by a discussion of the depositional environments and paleoclimate as they changed over time at this site.

Four optical luminescence dating samples were obtained at the Mikhailovka site to help constrain and correlate the upper portion of the stratigraphic record. As is the case at the Korostylievo site, sullegic and strategic factors dictated that of these four samples, only the lower three samples (MCSL 2 through 4) were analysed. Ages of these samples are as follows: 40 ± 2 ka (MCSL 2), 56 ± 4 ka (MCSL 3) and 132 ± 22 ka (MCSL 4). The application and implications of these ages are discussed below and in Chapter 4 - Chronostratigraphy. Procedures used to obtain these ages follow from Little *et al.* (in press, Appendix B); data plots and tables are also available in Appendix B.

Mikhailovka Site: relative data interpretations

Grain size, rock magnetic properties, and LOI are discussed below in a relative context in order to understand the relationship between pedogenesis and sedimentation processes through time. Grain size, although relatively fine, given the interpreted nature of the deposit (*vide post*), correlates to the observed stratigraphy. Both magnetic susceptibility and frequency dependence of magnetic susceptibility (F_D), being proxies for pedogenesis and soil productivity respectively (*vide* Chapter 2), are invaluable for discerning some of the weaker paleosols. LOI,

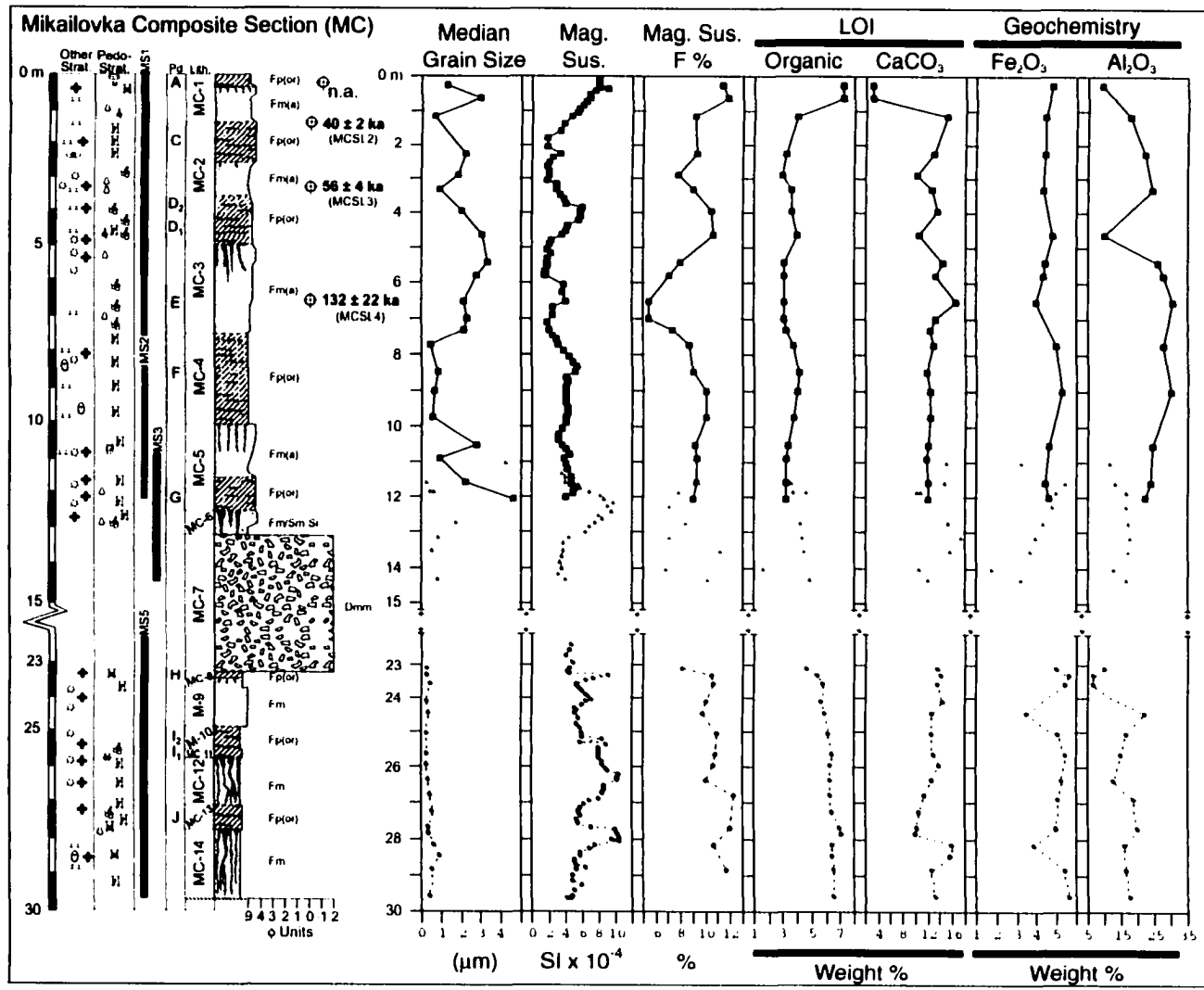


Figure 3.31. Mikhailovka composite section. Correlation between sections is done through visual leveling (e.g., MS1 and MS2), horizon identification, physical properties (e.g., MS1 and MS3) and estimated average thickness of the diamicton unit between MS3 and MS5.

The black line represents MS1 and MS2 data, the red line represents MS3 data and the blue line represents MS5 data.

organic content (wt.%) and CaCO_3 content (wt.%) correlates to the observed pedostratigraphy and allows identification organic-rich horizons and carbonate-rich horizons. Geochemistry of sediments at the Mikhailovka site is not as revealing as in other cases, possibly due to insufficient data resolution, hence these data are only briefly discussed.

Grain size values obtained from the Mikhailovka site are very fine (Figure 3.31 and Appendix D), but internally, these data still exhibit patterns/trends that can be tied to the stratigraphy. Given the grain size trends and observed stratigraphy and structures (or the lack thereof), most of the sediment deposited at this site is interpreted to be the product of aeolian processes. However, the fineness of the sediments (obtained from the grain size analysis) suggest that these deposits are not loess (hence the commonly used descriptive Russian term “loess-like”). One possible explanation for the overall fineness of the deposit may be the disaggregation of aeolian silt-sized aggregates. The disaggregation process used as a pretreatment to the grain size analysis may have broken these particles down to their primary constituents, thereby causing a clay spike to occur in the frequency distribution of samples. To test this hypothesis, samples from sections at both Yichuan (unit L-1-1, LGM) and Weinan (unit L-1-1, LGM) of the Chinese Loess Plateau were processed and analysed using the same methods as those used on the Russian samples; striking similarities are observed (Figure 3.32). All tests resulted in the enrichment of clay-sized material, which is, in all likelihood a function of both disaggregation of silt-size aggregates and clay illuviation. However, because some degree of enrichment does occur in all of the Russian Plain samples regardless of pedogenic position within the stratigraphic column (additional tests were run on glacial flour, and other sediments from known depositional environments; some of these samples did not yield the enrichment in clay - *vide* Appendix D), the laboratory disaggregation process is thought to produce the majority of the clay enrichment. The factors that support an aeolian origin include:

- 1) no primary stratification is present with the exception of the sandy facies of MC-6 (Figure 3.28b), where the texture and structure of these sediments would suggest (glacio)fluvial-type processes;**

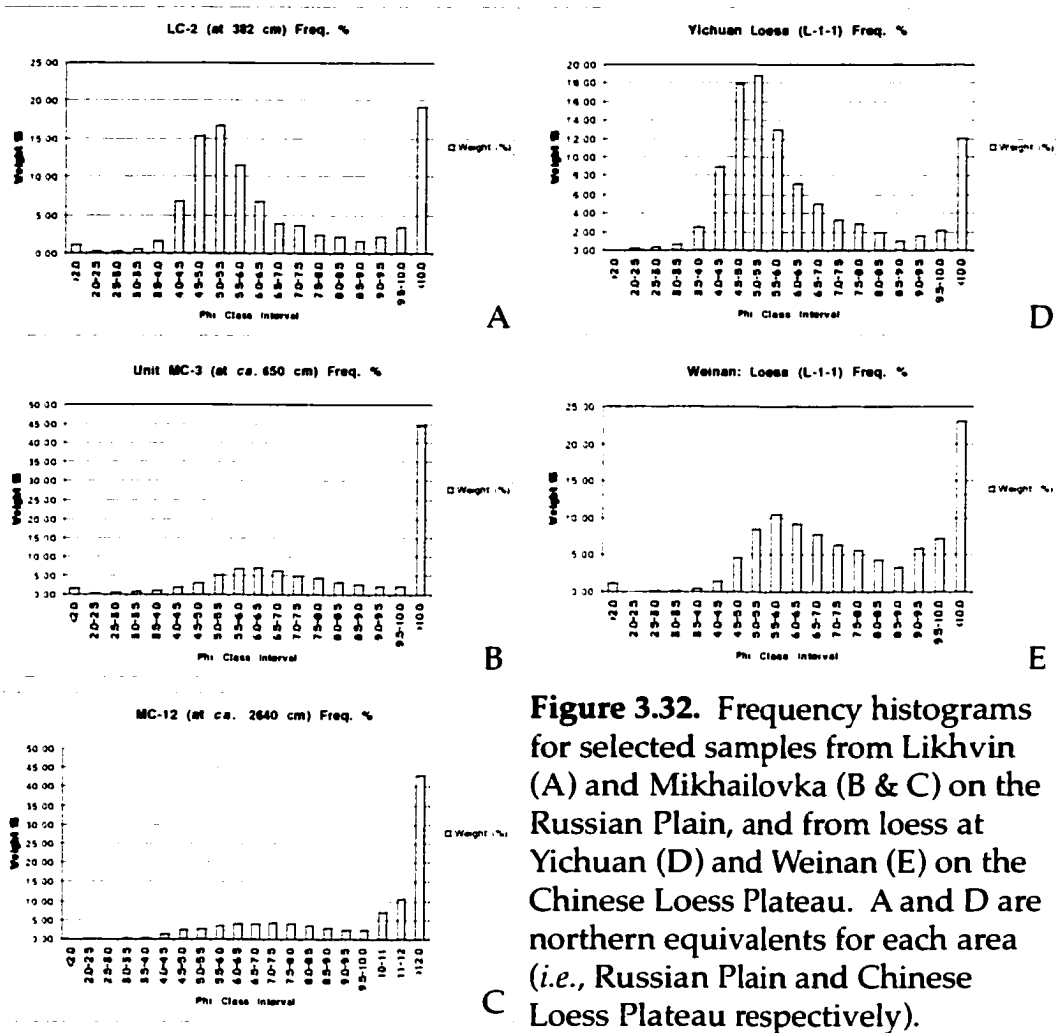


Figure 3.32. Frequency histograms for selected samples from Likhvin (A) and Mikhailovka (B & C) on the Russian Plain, and from loess at Yichuan (D) and Weinan (E) on the Chinese Loess Plateau. A and D are northern equivalents for each area (*i.e.*, Russian Plain and Chinese Loess Plateau respectively).

Likewise B, C, and E are southern equivalents. Each graph depicts peaks in the silt fraction (standard loessic curves; *cf.* Pye 1995) and also in the clay fraction. This enrichment of clay-sized particles in all samples is thought to be a product of laboratory procedure; most likely due to disaggregation of wind transported silt-sized aggregates composed of smaller fine silt and clay-sized particles. The disaggregation method has broken down these aggregates into their primary particle constituents. Since all samples presented in the dissertation have been prepared through the same methods, internally, the grain size data can be compared in a relative context.

- 2) grain size frequency distributions (Figure 3.32) all depict silt-peaks that can be diagnostic of loess-type material, and;**
- 3) the hypothesized enrichment of clay through laboratory disaggregation may be the cause of some of the fine median grain size values (Figure 3.31).**

However, because all samples were prepared using the same methodology, relative comparisons can be made between any grain-size data set presented herein. The entire digital grain-size database is referenced in Appendix D.

Rock magnetic properties (magnetic susceptibility and F_D) exhibit peaks and plateaus that correspond to all but one of the identified paleosols. Clear peaks in magnetic susceptibility are observed in the modern soil (used as an analogue for interpretation), and all of the underlying paleosols. Frequency dependence shows a relative peak in the modern soil, but also exhibits peaks in paleosols D, F, H, I and J. Weak peaks and /or plateaus in the F_D data are observed in paleosols C and G. One inverse relationship in the frequency dependence is observed in figure 3.31; a trough which corresponds to physical evidence of paleosol-E (origin of fissures and granular structure) and to a peak in magnetic susceptibility.

Above the till unit, all of the well developed paleosols exhibit relative peaks in organic content and corresponding peaks in CaCO_3 content immediately beneath (*e.g.*, soil-A and paleosols D, F, and G). The more weakly developed paleosols (*i.e.*, C and E), however, show moderate increases (*e.g.*, CaCO_3 increase below paleosol C) to negligible differences in either of these parameters (*e.g.*, paleosol E).

As stated above, a low sample resolution for the geochemical data has made interpretation of the available data enigmatic and therefore there is very little information that can be extracted. There does, however, appear to be an accumulation of Al_2O_3 (aluminium sesquioxides) below paleosols D, H, and I. Future research should include higher resolution data analysis in order to enhance the interpretive potential for pedogenic processes that affected the Mikhailovka primary sediments.

Mikhailovka Site Depositional Environment: overview

The sediments at the Mikhailovka site have yielded extremely fine grain sizes and therefore, many of the units are not considered to be loess in the traditional sense, as defined Pye (1995, p. 653), *i.e.*, "terrestrial clastic sediment composed predominantly of silt-sized particles, which is formed essentially by the accumulation of wind-blown dust".

Instead, a hypothesis put forth in the foregoing section suggests that, based on the evidence presented therein, some of the particles deposited in the Mikhailovka sections were originally deposited as silt-sized aggregates that have been subsequently disaggregated during laboratory pretreatment procedures. This has caused a laboratory-induced reduction in the median and mean grain sizes by enriching sample in clay-sized particles. Therefore, the overall interpretation of many of the units (*vide post*) considers aeolian dust accumulation as the primary depositional mode, but due to the grain size results (many samples have <51% silt), a standard "loess" definition (*cf.* Pye 1995) can not be applied. Nevertheless, because each sample has been pretreated in the same manner, the sample results are internally consistent and grain size relationships to stratigraphy and other data sets (such as rock magnetic properties and LOI results) are clearly observed (Figure 3.31).

Units MC-14 through MC-8 are composed of extremely fine sediments (median grain sizes < 2 μm). Since there is a lack of primary structures that would be expected in typical sediments deposited within lacustrine or alluvial depositional environments, and grain size frequencies mimic loess-type distribution, both lacustrine and fluvial interpretations are not accepted. Alternatively, a hypothesis proposing that the grain size data are clay enriched because of laboratory procedures is advanced. This hypothesis, and the presence of paleosols (clearly subaerial), all support the possibility that these units may have formed from the subaerial accumulation of fine-grained dust (*i.e.*, loess).

Soil parameters below the till (MC-7) are quite pronounced. The lower-most horizon (MC-14) is marked primarily by a twofold increase in CaCO_3 content relative to the overlying horizon (Figure 3.31). This significant increase, which is visually corroborated from section observations (Figure 3.30; below paleosol-J), is interpreted as the B- and C-horizons of paleosol-J. In MC-13, the Ah-horizon of paleosol-J is observed in section (Figure 3.30) and also exhibits peaks in magnetic susceptibility and organic content. This horizon also exhibits an initial increase in the F_D data that leads into a plateau in the overlying unit (Figure 3.31), possibly suggesting a relative increase in the strength of pedogenic processes which were initiated during the formation of paleosol-J.

Large narrow fissures infilled with organic rich sediment from overlying units are observed within MC-14 and MC-12, whereas smaller versions are present within unit MC-8. The morphology of these fissures closely resembles modern-day fissures beneath the Ah-horizon in unit MC-1 with the exception that the paleoversions within units MC-12 and MC-14 are 6 to 7.5 times larger (respectively) than their modern-day counterparts. The formation of the observed modern-day fissures is through desiccation (summer) and frost-cracking (winter) processes. Although the size of the fissures observed in units MC-14 and MC-12 is relatively large, they do not exhibit the morphology of ice-wedge pseudomorphs (*cf.* Figure 3.12C) and are therefore, not interpreted as being related to continuous permafrost conditions. Alternatively, the formation of these large fissures is interpreted to be a function of desiccation, differential frost heave and thermal gradients similar to the minimum frost scenario hypothesis of van Vliet-Lanoë (1988, p. 94). This hypothesis is supported by comparing fissures from units MC-14 and MC-12 with fissures of similar morphology and size from soil profiles in Padjelanta National Park, Sweden, which were interpreted to have been formed under discontinuous permafrost conditions (Rapp and Clark 1971, their figures 9 and 10, pp. 78-79).

Given the location (spatial and relative temporal) and genetic interpretation of unit (MC-7) as till (*vide ante*), it is associated with the Don Glaciation (*cf.* Figure 1.8). The base of the till marks a major unconformity that represents a significant hiatus as it crosscuts all three paleosols (H, I and J) in the western part of the Mikhailovka site. A discussion on the age of the Don Till and the significance of the underlying hiatus are presented in Chapter 4 -- Chronstratigraphy. Also, the basic lithologies observed within this till suggest a northern source. However, no data were collected that could refine the location of the source area (*e.g.*, Urals or Scandanavia). Therefore, further evaluation of source areas for the Don Till remains unsolved (Glushankova *et al.* 1995). There is, however, speculation on both Scandinavian and Uralian sources for the Don Ice Sheet, depending on the location of a till exposure relative to ice sheet extent (Glushankova *et al.* 1995).

The sharp wavy transition between the till and the overlying sediments of unit MC-6 suggests a rapid change in modes of deposition and

the removal of some material. There is no evidence to suggest that the unconformity between units MC-7 and MC-6 represents a major hiatus between the deposition of the two units. Therefore, the interpretation of unit MC-7 follows the simplest scenario: unit MC-6 records proglacial deposition of glaciofluvial sands and silts following the retreat of the glacier responsible for the deposition of MC-7, but still within the deglacial period. Eventually, as the climate ameliorated, this deposition slowed or ceased, thereby allowing the formation of paleosol-G which marks the succeeding interglacial. The upper portions of MC-5 record a gradual coarsening of the aeolian sediments and reduced pedogenic processes that are related to the climatic deterioration that followed paleosol-G formation.

The gradual change between units MC-5 and MC-4 and the slight increase of the F_D data and organic content suggest that soil forming processes had increased relative to the accumulation rate. The low contrast in F_D data and organic content suggest that the ratio between pedogenic processes and accumulation were relatively constant throughout the formation of MC-4. This scenario supports the interpretation of subaerial deposition of these fine grained sediments (loess) and suggests that the two processes were coeval. The magnetic susceptibility peak in the upper portions of unit MC-4, however, may also suggest that climatic optimum occurred in the latter stages of this soil forming interval.

A significant rise in the median grain size, and a corresponding decrease in the rock magnetic parameters and organic content, mark the formation of MC-3 and record paleosol-E formation. The physical properties identified in the field are the best evidence for paleosol-E. Evidence includes granular structure, and the presence of a paleosurface that is inferred from the light coloured fissures that penetrate into the darker organic horizons of paleosol-F (Figure 3.26). The trend of the median grain size that gradually increases up-section (Figure 3.31) through paleosol-E may be the result of deteriorating climatic conditions. Therefore, paleosol-E represents a punctuation in climatic deterioration. During this episode, relatively weak pedogenic processes were able to overprint the parent material. These processes began to wane once the rate of climatic deterioration and associated accumula-

tion rates exceeded the ability of pedogenesis to overprint the parent material. A fining that occurs above the grain-size peak at approximately 540 cm suggests waning winds during the initiation of climatic amelioration. The end result is the termination of this cold period marked by the formation of paleosol D_1 . This paleosol overprints the finer sediments deposited during the deglacial phase of the preceding cold period (represented by unit MC-3). Significant increases in rock magnetic properties, organic matter, leached carbonate in the lower soil profile (in MC-3), and the presence of abundant pedogenic structures and krotovena suggest a strong soil forming interval. Subsequent climatic deterioration increased the rate of deposition and reduced the effects of pedogenic processes. This resulted in the formation of MC-2 and the development of D_2 during the initial transition from warm period to subsequent cold period. Continued climatic deterioration allowed the formation of permafrost which overprints the upper portions of the underlying unit (MC-3). Ground wedges that overprint krotovena related with the genesis of paleosol D_1 are interpreted as ice-wedge pseudomorphs based on their morphology; these permafrost features developed during this significant cold phase that followed D_2 soil formation. Furthermore, krotovena observed above paleosol- D_2 exhibit a different morphology than those associated with paleosol- D_1 (*cf.* krotovena in Figure 3.25b and c) thereby supporting the notion of a change in climate (*i.e.*, change in land-mammal assemblage) from climatic optimum to cold glacial-steppe conditions.

A minor period of warming during the deposition of MC-2 is recorded by minor peaks in the rock magnetic parameters, a slight darkening of the unit and the presence of pedogenic structures related to the genesis of paleosol-C. This is followed by a return to cold conditions and the deposition of MC-1, as pedogenesis is reduced during the late glacial period. The formation of soil-A that overprints unit MC-1 marks the final climatic amelioration to affect the region; this phase of pedogenesis is associated with the Holocene Epoch.

Distal Section Correlation

Allostratigraphy allows long range correlation of heterogeneous units based on the occurrence of mappable bounding discontinuities. Soils and paleosols represent discontinuities in depositional processes and are viable boundaries of allostratigraphic units. As discussed earlier, paleosols are prevalent within the sections at each of the four sites. In some cases, these paleosols are mappable and the vertical sequence of their relative development (*e.g.*, soil-A, paleosol-C and paleosol-D sequence), in addition to the identification of marker beds (*e.g.*, paleosol-D, Don Till *etc.*), will allow the construction of an allostratigraphic framework for long-range, site-to-site correlation.

Allostratigraphic Framework: introduction

Having completed the description of the lithic and basic pedologic characteristics, and having presented the local correlation between sections at each of the four study sites (*vide ante*), it is now possible to link the composite sections using marker beds and paleosols, trends in magnetic susceptibility data (where possible) and approximate time lines given by optical dating studies (*vide post*).

The construction of the allostratigraphic framework (Figure 3.33: insert) consisted of 4 integral phases: 1) identification of suitable bounding discontinuities; 2) classification of the reliability and status (*e.g.*, member or formation) of each allo-boundary (clear or inferred); 3) recognition of readily identifiable marker horizons for relative temporal control, and; 4) integration of absolute ages (*e.g.*, optical luminescence) which provide an independent check on the validity of the allostratigraphic framework. Once phases one through four were completed, each composite section was evaluated in relation to adjacent sections and informal alloformations were named and subdivided into allomembers. An alloformation designation consists of the letter "A" (for Allostratigraphy) followed by a unit number (*e.g.*, A-3). These can be further subdivided into allomembers, designated by a lower-case letter following the alloformation name (*e.g.*, A-3a). This alphanumeric sequence increases down-section to allow for future additions to the allostratigraphic framework. A detailed explanation of the construction of this allostratigraphy is presented in Appendix C.

Allostratigraphic Framework: discussion

The allostratigraphic succession observed (Figure 3.33) over the *ca.* 700 km north-south transect can be divided into three complete and definitive alloformations (A-1 through A-3), one complete, possible alloformation (A-4: *vide ante*) and three incomplete but possible alloformations (A-5 through A-7: *vide ante*). The three lowermost alloformation boundaries are given "formation" status based on the degree of development of the soils and the magnitude of the magnetic susceptibility signal relative to other interglacial soils above unit MC-7 (*cf.* figure 3.31: paleosols J, I, H, G, D and A). The upper two alloformations are further subdivided into 4 complete and definitive allomembers based on the presence of relatively weak, mappable paleosols. This endeavour represents the first attempt to develop an allostratigraphic framework on Russian Plain sediments.

The recognition of these allo-units suggests seven primary phases of deposition (A-1 through A-7), the major unconformity observed below unit MC-7 suggests the possibility that some primary phases of deposition may have been removed, as is the case west of MS5 (*vide* Chapter 4 for details). Even so, the identification of major bounding discontinuities allows the identification of seven depositional cycles punctuated by periods of enhanced pedogenesis.

The validity of the upper portion of the allostratigraphic correlation can be evaluated through the use of absolute age constraints. Here, optical dating is used and gives rise to the following implications:

- 1. All optical ages from below paleosol-D are minimum ages that corroborate and chronologically constrain the long-range correlation of alloformation A-2.**
- 2. All optical ages from between paleosol-D and paleosol-C suggest that the latter soil formed during an interstadial of the last glaciation at each site, thereby corroborating the stratigraphic framework.**
- 3. Optical ages above paleosol-C at Likhvin and Gololobovo support the allostratigraphic framework. However, the age at Mikhailovka is problematic (*vide post*).**

There are two possibilities for the older age for MCSL2 (Figure 3.33). If paleosol-C is entirely overprinting, then it is possible that the age of 40 ± 2 ka represents the timing of deposition of the parent material in which paleosol-C subsequently developed. However, pedogenic evidence suggests that the soil is a cumulic regosol which contradicts this proposal. Alternatively, grain size experiments have suggested that finer particles were transported to this site as silt-clay aggregates that were broken down into their primary constituents during laboratory pretreatment procedures (Figure 3.32). Also, high calcium carbonate percentages were noted in this portion of the record (Figure 3.31). Without doubt, some of the carbonate was mobilized during soil-A formation. However, the older-than-expected optical ages may suggest that the one source of this carbonate was calcium cement (*e.g.*, Plate 3.9 F) that held the silt-clay aggregates together during entrainment and transport to this location, but also prevented the silt grains from being reset with respect to optical dating principles (*cf.* Prescott and Robertson 1997), thereby explaining an age that is too old by a factor of approximately two.

The allostratigraphic construction presented above allows natural depositional cycles to be identified on the basis of physical evidence **rather than** climatic interpretations. The result: alloformations approximate glaciations punctuated by, or terminated by interglacials (*i.e.*, represented by relatively well developed paleosols/soils), and allomembers (where subdivisions of an alloformation are identified) approximate stadials within glaciations that are punctuated by interstadial events (*i.e.*, relatively weakly developed paleosols).

The realization of the foregoing relationship between the allostratigraphic units and their interpreted glacial cycle implications allows the construction of a stratigraphic scheme based on tangible and mappable evidence (*i.e.*, physical characteristics, bounding discontinuities and paleosol-sequence relationships). Climatic interpretations, which may change with further research, can be easily extracted from this independent allostratigraphic foundation, rather than using evolving climatic interpretations as the basis of the entire stratigraphy, *i.e.*, climatostratigraphy (*cf.* North American Commission on Stratigraphic

Nomenclature 1983; for further discussion, see Appendix C). The presented allostratigraphic scheme provides the potential to avoid future enigmatic stratigraphies similar to those presented in Chapter 1 (Figure 1.6). Furthermore, with the appropriate data, investigations can be made into the timing of the inferred depositional events (Chapter 5).

Chapter Summary

This chapter presented basic section descriptions, local correlations, composite section construction and regional inter-site correlations. Initially, basic stratigraphic concepts used throughout this chapter were briefly discussed (detailed discussions are found in Appendix C) in order to give the reader background information as to the logical progression and development of final stratigraphic scheme. This discussion was followed by site-by-site descriptions and interpretations of units and paleosols, followed by composite section construction for the stratigraphy observed at each site. Once the composite sections were completed, allostratigraphic concepts were applied. The resulting allostratigraphic scheme allows each composite section along the transect to be compared and contrasted, and aids in the construction of an age model presented in the ensuing chapter.

CHAPTER 4 - CHRONOSTRATIGRAPHY

Introduction

This chapter will place the allostratigraphic units (and their lithic and pedogenic components) that were presented in Chapter 3 (Figure 3.33) into a temporal context through empirical data correlations and geologic interpretations of physical evidence.

Detailed field and laboratory magnetic susceptibility measurements obtained from both Korostylievo and Mikhailovka sites yielded magnetic susceptibility enhancement patterns of the parent material that are similar to those observed in the Chinese Loess Plateau (*cf. Evans et al. 1997*), and which track the marine $\delta^{18}\text{O}$ record (*Ding et al. 1994, Rutter et al. 1996, Vandenberghe et al. 1997*). This initial observation led to a more detailed correlation between Russian Plain magnetic susceptibility and SPECMAP. From this analysis, supporting optical ages and the paleomagnetic chron boundary detected at Mikhailovka, a new age model spanning *ca. 800 ka* is developed for Quaternary stratigraphy of Russian Plain.

Organization

The magnetic susceptibility data from Korostylievo and Mikhailovka are presented with a correlation to SPECMAP. Implications of the terrestrial-oceanic correlation are then discussed, focusing on uncertainties within the currently accepted stratigraphy (*i.e., Velichko et al. 1999; Fig. 1.6*). Based on the data presented, solutions to long-standing stratigraphic problems are proposed and a new chronostratigraphic scheme for the Russian Plain is developed.

Construction of SPECMAP Correlations

Each of the sub-figures ("A" and "B") within figure 4.1 (insert) are constructed in the same manner; the composite stratigraphies of Korostylievo and Mikhailovka are adopted from figures 3.16 and 3.31 respectively. The allostratigraphy is obtained directly from figure 3.33. The SPECMAP record of *Imbrie et al. (1984)*, as modified by *Bassinot et al. (1994)*, was first digitized, followed by sequential peak/trough matching (*cf. Imbrie et al. 1984; Ding et al. 1994*) to the magnetic susceptibility versus depth data. In each case, absolute ages obtained from optical

dating and paleomagnetic reversals were first used to constrain the peak/trough matching within the youngest (<150 ka) and oldest (*ca.* 800 ka) portions of the stratigraphy, respectively. Each of the site correlations to SPECMAP were done independently; the interpreted stratigraphy and allostratigraphy are also independent of the magnetic susceptibility/SPECMAP records and correlations. At Mikhailovka, consideration is given to the observable presence of a major unconformity crosscutting at least three paleosols below the till associated with the Don Glaciation (Figure 4.2: insert). Further, since the time-span of the sedimentary record is thought to exceed 300 ka, the refined SPECMAP record of Martinson *et al.* (1987) was not used.

Stratigraphic Time Scale Development

The new time scale (Figure 4.3) utilizes currently accepted ages and MIS association for key marker horizons which include: Holocene soil (modern-day), Bryansk Paleosol (*ca.* 34-27 cal. yrs. BP; corrected after Velichko *et al.* 1964; Velichko and Morozova 1972, 1987; Dobrodeyev and Parunin 1973; Chichagova 1972, 1985; Velichko *et al.* 1992; Tsatskin 1997), Salyn Paleosol (*ca.* 130 -120 cal. yrs. BP; Velichko *et al.*, 1999; Figure 1.6) and the Brunhes/Matuyama boundary (780 ka: Cande and Kent 1995).

The following outlines the major factors that contributed to the development of the new time scale. The implications of these factors are discussed in the following subsection.

- 1) the site-independent, peak/trough tracking of the terrestrial magnetic susceptibility record to the SPECMAP record;**
- 2) the optical ages between paleosols C and D agree with inferred ages obtained from SPECMAP/magnetic susceptibility correlation at all four sites;**
- 3) the unconformity below unit MC-7 (till) may represent hundreds of thousands of years of erosion (figures 4.2 and 4.3);**
- 4) the identification of the Brunhes/Matuyama boundary (780 ka; Cande and Kent 1995) near the base of unit MC-12 (Semenov pers. com., 2001), and;**

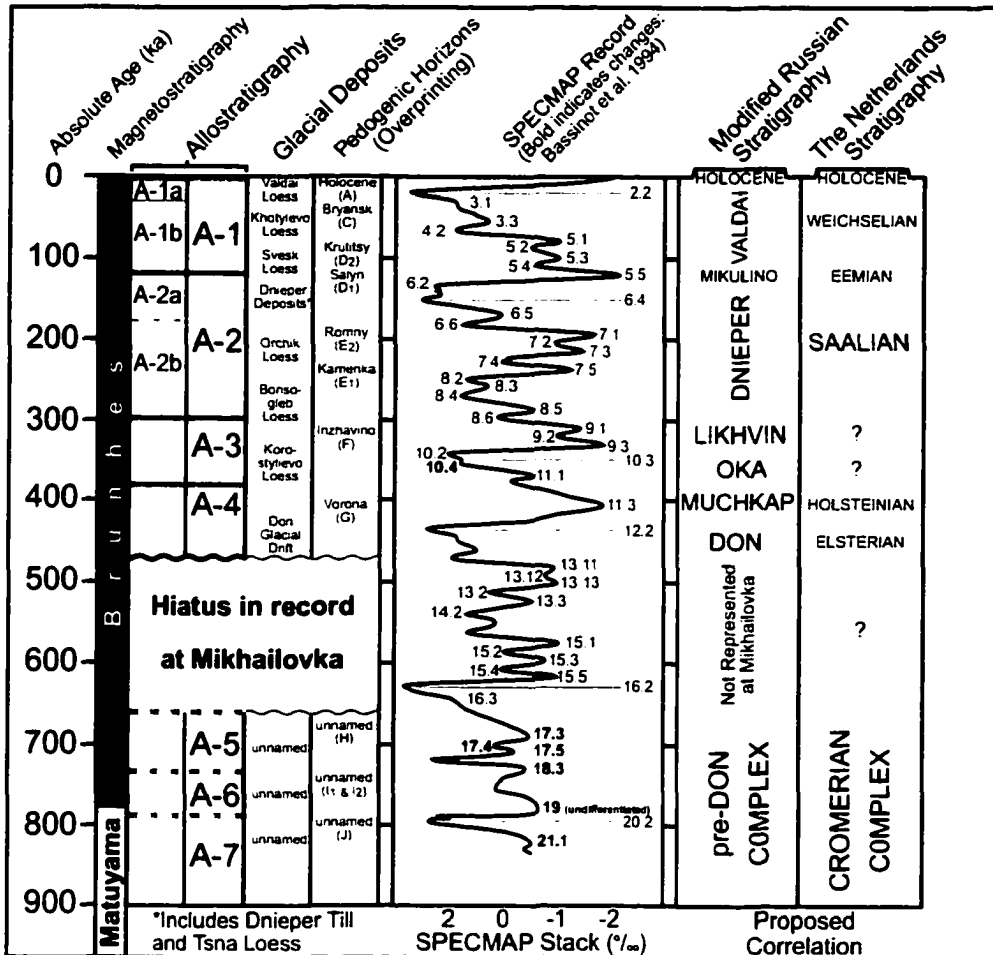


Figure 4.3. The newly proposed chronostratigraphic and geochronologic schemes for the Russian Plain are plotted versus absolute time as determined through SPECMAP correlations. Correlations are based on magnetic susceptibility data, optical dating, paleosol sequences, the presence of the Brunhes / Matuyama boundary within alloformation A-6 (Semenov pers. com. 2001) and the identification / consideration of major unconformities in the geologic record. Major advances between this scheme and the scheme presented by Velichko *et al.* 1999 include: 1) expansion of the Dnieper Glaciation to include MIS 8 and MIS 6; 2) development of the Romny and Kamenka paleosols within interstadials of the Dnieper Glaciation; 3) empirical support for the correlation of the Inzhavino Paleosol (Likhvin Interglacial) with MIS 9; 4) association of the Vorona Paleosol (Muchkap Interglacial) with MIS 11 and the corresponding disassociation of the Likhvin Interglacial with the Holsteinian Interglacial of western Europe, and; 5) the correlation of alloformations A-5 through A-7 with MIS 17 through 21 respectively and their corresponding association with the Cromerian Complex of western European schemes. Symbols presented in this diagram follow from figures 3.33 and 4.1.

5) the stratigraphic location of the Brunhes/Matuyama boundary corroborates the location of MIS 19 (cf. Bassinot *et al.* 1994) which was inferred from the magnetic susceptibility/SPECMAP correlations.

Together, these factors support the correlation between terrestrial magnetic susceptibility in the Russian Plain and the SPECMAP record of Imbrie *et al.* (1984) and Bassinot *et al.* (1994). However, two optical ages at Mikhailovka are somewhat problematic: MCSL4 at 132 ± 22 ka appears to correspond to MIS 7.3 and MCSL2 at 40 ± 2 appears to correspond to MIS 2. A solution to the latter has already been proposed in Chapter 3. The former is easily explained: due to anomalous fading of very old ages, and given the presence of younger material being mobilized downward and infilling fissures, MCSL4 represents a minimum age. It is therefore used to add validity to the inferred age of paleosol-D and alloformation A-2, but lacks the resolution to constrain the sediments to a specific oxygen isotope stage.

One critical implication of the MIS correlation to Korostylievo and Mikhailovka (Figure 4.1): physical evidence at these sections does not support the currently accepted chronostratigraphy for the Russian Plain in its entirety (Velichko *et al.* 1999; cf. Figure 1.6). This can be validated, by not accepting luminescence ages beyond 150 ka¹ (Wintle and Huntley 1982; Prescott and Robertson 1997; Huntley and Lian 1999; Lian and Huntley 2001; Little *et al.* in press) and any age relationships based on those data (*e.g.*, age of land mammal assemblages) that have been reported for strata of the Russian Plain -- an important consideration since these types of data have previously formed a keystone of Russian Plain Quaternary chronostratigraphy for the last 3 decades (Little *et al.* in press and references therein).

¹A single exception is the optical dating results of van Heteran *et al.* (2000) who, under special circumstances where K-feldspar were included within quartz grains, was able to demonstrate that some back-shore dunes along the coasts of Australia progressively increased in age landward up to *ca.* 400 ka -- corresponding to interglacial events.

Stratigraphic Implications: Discussion

Several stratigraphic implications arise from SPECMAP correlation to rock magnetic parameters. The younger, well dated deposits generally support the currently accepted Russian Plain stratigraphy. However, results presented herein significantly alter the chronology of events that took place prior to *ca.* 100 ka. The ensuing paragraphs outline, in chronological order, the implications of this research on the Russian Plain stratigraphy.

Brunhes/Matuyama Boundary within MC-12

The discovery of the Brunhes/Matuyama within MC-12 (Semenov, pers. com. 2001) serves as a lower control point for magnetic susceptibility - SPECMAP correlations.

Proposed Ages Units A-7 Through A-5

The lower three soils range from *ca.* 666 ka (paleosol-H) to *ca.* 820 ka (paleosol J). These ages are based on the magnetic susceptibility correlation to the SPECMAP orbitally tuned time scale (Imbrie *et al.* 1984) as modified by Bassinot *et al.* (1994) and the identification of the Brunhes/Matuyama boundary therein (*vide ante*). Given this information, these paleosols likely correspond to late Cromerian deposits of The Netherlands Quaternary Stratigraphic Record (Zagwijn 1996).

Reassessment of the Age of the Don Till on the Russian Plain

Presently, the Don Glaciation is presumed to be associated with MIS 16 (Velichko 1990; Glushankova and Sudakova 1995; Sudakova and Faustova 1995; Zagwijn 1996; Lowe and Walker 1997; Velichko *et al.* 1999). However, given the evidence from both Korostylievo and Mikhailovka, it is difficult to support this conclusion. The following summarises relevant physical evidence based on the author's research:

- 1) a till (KC-7 and MC-8) extends southward to a latitude of at least 50° 06' N which supports the all-time Pleistocene maximum glacial advance of the Don Till;**
- 2) a minor deglacial unconformity at the top of this till unit at both Korostylievo and Mikhailovka, and;**

3) a major erosional surface along the base of the Don till at Mikhailovka (Figure 4.2) that crosscuts three paleosol. When comparing the magnetic susceptibility to the SPECMAP time scale, this observed unconformity represents a major (ca. 185 ka) hiatus.

This leaves two possible alternatives: **A.** The till is not the Don Till and therefore represents an earlier glacial advance; or, **B.** the Don Till is much younger than previously thought. The first alternative (**A**), which invokes a major hiatus at the KC-8/-7 and MC-7/-6 boundaries does not allow for the lower, major unconformity (Figure 4.2) given the presence of the Brunhes/Matuyama boundary within MC-12. The second alternative (**B**) is therefore favoured for the following reasons:

- 1) accounts for both the upper (minor) and lower (major) unconformities and the hiatuses that they represent;**
- 2) the presence of early Cromerian land mammals (e.g., *Miomys intermedius* Newton) in sediments immediately below (but not within or above) the Don Till (Lomonosova 1987); and,**
- 3) recent work by Pospelova *et al.* (1997) who “tentatively” associate Don Glacial beds with MIS 12.**

Point three is based on the presence of a paleomagnetic excursion associated with MIS 12, but occurring within sediments of the Don Glaciation (Pospelova *et al.* 1997, p. 781). This evidence supports the association of the Don Till with MIS 12 (figures 4.1, 4.2 and 4.3).

Age Associations for units overlying KC-8 and MC-7

The age-associations of the supra-Don Till stratigraphic sequence are determined by using existing relative paleosol sequence (*cf.* Figure 1.6 - Velichko *et al.* 1999) as a guide, and by the evaluation of marker beds associated with: MIS 9 (*i.e.*, Inzhavino Paleosol: Zagwijn 1996; Velichko *et al.* 1999; Velichko *per. com.* 2001), MISS 5.5 (*i.e.*, Mezin Paleosol Complex, Velichko *et al.* 1999), MIS 3.3 (*i.e.*, Bryansk paleosol, Velichko *et al.* 1999) and the present-day soil (*i.e.*, MIS 1). Referring to Figure 4.1, one can clearly denote paleosols A through G, their associated peaks in the magnetic susceptibility data set and their suggested association with

the marine isotope stages of the SPECMAP record (Imbrie *et al.* 1984; Bassinot *et al.* 1994).

With reference to the newly proposed age model for the Russian Plain (Figure 4.3), the time-stratigraphic position of paleosol-G differs from the currently accepted Russian Plain stratigraphic scheme of Velichko *et al.* (1999: *cf.* Figure 1.6). This difference is based on the following:

- 1) the recognition and status classification of unconformities (*vide ante*) in the stratigraphic record;**
- 2) the correlation of paleosols A, C, D, and F to the SPECMAP record;**
- 3) the association of the upper portion of allunit A-4 and paleosol-G with SPECMAP MIS 11 (364 ka - 427 ka; Bassinot *et al.* 1994),and;**
- 4) the stratigraphic position of paleosol-G (*i.e.*, between the Inzhavino Paleosol of MIS 9 and the Don Till (*e.g.*, pre-MIS 11).**

Together, not only do these relationships suggest that paleosol-G is the Vorona Paleosol (Figure 4.3) of the Muchkap Interglacial (Zubakov 1993; *cf.* Figure 1.6 - Velichko *et al.* 1999), but also that these stratigraphic and geochronologic units (respectively) are associated with MIS 11 (figure 4.1 and 4.3) and not MIS 15 as suggested by Velichko *et al.* (1999: *cf.* Figure 1.6). This in turn implies that the Muchkap Interglacial is associated with the Holsteinian Interglacial of western European schemes, rather than the more frequently quoted Likhvin-Holsteinian Interglacial association (*cf.* Little *et al.* in press and references therein; Appendix B). This may initially seem unlikely, but, the timing of the Holsteinian Interglacial has been highly contentious as it has been reported to occur anywhere between MIS 7 and MIS 15 (*cf.* Zagwijn 1992, 1996; van Kolfschoten 1993; Zubakov 1993; Lowe and Walker 1997; Velichko *et al.* 1997; Turner 1996; Poore *et al.* 1998). Therefore the correlations presented herein between the Muchkap and the Holsteinian become, at the very least - plausible and should therefore be considered as an alternative to be tested.

The subsequent Likhvin Interglacial resulted in the formation of the Inzhavino soil (Velichko *et al.* 1999). The timing of this interglacial event has been previously based on correlations to MIS 9 (Velichko pers. com. 2001) and to the Holsteinian Interglacial of Europe (*e.g.*, Lowe and Walker, 1997). However, the correlation of the Holsteinian of the Netherlands stratigraphic record and MIS 9 has been recently discredited (*e.g.* Zagwijn 1992, 1996; Turner 1996; Poore *et al.* 1998). Therefore a re-evaluation of the Inzhavino Paleosol and corresponding Likhvin interglacial is required. To facilitate this re-evaluation, magnetic susceptibility-SPECMAP associations were examined at Korostylievo and Mikhailovka. Results suggest that paleosol-F is associated with MIS 9; this association occurs at both Korostylievo and Mikhailovka, although it is more easily identified at the former site (Figure 4.1). Given the pedostratigraphy and the lack of observable unconformities above this pedogenic horizon, paleosol-F is interpreted as the Inzhavino Paleosol. Hence, the data presented (Figure 4.1) supports the current notion (Velichko *et al.* 1999) that the Likhvin Interglacial occurred during MIS 9. A major implication of this interpretation, however, is that the Likhvin Interglacial is not associated with the Holsteinian Interglacial (*vide ante*). Also, the newly proposed age model clarifies other long standing enigmas: In recent schemes, the Likhvin Interglacial is commonly presented as a “*sensu lato*” geochronologic unit (Sudakova and Faustova 1995) or as “uncertainties” within the stratigraphic scheme (*cf.* Figure 1.6; Velichko *et al.* 1999). These types of uncertainties associated with the timing of the Likhvin Interglacial suggest inherent problems with its correlation to the MIS and other stratigraphic schemes. The age model proposed herein (figures 4.1 and 4.3) presents empirically-based solutions to this and other Russian Plain stratigraphic enigmas (Figure 4.3).

Currently, the Dnieper glacial deposits are associated with MIS 6, and the Romny and Kamenka paleosols are interpreted as having been developed prior to Dnieper glacial advance (figures 1.6 and 1.8; Velichko *et al.* 1999). However, other interpretations suggest that the Moscow event and Dnieper event should be classified into two glaciations separated by the Ordinstovo Interglacial (Sudakova and Faustova

1995). Again, the chronostratigraphy proposed herein, presents a solution that encompasses both ideas and explains the timing of these events based not only on the correlation of magnetic susceptibility and SPECMAP data, but also on the relative development of soil horizon sequences. Figure 4.3 classifies the Dnieper event as a glaciation that spans MIS 8 to MIS 6. Within this glaciation, there was a relatively weak climatic amelioration represented by paleosols E_1 and E_2 (coalesced into paleosol-E at the Mikhailovka site). This paleosol set is much weaker than other paleosols that have been classified as “interglacial soils” (cf. soil-A and paleosols D, F and G) and hence paleosol-E (paleosols E_1 and E_2 *sensu stricto*) is given an interstadial status. The timing of soil development for these weaker paleosols is based on the data presented in Figure 4.1 which suggest that they range between 186 ka and 236 ka (MISS 7.0 to MISS 7.5; Bassinot *et al.* 1994). The two inferred stadials, MIS 8 and MIS 6, are not named in the proposed scheme of figure 4.3, but may represent the Moscow and Dnieper stadials of the Dnieper Glaciation respectively (Figure 1.6).

The magnetic susceptibility peak occurring within paleosol-D at the Korostylievo and Mikhailovka sites exhibits a reasonable correlation to MIS 5 of the SPECMAP record (Figure 4.1). Furthermore, allostratigraphic correlation of optically dated samples above and below paleosol-D supports this conclusion (Little *et al.* in press). Both these lines of evidence suggest that paleosol-D (which includes D_2 and D_1) is the Mezin complex; D_1 is interpreted to be the Salyn Paleosol (MIS 5.5) of the Mikulino Interglacial while D_2 is interpreted to be associated with the Krutitsy phase of soil formation (late MIS 5 or MIS 4).

The Late Pleistocene (*i.e.*, last glacial cycle) is represented by alloformation A-1 and its subordinate members. Within this portion of the record at Korostylievo and Mikhailovka, the magnetic susceptibility pattern closely tracks MIS 1 through MIS 5 of the SPECMAP record (Imbrie *et al.* 1984) (Figure 4.1). This is in addition to corroborating evidence from optical dates that validate the allostratigraphic correlation. The Late Pleistocene record at these two sites, however, is not without problems. When comparing the Korostylievo and Mikhailovka records, the A-1a/b boundary (Figure 4.1) appears to occur at different

positions in the SPECMAP record: below and above MIS 2.2 respectively. A possible reason for this is that the A-1a/b boundary at Mikhailovka has been placed at the upper limit of pedogenesis, which may not be associated with the main phase of pedogenic development during the MIS 3 interstadial. A closer examination of both records reveals a sharp upper contact of Korostylievo paleosol-C (Bryansk Paleosol; figures 4.1 and 4.3) whereas the upper contact of the corresponding paleosol-C at Mikhailovka exhibits a diffuse upper contact. This suggests that paleosol-C at Korostylievo was an overprinting soil that developed downwards into the underlying parent material, while at Mikhailovka paleosol-C pedogenesis may have been followed by a phase of cumulic soil development. At Korostylievo, a proximal ice-sheet margin location gave rise to increased accumulation rates which inhibited pedogenesis and buried paleosol-C, preserving a clear upper contact. At Mikhailovka, however, the southern-most locality of the site, and its distal position to the ice-sheet margin allowed weak pedogenesis to continue following the main pedogenic phase of the interstadial. This weak cumulic pedogenesis, which forms the upper portion of paleosol-C at Mikhailovka, may mask the paleosurface associated with main phase of soil development and so, the peak in magnetic susceptibility observed at a depth of 250 cm (Figure 4.1) within unit MC-2 may represent optimal pedogenic conditions during the MIS 3 interstadial. If this is the case, then the A-1a/b boundary should be lowered accordingly in the Mikhailovka record, yielding a SPECMAP correlation similar to that observed at Korostylievo. Further investigations as to the nature of these contacts are needed in order to examine the validity of this argument.

The Holocene is clearly marked in the correlation of the magnetic susceptibility record and the SPECMAP record. This correlation acts as a unmistakable marker bed, as well as an analog of the rock-magnetic signatures for underlying paleosols, their correlation to the SPECMAP record and for other allostratigraphic boundaries.

Chapter Summary

Geologic interpretations and magnetic susceptibility versus depth data are correlated to the SPECMAP record using optical ages and the Brunhes/Matuyama paleomagnetic boundary to constrain the upper (<150 ka) and lower portions of the correlation, respectively. Correspondence between these two data sets allowed the development of a newly proposed age model for the Russian Plain. The final result is a stratigraphic scheme that proposes solutions to problematic issues related to Russian Plain stratigraphy:

- 1. Expansion of the Dnieper Glaciation to include both MIS 8 and MIS 6.**
- 2. Places the development of the Romny and Kamenka paleosols within interstadials of the Dnieper Glaciation.**
- 3. Corroboration of the MIS 9 association with the Likhvin Interglacial and its corresponding disassociation with the Holsteinian Interglacial of western Europe.**
- 4. Association of the Vorona Paleosol of the Muchkap Interglacial with MIS 11.**
- 5. The recognition of a major unconformity cross-cutting three paleosols below the Don Till at Mikhailovka which represents a hiatus spanning *ca.* 185 ka.**
- 5. Association of alloformations A-5 through A-7 with MIS 17 through 21 respectively, and the corresponding association of these allostratigraphic units with the Cromerian Complex of western Europe.**

The new stratigraphic scheme presented in this chapter forms the basic geologic foundation from which Quaternary geologic evolution and paleoclimatic interpretations are based in ensuing chapters.

CHAPTER 5 - RUSSIAN PLAIN QUATERNARY HISTORY

Introduction

This chapter focuses on relating the depositional environments and inferred climates between sites along the north-south transect in order to construct a regional view of Quaternary History on the Russian Plain.

Quaternary History of the Study Area

The following subsections present an interpretation of the sequence of events that contributed to the geologic evolution of the study area during the last *ca.* 800 ka of the Pleistocene Epoch. They are presented in chronological order starting with the pre-Don Till sedimentary sequence (allunits A-7 through A-5). However, because the pre-Don Till sequence is observed at only one site, this portion of the geologic record can not be placed in a regional context. Furthermore, the modern-day soil (A) and to some degree, the Mezin Paleosol Complex (D) have been intensively studied at northern and central locations, therefore, these will not be fully reinterpreted herein. They will, however be used as analogs to aid the paleoclimatic interpretations of older paleosols (*cf.* Table 5.1). Also, the Likhvin and Gololobovo sites will be considered as a single site for the purpose of interpreting the regional Quaternary history based on the following criteria:

- 1) latitudinal zonation of bio-climatic zones (*e.g.*, Figure 1.2);**
- 2) the proximity of the Likhvin and Gololobovo sites (north-south separation distance of only 100 km);**
- 3) both sites fall within modern day limits of mixed forest/forest-steppe zones of the temperate belt (Figure 1.2; Shcherbakova 1998);**
- 4) both sites fall within modern and Mikulino mixed-broadleafed forest vegetation zones (Shcherbakova 1998; Velichko *et al.* 1999), and;**
- 5) both sites fall within the same soil great group regions for the Holocene and Mikulino interglacials (Shcherbakova 1998).**

Table 5.1. Paleosol summary table outlining the pedofacies changes between site localities. Highlighted regions represent paleosols that could not be reasonably subdivided.

Paleosol Horizon	Gololobovo 55° 03'N; 38° 34'E	Likhvin 54° 06'N; 36° 16'E	Korostylievo 51° 51'N; 42° 22'E	Mikhailovka 50° 06'N; 43° 14'E
A	Luvisol (undif.)	Brunisol (undif.) ¹	Orthic Black Chernozem	Eluviated Brown Chernozem
B	N/A	Cumulic Regosol ³	N/A	N/A
C	Cumulic Regosol	Cumulic Regosol	Eluviated Brown Chernozem	Cumulic Regosol ³
D ₂	Luvisol (undif.)	Grey Brown Chernozem (upper) and Luvisol (lower)	Calcic Dark Brown Chernozem	Cumulic Regosol ³
D ₁			Orthic Dark Brown Chernozem	Solonchic Dark Brown Chernozem ³
E ₂	Luvisol (undif.)	Luvisol (undif.)	Orthic Brown Chernozem	
E ₁	Eluviated Brown Chernozem	Eluviated Brown Chernozem ¹	Cumulic Regosol	Cumulic Regosol ³
F ₂	Grey-Brown Luvisol	Luvisol (undif.)	Eluviated Brown Chernozem	Rego Brown Chernozem ³ to Calcareous Brown Chernozem ³ Catena
F ₁			Dark Grey Chernozem	
G	N/A	N/A	Luvisol (undif.) ²	Dark Grey Chernozem ³
H	N/A	N/A	N/A	Luvic Gleysol ³
I ₂	N/A	N/A	N/A	Eluviated Brown Chernozem ³
I ₁	N/A	N/A	N/A	Dark Grey Chernozem ³
J	N/A	N/A	N/A	Calcareous Brown to Dark Brown Chernozem ³

¹Alternatively, this may have been a brunisol.

²This paleosol is polygenetic: The luvisolic phase overprints a calcic brown chernozemic phase.

³These paleosols were interpreted from field and laboratory data only. Sollelic factors prevented micromorphological analysis.

Allunits A-7 through A-5 (pre-Don sediments) MIS 21-17

The progression of paleosols through time, from a calcareous brown to dark brown chernozem (paleosol-J) through dark grey and eluviated brown chernozems (paleosol-I₁ and I₂) to a luvic gleysol (paleosol-H) suggest an increase in available moisture during each successive interglacial. Likewise, the observed decrease in the size of the seasonal frost/desiccation fissures progressively up-section (Figure 3.30) supports this interpretation for the intervening cold intervals. Furthermore, the accumulation rate for the pre-Don Till sediments generally increases through time, culminating below the Till/Paleosol-H unconformity (Figure 5.1, A-7 through A-5). Therefore, it appears as though the general climatic environment at Mikhailovka was deteriorating, while available moisture was increasing through MIS 21 to MIS 17. The subsequent ice-sheet advance during the Don Glaciation eroded sediments that may have been deposited during MIS 16 through MIS 13, and deposited the till unconformably over what remains of paleosol-H.

Allunit A-4 (Don-Muchkap cycle) MIS 12-11

The presence of the Don Till at both Korostylievo and Mikhailovka in the south, suggests that a large ice sheet advanced from the north (presumably covering both Likhvin and Gololobovo, Velichko, pers. com

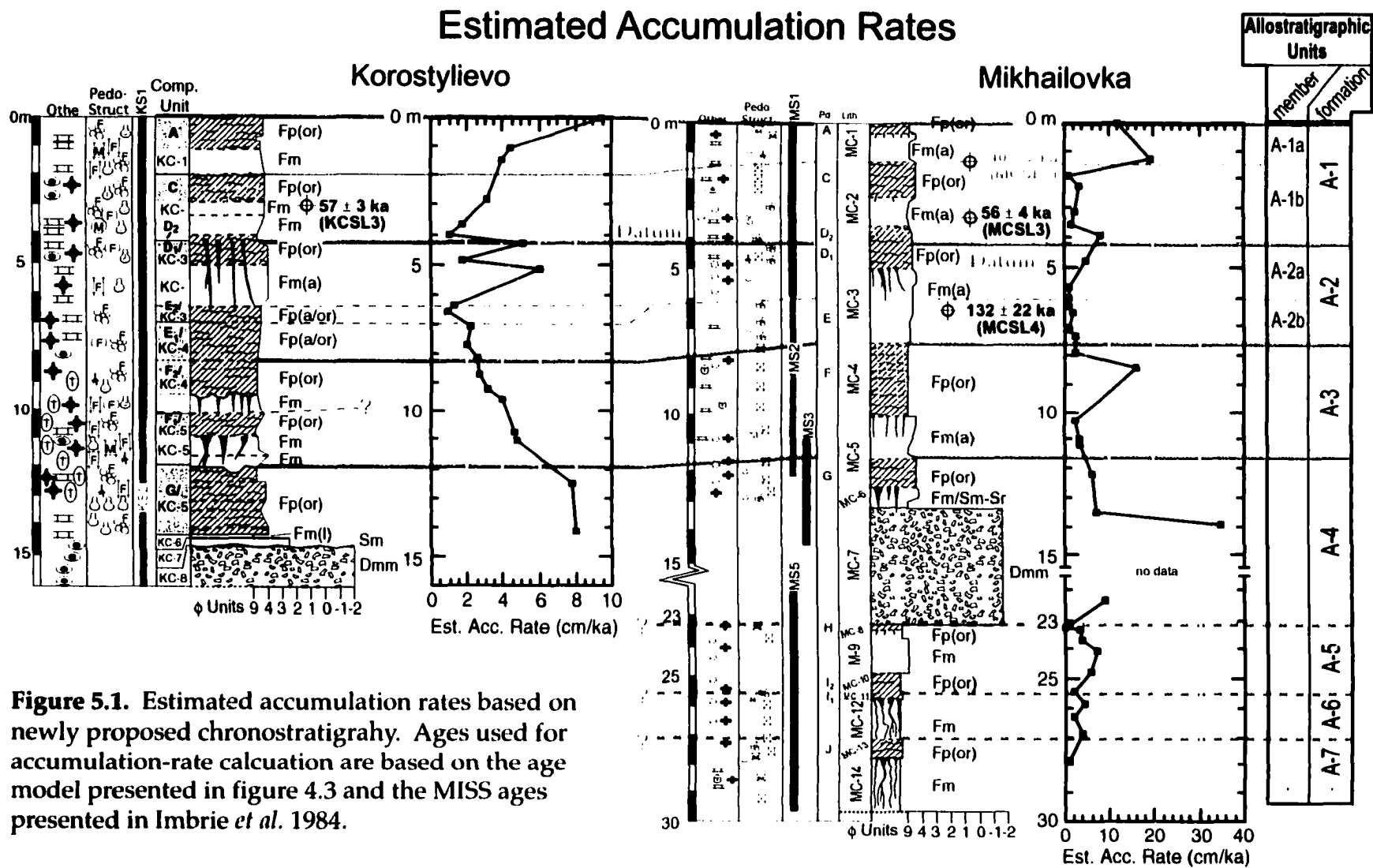


Figure 5.1. Estimated accumulation rates based on newly proposed chronostratigraphy. Ages used for accumulation-rate calculation are based on the age model presented in figure 4.3 and the MISS ages presented in Imbrie *et al.* 1984.

1996) onto the Oka-Don Plain (Figure 5.2). The southern mapped extent of this till suggests that it was deposited during the all-time Pleistocene maximum advance of the European ice sheet (*cf.* figures 1.8 and 5.2). Given the evidence presented in preceding chapters, the Don Glacial advance is associated with MIS 12 (*ca.* 468-427 ka from Bassinot *et al.* 1994) rather than the currently accepted (and problematic) age association with MIS 16 (*ca.* 550-630 ka in Velichko *et al.* 1999 or *ca.* 621-642 ka from Bassinot *et al.* 1994).

As the Don ice sheet retreated from Korostylievo and Mikhailovka, glaciofluvial sediments were deposited. The ever-increasing distance-to-the-glacial-margin is evident in these deglacial sediments from decreasing accumulation rates (Figure 5.1) and median grain sizes (figures 3.16 and 3.31). Eventually, glaciofluvial deposition (Figure 5.1) at these sites gave way to aeolian dust accumulation followed by soil formation during the Muchkap Interglacial (MIS 11).

The Muchkap Interglacial, a major interglacial period, is represented by the Vorona Paleosol (paleosol-G) at both Korostylievo and Mikhailovka (Table 5.1). The character of this paleosol suggests a forest influence at both sites, although this influence is much stronger at Korostylievo (*cf.* undifferentiated luvisol at Korostylievo versus dark grey chernozem at Mikhailovka). The presence of forest-related soils where chernozems are presently forming suggests a significant difference in climate: From these interpretations, the inference is made that the climate over the Russian Plain was warmer and more moist during the Muchkap (*cf.* Holsteinian, Figure 4.3) Interglacial than in all subsequent interglacials, including that of the modern-day. The Vorona Paleosol (paleosol-G) of the Muchkap Interglacial was subsequently buried as climatic deterioration re-initiated aeolian deposition during the Oka Glaciation (MIS 10).

Allunit A-3 (Oka-Likhvin cycle): MIS 10-9

When compared with the Don (MIS 12) or the Dnieper (MIS 8-6), the Oka glaciation is a relatively weak (*i.e.*, less extensive) glaciation (*e.g.*, Figure 5.2). Although no direct evidence for this glaciation (*i.e.*, till) was observed in the northern portion of the field area during the course of this study, the Oka Glacial advance has been mapped south of both

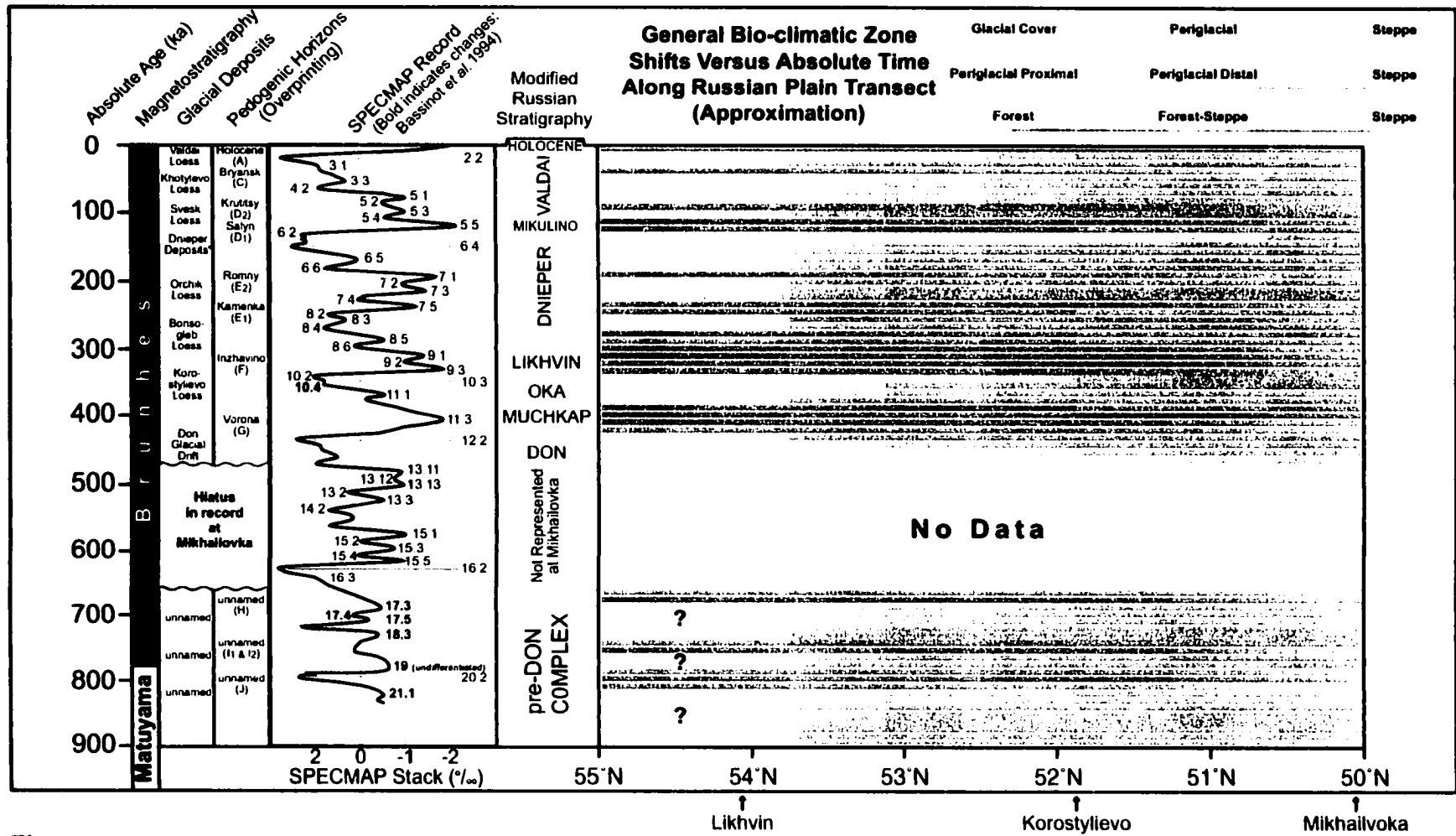


Figure 5.2. Diagrammatic illustrating general bioclimatic shifts and glacial advance relationships associated with the allostratigraphy, geochronology and the newly proposed age model for the Russian Plain.

Likhvin and Gololobovo down to approximately 53° north latitude by other researchers (*e.g.*, Figure 1.8). The initial phase of this glacial period is characterized by an accumulation-rate decrease (Figure 5.1) from approximately 7 cm/ka to 4.6 cm/ka at Korostylievo, and from approximately 5 cm/ka to 3 cm/ka at Mikhailovka. This drop in accumulation rates between these two sites is consistent with an increasing distance-from-source (north to south respectively) scenario for aeolian deposition. Within the zones of pedogenesis, however, the two sites diverge: at Korostylievo, multiple data points illustrate continued decrease in accumulation rate over time, whereas one data point at Mikhailovka depicts a drastic increase from 3 cm/ka to 16 cm/ka. Presently, more credibility is given to the former as it presents a superior data set and supports increased pedogenesis during a period of decreased sedimentation. At Mikhailovka, higher resolution accumulation-rate data in the upper portion of alloformation A-3 are required before reliable interpretations and correlations to other localities can be achieved. The climatic amelioration that followed the short-lived Oka Glaciation is referred to as the Likhvin Interglacial, and is observed at all four sites.

The Likhvin Interglacial is characterized by the migration of the forest-steppe transition zone at least as far south as Korostylievo (paleosol-F₁, Table 5.1). In the north, both Likhvin and Gololobovo exhibit paleosols much more developed than modern-day soils, perhaps suggesting climatic conditions during the Likhvin Interglacial that were intermediate between the present-day conditions and the Muchkap Interglacial conditions (MIS 11).

Allunit A-2 (Dnieper-Mikulino) MIS 8-5.5

Low accumulation rates of approximately 2-3 cm/ka at both Korostylievo and Mikhailovka (Figure 5.1, A-2b) suggest a slow-gradual transition from the Likhvin Interglacial to the initial stages of the Dnieper Glaciation.

The first major cold phase (*ca.* MISS 8.4-8.2: 266-248 ka, Bassinot *et al.* 1994) of the Dnieper Glaciation produced a weak ice-sheet advance commonly associated with the Moscow Stadial of the Dnieper Glaciation. This early Dnieper ice-sheet advanced southward onto the Rus-

sian Plain and stopped just north of Moscow (figures 1.8 and 5.2). Increased oscillation of the SPECMAP record during MIS 7 suggests climatic instability which is corroborated by the formation of two relatively weak paleosols (E_1 and E_2) and an intervening loess. The latter paleosol represents warmer climatic conditions and is associated with the Romny Interstadial. During this time, ice retreated and forests briefly returned to Gololobovo and Likhvin while brown chernozems and cumulic regosols formed in cold steppe environments farther south at Korostylievo and Mikhailovka respectively. The burial of the Romny Paleosol (paleosol- E_2) by loess is characterized by increased accumulation rates at both Korostylievo and Mikhailovka (Figure 5.1). The increase in loess accumulation was forced by the advance of the main Dnieper Ice Sheet during MIS 6 (figures 1.8, 4.3 and 5.2) which eventually resulted in till deposition at Likhvin (lithic unit LC-6) and proglacial lake formation in the vicinity of Gololobovo (lithic unit GC-7; Figure 3.33). The latter was caused by ice damming to the north and was followed by loess accumulation and colluviation. Relationships between the increasing distance to the ice sheet front and loess median grain sizes are clearly identified in all A-2a loess units (Figure 5.3).

Climatic amelioration during the Dnieper deglaciation ultimately lead to the Mikulino Interglacial (MISS 5.5). During this climatic optimum, forests once again returned to the northern reaches of the transect while chernozems formed in the warm steppe environments that dominated to the south (Table 5.1). Extensive research compiled on the Mikulino Interglacial paleosols has resulted in a regionally extensive, small-scale paleosol map of the Russian Plain (*e.g.*, Morozova, 1995). This research is presented in Figure 5.4 along with a map of modern-day soils to allow easy comparisons. The primary differences between Mikulino Interglacial paleosol extents and modern-day soil extents are outlined below:

- 1. Less taiga during the Mikulino Interglacial suggests an increased sensitivity to climate change at northern latitude sites, and that these sites experienced a warmer climate relative to modern-day.**
- 2. The forest-steppe transition zone was much more extensive during the Mikulino Interglacial.**

**Distance-to-glacial-margin relationships
for allomember A-2a (MIS 6) and A-1a (MIS 2) Loess
Along the North-South Transect**

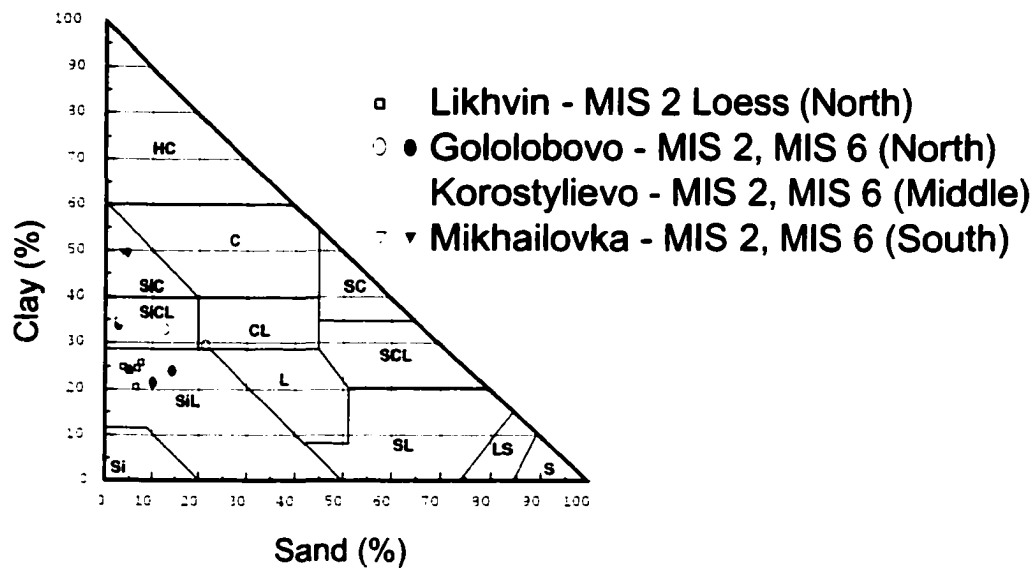


Figure 5.3. Distance-to-source relationships between correlative loess units along the 700 km long north-south transect. General median grain-size fining occurs from Gololobovo to Mikhailovka during MIS 6, and from Likhvin to Mikhailovka during MIS 2. Approximate ice margin locations for the Dneiper maximum ice advance (MIS 6) and Valdai ice advance (MIS 2) are given in Figure 1.8.

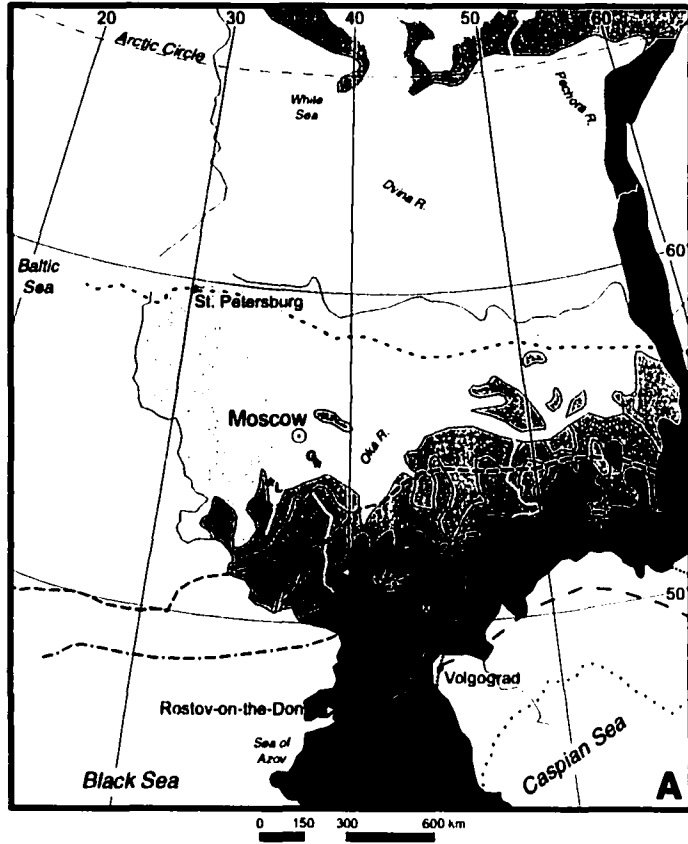
3. There is a notable southeastern shift of the mapped calcic black chernozems during the Mikulino.

In all, the available data suggest that the Mikulino Interglacial was slightly warmer with more available moisture than present-day climatic conditions on the Russian Plain.

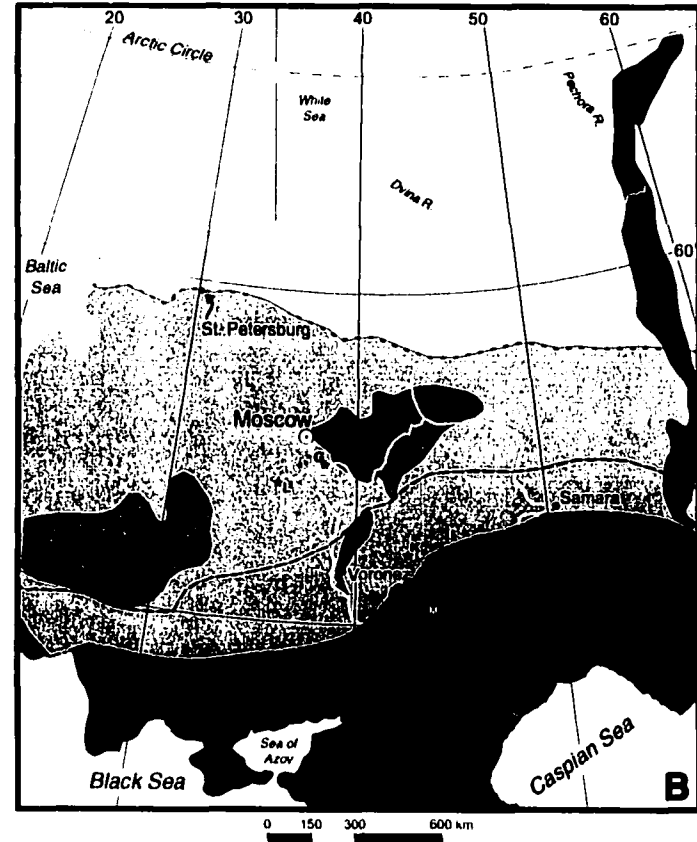
Allunit A-1 (Valdai-Holocene) MIS 5.4-1

The climatic oscillation inferred from the MISS 5.4 through MISS 5.0, and interpreted from paleosol D₂ suggest that the climatic environment immediately following the Mikulino interglacial was on the verge of change and hence, represents the onset of the last glaciation (*i.e.*, Valdai) of the Pleistocene Epoch. The initial stages of the Valdai Glaciation are marked by loess accumulation at each of the four sites, punctuated in places by local ponding of water (*e.g.*, Gololobovo) due to ice-dammed drainage networks (*e.g.*, Mangerud *et al.* 2001). In the south, a trend

Modern-Day Soil Map (modified after Shcherbakova 1998)



Mikulino Soil Map (modified after Morozova 1995)



Key to Modern-Day and Mikulino Soil Maps

- Cryosols (1)
 - Taiga Podzols (4)
 - Mixed Forest Luvisol
 - GB Luv to DG Chern (6&7)
 - E1 Bi Chern (8)
 - O Bi Chern (9)
 - Ca Bi Chern (12)
 - Brown Semi-Desert Soils (13)
 - Mountain Soil (17-20)
 - Luvisols on Sands (Mikulino only)
 - Deciduous Brunisols (Mikulino only)
 - G1 Bi to O Bi Chern (Mikulino only)
 - No Data
 - Water
 - River
 - Capital City
 - City
 - Study Site
- Southern Boundaries of Mikulino soils Overlay on Modern Soil Map**
- Mixed Forest Luvisol
 - GB Luv to DG Chern (6&7)
 - E1 Bi Chern (8)
 - O Bi Chern (9)
 - Ca Bi Chern (12)
 - G1 Bi to O Bi Chern (Mikulino only)

Figure 5.4. Modern-day (A) and Mikulino Interglacial (B) soil maps for the Russian Plain Region. Paleosol boundaries from B are transposed onto A for easy comparison. Numbers in parentheses relate to the original soil designators in Shcherbakova (1998).

towards increasing accumulation in allunit A-1b is clearly observed at Korostylievo (Figure 5.1) and to a lesser extent at Mikhailovka above paleosol-D₂. During paleosol-C formation, it appears that accumulation rates were slightly reduced at Korostylievo, but at Mikhailovka the enigmatic upper horizon of paleosol-C makes accumulation rate estimates questionable. The age of loess horizons at 3 of the four sites suggests the age of paleosol-C is less than 55 ka, whereas at Gololobovo the lower confining age on loess below the paleosol is *ca.* 34 ka. These data agree with an accepted age of 30 ± 1 k to 23 ± 1 k ¹⁴C years for correlative horizons at other Russian Plain sections. Cooler temperatures and increased aeolian deposition terminated the development of paleosol-C. During this time, accumulation rates peaked with over 250 cm of typical loess being deposited between the tops of paleosols C and B at Likhvin, and rates exceeding 8 cm/ka at Korostylievo and possibly up to 20 cm/ka at Mikhailovka; the latter, however, is questionable as higher resolution dating is required to solve the chronostratigraphic enigma identified in chapters 3 and 4. As was the case during MIS 6 loess deposition, a fining in the median grain size is also observed for the A-1a (MIS 2) loess as distance from the ice-sheet margin increases to the south (Figure 5.3). Further, at Likhvin, there is a minor soil-forming event (Paleosol-B) that is post-MIS 3 and pre-MIS 1. Based on stratigraphic position, relative pedogenic development and correlative units at other Russian Plain sites, paleosol-B at Likhvin is interpreted as the Trubchevsk Paleosol (*vide* Figure 1.6) and has an accepted age range of *ca.* 15 to 17 k ¹⁴C years (*e.g.*, Velichko and Morozova 1987; Velichko, 1990), or 18 ka to 20 ka calendar years (*vide ante* for method). It is possible that this soil-forming event may be correlative with the recently identified 15 m rise in sea-level that occurred at *ca.* 16.5-16 k ¹⁴C years BP (Lambeck *et al.* 2000). Hence, the formation of the Trubchevsk Paleosol (paleosol-B) may provide a forcing mechanism link for rapid ice-sheet decay (Clark and Mix 2000; Yokoyama *et al.* 2000) and resulting early deglacial sea-level rise referred to in Lambeck *et al.* (2000).

With the exception of Likhvin, each of the four sections is capped by the modern-day soil which is developing in sediments deposited during MIS 2 and MIS 1. At Likhvin, the modern-day soil has formed atop 2 m of anthropogenically disturbed loessic and colluviated sediments,

as suggested by the fire pit with an age of 2770 ± 60 ^{14}C years BP. Based on field and micromorphological observations, the classification of modern soils observed at each of the four sites is given in Table 5.1; their distributions are presented in Figure 5.4A.

Chapter Summary

Utilizing depositional histories and classified paleosols that are placed into a newly developed age model for the Russian Plain, a Quaternary history spanning the last *ca.* 800 ka is presented. This history interrelates environmental conditions that span a *ca.* 700 km north-south transect revealing relative shifts in bio-climatic zones within the study area over time. Further, the Trubchevsk Paleosol (paleosol-B) is associated with an early deglacial 15 m sea-level rise at *ca.* 16.5-16k ^{14}C years BP. The warming associated with Trubchevsk Paleosol development may provide a link for rapid ice-sheet decay following the last glacial maximum.

CHAPTER 6 - EURASIAN CORRELATION: APPLICATION OF PROPOSED RUSSIAN PLAIN ALLOSTRATIGRAPHY

The ensuing discussions attempt to correlate the allostratigraphic scheme developed in this dissertation with stratigraphic data compiled by other researchers, both within the extent of the Russian Plain and to sites in Siberia and China. The intent is to test the validity of the allostratigraphic scheme thereby providing a reliable link for future climate forcing investigations.

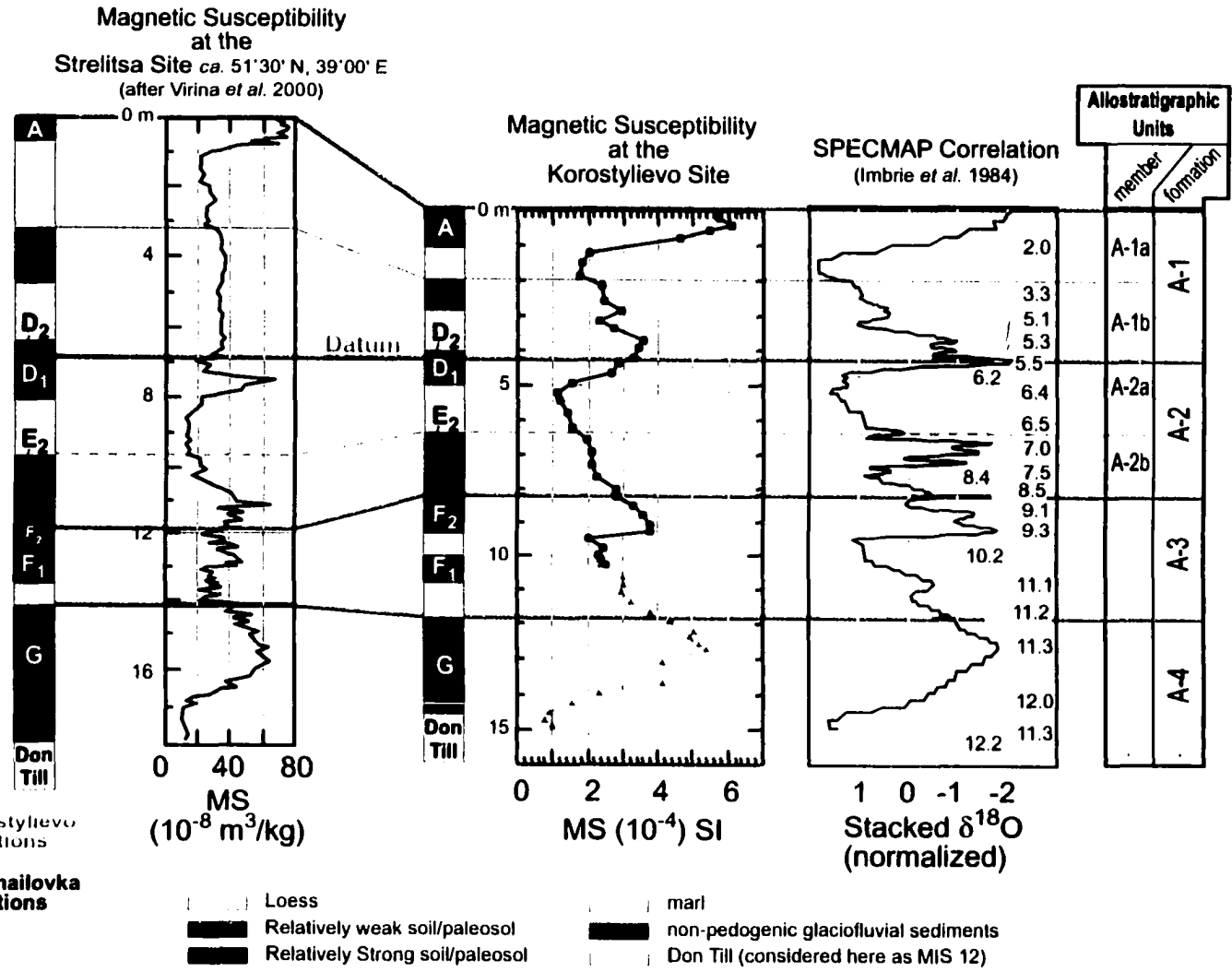
Correlation to other research within the Russian Plain

Only recently has the paleoclimate influence on rock magnetic properties been examined at sites in the European Plain (*e.g.*, Tsatskin *et al.* 1998, Virina *et al.* 2000). These data allow cross-referencing between empirical data and allostratigraphic correlations.

The Strelitsa type-section (*vide* inset map, Figure 6.1) exhibits a strikingly similar paleosol-loess-till stratigraphic sequence to that observed at the Korostylievo site, located approximately 200 km to the east-northeast (Figure 6.1). The similarities between these two sites are also observed in the magnetic susceptibility data (Figure 6.1). Together, these two Quaternary stratigraphic sequences allow an unprecedented opportunity to compare and contrast data sets collected by researchers working independently.

Given the litho- and pedo-sequences at both sites, allostratigraphic correlation of bounding discontinuities was relatively simple. Furthermore, Virina *et al.* (2000) present paleosol horizons that allowed subdivisions of their stratigraphic units. For instance, their Inzhava Paleosol (paleosol-F) could be subdivided based on the presence of two distinct A-horizons giving rise to the F_1 and F_2 pedounits presented in figure 6.1. In this regard alone, the allostratigraphic correlation was successful. Furthermore, corroboration of the allostratigraphic correlation is clearly observed in magnetic susceptibility and SPECMAP comparisons. Alloformation A-1 (Figure 6.1) exhibits a strong susceptibility peak denoting soil-A at both sections that correlate to MIS 1 of SPECMAP. Alloformation A-2 exhibits susceptibility peaks at, or near both its upper and lower boundaries. Alloformation A-3 exhibits a generally

Figure 6.1. Allostratigraphic scheme applied to Korostylevo (this study) and Strelitsa stratigraphy and magnetic susceptibility. Strelitsa striplog is summarized from Figure 3 of Virina *et al.* (2000) considering their interpreted pedogenic horizons and stratigraphic name associations. Soil designators (*e.g.*, A, C, F₂ *etc.*) are applied as per this study given their stratigraphic name associations.



broad, gradually increasing (with depth) magnetic susceptibility peak that is truncated by a distinct drop in susceptibility; these correspond to MIS 9 and MIS 10 respectively. Finally, the broad peak that characterizes the magnetic susceptibility of the Vorona paleosol (paleosol-G; Figure 6.1) at both Strelitsa and Korostylievo corresponds to the broad $\delta^{18}\text{O}$ peak (MIS 11) in the SPECMAP record. Finally, both sections exhibit the Don Till underlying glaciofluvial sands.

Although the two sites correspond reasonably well, the new age model presented herein elucidates some unsubstantiated age relationships put forth by Virina *et al.* (2000). In their work, no absolute dating or independent magnetic susceptibility/marine isotope correlations are presented. Therefore it is the opinion of this author that the age discrepancies are the result of Virina *et al.* (2000) forcing their litho- and pedo-stratigraphy into the marine isotope associations of the currently accepted stratigraphy (*e.g.*, Velichko *et al.* 1999), given their interpreted stratigraphic units (their Figure 3, p. 492). Furthermore, temporal associations between correlative units at the two sites vary considerably below MIS 10 (*ca.* 335 ka: Bassinot *et al.* 1994). Virina *et al.* (2000) associate the Inzhavino Paleosol (paleosol-F) to MIS 10 and 11, inferring that the development of this paleosol spanned nearly 72 ka (Bassinot *et al.* 1994). In contrast, the present study associates this paleosol with MIS 9 (301-328 ka: Bassinot *et al.* 1994), given the empirical correlations of the magnetic susceptibility record with SPECMAP. The Korostylievo Loess between paleosols G and F, and the upper portion of the Vorona Paleosol (paleosol-G) were associated with MIS 12 in Virina *et al.* (2000) whereas empirical correlations of their data as presented herein (Figure 6.1) suggest that the entire paleosol-G, a predominant pedogenic horizon, is associated with MIS 11 (364-406 ka: Bassinot *et al.* 1994). This is consistent with occurrence of the major interglacial known as the Holsteinian (MIS 11) in the Netherlands' stratigraphic scheme (*e.g.*, Turner 1996; Poore *et al.* 1998). Furthermore, following their scheme, Virina *et al.* (2000) associate the lower portion of the Vorona Paleosol (paleosol-G) with MIS 13 through MIS 15 suggesting that these sediments and the pedogenic horizons (lower parts of paleosol-G only) developed over *ca.* 188 ka (Bassinot *et al.* 1994). With regards to the Don

Till, Virina *et al.* (2000) acknowledge previous associations of the Don Glaciation with both MIS 12 and MIS 16, but choose to correlate the Don Till at the base of the Strelitsa type-section with MIS 16, based solely on their acceptance of available previous works (Virina *et al.* 2000, p. 488). Finally, the above age associations put forth by Virina *et al.* (2000) are exceedingly difficult to correlate outside the East European Plain (*cf.* Figure 1.6 and 1.7).

The agreement between the magnetic susceptibility correlations at the Korostylievo and Strelitsa sections, and the correlation of these two sites to the SPECMAP record (Figure 6.1), in addition to the enigmatic nature of the geochronology proposed by Virina *et al.* (2000), help to validate the allostratigraphic and chronostratigraphic and geochronologic schemes presented herein.

Correlation of the Russian Plain Quaternary Sequence to Siberian and Chinese Records

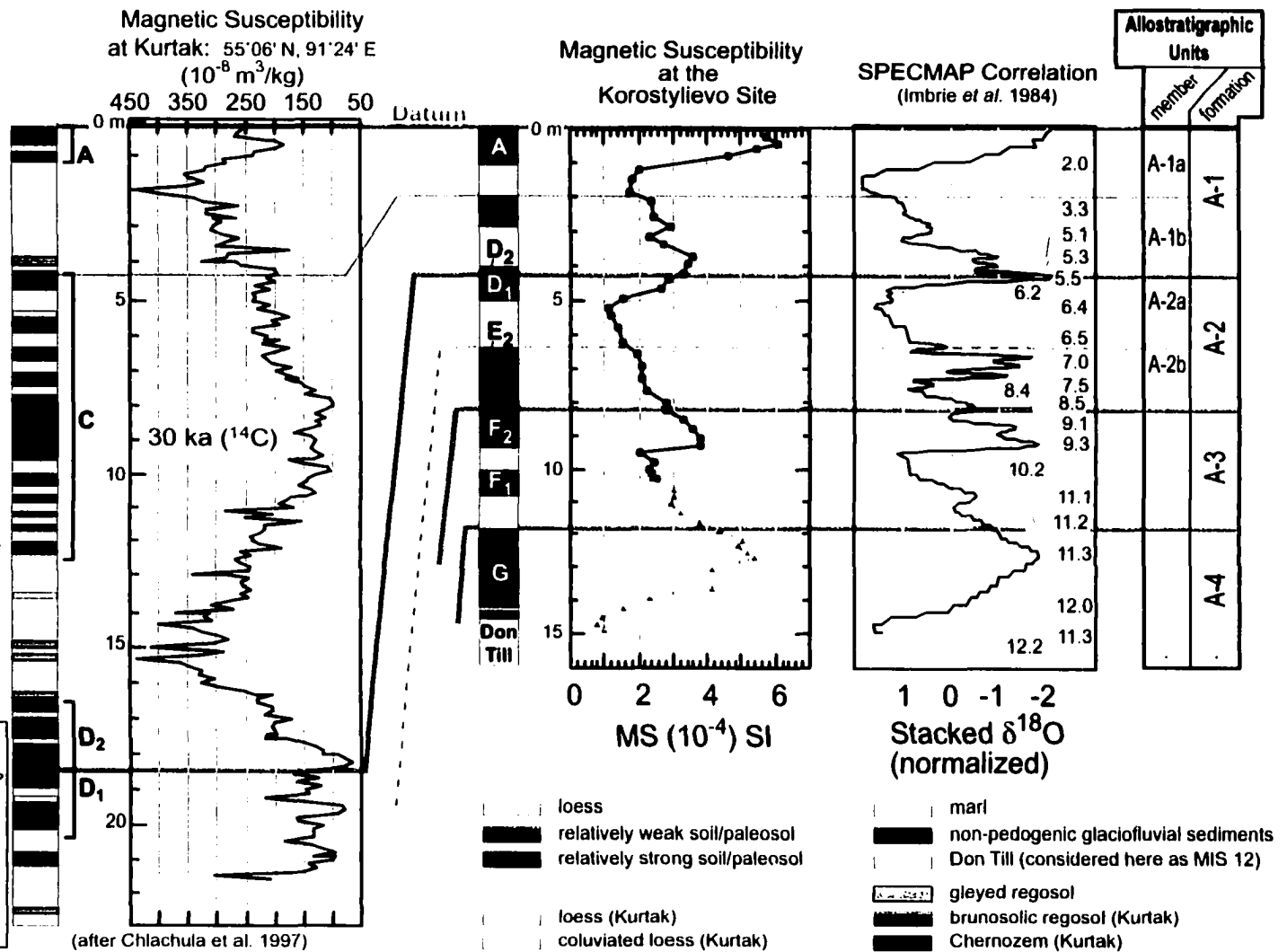
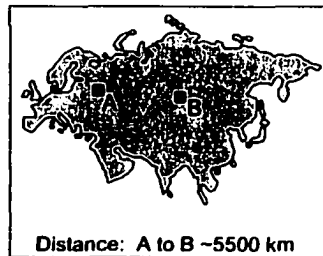
Having shown that it is possible to correlate the allostratigraphic scheme developed herein to another Russian Plain Quaternary section, the stratigraphic scheme is further tested by comparison to records outside the Russian Plain. Below, last glacial cycle correlations are made between Korostylievo and Kurtak (Siberia), whereas the *ca.* 800 ka record at Mikhailovka is compared to the Baoji Section on the Chinese Loess Plateau.

Russian Plain Correlation to Siberian Records

The late Quaternary loess-paleosol sequence recorded at Kurtak, Siberia has yielded high-resolution correlations to marine isotope stages (Chlachula *et al.* 1997). Exceedingly high accumulation rates following the penultimate glacial (*ca.* MISS 6.1) have resulted in a sensitive record of multiple pedogenic events. These events have been interpreted and classified according to the scheme presented in this dissertation (Figure 6.2) based on relative degree of development and stratigraphic position. Both stratigraphic and magnetic susceptibility data sets are compared to those of Korostylievo and the allostratigraphic framework; alloformation and allomember boundaries are correlated based on observed similarities.

Figure 6.2. Allostratigraphic scheme applied to Korostyliievo (this study) and Kurtak stratigraphy and magnetic susceptibility. Kurtak striplog is modified after Chlachula *et al.* (1997). Allostratigraphic correlations are based on comparison of both susceptibility and pedostratigraphy.

Note: Kurtak mag. susceptibility plot is reversed.



Although the two data sets have very different resolutions and opposite signal sign (*cf.* Chlachula *et al.* 1997, p. 684), distinct changes in magnetic susceptibility can be compared (Figure 6.2):

- 1. paleosol-A at both sections is characterized by prominent trough (Kurtak) and peak (Korostylievo), both of which correspond to MIS 1 (SPECMAP);**
- 2. immediately above the A-1a/b boundary, sharp reductions in magnetic susceptibility at Korostylievo and $\delta^{18}\text{O}$ (SPECMAP) correspond to a drastic increase in magnetic susceptibility at Kurtak;**
- 3. immediately below the A-1a/b boundary (paleosol-C) the magnetic susceptibility data exhibit plateaux that are followed (down-section) by a trough (Kurtak, *ca.* 5-7 m) and a peak (Korostylievo, *ca.* 2-2.5 m);**
- 4. the lower portions of allomember A-1b are characterized by a high-amplitude fluctuation in magnetic susceptibility that corresponds to MIS 3.3 through MIS 5.1, and;**
- 5. the D_1/D_2 contact is situated within a prominent trough (Kurtak) and peak (Korostylievo) that occurs within MIS 5.**

The above similarities are hampered by differences in resolution and a lack of age control. Nonetheless, both sections suggest that the paleosol- D_1 event was followed by weaker climatic amelioration prior to entering full glacial conditions during MIS 4. Furthermore, the pedogenic event associated with paleosol-C at Kurtak displays multiple paleosols that presumably represent climatic events of short duration. All of these events correspond to the single eluviated brown chernozem at Korostylievo. If the correlation is correct, then the single paleosol at Korostylievo and at other locations in the Russian Plain represents multiple climate events masked by pedogenic overprinting during successive warmer periods and low loess accumulation rates relative to Kurtak. Likewise, the Mezin Paleosol complex (paleosol-D) at Korostylievo may reflect multiple climatic events.

Russian Plain Correlation to Chinese Records

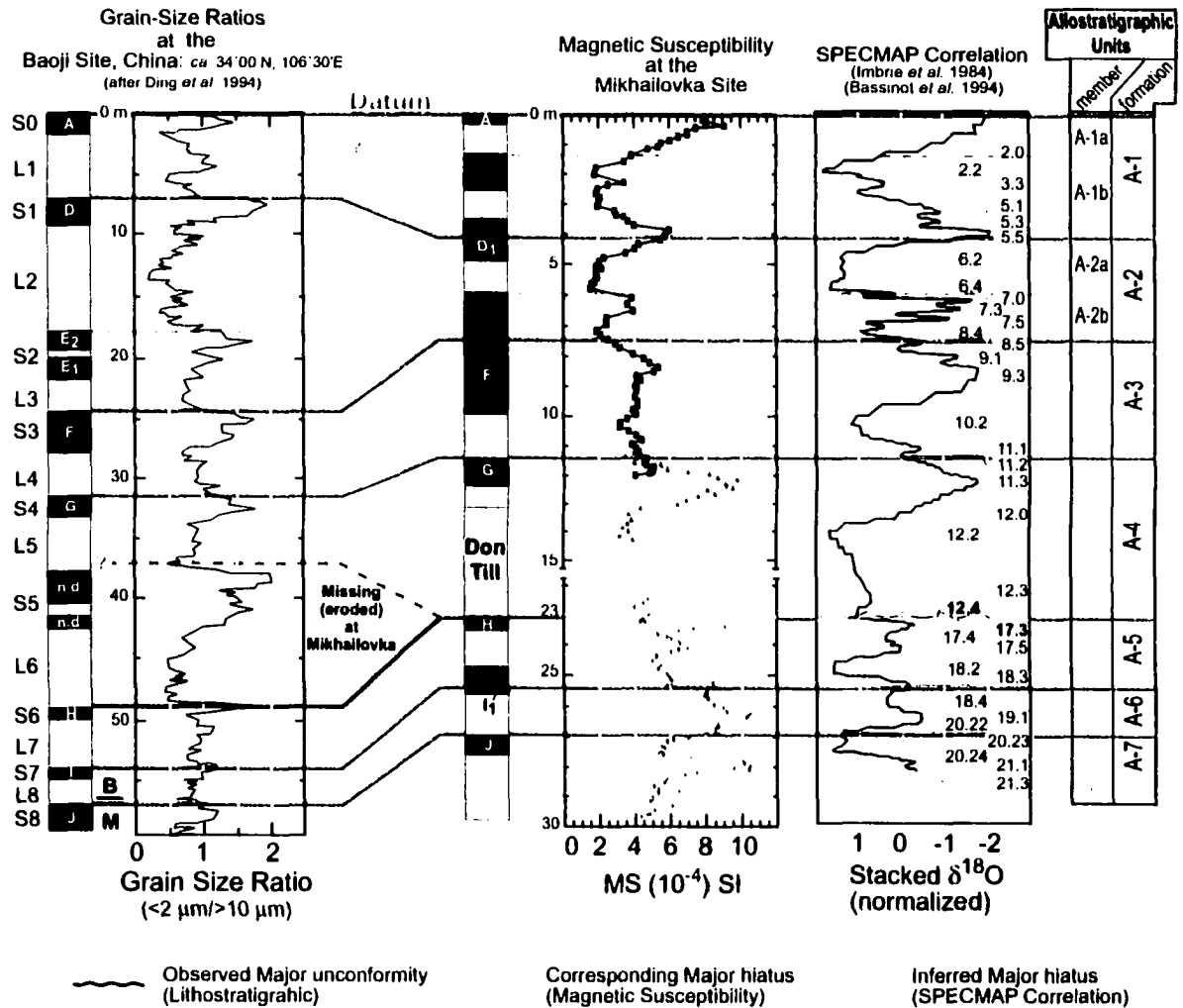
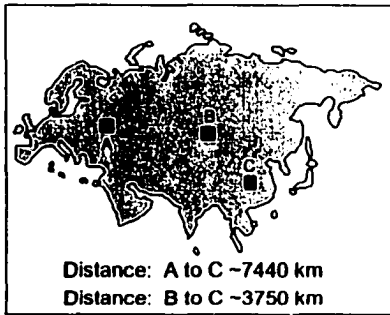
The Baoji section, China represents one of the most continuous terrestrial Quaternary records spanning the last *ca.* 2.5 Ma (*e.g.*, Ding *et al.* 1994, Rutter *et al.* 1996). Furthermore, this section has been tuned to the orbital time scale *via* SPECMAP correlations in order to produce independent, chronologically constrained grain-size-ratio data (Ding *et al.* 1994). The grain-size ratio to SPECMAP correlation is considered to be more robust than magnetic susceptibility correlations at Baoji (*e.g.*, Kukla *et al.* 1988) due to complicated origins of the magnetic susceptibility signal such as spatially dependant magnetic susceptibility values and a quasi-constant magnetic flux (Ding *et al.* 1994, pp. 40-41). Direct comparisons of absolute ages inferred from Baoji with those from Mikhailovka are not entirely feasible, however, as the modified age of the Brunhes/Matuyama boundary at 780 ka (Cande and Kent 1995) and the modifications to the SPECMAP time-scale proposed by Bassinot *et al.* (1994) were not available to Ding *et al.* (1994). Nevertheless, reasonable correlations between grain-size ratio (Baoji), magnetic susceptibility (Mikhailovka) and SPECMAP (Imbrie *et al.* 1984 as modified by Bassinot *et al.* 1994) data are possible (Figure 6.3).

The A-1 alloformation at both sites exhibits peaks and troughs that correspond to MIS 1 and 5 respectively. However, as discussed in chapters 3 and 4 (*vide ante*) the placement of paleosol-C at Mikhailovka into a temporal sequence is enigmatic. This is further complicated by the lack of a paleosol-C equivalent horizon within the Chinese stratigraphy (Figure 6.3). Hence, the correlation and placement of the associated A-1a/b boundary is problematic. Regardless, each record depicts a clear peak situated between MIS 1 and MIS 5 that is tentatively associated with MIS 3.

The A-2 alloformation is better represented at both sites, with clear correlations being made at MIS 5, MIS 7 and *ca.* MIS 8.5. Furthermore, the presence of paleosol-E at Mikhailovka, and paleosols E₁ and E₂ (*cf.* Korostylievo) at Baoji define the A-2a/b boundary that is clearly associated with the climatic oscillations inferred from MIS 7 (*cf.* Ding *et al.* 1994).

Figure 6.3. Allostratigraphic scheme applied to the stratigraphy and magnetic susceptibility of Mikhailovka, and the orbitally tuned grain-size ratio record at Baoji, China (Ding *et al.* 1994). For the Baoji striplog, both Chinese paleosol-loess designators and Russian Plain paleosol designators are used for comparison. Allostratigraphic correlations are based on the comparison of both pedostratigraphic position and grain-size ratio/magnetic susceptibility trend similarities at Baoji and Mikhailovka respectively.

- loess
- relatively weak soil/paleosol
- relatively strong soil/paleosol
- Don Till (considered here as MIS 12)



The Baoji data closely track SPECMAP in alloformation A-3, but similarities to the Mikhailovka magnetic susceptibility data are also apparent (Figure 6.3):

- 1. peak below A-2/3 boundary relating to the S3 paleosol (Baoji), the Inzhavino Paleosol (paleosol-E, Russian Plain) and MIS 9;**
- 2. plateau with minor trough at Mikhailovka corresponding to troughs at Baoji (ca. 27 m) and MIS 10.**
- 3. a relatively broad-peak corresponding to the S4 paleosol (Baoji), the Vorono Paleosol (paleosol-G, Russian Plain) and MIS 11.**

The top of paleosol-G marks the A-3/ A-4 boundary, below which, the all-time Pleistocene European glacial maximum (Don Till) is correlated with the all-time Pleistocene desert expansion in Mongolia and China (Ding *et al.* 1994); both of which are associated with MIS 12. The observed unconformity below the Don Till at Mikhailovka represents the removal of approximately 185 ka of sediment and paleosol formation, therefore MIS 13 through MIS 16 can not be correlated between these two sections.

Below the Don-Till unconformity at Mikhailovka, the stratigraphic sequence is associated with MIS 17 through 21 and exhibits striking similarities to the Baoji grain-size ratios. These correlations are further corroborated by the presence of the Brunhes/Matuyama reversal (MIS 19: Bassinot *et al.* 1994) near the base of alloformation A-6 in both sections.

The glacial--interglacial events show reasonable correspondence over a distance of approximately 7440 km. The presence of the chronologically constrained upper formation (considering all Russian Plain sections in the Allostratigraphic scheme) and the presence of the Brunhes/Matuyama boundary (MIS 19) temporally constraining the base of alloformation A-6 (ca. 780 ka) adds further validity to the trend comparisons between Chinese Loess Plateau and Russian Plain data sets.

Chapter Summary

Correlations to other sites within the Russian Plain and to Siberia and China were tested by comparing relevant data sets (magnetic susceptibility, grain-size ratios and the SPECMAP stack). The results clearly show a correspondence between sites at a hemispheric scale, and add validity to the use of the allostratigraphic and chronostratigraphic schemes in other regions. Through these correlations, relationships between major climatic events can be elucidated. Of major importance: the all-time Pleistocene maximum ice-sheet advance in Europe is correlated to the all-time Pleistocene maximum desert expansion in China. Correlations such as this will enable climate modellers to better understand climate systems, and their evolution over the Eurasian land-mass by linking Quaternary paleoclimatic records from different regions.

CHAPTER 7 - SUMMARIES, CONCLUSIONS AND FUTURE RESEARCH

Four stratigraphic type-sections were studied along a 700 km long north-south transect within the Russian Plain between Moscow and Volgograd, Russia. Composite stratigraphic sequences from each of these sites yielded a geologic record that spans the last *ca.* 350 ka in the north, and up to *ca.* 800 ka in the south. Lithostratigraphic and pedostratigraphic analyses were supported by physical data (*e.g.* rock-magnetic properties, textural analyses, loss-on-ignition), geochemical data and micromorphological investigations. Optical dating and paleomagnetic chron identification provided independent chronological constraints for development of an allostratigraphic framework and SPEC-MAP correlations. Together, these analyses allowed a reinterpretation of Russian Plain chronostratigraphy, thereby providing solutions to previous, enigmatic Russian Plain geochronologic schemes. The new stratigraphic framework is corroborated by reasonable correlation to other records within the Russian Plain and to sites in Siberia and China.

Composite Type-Sections: the 700 km north-south transect revisited

Abridged descriptions of the lithostratigraphic and pedogenic findings at each of the four sites are presented in the following subsections.

Summary of Likhvin Site

The Likhvin composite section comprises a variety of sediments that include aeolian (primary and reworked), local lacustrine, glaciofluvial and till deposits. In addition to the variety of sediments, portions of the sedimentary record have been overprinted by pedogenic and cryogenic processes. This inherent heterogeneity of the Likhvin section renders magnetic susceptibility correlation to the marine isotope stages (MIS) untenable. Therefore, litho- and pedo-stratigraphic units in addition to absolute dating techniques were instrumental correlation tools that allowed the Likhvin section and the associated depositional and paleoclimatic environments to be correlated to other sections in the Russian Plain.

Summary of Gololobovo Site

Similar to the Likhvin site, the Gololobovo site consists of a variety of sediments. The lack of diamictons and associated glaciofluvial sediments, however, suggests that this site was not glaciated in the recent

geologic past. Instead, the site experienced fluctuating hydrologic cycles that periodically flooded and dried the basin, depositing heavy clays, fine grained stratified sediments or massive loess units.

Depositional phases were punctuated by periods of pedogenesis. Both moderate and well developed paleosols are present at the site representing both major and minor periods of climatic amelioration. The developmental states of these paleosols can be compared allowing a sequence of climatic events (summarized below) to be constructed. Further, the Gololobovo soil sequence correlates well with Likhvin.

Summary of the Korostylievo Site

Strata observed at the Korostylievo site record deposition in two distinctly different environments: proximal to- and distal to- glacier fronts. The till, glaciofluvial and ponded sediments of units KC-8 through KC-6 reflect deposition at/beneath and relatively close to a glacier margin, respectively. Strata overlying the glaciogenic sediments (units KC-5 through KC-1) reflect a more distal environment dominated by aeolian deposition. Attenuation of aeolian sedimentation allowed for soil formation. The relative strengths of these two competing processes gives rise to three different scenarios (in order of decreasing accumulation relative to pedogenic processes): little to no observed pedogenesis, accretionary or cumulic pedogenesis (*e.g.*, paleosol-E₁), or entirely overprinting soils (*e.g.*, paleosols G and D₁).

Summary of the Mikhailovka site

Two sequences of aeolian sediment deposition and paleosol formation are separated by till emplacement. The lower sedimentary sequence exhibits three soil-forming phases that are developed within extremely fine-grained, aeolian sediments. Infilled fissures observed between the darker Ah horizons of each paleosol are interpreted as desiccation cracks and segregated ice infillings that formed in a discontinuous permafrost environment. Above paleosol-H, the climatic deterioration was significant enough to cause a glacial advance (*vide ante*) which, in places, eroded significant amounts of underlying material as it crosscuts paleosols H, I and J. The deglacial phase that followed till deposition produced a unit that exhibits both an aeolian facies and a glaciofluvial facies in which paleosol-G developed. Sediment immedi-

ately overlying paleosol-G marks the beginning of the second sequence aeolian of deposition and paleosol formation. This phase of deposition is dominated by aeolian accretionary processes that wane (relative to pedogenesis) during the genesis of paleosol-F and -E (the former being stronger). Paleosol-E developed in the intermediate phases of the glaciation that followed the development of paleosol-F. The ensuing glacial maximum is recorded by a lack of pedogenic processes and gradually increasing median grain sizes and accumulation rates. The deglacial phase within this formation is marked by a subsequent decrease in median grain size and the development of paleosol-D₁. The climatic deterioration of the last glacial cycle allowed the formation of ground wedges that crosscut krotovena that formed contemporaneously with paleosol-D₁. A brief warming within the last glacial cycle is evident from paleosol-C. The final stages of deposition likely occurred during the deglaciation phase. Subsequent soil formation during the Holocene resulted in the formation of soil-A capping the sequence.

Allostratigraphy and Chronostratigraphy: review

The characterization, classification and correlation of discontinuities in sedimentation that are represented by pedogenic events (*i.e.*, paleosols) have allowed the development of an allostratigraphy that provides reliable correlation between sections separated by significant distances (Chapter 3). Along the *ca.* 700 km transect presented in Chapter 3, allostratigraphic correlations proved to be essential to the advancement of the Russian Plain age model proposed in Chapter 4.

Allostratigraphy

In addition to aiding in distal section correlation, the allostratigraphy presented herein inherently identifies a series of depositional megacycles that can be correlated to glacial-scale events; seven of these cycles were identified. Considering the major hiatus inferred from the unconformity at Mikhailovka, this agrees with the eight major cycles observed in the Chinese Loess Plateau and SPECMAP records during the last *ca.* 800 ka.

The oldest of the megacycles (A-7 through A-5) are well constrained by the presence of the Brunhes/Matuyama boundary near the base of A-6, and the correlation between magnetic susceptibility trends

(Mikhailovka), grain-size ratio trends (Baoji) and SPECMAP. These data suggest that the lowermost sedimentary sequence at Mikhailovka and the intermediate sequence at Baoji span MIS 21 through MIS 17. Above the observed major unconformity marking the base of alloformation A-4, the magnetic susceptibility data and SPECMAP correlations suggest deposition of the till during MIS 12. Three megacycles of deposition are observed above alloformation A-4 at each of the four sites. Of these, alloformation A-2 represents the strongest of the three glacial intervals and exhibits two allomembers. Allomember (A-2b) exhibits a till which is associated with an ice sheet that advanced over the Likhvin site, while decreasing median grain-size values from Gololobovo to Mikhailovka agree with increasing distance-to-source aeolian deposition. Within A-1, the depositional megacycle can be subdivided into two allomembers. Similar to the A-2b loess, reduced grain-size with increased distance-to-source relationships are observed for MIS 2 loess (A-1b) at all four sites.

Chronostratigraphy

Lithostratigraphic, pedostratigraphic, and allostratigraphic analyses in conjunction with independent absolute dating techniques and a reasonable correlation to SPECMAP have resulted in a reinterpretation of the temporal sequence of events that led to evolution of Russian Plain. The significant advances between the chronostratigraphic scheme presented herein (Chapter 4) and enigmatic previous versions (*vide* Chapter 1) are summarized under conclusions (*vide post*).

Correlation to other Quaternary Research: Regional and Eurasian-wide scales

The results presented herein provide a better understanding of the Russian Plain geochronologic and chronostratigraphic (*sensu lato*) schemes. This has been clearly demonstrated by the capability of extending these schemes beyond the regional scope of the 700 km north-south transect. Through correlation to the Strelitsa type section, approximately 200 km southwest of Korostylievo, the magnetic susceptibility and allostratigraphy were corroborated. Correlation of the allostratigraphy to the high-resolution record at Kurtak, Siberia for the last glacial-interglacial cycle lends support to the allostratigraphic scheme.

Thirdly, correlation between the Mikhailovka section and the orbitally tuned grain-size ratios of the Baoji section, Chinese Loess Plateau provide further corroboration to the time-stratigraphic interpretations presented in this dissertation.

Finally, the teleconnection between the Russian Plain, Siberia and China paleosol sequences obtained through the allostratigraphic scheme now provides a more reliable means to evaluate terrestrial Eurasian-scale climate systems and dynamics.

Conclusions

A newly developed age model for Russian Plain Quaternary stratigraphy has enabled a re-evaluation of chronostratigraphic (*sensu lato*) and geochronologic units, thereby allowing reinterpretations of the Quaternary evolution of the Russian Plain. Major advances of the newly proposed stratigraphy include:

- 1) expansion of the Dnieper Glaciation to include MIS 6 and MIS 8;**
- 2) development of the Romny and Kamenka paleosols within punctuated interstadials (substages of MIS 7) of the Dnieper Glaciation;**
- 3) empirical support of the correlation of the Inzhavino Paleosol (Likhvin Interglacial) to MIS 9;**
- 4) association of the Vorona Paleosol (Muchkap Interglacial) with MIS 11 and the corresponding disassociation of the Likhvin Interglacial with the Holsteinian Interglacial of western Europe;**
- 5) association of the Don Glacial with MIS 12 rather than its generally accepted association with MIS 16, and;**
- 6) correlation of alloformations A-5 through A-7 with MIS 17 through 21 respectively and their corresponding association with the Cromerian Complex of western European schemes.**

Together, these represent major changes to the chronostratigraphic record and significantly alter Middle Pleistocene geologic history and climatic interpretations inferred from sedimentary deposits and paleosol classification.

Pedogenic events identified within the stratigraphic record have yielded evidence of latitudinal bio-climatic shifts. The warmest of these periods occurred during the last *ca.* 400 ka and is associated with the Muchkap (Holsteinian) Interglacial paleosol. During this interglacial, forested environments were present down to at least *ca.* 50° north latitude in the vicinity of Mikhailovka; presently, arid steppe conditions occupy the region. Also, the interglacials of the last *ca.* 400 ka have been interpreted to be warmer and possibly more moist than present day climatic conditions. The warmest of these interglacials was the Muchkap Interglacial (Holsteinian equivalent) of MIS 11.

Through allostratigraphic concepts, seven glacial-interglacial events have been recognized. Of these, only three glaciations produced ice sheets that extend south of Moscow: the Don Glaciation (MIS 12) representing the all-time Pleistocene maximum glacial advance; the Oka Glaciation (MIS 10), inferred from previous work, and; the Dnieper Glaciation. The latter glaciation appears to be more complex as it exhibits an earlier limited advance associated with MIS 8, and a more extensive later advance associated with MIS 6. These two glacial stadials are separated by a period of climatic fluctuation associated with MIS 7, during which climatic fluctuations resulted in two minor paleosols and an intervening loess. Along the transect between Likhvin and Mikhailovka, the youngest glacial period, as well as the pre-Don Glacial events, resulted in cold steppe conditions that were (generally) dominated by loess deposition in a continuous permafrost environment (north) or loess deposition in a discontinuous permafrost environment (south).

Correlations between the allostratigraphy and other records within and outside the Russian Plain lend support to the newly developed stratigraphy. Through independent constraints from optical dating, the identification of a paleomagnetic chron boundary and SPECMAP correlations, comparisons between paleoclimatic conditions over the Russian Plain and in China were attempted. They suggest that the all-time Pleistocene European glacial maximum in Russia (MIS 12) and the all-time Pleistocene Asian desert expansion in China are isochronous (at the resolution presented herein).

Being able to make this type of Eurasian-scale correlation will provide new insight for climate modellers, allowing a better understanding of climate forcing mechanisms at hemispheric scales.

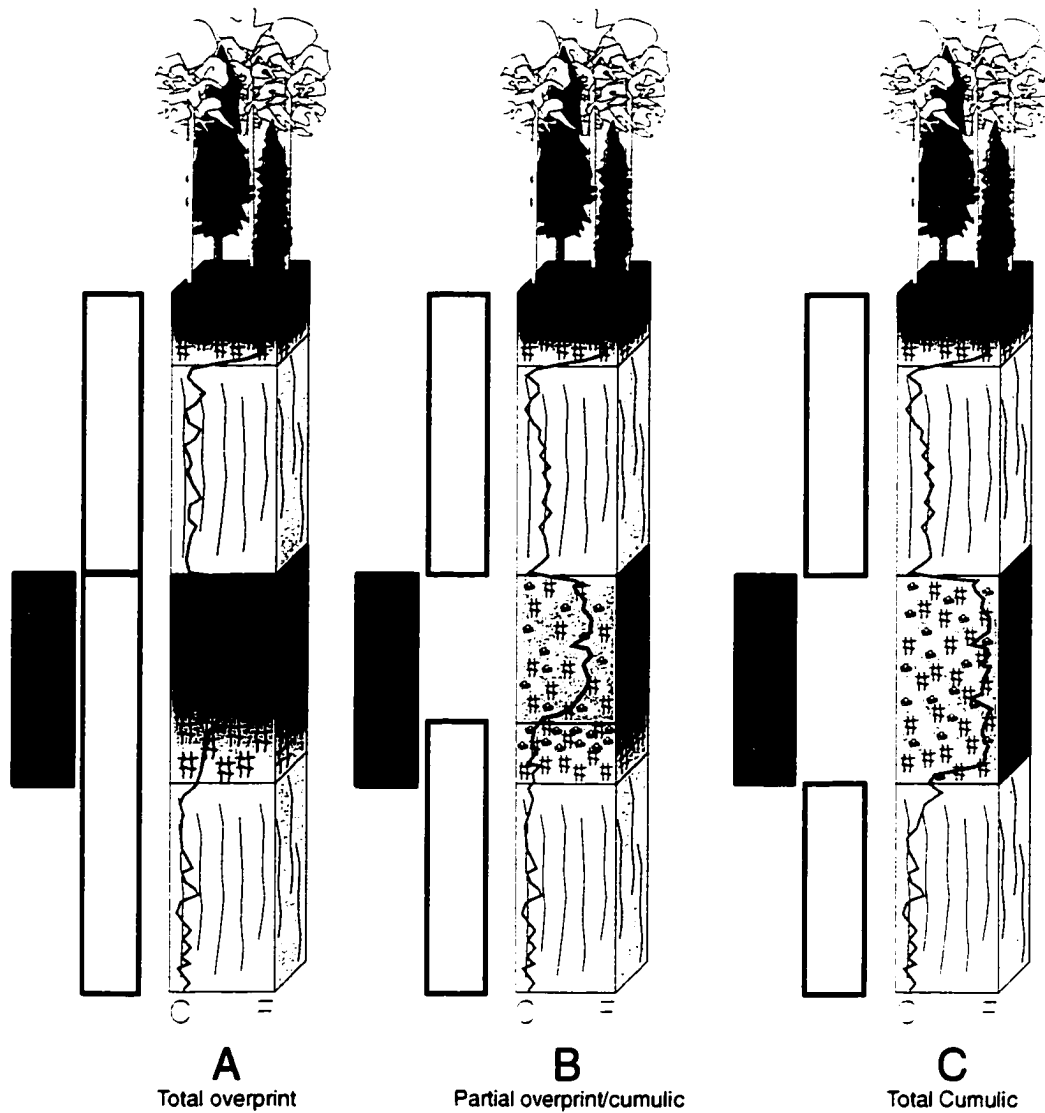
Recommendations for Future Research

There are two main foci for research that should be undertaken in the immediate future: continued evaluation of the newly proposed stratigraphy and evaluation of hemispheric-scale paleoclimatic models over the last *ca.* 800 ka of earth history. Of major importance is the continued focus on understanding the timing of events during the Middle Pleistocene.

Shifting the inferred age of the Don Till, a chronostratigraphic marker bed, by nearly 200 ka has significant implications for European Quaternary stratigraphy and paleoclimatology. Therefore, future research should continue to test the allostratigraphic, chronostratigraphic and geochronologic schemes put forth herein. This would involve rigorous re-evaluation of paleontologic data previously used to constrain the age of the Don beds.

The long-range correlations presented in Chapter 5 have the potential to help evaluate current Eurasian-scale climate models that focus not only on the last glacial cycle, but also on climate models that cover a much larger span of time -- *ca.* 800 ka. Thus, relationships such as the all-time maximum Pleistocene glacial advance for Europe being equated to the all-time maximum Pleistocene desert expansion in China may help climate modellers to elucidate climate forcing mechanisms and link paleoclimate conditions at hemispheric scales.

Lastly, higher-resolution records will be required to elucidate paleoclimatic leads and lags between geographically separated sites (e.g., Russian Plain and China) in order to further evaluate climatic forcing mechanisms. However, in order to do this, researchers must consider relationships between the rate of pedogenesis and sediment accumulation at a resolution much greater than the stratigraphic framework presented herein allows. This is necessary in order that they account for different degrees of pedogenic overprinting, such as those interpreted for paleosols G, D₁/D₂ and C, and the inferred chronologic implications for the associated SPECMAP correlations (e.g., Figure 7.1).



Blue=deposition during cold MIS
 Red=soil formation during warm MIS

Where red and blue overlap, then the soil overprints the original deposit.

Figure 7.1. Diagrammatic illustration of three possible origins for loess-paleosol genesis. A. paleosol-G scenario; B. paleosol-D1/D2 scenario; C. paleosol-C scenario. The grain-size curve is a hypothetical curve based on observations made from Chinese data; it could, however, represent any climate-proxy data. These scenarios must be considered in future high-resolution studies of loess-paleosol sequences.

REFERENCES

- Agadjanyan, A. K. & Glusjankova, N. I. (1987) Paleogeografiya Pleistotsena Oksko-Donskoi Ravnini (Paleogeography of the Pleistocene Oka-Don Plains). In: *Teoreticheskiye i metodicheskiye problemi paleogeografii* (Theoretical and Methodological Problems in Paleogeography) (Ed. by M. B. Lomonosova), pp. 145-169. Uzdatelstvo Moscovskovo universiteta (Publishing House of Moscow University), Moscow.
- Aleksandrova, L. N. (1983) Founder of the Study of Geographic Patterns of Soil Humus. *Soviet Soil Science*, **15**(3), 40-43.
- Anderson, J. and Buckton, D. (1999) Physical Europe (map). *Heritage Atlas: Firefly World Atlas Millennium Edition*. Firefly Books Ltd., Willowdale Ontario, Canada.
- Arinushchikina, E. V. (1970) Rukovodstvo po ximicheskomu analizu pochv (Guide to the chemical analysis of soils). In: *unknown* (Ed.), pp. 116-207. Izdatelstvo Moskovskovo Universityeta (Moscow Univeristy Publishing House), Moscow.
- Arhipov, S. A., Bepaly, M. A., Faustova, M. A., Yu, O., Glushkova, L. L., Isaeva, L. L. & Velichko, A. A. (1986) Ice-Sheet Reconstructions. *Quaternary Science Reviews*, **5**, 475-483.
- Astakhov, V. I., Svendsen, J. I., Matiouchkov, A., Mangerud, J., Maslenikova, O. & Tveranger, J. (1999) Marginal formations of the last Kara and Barents ice sheets in northern European Russia. *Boreas*, **28**(1), 23-45.
- Bard, E., Arnold, M., B., H., N., T.-L. & G., C. (1998) Radiocarbon calibration by means of mass spectrometric ^{230}Th , ^{234}U and ^{14}C ages of corals: An updated database including samples from Barbados, Mururoa and Tahiti. *Radiocarbon*, **40**, 1085-1092.
- Barrett, P. J. & Brooker, M. R. (1989) Grain Size Analysis at VUW, pp. 1-22. Unpublished, Research School of Earth Sciences, University of Wellington, New Zealand.
- Bassinot, F. C., Labeyrie, L. D., Vincent, E., Quidelleur, X., Shackleton, N. J. & Lancelot, Y. (1994) The astronomical theory of climate and the age of the Brunhes-Matuyama magnetic reversal. *Earth and Planetary Science Letters*, **126**, 91-108.

- Bolikhovskaya, N. S. & Sudakova, N. G. (1996) The Chekalin (Likhvin) reference section in the Russian Plain and its significance for Pleistocene stratigraphy and correlation. *Stratigraphic and Geologic Correlation*, **4**(3), 294-304.
- Bullock, P., Federoff, N., Jongerius, A., Stoops, G., Turnsina, T. & Babel, U. (1985) *Handbook for Soil Thin Section Description*. Waine Research, Wolverhampton, U.K., 152 pp.
- Cande, S. C. & Kent, D. V. (1995) Revised calibration of the geomagnetic polarity timescale for the Late Cretaceous and Cenozoic. *Journal of Geophysical Research*, **100**(B4), 6093-6095.
- Catt, J. A. (1990) *Paleopedology Manual*. Pergamon Press, Oxford, 95 pp.
- Chichagova, O. A. (1972) *Vozrast verkhnepleystotsenovykh iskopayemykh pochv po radiouglerodnym dannym (Radiocarbon age of upper Pleistocene fossil soils)*. Akademii Nauk SSSR, Institut Geografii (Academy of Sciences USSR, Institute of Geography), Moscow, 119-137 pp.
- Chichagova, O. A. (1985) Radiocarbon dating of the soil humus. In: *Nauka (In Russian)*, pp. 142. Moscow State University Press, Moscow.
- Chlachula, J., Rutter, N. W. & Evans, M. E. (1997) A Late Quaternary Loess-Paleosol record at Kurtak, southern Siberia. *Canadian Journal of Earth Sciences*, **34**, 679-686.
- Clark, P. U. & Mix, A. C. (2000) Ice sheets by volume. *Nature*, **406**, 689-690.
- Dean, W. E., Jr. (1974) Determination of Carbonate and Organic Matter in Calcareous Sediments and Sedimentary Rocks by Loss-On-Ignition: Comparisons with Other Methods. *Journal of Sedimentary Petrology*, **4**, 242-248.
- Ding, Z., Yu, Z., Rutter, N. W. & Liu, T. (1994) Towards an orbital time scale for Chinese Loess. *Quaternary Science Reviews*, **13**, 39-70.
- Dobrodeyev, O. P. & Parunin, O. B. (1973) New data on the absolute age of Pleistocene fossil soils on the Russian Plain. *Transactions (Doklady) of the Russian Academy of Science, Earth Science Section (In Russian)*(209), 426-427.
- Dokuchayev, V. V. (1883) *Russkiy Chernozm (The Russian Chernozem)*, St. Petersburg.

- Dokuchayev, V. V. (1893) *O proiskhozhdenii Russkovo liossya (On the formation of loess in Russia)*, Esna-Rennes (1974).
- Dreimanis, A., Hütt, G., Raukas, A. & Whippey, P. W. (1978) Dating methods of Pleistocene deposits: 1. Thermoluminescence dating. *Geoscience Canada*, **5**, 55-60.
- Dukes, P. (1990) *A History of Russia: Medieval, Modern, Contemporary*. MacMillan Education Ltd., London, 425 pp.
- Evans, M. E. (1999) Magnetoclimatology: a test of the wind-vigour model using the 1980 Mount St. Helens ash. *Earth and Planetary Science Letters*, **172**, 255-259.
- Evans, M. E., Heller, F., Bloemendal, J. & Thouveny, N. (1997) Natural magnetic archives of past global change. *Surveys in Geophysics*, **18**, 183-196.
- Eyles, N., Eyles, C. & Miall, A. (1983) Lithofacies types and vertical profile models; an alternative approach to the descriptive and environmental interpretation of glacial diamict sequences. *Sedimentology*, **30**, 393-410.
- Faustov, S. S., Il'ichev, V. A. & Bol'shakov, V. A. (1974) Paleomagnetic and thermoluminescence analysis of the Likhvin Section. *Doklady Akademii Nauk SSSR, Earth Science Section*, **214**, 123-125.
- Fulton, R. J. (1989) Foward to the Quaternary Geology of Canada and Greenland. In: *Quaternary of Canada and Greenland, Vol. Geology of Canada No. 1* (Ed. by R. J. Fulton), pp. 1-11. Geological Survey of Canada, Ottawa.
- Gerasimov, I. P. (1971) Nature and originality of paleosols. In: *Paleopedology, origin, nature and dating of paleosols*. (Ed. by D. H. Yaalon), pp. 15-27. International Soil Science Society, Jerusalem. *Papers of the symposium on the age of parent materials in soils, Amsterdam, The Netherlands, August 10-15, 1970*.
- Gerasimov, I. P., Velichko, A. A., Markov, A. K. & others (1980) Prirodnoklimaticheskiye etapi v lednikovoi periglatsialnoi i premoskoi oblastiakh vostoschno-evropeiskovo sektora (Natural climatic stages in the glacial, periglacial and coastal regions of the east-European sector). In: *Kratkii istoricheskii obzor izucheniya stratigrafi chetvertichnoi sistemi (Brief historical review of the study of the stratigraphy of the Quaternary*

- System*), Vol. 1 (Ed. by B. G. Gerbova and I. I. Krasnov), pp. 34-37. Bcecoyuzni nayuchno-issledivatyelski geologichski institut (All-union Scientific-Research Geologic Institute, Bcecoyuzni nayuchno-issledivatyelski geologichski institut (All-union Scientific-Research Geologic Institute).
- Gerasimova, M. I., Gubin, S. V. & Shoba, S. A. (1992) *Micromorfologiya pochv pripodnix* (Micromorphology of Natural Soils), pp. 214. Pushchinski Nauchni Tsentri, RAN (Pushchino Science Centre, RAS), Moscow.
- Gerasimova, M. I., Gubin, S. V. & Shoba, S. A. (1996) *Soils of Russia and Adjacent countries: Geography and Micromorphology*. Moscow State University, Moscow, 204 pp.
- Gerbova, B. G. & Krasnov, I. I. (1982) *Kratkii istoricheskii obzor izucheniya stratigrafi chetvertichnoi sistemi* (Brief historical review of the study of the stratigraphy of the Quaternary System). In: *Chetverichnaya Sistema (Quaternary System)*, Vol. 1 (Ed. by E. V. Shantser), pp. 9-44. Bcecoyuzni nayuchno-issledivatyelski geologichski institut (All-union Scientific-Research Geologic Institute, Moscow. *Stratigraphiya SSSR*.
- Glinka, K. D. (1904) *Zadachi istoricheskovo pochvovedeniya* (Objectives of Historical Soil Science). Science, Moscow, 278 pp.
- Glushankova, N. I. & Sudakova, N. G. (1995) *Glacial Stratigraphy of the Lower Pleistocene in the Oka-Don Region*. In: *Glacial Deposits in North-East Europe* (Ed. by J. Ehlers, S. Kozarski and P. Gibbard), pp. 157-160. A.A. Balkema, Rotterdam.
- Glushankova, N. I., Gribchenko, Y. N. & Sudakova, N. G. (1995) *Lithology of Lower Pleistocene Tills in the southern glaciated area of Russia*. In: *Glacial Deposits in North-East Europe* (Ed. by J. Ehlers, S. Kozarski and P. Gibbard), pp. 161-166. A.A. Balkema, Rotterdam.
- Grosswald, M. G. (1980) *Late Weichselian Ice Sheet of Northern Eurasia*. *Quaternary Research*, **13**, 1-32.
- Grosswald, M. G. (1993) *Extent and melting history of the Late Weichselian ice sheet, the Barents-Kara continental margin*. In: *Ice in the Climate System* (Ed. by W. R. Peltier), pp. 1-20. Nato ASI Series-I, Springer Verlag, Berlin/Heidelberg.

- Heller, F. & Evans, M. E. (1995) Loess Magnetism. *Reviews of Geophysics*, **33**, 211-240.
- Huntley, D. J., Godfrey-Smith, D. I. & Thewalt, M. L. W. (1985) Optical Dating of Sediments. *Nature*, **313**, 105-107.
- Huntley, D. J. & Lian, O. B. (1999) Determining When A Sediment Was Last exposed to Sunlight by Optical Dating. In: *Holocene Climate and Environmental Changes in the Palliser Triangle, Southern Canadian Prairies: Geological Survey of Canada Bulletin*. (Ed. by D. S. Lemmen and R. E. Vance), pp. 211-222. Geological Survey of Canada Bulletin 534.
- Imbrie, J., Hays, J. D., Martinson, D. G., McIntyre, A., Mix, A. C., Morley, J. J., Pisias, N. G., Prell, W. L. & Shackleton, N. J. (1984) The orbital theory of Pleistocene climate: Support from a revised chronology of the marine $d^{18}O$ record. In: *Milankovitch and Climate, Understanding the Response to Astronomical Forcing, Vol. 126 (1)* (Ed. by A. Berger, J. Imbrie, J. Hays, G. Kukla and B. Saltzman), pp. 269-305. Reidel publishing Company, Boston and Lancaster. *NATA ASI Series C: Mathematical and Physical Sciences*.
- Kitagama, H. & van der Plicht, J. (1998) Atmospheric radiocarbon calibration to 45,000 yr B.P.; late glacial fluctuations and cosmogenic isotope production. *Science*, **279**(5354), 1187-1190.
- Krasnenkov, R. V., Kholmovoi, G. V., Glushkov, B. V. & others, a. (1984) *Oporniye razrezi inzhnevo Pleistocina bassina verkhnevo Dona (Supporting Sections for the Early Pleistocene from Upper Don Basin)*. Izdatelstvo Voronezhskovo Universityeta (Voronezh University Publishing House), Voronezh, 212 pp.
- Krasnov, I. I. & Shantser, E. V. (1982) Klassifikantsiya i terminologiya stratigraficheskikh podrazdeleni chetvertichnoi [antropogenovoi] sistemi (Classification and Terminology for stratigraphic subdivisions of the Quaternary [Anthropogenic] System. In: *Chetverichnaya Sistema (Quaternary System)*, Vol. 1 (Ed. by E. V. Shantser), pp. 110-119. Bcecoyuzni nayuchno-issledivatyelski geologichski institut (All-union Scientific-Research Geologic Institute, Moscow. *Stratigraphiya SSSR*.
- Kukla, G., Heller, F., Liu, X. M., Xu, T. C., Liu, T. S. & An, Z. S. (1988) Pleistocene climates in China dated by magnetic susceptibility. *Geology*, **16**, 811-814.

- Lambeck, K., Yokoyama, Y., Johnston, P. & Purcell, A. (2000) Global ice volumes at the Last Glacial Maximum and early Lateglacial. *Earth and Planetary Science Letters*, **181**, 513-127.
- Larsen, E., Svend, F. & Thiede, J. (1999) Late Quaternary history of northern Russia and adjacent shelves - a synopsis. *Boreas*, **28**(1), 6-11.
- Lian, O. B. & Huntley, D. J. (2001) Luminescence Dating. In: *Tracking Environmental Change Using Lake Sediments: Physical and Chemical Techniques* (Ed. by W. M. Last and J. P. Smol). Kluwer Academic Publishers, The Netherlands.
- Little, E. C., Lian, O. B., Velichko, A. A., Morozova, T. D., Nechaev, V. P., Dlussky, K. G. & Rutter, N. W. (in press) Optical dating studies of loess from east European Plain (Russia) and their stratigraphic implications. *Quaternary Science Review*.
- Lomonosova, M. V. (1987) *Teoreticheskiye i metodicheskiye problemi paleogeografii (Theory and Methodology of problems in paleogeography)*. Izdatelstvo Moskovskovo Universiteta (Moscow University Publishing House), Moscow, 144-169 pp.
- Lowe, J. J. & Walker, M. J. C. (1997) *Reconstructing Quaternary Environments*. Addison Wesley Longman Ltd., Essex, England, 446 pp.
- Lydolph, P. E. (1977) Climates of the Soviet Union. In: *World Survey of Climatology, Vol. 7*, pp. 442. Elsevier Scientific Publishing Co., Amsterdam, The Netherlands.
- Lysenko, M. P. (1971) *Loessal Rocks of the European USSR*. Israel Program for Scientific Translations, Jerusalem.
- Mangerud, J., Svendsen, J. I. & Astakov, V. I. (1999) Age and Extent of the Barents and Kara Ice Sheets in Northern Russia. *Boreas*, **28**, 46-80.
- Mangerud, J., Astakhov, V., Jakobsson, M. & Svendsen, J. I. (2001) Huge Ice-age lakes in Russia. *Journal of Quaternary Science*, **16**, 773-777.
- Martinson, D. G., Pisias, N. G., Hays, J. D., Imbrie, J., Moore, T. C. J. & Shackleton, N. J. (1987) Age dating and the orbital theory of the ice ages; development of a high-resolution 0 to 300,000-year chronostratigraphy. *Quaternary Research*, **27**(1), 1-29.

- Morozova, T. D. (1972) *Micromorphological peculiarities of fossil soils and some problems of paleogeography of the Mikulino (Eemian) Interglacial on the Russian Plain*. Panstvove Vidavnistvo Naukove, Warsaw, 595-606 pp.
- Morozova, T. D. (1995) Identification of paleosol types and their applicability for paleosol reconstructions. *Geojournal*, **36**, 199-205.
- Morozova, T. D. & Nechayev, V. P. (1997) The Valdai Periglacial Zone as an area of crygenic soil formation. *Quaternary International*, **41/42**, 53-58.
- Morrison, R. B. (1998) How can the treatment of pedostratigraphic units in the North American Stratigraphic Code be improved? *Quaternary International*, **51/52**, 30-33.
- Moskvitin, A. I. (1976) *Opornye razrezi Pleistotsena Russkoi ravnini (Supporting [Stratotype] Sections for the Pleistocene of the Russian Plain)*. Nauka (Science), Moscow, 203 pp.
- Mücher, H. J. & Morozova, T. D. (1983) The Application of Soil Micromorphology in Quaternary Geology and Geomorphology. In: *Soil Micromorphology* (Ed. by P. Bullock and C. P. Murphy), pp. 151-194. A.B. Academic Publications, Berkhamsted, England.
- Nalivkin, D. V. (1960) *The Geology of the USSR: a short outline*. Pergamon Press, Oxford, 170 pp.
- Nalivkin, D. V. (1973) *Geology of the USSR*. Oliver and Boyd, Edinburgh, 855 pp.
- Nikitin, S. N. (1885) Limits of glaciation traces in central Russia and the Urals. *Proceedings of Geology Committee (in Russian)*, **4**, 8.
- North American Code of Stratigraphic Nomenclature (1983) The North American Stratigraphic Code. *American Association of Petroleum Geologists Bulletin*, **67**, 841-875.
- Norrish, K. & Tiller, K. G. (1976) Subplasticity in Australian soils: V. factors involved and techniques of dispersion. *Australian Journal of Soil Research*, **14**, 273-289.
- Obruchev, V. A. (1945) Loess Types and Their Origin. *American Journal of Science*, **243(5)**, 256-262.
- Okulitch, A. V. (1999) Geological time scale, 1999. Geological Survey of Canada, Ottawa.

- Pécsi, M. (1995) Concepts of loess, a comprehensive information. In: *Concept of Loess, Loess-Soil Stratigraphy* (Ed. by M. Pécsi and F. Schweitzer), pp. 9-22. Geographical Research Institute, Hungarian Academy of Science, Budapest.
- Pécsi, M. (1990) Loess is not just the accumulation of dust. In: *Loess and the Environment, Vol. 7/8* (Ed. by M. Pécsi and D. Loczy), pp. 1-21. Pergamon Press, Oxford.
- Poore, R. Z., Burckle, L., Droxler, A. & McNulty, W. E. (1998) Marine Isotope Stage 11 and associated Terrestrial Records: Workshop Report. USGS, http://chht-ntsrv.er.usgs.gov/warmclimates/products/s11_work.txt.
- Pospelova, G. A., Semenov, V. V., Sharonova, Z. V. & Mironov, T. V. (1997) An Early Pleistocene Excursion of the Geomagnetic Field in the Upper Don Subaerial Deposits. *Doklady Akademii Nauk SSSR, Earth Science Section*, **355**(5), 778-782.
- Prescott, J. R. & Robertson, G. B. (1997) Sediment Dating by Luminescence. *Radiation Measurements*, **27**, 893-922.
- Pye, K. (1995) The Nature, Origins and Accumulation of Loess. *Quaternary Science Reviews*, **14**(7-8), 653-667.
- Rapp, A. & Clark, G. M. (1971) Large non-sorted polygons in Padjelanta National Park, Swedish Lappland. *Geografiska Annaler*, **53**, 71-85.
- Rutter, N. W. (1995) Problematic Ice Sheets. In: *IGCP 253 - Termination of the Pleistocene- Final Report, Vol. 28* (Ed. by J. Lundqvist, M. Saarnisto and N. W. Rutter), pp. 19-37. Pergamon Press, Oxford. *Quaternary International*.
- Rutter, N. W., Ding, Z. & Liu, T. (1996) Long Records From China. *Geophysica*, **32**, 7-34.
- Sanko, A. F. (1995) The Problems of Middle Pleistocene Stratigraphy in Belarus. *Acta Geographica Lodziensia*, **68**, 163-171.
- Shackleton, N. J. & Opdyke, N. D. (1976) Oxygen-isotope and paleomagnetic stratigraphy of Pacific Core V28-239, late Pliocene to latest Pleistocene. In: *Investigation of late Quaternary paleoceanography and paleoclimatology, Vol. 145*, pp. 449-464. Geological Society of America, Boulder, CO.

- Shcherbakova, V. I. (1998) *Geografiya Rossii Atlas (Geographic Atlas of Russia)*, pp. 54. Federalnaya Sloozhba Geodezii i Kartografii Rossii (Federal Service for Geodesy and Cartography of Russia), Moscow, Russia.
- Sheldrick, B. H. & Wang, C. (1993) Particle Size Distribution. In: *Soil Sampling and Methods of Analysis* (Ed. by M. R. Carter), pp. 499-511. Lewis Publishers, Ann Arbor, USA.
- Shelkopyas, V. N. & Morozov, G. V. (1965) *Nekotoryye rezul'taty issledovaniya Chetvertichnykh otlozheniy termolyuminescentnym metodom (Some results of investigations of Quaternary deposits by the thermoluminescence method)*. Akademiya Nauk Ukrainskoy SSR, Institut Geologicheskikh Nauk, Komissiya po Izucheniyu Chetvertichnogo Perioda (Ukrainian SSR Academy of Science, Institute of Geological Sciences, Commission for the Study of the Quaternary Period, Kiev, USSR, 83-90 pp.
- Shevirev, L. T., Raskatov, L. I. & Alekseeva, L. I. (1979) Shkurlatovskoe mestonakhozhdeniye fauni mlekopetayushchukh mikilinskovo vremeni [Voronezhskaya oblast] (Shuratov Locality for Mammilian Fauna of the Mikulino Time). *Byul. Komis. po izucheniyu chetvertichn perioda (Bulletin on the Commission for the study of the Quaternary Period)*(49).
- Soil Classification Working Group. (1998) *The Canadian System of Soil Classification*. Agriculture and Agricultural Foods Canada, Ottawa, 187 pp.
- Sokolov, I. A. & Targulian, V. O. (1976) Vzaimodeistviye pochvi i sredi: pochva-pamyat i pochva momyent (Interactions of soils and environments: soil of the past and soil of the present). In: *Environmental study and development of periods*, pp. 150-164, Moscow.
- Spoooner, N. A. (1994) The anomalous fading of infrared stimulated luminescence from feldspars. *Radiation Measurements*, **23**, 625-632.
- Stephenson, A. (1971) Single Domain Grain Distributions I: a method for the determination of single domain grain distributions. *Physics of the Earth and Planetary Interiors*, **4**, 353-360.

- Sudakova, N. G. & Faustova, M. A. (1995a) Glacial History of the Russian Plain. In: *Glacial Deposits in North-East Europe* (Ed. by J. Ehlers, S. Kozarski and P. Gibbard), pp. 151-156. A.A. Balkema, Rotterdam.
- Svendsen, J. I., Astakhov, V. I., Bolshiyarov, D. R., Demidov, I., Dowdeswell, J. A., Vataullin, V., Hjort, C., Hubberten, H. J., Larsen, E., Mangerud, J., Melles, M., Möller, P., Saarnisto, M. & Siegert, M. J. (1999) Maximum extent of the Eurasian ice sheets in the Barents and Kara Sea region during the Weichselian. *Boreas*, **28**(1), 234-242.
- Tsatskin, A. (1997) A History of Soviet Paleopedological Studies and Their Relation to Soil Science and Quaternary Geology. In: *History of Soil Science, Vol. 29* (Ed. by D. H. Yaalon and S. Berkowicz), pp. 277-291. Catena Verlag, Reiskirchen, Germany. *Advances in GeoEcology*.
- Tsatskin, A., Heller, F., Hailwood, E. A., Gendler, T. S., Hus, J., Montgomery, P., Sartori, M. & Virina, E. I. (1998) Pedosedimentary division, rock magnetism and chronology of the loess / palaeosol sequence at Roxolany (Ukraine). *Palaeogeography, Palaeoclimatology, Palaeoecology*, **143**, 111-133.
- Turner, C. (1996) A brief survey of the early Middle Pleistocene in Europe. In: *The Early and Middle Pleistocene in Europe* (Ed. by C. Turner), pp. 295-318. A.A. Balkema, Rotterdam.
- van Heteran, S., D.J., H., van de Plasche, O. & Lubberts, R. K. (2000) Optical dating of dune sand for the study of sea-level change. *Geology*, **28**(5), 411-414.
- van Kolfschoten, T., Roebroeks, W. & Vandenberghe, J. (1993) The Middle and Late Pleistocene sedimentary and climatic sequence at the Maastricht-Belvédère Interglacial. In: *Maastricht-Belvédère: stratigraphy, palaeoenvironment and archaeology of the Middle and Late Pleistocene deposits; Part II, Vol. 47* (Ed. by J. Vandenberghe, W. Roebroeks and T. Van Kolfschoten), pp. 81-91. Mededelingen Rijks Geologische Dienst.
- van Vliet-Lanoë, B. (1988) The significance of cryoturbation phenomena in environmental reconstruction. *Journal of Quaternary Science*, **3**, 85-96.
- Vandenberghe, J., An, Z., Nugteren, G., Lu, H. & van, H. K. (1997) New absolute time scale for the Quaternary climate in the Chinese loess region by grain-size analysis. *Geology (Boulder)*, **25**, 35-38.

- Vangengyem, E. A. (1982) Paleozoogeograficheskiye obozneniya rasprostraneniya mlekopitayushchikh. In: *Chetverichnaya Sistema (Quaternary System)*, Vol. 1 (Ed. by E. V. Shantser), pp. 279-282. Bcecoyuzni nayuchno-issledivatyelski geologichski institut (All-union Scientific-Research Geologic Institute, Moscow. *Stratigraphiya SSSR (Stratigraphy of USSR)*).
- Velichko, A. A. (1973) *Prirodnyy protsess v Pleistotsen (Natural Processes in the Pleistocene)*. Nauka (Science), Moscow, 256 pp.
- Velichko, A. A. (1990) Loess-Paleosol Formation on the Russian Plain. In: *Loess and the Paleoenvironment*, Vol. 7/8 (Ed. by M. Pecs and D. Loczy), pp. 103-114. Pergamon Press, Oxford. *Quaternary International*.
- Velichko, A. A. (1995) Climate rhythms in Europe during two late glacial-interglacial cycles and the Holocene. In: *Climate and Environment Changes of East Europe during Holocene and Late-Middle Pleistocene* (Ed. by A. A. Velichko), pp. 4-13. Institute of Geography of Russian Academy of Sciences, Moscow.
- Velichko, A. A. & Morozova, T. D. (1972) *Obozneniya stroeniya sredne-verkhne-pleistotsenovikh iscopaemikh pochv na Russkoi ravninye (Characteristic structure of the Middle-Upper-Pleistocene Fossil Soils on the Russian Plain)*. Moscow Nauka, Moscow.
- Velichko, A. A. & Morozova, T. D. (1987) The Role of Loess-Paleosol Formation in the Study of the Regularities of Pedogenesis. *Catena*, **9**, 55-66.
- Velichko, A. A., Devirts, A. A., Dobkina, E. I., Markova, A. K. & Morozova, T. D. (1964) First absolute ages of fossil soils in the loess sequences of the Russian Plain. *Transactions (Doklady) of the Russian Academy of Science, Earth Science Section (In Russian)*, **155**, 555-558.
- Velichko, A. A., Morozova, T. D. & Udartsev, V. P. (1986) Stratigraphy of Loesses and of Fossil Soils within the Russian Plain and Their Correlation with the Rhythms of Oceanic Bottom Deposits. *Annales Universitatis Mariae Curie-Sklodowska Lublin-Polona*, **41(5)**, 87-109.
- Velichko, A. A., Morozova, T. D. & Nechayev, V. P. (1992) Soil formation and cryogenesis on the Russian Plain during the last 125 000 years. In: *Joint Russian-American seminar on cryopedology and global change*, pp. 122-131. Russian Academy of Sciences, Pushchino, Russia.

- Velichko, A. A., Borisova, O. K., Doskach, A. G., Morozova, T. D., Spasskaya, I. I. & Faustova, M. A. (1993) Russkaya Ravnina (Russian Plain). In: *Razvitiye Landshaftov i Klimata Cevyernoy Evrazii: Pozdni Pleistotsen-Golotsen Elementi Prognoza (Development of Landscape and Climate of Northern Europe: Late Pleistocene-Holocene Elements of Prognosis)*, Vol. 1 (Ed. by A. A. Velichko), pp. 11-18. Moscow Nauka, Moscow.
- Velichko, A. A., Morozova, T. D. & Nechaev, V. P. (1995) Correlation of the Late and Middle Pleistocene Events in the Periglacial Zone of Eastern Europe. In: *Climate and Environment Changes of East Europe during Holocene and Late-Middle Pleistocene* (Ed. by A. A. Velichko), pp. 75-79. Institute of Geography of Russian Academy of Sciences, Moscow.
- Velichko, A. A., Gribchenko, Y. N., Gubonina, E. P., Morozova, T. D., Nechayev, V. P., Cicheva, C. A., Timireva, C. N., Udartsev, V. P., Khalcheva, T. A., Tsatskin, A. I. & Chikolini, N. I. (1997) Osnovniye cherti stroyeniya lessovo-pochnennoi formtsii (Essential structural traits of loess-paleosol formation). In: *Lessovo-Pochvennaya Formatsiya Vostochno-Evropoyeskoy Ravnini: Paleogeografiya i Stratigraphiya (Loess-Soil Formation of the Eastern-European Plain: Paleogeography and Stratigraphy)* (Ed. by Velichko), pp. 5-24. Russian Academy of Science, Institute of Geography, Moscow.
- Velichko, A. A., Akhlestina, E. F., Borisova, O. K., Gribchenko, Y. N., Zhidovinov, N. Y., Zelikson, E.M., Iosifova, Y. I., Klimaniov, V. A., Morozova, T. D., Nechaev, V. P., Pizariva, V. V., Svetlitskaya, T. V., Spasskaya, I. I., Udartsev, V. P., Faustova, M. A. & Shik, S. M. (1999) Glava 3: Bostochno-Evropayskaya Ravnina (Chapter 3: East European Plain). In: *Izmeneniye klimata i landshaftov za posledniye 65 millionov let [Kainozoi: ot paleotsena do golotsena] (Climate and Environmental Changes during the last 65 Million Years [Cenozoic: from Paleocene to Holocene])* (Ed. by A. A. Velichko and V. P. Nechayev), pp. 43-83. GEOS, Moscow.
- Verosub, K. L. & Roberts, A. P. (1995) Environmental magnetism: Past, present, and future. *Journal of Geophysical Research*, **100**, 2175-2192.

- Virina, E. I., Heller, F., Faustov, S. S., Bolikovskaya, N. S., Krasenkov, R. V., Gendler, T., Hailwood, E. A. & Hus, J. (2000) Palaeoclimate record in the loess-palaeosol sequence of the Strelitsa type section (Don glaciation area, Russia) deduced from rock magnetic and palynological data. *Journal of Quaternary Science*, **15**, 487-499.
- Wintle, A. G. & Huntley, D. J. (1982) Thermaluminescence dating of sediments. *Quaternary Science Reviews*, **1**, 31-53.
- Yaalon, D. H. (1971) Soil forming processes in time and space. In: *Paleopedology, origin, nature and dating of paleosols*. (Ed. by D. H. Yaalon), pp. 29-39. International Soil Science Society, Jerusalem. *Papers of the symposium on the age of parent materials in soils, Amsterdam, The Netherlands, August 10-15, 1970*.
- Yakimenko, E. Y. (1995) Pleistocene paleosols in the loess and loess-like sediments of the central part of the Russian Plain. *Quaternary Science Reviews*, **14**, 747-753.
- Yokoyama, Y., Lambeck, K., De Deckker, P., Johnston, P. & Fifield, K. (2000) Timing of the Last Glacial Maximum from observed sea-level minima. *Nature*, **406**, 713-716.
- Zagwijn, W. H. (1992) The beginning of the ice age in Europe and its major subdivisions. *Quaternary Science Reviews*, **11**, 583-591.
- Zagwijn, W. H. (1996) The Cromerian Complex Stage of the Netherlands and correlation with other areas of Europe. In: *The Early and Middle Pleistocene in Europe* (Ed. by C. Turner), pp. 145-172. A.A. Balkema, Rotterdam.
- Zonenshain, L. P., M.I., K. & Natapov, L. M. (1990) *Geology of the USSR: A plate-tectonic synthesis*. American Geophysical Union, Washington, D.C., 242 pp.
- Zubakov, V. A. (1974) Predvaritelnaya klimatokhronologicheskaya shkala pleistotsena [vosrast po TL v tis. lyet] (Preliminary Climato-chronological scale of the Pleistocene [Age from TL in thousands of years]). In: *Kratkii istoricheskii obzor izucheniya stratigrafi chetvertichnoi sistemi (Brief historical review of the study of the stratigraphy of the Quaternary System)*, Vol. 1 (Ed. by B. G. Gerbova and I. I. Krasnov), pp. 44. Bcecoyuzni nayuchno-issledivatyelski geologichski institut (All-union Scientific-Research Geologic Institute).

Zubakov, V. A. (1976) *Globalnye klimaticheskiye sobitiya Pleistotsena (Global Climatic Events of the Pleistocene)*. Gridrometeizdat, Leningrad (St. Petersburg), 288 pp.

Zubakov, V. A. (1993) Trans-Eurasian correlation and the general climatostratigraphic scale of the Pleistocene. *Newsletters of Stratigraphy*, **29**(1), 1-19.

APPENDIX A: MODERN CLIMATE DATA

Appendix A presents modern climate data for three regions that approximate climatic conditions for each of the regions in which the study sites are located. Some of this data (*i.e.*, temperature and precipitation data) was also used to construct the climatograms presented in Figure 1.3. These data were obtained from Lydolph 1977, *Climates of the Soviet Union*.

Climate Table for Moscow

Latitude 55° 45'N; Longitude 37° 34'E

Elevation 156m

Month	Air Pressure (mbar)		Wind prevailing direction	Temperature (°C)				Humidity		Precipitation (mm)				
	sea level	station		mean speed (m/s)	mean	mean daily range	max.	min.	vapour pressure (mm)	relative (%)	mean	max.	min.	max. in 24h
January	1019.2	997.9	W	5.0	-10.3	7.8	4	-42	2.2	85	31	67	8	20
February	1019.0	997.7	SE	4.9	-9.7	12.0	6	-40	2.1	82	28	75	7	21
March	1017.1	996.2	W	5.2	-5.0	11.0	15	-32	2.8	77	33	98	6	21
April	1016.4	996.2	SE	4.7	3.7	10.1	28	-19	4.7	71	35	100	3	25
May	1015.8	996.3	N	4.5	11.7	13.3	32	-7	6.8	64	52	103	2	33
June	1011.5	992.3	NW	3.9	15.4	13.3	35	-2	9.4	66	67	174	5	51
July	1010.5	991.5	NW	3.5	17.8	11.8	37	4	11.2	69	74	169	25	79
August	1011.8	992.7	NW	3.5	15.8	13.0	37	1	10.2	74	74	164	1	63
September	1015.8	996.2	W	4.3	10.4	13.1	32	-5	7.7	79	58	131	7	52
October	1018.0	997.9	W	4.7	4.1	11.8	24	-20	5.3	82	51	143	6	42
November	1018.6	997.9	SW	4.9	-2.3	7.3	13	-33	3.7	85	36	114	11	22
December	1019.2	997.9	S	4.7	-8.0	7.0	8	-39	2.5	86	36	82	7	26
Year	1016.0	995.9		4.5	3.6		37	-42		77	575	819	354	79

Climate Table for Tambov

Latitude 52° 44'N; Longitude 41° 28'E

Elevation 139m

Month	Air Pressure (mbar)		Wind prevailing direction	Temperature (°C)				Humidity		Precipitation (mm)			
	sea level	station		mean speed (m/s)	mean	mean daily range	max.	min.	vapour pressure (mm)	relative (%)	mean	max.	min.
January			SE	4.2	-10.8	6.9	4	-39	2.7	85	34	88	9
February			SE	4.4	-10.2	7.6	5	-37	2.9	84	29	105	1
March			SE, S	4.4	-5.1	7.8	18	-31	3.8	83	30	62	8
April			SE	3.8	5.1	9.4	30	-18	6.7	72	34	67	3
May			N, SE	3.8	13.9	12.0	34	-8	9.3	60	50	125	5
June			N	3.4	18.0	12.2	38	-1	12.7	60	53	121	6
July			NW	3.1	20.2	11.9	40	4	15.1	65	64	172	3
August			N	2.9	18.5	11.8	38	1	14.3	68	53	155	1
September			W	3.2	12.2	11.1	37	-7	10.3	72	45	114	1
October			W	3.7	5.3	7.8	27	-19	7.0	80	44	106	0
November			SE	4.1	-2.0	5.8	16	-34	4.8	84	39	104	9
December			SE	4.2	-7.7	5.8	8	-37	3.6	86	38	117	2
Year			SE	3.8	4.8		40	-39	7.8	75	513	735	337

Climate Table for Volgograd

Latitude 48° 42'N; Longitude 44° 31'E

Elevation 42m

Month	Air Pressure (mbar)		Wind prevailing direction	Temperature (°C)				Humidity		Precipitation (mm)			
	sea level	station		mean speed (m/s)	mean	mean daily range	max.	min.	vapour pressure (mm)	relative (%)	mean	max.	min.
January	1023.6		NE	6.1	-9.6	7.3	11	-35	2.1	85	23	60	1
February	1022.7		NE	7.1	-8.9	9.2	10	-31	2.1	85	20	63	1
March	1020.4		NE	5.3	-2.6	10.2	23	-26	3.3	84	18	67	4
April	1017.8		NE	5.2	8.2	12.4	31	-14	5.3	65	19	63	0
May	1015.8		E	4.8	17.0	13.3	35	-4	7.6	56	27	79	0
June	1011.4		NE	4.9	21.4	13.0	40	4	10.2	49	40	137	0
July	1010.1		N, NW	4.2	24.2	13.2	42	9	11.4	47	33	103	0
August	1012.6		N	4.6	22.7	13.5	43	6	10.2	51	23	116	0
September	1017.8		N, SE, S	4.3	15.9	13.6	36	-2	8.0	57	27	74	1
October	1021.9		W	4.6	8.2	12.9	32	-14	5.9	71	23	66	0
November	1023.4		NE	5.0	0.2	8.9	22	-25	4.3	82	34	76	1
December	1023.5		NE	5.8	-6.3	7.4	12	-31	2.8	86	31	117	3
Year	1018.4		NE	5.1	7.5		43	-35		68	318	571	156

APPENDIX B: OSL DATING METHODS

Appendix B outlines the methods used to obtain the OSL ages presented throughout the dissertation. It is presented in manuscript form for OSL samples obtained from Likhvin and Gololobovo, and in table and figure form for samples from Korostylievo and Mikhailovka.

Manuscript Acceptance Letter.

November 20th 2001

Dr Edward C. Little,
 Canada-Norway Geoscience Centre
 P.O. Box 2319,
 Iqaluit, Nunavut, X0A 0H0,
 Canada

Dear Edward,

QUATERNARY SCIENCE REVIEWS

**Quaternary stratigraphy and optical dating studies of loess from the east
 European Plain (Russia)**

by
**E.C. Little, O.B. Lian, A. A. Velichko, T.D. Morozova, V.P. Nechaev, K.G.
 Dlussky, N.W. Rutter**

I'm delighted to say that your paper is now acceptable for publication and has
 been sent to the publisher. You should receive the proofs within about two months
 and the paper will be published in the middle of 2002.

Very best wishes,

Yours sincerely,

A handwritten signature in black ink, appearing to read "J. Rose".

Professor J. Rose
 Editor in Chief, Quaternary Science Reviews

Quaternary stratigraphy and optical dating of loess from the east European Plain (Russia).

Edward C. Little¹

*Department of Earth and Atmospheric Sciences, The University of Alberta,
Edmonton, Alberta, Canada T6G 2E3.*

Olav B. Lian²

*School of Earth Sciences, Victoria University of Wellington, P.O. Box 600,
Wellington, New Zealand.*

A. A. Velichko

*Laboratory of Evolutionary Geography, Institute of Geography, Russian Academy
of Sciences, Staromonetny 29, Moscow 109017 Russia (paleo@glasnet.ru).*

T.D. Morozova

*Laboratory of Evolutionary Geography, Institute of Geography, Russian Academy
of Sciences, Staromonetny 29, Moscow 109017 Russia (paleo@glasnet.ru).*

V.P. Nechaev

*Laboratory of Evolutionary Geography, Institute of Geography, Russian Academy
of Sciences, Staromonetny 29, Moscow 109017 Russia (paleo@glasnet.ru).*

K.G. Dlussky

*Laboratory of Evolutionary Geography, Institute of Geography, Russian Academy
of Sciences, Staromonetny 29, Moscow 109017 Russia (paleo@glasnet.ru).*

N. W. Rutter

*Department of Earth and Atmospheric Sciences, The University of Alberta,
Edmonton, Alberta, Canada T6G 2E3 (nat.rutter@ualberta.ca).*

¹ Present address: Canada-Nunavut Geoscience Office, P.O. Box 2319, Iqaluit, Nunavut, Canada X0A 0H0 (elittle@NRCan.gc.ca).

² Present address: Department of Physics, Simon Fraser University, 8888 University Drive, Burnaby, British Columbia, Canada V5A 1S6 (olian@sfu.ca).

Abstract

Optical dating of silt-sized potassium feldspar grains was found to be suitable for dating the formation of key loess units at two sites on the central east European Plain. Loess bracketing the Bryansk palaeosol yielded optical ages in agreement with the well-dated radiocarbon chronology when corrected for anomalous fading. Optical ages from loess bracketing a significant pedogenic unit below the Bryansk palaeosol support our lithostratigraphic interpretation that it is the Mezin palaeosol complex, and its formation during the Last Interglaciation, Oxygen Isotope Stage (OIS) 5. Optical ages from a stratigraphically older loess unit directly underlying a significant (~10 m thick) till unit, in conjunction with its regional stratigraphic context, suggest that the loess, and the till were deposited during the Dnieper Glaciation, which probably occurred during OIS 6.

1. Introduction

The east European Plain (Fig. 1A), is one of Earth's largest physiographic regions. It is capped with till, glaciofluvial, glaciolacustrine, alluvial, and aeolian deposits that represent several glacial and nonglacial intervals thought to span much of the Quaternary Period. Of particular interest are the widespread loess sheets that show extensive pedogenic and (or) cryogenic overprinting, making them ideal for the study of Quaternary palaeoecology and climate.

Understanding of the Quaternary geology and geography of the east European Plain has evolved dramatically over the last c. 115 years – from the pioneering work of Nikitin (1885) and Pravoslavlev (1907), to the discovery of early glaciations in the Oka and Don river basins (Gerbova and Krasnov, 1982 and references cited therein), to the relatively recent work on loess-palaeosol sequences (e.g., Velichko et al., 1997, 1999). Lithostratigraphic units have generally been placed into a relative stratigraphic context through the correlation of in-situ fossil assemblages, some of which have been associated with global marine oxygen isotope stages (OIS) (Velichko, 1990; Ehlers et al., 1995). However, there is still much uncertainty as to the timing of local geo-climatic events, and how these relate to global climatic events. Recent stratigraphic schemes for the east European Plain, and adjacent regions, are discussed below.

In order to infer Quaternary climates from the sedimentology and palaeoecology of the east European Plain, a variety of techniques have been employed (e.g., Markova, 1975; Morozova, 1981; Velichko and Nechayev, 1984; Velichko et al., 1984; Grichuk, 1984; Velichko and Svetlitskaya, 1987; Agadjanyan, 1992). This multi-disciplinary research approach has significantly advanced the understanding of the physical processes that have contributed to the development of the region (Velichko, 1990, 1995). Establishing an absolute chronology has been of particular importance, as it is needed to correlate key units over distances of 10 km or more. Radiocarbon dating has been routinely employed, but has only allowed for the development of a reliable stratigraphic framework over the last ~40 ka (e.g., Dobrodeyev and Il'ichev, 1974; Arslanov et al., 1977; Velichko and Shik, 1992; Velichko et al., 1986, 1994, 1997). For deposits older than ~40 ka, the geology has been much more difficult to place in an absolute temporal context; in most instances only relative ages have been obtained from palaeoecological information (e.g., Agadjanyan and Glushankova, 1987; Velichko, 1990; Velichko et al., 1997). Absolute chronologies beyond the limit of radiocarbon dating have come almost exclusively from thermoluminescence (TL). The most comprehensive suite of TL ages (at least 23 ages) from a single site, is probably that from the Chekalin (Likhvin) type section. They range from about 560 ka to 25 ka, and were reported by Faustov et al. (1974) and Dobrodeyev and Il'ichev (1974), and are summarised by Dreimanis et al. (1978). Dobrodeyev and Il'ichev (1974) also show, and correlate, 19 other TL ages from ten sections on the east European Plain.

Although these TL ages are generally consistent from section to section, and increase with depth, their validity has been seriously questioned on the basis of inappropriate laboratory technique – see discussions by Dreimanis et al. (1978) and Wintle and Huntley (1982). However, since many of these early TL ages are still being used in stratigraphic work, and the youngest (<50 ka) appear to be consistent with associated radiocarbon ages, we feel it will be useful to compare them with the results presented here.

More recently, optical dating has been employed on loess from the east European Plain (Yakimenko, 1995). However, the mineral(s) dated

and the laboratory procedures used were not reported or discussed, so an assessment of reliability is not possible.

Also of concern is that the Russian literature commonly reports luminescence ages that exceed 500 ka, when Western laboratories are rarely able to produce accurate ages of this magnitude, even when established laboratory techniques are used and sedimentological and dosimetric circumstances are ideal, (e.g., see the review by Prescott and Robertson, 1997). Indeed, in most cases, established luminescence dating techniques are reliable only in the range c. 1 ka to 150 ka (Prescott and Robertson, 1997).

There have been few independent studies published on the utility of using luminescence to date loess from regions of the former Soviet Union. One relatively recent test by Zhou et al. (1995) focused on re-dating the fine-grain fraction of loess at a key section in Orkutsay, Uzbekistan. These workers succeeded in producing TL ages up to ~130 ka, but stated that their ages must all be considered lower limits because of the presence of anomalous fading. This in turn led them to seriously question all but the youngest (c. <50 ka) previously reported TL ages on loess from the former Soviet Union. Such data have only added vagueness to the timing of the older geo-climatic events (Velichko, 1995).

In light of this, and because of our present and ongoing research on the palaeoclimates of the east European Plain region (e.g., Velichko, 2000; Dlussky, 2001), we decided to develop an independent chronology using optical dating techniques that have been well-tested on a variety of deposits from different parts of the world. In this paper we present a detailed account of the procedures used to obtain our first set of optical ages. We then discuss their limitations and compare them with information already in the literature.

We collected eight samples of loess associated with palaeosols from two key sites in the east European Plain. Four were from the Chekalin type section (hereafter referred to as the Likhvin section), and four were from a site at Gololobovo (Fig. 1B). Four of the samples are associated with a palaeosol whose age-range is relatively certain; these samples were chosen in order to test our methods. The other samples were

associated with significantly older palaeosols, and a till, whose absolute ages are less secure.

2. Recent stratigraphic schemes for the east European Plain region

Developments in Quaternary stratigraphy of the east European Plain during the 1980's and 1990's followed from studies undertaken in preceding decades, which had focused mainly on establishing the timing of glacial/interglacial events. Several stratigraphic schemes were produced, but with only limited consistency. The three most recent, and most widely accepted, schemes are briefly discussed below and are illustrated in Fig. 2.

During the 1980's, a stratigraphic scheme was developed that expanded upon the work of Gerasimov et al. (1980) and Zubakov (1974). It consisted of a comprehensive stratigraphic framework that became one of the most widely accepted schemes for the Quaternary of European U.S.S.R. and western Europe (Krasnov and Shantser, 1982, their Table 19 which was compiled by K.V. Nikiforova, I.I. Krasnov, L.P. Aleksandrova, Yu. M. Vasilev, N.A. Konstantinova, and A.L. Chepalyga). This compilation included magnetostratigraphic, biostratigraphic, and climatostratigraphic information that spanned the last c. 3.5 Ma, some of which was subsequently correlated to archaeological records and marine data (Fig. 2).

Velichko (1990), and Velichko et al. (1997), expanded on the aforementioned scheme, but retained the stratigraphic subdivisions of Gerasimov et al. (1980). In Velichko's stratigraphic scheme, rather than correlating terrestrial records to oceanic records through coastal sections, terrestrial climate proxies were established from palaeosols and cryogenic features, and these were used to infer estimates of mean January temperatures as a function of time, which were in turn compared to the global oxygen isotope record (Fig. 2).

The most recent stratigraphic framework was developed in 1997 and includes information compiled over the last 30 years Velichko et al. (1999). This scheme includes stratigraphic units in both glacial and periglacial zones, and an absolute time scale; an abridged version is shown in Fig. 2.

Several differences can be noted between these three schemes. The most significant of these are the changes in the timing of many upper and lower zone boundaries. One example is the placement of the Mikulino Interglacial, which was shown as an early to middle OIS 5 event in the 1982 scheme, but was later (1990 scheme) shown to encompass the whole of OIS 5, and is currently (1997 scheme presented in Velichko et al., 1999) considered to be associated only with the OIS 5 climatic optimum, Oxygen Isotope Substage (OISS) 5e.

For this study, we will adhere to the stratigraphic scheme of Velichko et al., (1999).

3. Physical setting, stratigraphy, and sample locations

The Likhvin site is located along the Oka River near the town of Likhvin (formerly known as Chekalin), in the northern part of the Central Russian Upland (Fig. 1C) (Velichko et al., 1997). The landscape of this region is dissected by river valleys, gullies and ravines; river incision in the order of 50–70 m is common (Lysenko, 1971). Bedrock in the region consists mainly of dolomite, limestone, sandstone, and mudstone (Nalivkin, 1960, 1973).

The Gololobovo site is located ~250 km northeast of Likhvin, along the Oka River in the forest zone of the Oka Basin (Fig. 1B, C) (Velichko et al., 1997). The geomorphology of the region consists generally of gently rolling hills bordered by the Smolensk-Moscow Upland in the north, the Oka-Don Plain in the south, the Central Russian Upland to the west, and the Meshchera Depression in the east and southeast (Fig. 1C) (Lysenko, 1971). Bedrock of the Oka Basin in the vicinity of Gololobovo consists mainly of dolomite, limestone, anhydrite, gypsum and minor amounts of sandstone and shale with coal interstratification (Nalivkin 1960, 1973; Lysenko, 1971).

Initial stratigraphic correlation between sites on the east European Plain was typically made through comparison of loess and palaeosol sequences in over 100 sections within the Eastern European Plain (e.g., Velichko, 1990, 1995; Morozova, 1995; Velichko et al., 1997). In most cases marker beds, such as the Mezin palaeosol complex, were used as control points, and from these marker horizons the less well developed pedogenic horizons were fit into the loess-palaeosol relative-time se-

quence. Other stratigraphic tools such as palaeomagnetism, palaeoecology, micromorphology, radiocarbon and limited luminescence dating, have been used to strengthen correlation and provide absolute time constraints (Krasnov and Shantser, 1982; Velichko et al., 1992; Velichko, 1990, Pospelova et al., 1997; Velichko et al., 1999).

For this work, lithological characteristics and relative position were used to give a first-order approximation of the stratigraphy at both Likhvin and Gololobovo. The marker beds identified were: 1) the Holocene soil, which is the uppermost pedogenic horizon at both sites; 2) the Bryansk palaeosol, which is situated directly beneath the Holocene soil and typically is moderately-well developed, relative to the Holocene and immediately older interglacial palaeosols; 3), the Mezin palaeosol complex, which is associated with the Mikulino Interglacial (e.g., Velichko et al., 1997) and directly underlies the Bryansk palaeosol; 4) deposits of the Dnieper Glaciation – till at Likhvin and Tsna Loess at Gololobovo, and 5) a sequence of pre-Dnieper loess and palaeosols including: the Romny palaeosol, the Kamenka palaeosol and the Inzhavino palaeosol (Velichko et al., 1999).

Seven significant palaeosol units were identified and studied at both Likhvin and Gololobovo (Fig. 3). In the discussion below we refer to the palaeosols as units A (youngest) to F (oldest), whereas the non-organic (lithic) sedimentary units are labelled LC-1 to LC-12 (Likhvin) and GC-1 to GC-10 (Gololobovo).

3.1. *Likhvin Composite Section*

The Likhvin composite section (54°06' N 36°16' E) includes two sections about 300 m apart (Fig. 3). The upper ~7 m consists primarily of silt and clayey-silt showing three episodes of pedogenic overprinting. The Holocene soil (Ap horizon) occupies the upper 0.75 m of the section (unit A). The lithic unit in which unit A formed is interpreted to be a secondary (colluviated) loess (unit LC-1). Approximately 1 m below unit A there is a weakly-developed palaeosol (unit B) that is truncated by an intrusive pit-shaped feature; this feature also truncates a charcoal-rich horizon that yielded an AMS radiocarbon age of 2770 ± 60 years BP (TO-7408). Directly beneath the charcoal layer is about 3 m of massive calcareous silty clay (base) that grades to silty loam (unit LC-

2), that is interpreted to be primary loess. Within unit LC-2 there is a moderately-well developed organic-rich horizon (~1 m thick) that is interpreted to be the Bryansk palaeosol (unit C). Optical dating samples LCSL1 and LCSL2 consisted of loess collected about 50 cm above, and 24 cm below, the Bryansk palaeosol, respectively.

According to several investigations (e.g., Velichko et al., 1964a, 1992; Velichko and Morozova, 1972, 1987; Dobrodeyev and Parunin, 1973; Chichagova, 1985; Tsatskin, 1997) the Bryansk palaeosol formed during the period 30 ± 1 ka to 23 ± 1 ka radiocarbon years, or during 34 ± 1 ka to 27 ± 1 ka calendar years (i.e., late OIS 3), using the calibration data of Bard et al. (1998) and Kitagawa and van der Plicht (1998). Faustov et al. (1974) and Dobrodeyev and Il'ichev (1974) reported three TL age determinations for the Bryansk palaeosol at Likhvin: 36.7 ± 4.3 ka (MGU-KTL 60), 41.1 ± 5.2 ka, and 45.5 ± 5.1 ka, while Dobrodeyev and Il'ichev report seven TL ages for the palaeosol from five correlative sections; the ages span from about 22 ka to 28 ka.

Approximately 1 m beneath the Bryansk palaeosol (i.e., underlying unit LC-2) is a well-developed organic-rich complex that exhibits two sets of soil horizons that formed in silty-clay to silty-loam. On the basis of its stratigraphic position, and on its physical characteristics, this double set of palaeosol horizons (palaeosol D in unit LC-3, Fig. 3) is interpreted to be the Mezin palaeosol complex (Fig. 4A). On the basis of their degree of development, the upper Ah-B horizon set probably was formed during the Krutitsy Phase, which is commonly associated with OISS 5a and OISS 5c, whereas the lower set (Ah-Ae-B horizons) may have developed during the Salyn Phase (OISS 5e) of the last (Mikulino) interglacial (Fig. 2). The silty-clay to silty-loam (Fig. 4B) parent material in which the Mezin palaeosol complex developed (unit LC-3) is highly altered (pedogenically and cryogenically) and is therefore difficult to interpret; the tentative interpretation of this material, based on its high percentage of silt (50–79%), and the lack of any observable remnant primary structures, is a secondary (altered) loess. The Mezin palaeosol complex at this site is extremely cryoturbated, with ground wedges (cf. Harry and Gozdzik, 1988) penetrating into underlying units.

Faustov et al. (1974) and Dobrodeyev and Il'ichev (1974) reported a TL age of 186 ± 21 ka (MGU-KTL 58) and 105 ± 13 ka for sediments

directly underlying and overlying the Mezin palaeosol complex at Likhvin, respectively, whereas TL ages from correlative sections include 46 ± 14 ka and 115 ± 13 ka from the base of the palaeosol, and 107 ± 11 ka at the top (Dobrodeyev and Il'ichev, 1974). These TL ages collectively support the notion that the Mezin palaeosol complex formed during OIS 5. More recently Yakimenko (1995) presented two optical ages in the range "100–110 ka" for a palaeosol at Serpukhov (Fig. 1B) that she associated with the Mikulino interglaciation. Further chronological control has come from palynological data collected from a peat layer that interfingers the Mezin palaeosol horizon at its type section along the Densa River, which suggests its formation during the Salyn Phase (Velichko et al., 1964b), which occurred between about 130 ka and 123 ka (Martinson et al., 1987).

Approximately 50 cm below the base of the Mezin complex, the clay content increases from silty loam to silty-clay loam, and the sediment becomes laminated; the laminae are composed mainly of silt and are highly deformed. These sediments (unit LC-4) are interpreted to have been deposited in a glacial lake and were subsequently cryoturbated during the same cold event that cryogenically deformed the overlying unit (unit LC-3). Unit LC-4 is underlain by alternating beds of poorly-sorted fine to medium sand (LC-5 – upper); one of these beds consists of poorly sorted sandy-gravel. This sand and gravel unit is underlain sharply by clay, silt and sand beds that exhibit well-developed load structures. Directly beneath are medium to coarse sands (LC-5 – lower) which are well sorted and show trough and tabular cross-bedding. This sequence of bedded sand, silt clay, and gravel (unit LC-5) is interpreted to have been deposited in a glaciofluvial environment. Unit LC-5 lies sharply on ~10 m of diamicton (unit LC-6) which is interpreted to be till deposited during the Dnieper Glaciation. The Dnieper Glaciation is commonly associated with OIS 6, but some workers argue that it could be older (Velichko et al., 1999).

Three largely undeformed palaeosols (units E_2 , E_1 , F) were identified below the Dnieper till. Palaeosols units E_2 and E_1 occur in clay-rich silt and are relatively weakly developed, whereas palaeosol unit F is more strongly developed and exhibits krotovena and root traces. Based on its

degree of development and stratigraphic position, palaeosol unit F is interpreted to be part of the Chekalin horizon (referred to here as Inzhavino palaeosol) which is thought to have developed during the Likhvin Interglacial (Bolikhovskaya and Sudakova, 1996; Velichko et al., 1999). The Likhvin Interglacial is often equated to the Holsteinian Interglacial of northwestern Europe (e.g., Sudakova and Faustova, 1995; Zagwijn, 1996), but there is still considerable speculation about this. Moreover, the timing of the Holsteinian Interglacial is contentious, and has been reported to occur anywhere between OIS 7 and OIS 15 (cf. Van Kolfschoten, 1993; Zagwijn, 1992, 1996; Lowe and Walker, 1997; Velichko et al., 1997). However, there appears to be a growing consensus that the Holsteinian Interglacial should be associated with OIS 11 (Turner, 1996; Poore et al., 1998), and therefore the Likhvin Interglacial, if indeed correlative, may also have occurred during this period.

The sediments bracketing palaeosol units E₂, E₁, and F, and lithic units LC-7 through L-12 (Fig. 3), are interpreted to be loess (LC-8, -10, -11, -12), reworked loess (LC-7), and lacustrine (LC-9). However, limited exposure made it impossible to determine whether the loess units are primary or secondary deposits. Optical dating samples LCSL3 and LCSL4 were collected from loess units LC-8 and LC-9, about 2.5 m and 1.5 m, respectively below the Dnieper till (Fig. 3).

To our knowledge, the only quantitative age data associated with Dnieper glacial deposits are those reported by Faustov et al. (1974) for the Likhvin site. They include a TL age of 280 ± 31 ka (MGU-KTL 41) for Dnieper "stratified moraine", and a TL age of 336 ± 41 ka (MGU-KTL 44) for sediments associated with the "Likhvin soil horizon" (Faustov et al., 1974), which is probably correlated with our unit LC-12 (Fig. 3).

3.2. Gololobovo Composite Section

The Gololobovo composite section (55°03' N 38°34' E) consists of four sections, less than 800 m apart, that together expose sediments interpreted to span the last two major glacial cycles: Holocene–Mikulino and Mikulino–Likhvin (Fig. 2). To our knowledge, the only published material from Gololobovo is a summary of section descriptions, geochemical data, rock-magnetic properties and soil micromorphology (Velichko,

2000). Therefore, the data presented here will help to chronologically constrain the units at Gololobovo, thus adding to our knowledge of the Late Pleistocene stratigraphy of the east European Plain.

The sediments exposed at Gololobovo consist primarily of clay-rich silts that show at least six episodes of pedogenic overprinting (Fig. 3). The upper three pedogenic horizons, units A, C, D, are interpreted to be the Holocene soil (at the top), the Bryansk palaeosol, and the Mezin palaeosol complex, based on relative development and stratigraphic position. The Mezin palaeosol at this site consists only of A1, A2 and Bt horizons; the characteristic double set of A-B horizons observed in the Mezin palaeosol at Likhvin is not discernable here.

These palaeosols have developed within lithic units GC-1, GC-3, GC-4, which consist primarily of massive silty-clay loam with gradational contacts. Unit GC-2, is weakly stratified silty clay, whereas the silty loam of unit GC-5 exhibits weak oxidised banding that suggests alternating changes in grain size and porosity. Units GC-1, GC-3, and GC-4 are considered to be primary loess, whereas unit GC-2 is interpreted to be secondary loess that was redeposited in standing water in either a lacustrine or glaciolacustrine environment; unit GC-5 is interpreted to be a secondary (colluviated) loess. Optical dating sample GCSL1 was collected from unit GC-1, about 1 m below the Holocene soil, whereas sample GCSL2 was collected from unit GC-3, about 20 cm beneath the Bryansk palaeosol (Fig. 3).

Based on stratigraphy, the sediments below the Mezin complex are interpreted to have been deposited during the Middle Pleistocene (as defined by the Russian stratigraphic scheme, Fig. 2). Near the base of the Mezin complex, small (20 ¥ 45 cm), but distinct, ground wedges are observed intruding into parent material, which gradually coarsens downward to calcareous massive silt interpreted to be primary loess (unit GC-4). Optical dating samples GCSL3 and GCSL4 were both collected from unit GC-4, about 1 m below the base of the Mezin palaeosol complex, but from different sections (Fig. 3); the samples were taken at least 75 cm below the Mezin ground wedges. About 1.5 m below the location of samples GCSL3 and 4, clay content begins to gradually increase with depth, and weak to moderate, parallel, inclined

stratification is observed (unit GC-6). This unit is interpreted to consist of secondary (colluviated) loess. Unit GC-6 rests sharply on a ~1 m-thick bed of massive blue-grey clay that exhibits strong mottling (unit GC-7). Underlying the clay unit are three palaeosols, units E₂, E₁ and F, that have developed in clayey-silt parent material (unit GC-8 through to unit GC-10); these units are differentiated on the bases of colour, soil structure, and degree of cryoturbation (see Fig. 3 for details). The parent materials of units GC-8 and GC-9 are interpreted to be pedogenically altered secondary loess, whereas the secondary loess of unit GC-10 was altered by both pedogenic and cryogenic processes. Palaeosols units E₂ and E₁ are moderately and weakly developed, respectively, whereas palaeosol unit F is very well developed. Furthermore, palaeosol unit F exhibits well developed involutions and other evidence of pervasive cryoturbation. The degree of development, and post-pedogenic cryoturbation of the palaeosol unit F, in addition to its stratigraphic position, suggest that it formed during the Likhvin Interglacial and is therefore interpreted to be the Inzhavino Palaeosol (Fig. 2). The relatively weak soil development observed in palaeosol units E₂ and E₁ may represent warmer periods within OIS 7, or alternatively it may represent formation during OIS 7 and 9, respectively, depending on the placement of the Likhvin (Holsteinian?) Interglaciation with respect to the oxygen isotope record.

4. Optical dating

Optical dating is based on the fact that minerals, such as feldspar and quartz, contain structural defects that can act as traps for unbound (free) electrons. The rate at which such traps are filled is proportional to the rate at which free electrons are produced. This is in turn proportional to the environmental dose rate from α , β , and γ radiation produced during the decay of ²³⁸U, ²³⁵U, ²³²Th, their daughter products, and ⁴⁰K in the mineral grains and in the surrounding sediment. For samples near the ground surface, there is also a significant contribution from cosmic rays.

In the laboratory, the radiation dose absorbed since the sediment grains were last exposed to sunlight is estimated (the “equivalent dose”), and, together with a measure of the environmental dose rate,

the time elapsed since the sediment grains were last exposed to sunlight can be determined. The optical age is simply the equivalent dose divided by the environmental dose rate. Detailed and varied accounts of the theory and (or) laboratory procedures involved can be found in Berger (1995), Wintle (1997), Aitken (1998), Wagner (1998), Huntley and Lian (1999), Lian and Huntley (2001), and the papers published in *Radiation Measurements* (Vol. 27 5/6, 1997).

4.1 *Sample collection and laboratory preparation*

Carved blocks were collected from cleaned section faces during the summer of 1996. In order to protect the samples, they were fit into brass cylinders (10 × 8 cm), wrapped in aluminium foil, and made water tight.

Under subdued orange light (fluorescent light behind several layers of Lee 158 optical film), the sample cylinders were opened from the in-section end, and several centimetres of sediment was removed and discarded. Subsamples to be used to estimate water content were first collected, and then about 200 g (moist) of sediment was removed for dating. Care was taken to avoid contamination by sampling away from the walls of the cylinder. Of the material removed for dating, a representative subsample of about 30 g was dried and milled to a fine powder, to be used later for dosimetry.

The bulk samples consisted of 1–7 % sand (>63 µm diameter), 43–83% silt (2–63 µm diameter), and 11–50% clay (<2 µm diameter) which required us to use the fine grain method of optical dating. The fine silt (4–11 µm diameter) fraction was used for dating. Chemical and mechanical separation of the desired polymineral sediment fraction was performed using standard methods as described in Lian and Huntley (1999). For each sample about 70 aliquots were made by suspending the separated sediment in acetone, and depositing the suspension onto ~1 cm diameter aluminium discs.

4.2 *Determination of the environmental dose rate*

The environmental dose rate due to a, b, and g radiation was calculated from the concentrations of ²³⁸U, ²³²Th, and ⁴⁰K (Table 1), which were found using delayed neutron counting (DNC), neutron activation analysis (NAA), and inductively-coupled plasma atomic emission

spectrometry (ICP-AES), respectively. To test for the presence of radioactive disequilibrium in the U and Th decay chains, equivalent concentration of these parent radioisotopes were determined by thick-source alpha counting (TSAC) (Table 2). The presence of water and organic matter reduce the radiation absorbed by the relevant minerals, and must be accounted for in the dose rate calculations. For water content, an average of the as-collected and saturated values was used, with an uncertainty that was expected to account for dry and wet periods, and periods of permafrost, at two standard deviations. Organic matter was found to be insignificant in these samples, accounting for only 2–4% of the total dry mass (Table 2).

Dose rates due to a, b, and g radiation were calculated using standard formulae (e.g., Aitken, 1985) and the revised dose-rate conversion factors of Adamiec and Aitken (1998). For sediments that are near the surface, cosmic rays can make a significant contribution to the total dose rate. If sedimentation rates are known, the cosmic ray contribution can be calculated in detail. However, this can rarely be done since it is difficult, or impossible, to account for periods of erosion, nondeposition, and rapid sedimentation. For our samples, while at the surface, the dose rate due to cosmic rays would have been $\sim 0.3 \text{ Gy ka}^{-1}$ (less than $\sim 10\%$ of the present total dose rate), but it would have rapidly decreased with increasing burial depth. Since all of our samples are expected to have spent most of the time at depths $> 2 \text{ m}$, the contribution from cosmic rays is expected to be small, accounting for no more than $\sim 5\%$ of the total dose rate. For each sample, therefore, the dose rate due to cosmic ray radiation was estimated using the present burial depths (Table 3).

4.3. Determination of the equivalent dose

Equivalent doses were determined by constructing the dose response of each sample using the violet ($\sim 3.1 \text{ eV}$, 400 nm) luminescence emitted during excitation with infrared ($\sim 1.4 \text{ eV}$, 800–960 nm) photons. It was confirmed that this emission came from the desired mineral(s) by observing the samples' emission spectra, which was characteristic of that known to be associated with potassium feldspar. Semi-quantitative X-ray diffraction indicated that potassium feldspar accounted for 2–9% of

the minerals in the fraction used for dating. Plagioclase feldspar, found to account for 2–14%, is also excited by 1.4 eV photons, but its contribution to the measured luminescence was expected to be insignificant due to our choice of optical filters (below) and the low quantum efficiency (sensitivity) of our detector to the main 2.2 eV (~560 nm) emission from plagioclase feldspar.

Luminescence was detected using a EMI 9235QA photomultiplier tube mounted behind a Schott BG-39 (infrared absorbing) and Kopp 5-58 (violet band pass) optical filters. The apparatus used for all the luminescence measurements was the same as that used by Lian and Shane (2000). Laboratory bleaching was performed using red-infrared light from a quartz-halogen lamp behind a Schott RG715 optical filter (e.g., Huntley and Clague, 1996). The bleach was for 4 hours and reduced the luminescence to 3–6% of that of a similar unbleached aliquot. Laboratory irradiations were at 6.5 Gy min⁻¹ from a ⁹⁰Sr–⁹⁰Y b source. The efficiency (*h*-value) was determined by exposing some of the aliquots to ²⁴¹Am sources that delivered a radiation to the sample at 0.15 μm⁻² min⁻¹.

To assure that only sufficiently stable electron traps were sampled during the final measurements, all the aliquots were heated (“preheated”) at 140 °C for 7 days. The choice of this temperature and duration was based on its adequacy in several other studies (e.g., Huntley et al., 1993*b*; Lian et al., 1995; Lian and Shane, 2000). In order to find a more convenient preheat protocol using a heating time of 4 hours, we observed the ratio of the luminescence intensity from aliquots that had received a long laboratory bleach followed by a b dose approximately equal to their equivalent dose, to the luminescence intensity from aliquots that had not received a laboratory bleach or radiation dose (i.e., “naturals”). This ratio was first observed for aliquots measured at room temperature (~20 °C), and then at successive ~25 °C intervals up to 250 °C. When this ratio became relatively constant we presumed that stable traps were being similarly emptied in both sets, and from this we deduced that 175 °C for 4 hours would be sufficient. To test this we used both the new and the standard (140 °C / 7 day) preheat protocols on samples GCSL1 and LCSL1.

After preheating, all the samples were stored at room temperature for 90 days, and then measured for 100 s. Equivalent doses were deter-

mined using both the regeneration method (Huntley et al., 1993a; Huntley and Lian, 1999) and the additive-dose with thermal transfer correction (ADTT) method, as described by Huntley et al. (1993b) and Lian and Huntley (1999). The ADTT method is suitable when the dose response is linear, or nearly so. If this is not the case, then the regeneration method is required.

Dose response data were fitted with curves using maximum likelihood. For all samples the additive-dose and regeneration data were fitted with saturating exponential functions, whereas the thermal transfer correction data were fitted with straight lines. For both methods, dose-axis intercepts (ADTT method), or dose-axis shifts (regeneration method), were calculated for successive 10 s intervals. For the regeneration method, sensitivity change in the regeneration data was tested for by using a scaling parameter in the fit. Dose response data for most of the samples are shown in Figs. 5 and 6, whereas plots of dose-axis intercepts versus excitation time are shown in Fig. 7.

Anomalous fading is the term used to describe the reduction in measured luminescence arising from electrons leaving traps that are otherwise stable at ambient temperatures over geological time (e.g., see Aitken, 1998). It causes calculated optical ages to be too young, and it is likely that all feldspars suffer from this malign effect, but to various degrees. Whether or not anomalous fading is considered significant as far as dating is concerned depends on the rate of fading, and the accuracy required in the calculated ages. However, for samples within the linear portion of their dose response, the fading may be corrected by using the model of Huntley and Lamothe (2001). Estimates of the degree of anomalous fading were made for samples LCSL1, LCSL2, GCSL1, and GCSL3 using the method outlined in Lian and Shane (2000); a further test comes from comparison of our optical ages with the radiocarbon chronology of the Bryansk palaeosol.

4.4. Results

Concentrations of U and Th found from DNC and NAA, respectively, were in all cases consistent with those found using TSAC (Tables 1 and 2). From this we deduce that radioactive disequilibrium in the U and Th decay chains was insignificant at the time of sample collection, and

consideration of the depositional environment suggests that it was probably so throughout the lifetime of the deposit. The dose rates due to a, b, and g radiation were therefore calculated using the more precise values found from DNC and NAA.

For most of the samples dose-axis intercepts (ADTT method) and dose-axis shifts (regeneration method) were found to be constant with excitation time (Fig. 7). The exception was for sample LC SL2 for which the dose-axis intercepts found using the ADTT method showed a slight decrease with time. The reason for this decrease is unknown, but is probably a result of increasing scatter in the dose-response data with excitation time, as such a decrease was not observed for the regeneration data. For all the samples no sensitivity change was detected in the regenerative data. For sample LC SL4, however, the additive-dose and regenerative dose responses did not appear to define the same curve at high doses (see Fig. 6). For that sample the dose intercepts were calculated with the high dose (>4 kGy) points omitted.

For the both the ADTT and regeneration methods, equivalent doses used for the age calculation were found using the luminescence integrated over the entire excitation time. The procedures used are shown, and described, in Figs. 5 and 6. For all of the samples the equivalent doses found using both methods are consistent at 2s, most agree within 1s (Table 3). For samples GCSL1 and LC SL2, equivalent doses found using the 140°C/7 day and 175°C/4 hour ~~one~~ heat protocols were consistent (Table 3), which indicates that the shorter, more convenient combination, can be used for future work on samples from this region.

The anomalous fading tests performed on samples LC SL1, 2, and GCSL1 yielded ratios consistent with unity (Table 3). However, sample GCSL3 from Gololobovo yielded a fading ratio of 0.976 ± 0.006 (errors quoted as 1s). This was also the sample for which the results were most precise. It might therefore be expected that all the samples exhibit a similar degree of anomalous fading, since they are expected to consist mainly of sediments derived from similar source materials. For that reason we use the fading rate derived from the fading ratio measured for sample GCSL3 to correct all the ages. The validity of this assumption is tested on the optical age of sample LC SL1 which directly overlies the well-dated Bryansk palaeosol at Likhvin

4.5. Optical ages

Optical ages were calculated by dividing the equivalent dose, as found using both the ADTT and regeneration method, by the total dose rate (Table 3).

For samples GCSL1, 2, and LCSL1, 2 the curvature in the dose response was low enough that the equivalent doses found using both methods could be confidently used to calculate optical ages, and we use the weighted mean ages in the discussion below. Samples GCSL3, 4 and LCSL3, 4, however, were too far into the non-linear part of their dose response (Fig. 6), thus only the optical ages found using the regeneration method were used.

Our uncorrected optical ages (Table 3) range from about 22 ka to 150 ka, and are thus all within, or near, the established age limit for the method.

5. Discussion

In the following discussion we compare our optical ages with independent age data and the presently-accepted stratigraphy. Age limits used for global oxygen isotope stages are those of Martinson et al. (1987).

Samples LCSL1, LCSL2 and GCSL1, GCSL2, which bracket the well dated Bryansk palaeosol at the Likhvin and Gololobovo composite sections, respectively, serve as tests of our dating method. The optical ages for samples overlying the Bryansk palaeosol, 24 ± 2 ka (LCSL1) and 23 ± 1 ka (GCSL1) are consistent with the radiocarbon chronology, as is the optical age for sample LCSL2 (55 ± 4 ka) collected 24 cm beneath the palaeosol at Likhvin. However, the optical age for sample GCSL2, 27 ± 1 ka, collected 20 cm below the palaeosol at Gololobovo is too young by at least 10%, and we suspect this underestimation is the result of anomalous fading.

If we correct the optical age of sample GCSL2 for anomalous fading using the model of Huntley and Lamothe (2001), and use the most precise measured fading ratio (that for sample GCSL3) to calculate the fading rate (Table 3), the optical age for sample GCSL2 becomes 34 ± 3 ka, which is consistent with the calibrated radiocarbon age (34 ± 1 ka). Our corrected age for sample GCSL2 is also consistent with Faustov et

al.'s TL age of 37 ± 4 ka (MGU-KTL 60). The corrected optical age for sample GCSL1 is 28 ± 2 ka, and is now in better agreement with the calibrated radiocarbon age (27 ± 1 ka). The corrected optical age for the sample LCSL1 (29 ± 3 ka), overlying the Bryansk palaeosol at Likhvin, is also closer to the associated radiocarbon age.

Sample LCSL2 yielded an optical age of 55 ± 4 ka, but is probably far enough into the non-linear part of its dose response that fading cannot be corrected for using the present model, in which it is assumed that the electron traps responsible for the fading have not undergone significant repetitive filling and emptying (Huntley and Lamothe, 2001). For example, Huntley and Lamothe (2001) showed that a potassium feldspar sand-sized sample (their sample GP3), that yielded an optical age of 35 ± 3 ka, and a measured fading rate of $6.5 \pm 0.3\%$ per decade, gave a corrected optical age of 59 ± 5 ka, which is about 15% younger than its U-Th age. For sample LSCL2, therefore, the corrected optical age (70 ± 7 ka) must be considered a lower limit. Deposition of the portion of unit L-2 below the Bryansk palaeosol must therefore have occurred during OIS 4 (73–59 ka), or perhaps during early OIS 5.

At Gololobovo, samples GCSL3 and GCSL4, both of which were collected from the same stratigraphic position (unit GC-4), but from different sections (Fig. 3), gave optical ages of 94 ± 9 ka and 90 ± 14 ka, respectively. Both samples occurred ~1 m below the unit that we interpreted to be the Mezin palaeosol complex. Correcting our most precise optical age for unit GC-4 (94 ± 9 ka) for anomalous fading gives 122 ± 15 ka, which must, for the reason mentioned above, be considered a lower age limit. Our corrected ages therefore are consistent with deposition of the overlying palaeosol during OIS 5 (130–74 ka), and this is also consistent with Faustov et al.'s TL age of 186 ± 21 ka (MGU-KTL 58) for sediments directly underlying the Mezin palaeosol complex at Likhvin, and the palynological data of Velichko et al. (1964b) which suggests that the palaeosol formed during OISS 5e (130–123 ka).

Samples collected from unit LC-8 and LC-9, 1 and 2 m below Dnieper till at Likhvin (Fig. 3), gave optical ages of 105 ± 10 ka (LCSL4) and 153 ± 12 ka (LCSL3), respectively, and thus the corrected ages, 136 ± 17 (LCSL4) and 201 ± 14 ka (LCSL3), are interpreted to be lower limits for

the age of unit LC-8 and LC-9 respectively. Based on stratigraphy, Velichko (1990) and Velichko et al. (1999) argued that Dnieper till was deposited during OIS 6 (188–129 ka), whereas an earlier study (reported in Krasnov and Shantser, 1982) suggests that it formed during OIS 8 (c. 297–251 ka). The only previous quantitative age-data are the TL ages reported by Faustov et al. (1974) that include an age of 280 ± 31 ka (MGU-KTL 41) for on Dnieper drift, and an age of 336 ± 41 ka (MGU-KTL 44) from the “Likhvin soil horizon” (probably correlative with the Inzhavino palaeosol within our unit LC-12, Fig. 3). Therefore, our corrected optical ages for samples LCSL4 and LCSL3 cannot be used to refute, or to support the TL ages, and cannot be used to resolve whether Dnieper till was deposited during OIS 6 or 8. Until a method of correcting optical ages of this magnitude for anomalous fading is developed, all that can be inferred from our data is that the upper part of unit LC-8 is older than 136 ± 17 ka, and LC-9 is older than 201 ± 14 ka.

6. Conclusions

Optical dating using infrared excitation of potassium feldspar grains in the fine silt fraction of loess, from sections at Likhvin and Golobovo on the east European Plain (Russia), has yielded satisfactory ages for the well-dated Bryansk palaeosol when corrected for anomalous fading, and this lends support to our dating method. Optical ages obtained from loess directly underlying an older palaeosol were too old to be corrected for anomalous fading, and thus must be considered as lower limits, but nevertheless support our lithostratigraphic and pedological interpretation of it as being the Mezin palaeosol complex, and deposition sometime during OIS 5, probably during OISS 5e. Optical ages for loess directly underlying Dnieper till at Likhvin were also too old to be corrected for anomalous fading, and therefore all that can be said at this point is that the loess is older than 153 ± 12 ka, which in turns suggests deposition of the unit LC-9, and perhaps also the till (LC-6), during OIS 6, but deposition during OIS 8 instead is also possible.

For samples beyond the limit of radiocarbon dating, our optical ages are broadly consistent with the earlier TL ages of Faustov et al. (1974) and Dobrodeyev and Il'ichev (1974), but a useful comparison of the older ages can only be made after a method of correcting optical ages of

this magnitude for anomalous fading has been developed. The problem of anomalous fading can be avoided by dating the sand-sized quartz fraction, but for the deposits studied here there is so little sand (<7%) that standard multiple-aliquot techniques would be impracticable. Moreover, the luminescence intensity of quartz generally saturates at a much lower radiation dose than do feldspars, so using quartz to date the older deposits may be problematic. Nevertheless, the testing of single-aliquot/grain dating techniques (e.g., Galbraith et al., 1999; Roberts et al., 1999) for quartz from this region would be useful.

Acknowledgments

We thank N. Wang (VUW) for assistance with sample preparation and measurements, and M. A. Short (SFU) for measuring the emission spectra. D.J. Huntley and S.A. Wolfe critically read earlier versions of the manuscript and contributed to its improvement. The authors are also grateful to J. Chlachula and M. Frechen for providing critical reviews the manuscript. This work was funded in part by a Natural Sciences and Engineering Research Council of Canada grant to N.W. Rutter. The Victoria University of Wellington Luminescence Dating Laboratory was supported in part by an internal VUW research grant and a Public Good Science Fund (NZ) grant (VIC808). This is Geological Survey of Canada Contribution 2001112.

References (Optical Dating Manuscript)

- Adamiec, G., Aitkin, M. J. (1998). Dose-rate conversion factors: update. *Ancient TL*, 16, 37–50.
- Agadjanyan, A. K. (1992). Tape razvitiya melkix mlekopitayushchix pleistotsina sentralnix raionov Russkoi ravnini (Stages of small mammal evolution in the central Russian Plain during the Pleistocene). In A. A. Velichko, S. M. Shik (Eds.) *Stratigrafiya i paleogeografiya chetvertichnovo perioda vostochnoi Evropi (Stratigraphy and Paleogeography of the Quaternary Period of Eastern Europe)*, (pp. 37-49). Russian Academy of Sciences, Institute of Geography, Moscow.
- Agadjanyan, A. K., Glushankova, N. E. (1987). Paleogeografiya Pleistotsena Oksko-Donskoy Ravnini (Pleistocene Paleogeography of the Oka-Don Plain). In M. S. U. Geography Faculty (Eds.), *Teoreticheskie i metodicheskie problemi paleogeografii (Theoretical and methodological problems in paleogeography)*, (pp. 145–169). Moscow University Publishing House, Moscow.
- Aitken, M. J. (1985). *Thermoluminescence Dating*. Academic Press, London.
- Aitken, M. J. (1998). *An Introduction to Optical Dating*. Oxford University Press, Oxford.
- Anderson, J. and Buckton, D. (1999). Physical Europe (map). *Heritage Atlas: Firefly World Atlas Millennium Edition*. Firefly Books Ltd., Willowdale Ontario, Canada.
- Arslanov, K. A., Berdovskaya, G. N., Zaytseva, G. Y., Lavrov, A. S., Nikiforova, L. D. (1977). Stratigraphy, geochronology, and paleogeography of the Middle Valday interval in the northeastern part of the Russian Plain. *Doklady Akademii Nauk SSSR Earth Science Section*, 233, 39–41 .
- Bard, E., Arnold, M., Hamelin B., Tisnerat-Laborde N., Cabioch G. (1998). Radiocarbon calibration by means of mass spectrometric ^{230}Th , ^{234}U and ^{14}C ages of corals: An updated database including samples from Barbados, Mururoa and Tahiti. *Radiocarbon*, 40, 1085–1092.
- Bassinot, F. C., Labeyrie, L.D., Vincent, E., Quidelleur, X., Shackleton, N. J., Lancelot, Y. (1994). The astronomical theory of climate and the age of the Brunhes-Matuyama magnetic reversal. *Earth and Planetary Science Letters*, 126, 91–108.

- Berger, G. W. (1995). Progress in luminescence dating methods for Quaternary sediments. In N. W. Rutter, N. R. Catto (Eds.), *Dating methods for Quaternary deposits* vol. 2, (pp. 81–104). Geological Association of Canada, GEOtext.
- Bolikhovskaya, N. S., Sudakova, N. G. (1996). The Chekalin (Likhvin) reference section in the Russian Plain and its significance for Pleistocene stratigraphy and correlation. *Stratigraphic and Geologic Correlation*, 4, 294–302.
- Cande, S. C., Kent, D. V. (1995). Revised calibration of the geomagnetic polarity timescale for the Late Cretaceous and Cenozoic. *Journal of Geophysical Research*, 100, 6093–6095.
- Chichagova O.A. (1985). Radiocarbon dating of the soil humus. *Nauka*, Moscow. 142 p. (In Russian).
- Dlussky, C.D., (2001). Crednyepleistotsyenovoye pochvoobrazovaniye tsentra Bostochno-Evropeskoi Ravnini (Middle Pleistocene soil formation from the central East-European Plain), Extended PhD Abstract, Institute of Geomorphology and Evolutionary Geography, Russian Academy of Sciences, Moscow.
- Dobrodeyev, O. P., Il'ichev, V. A. (1974). Age of loess and fossil soils of the Russian Plain and their correlation with glacial events of the Pleistocene. *Transactions (Doklady) of the Russian Academy of Science, Earth Science Section*, 214, 54–56.
- Dobrodeyev, O. P., Parunin, O.B. (1973). New data on the absolute age of Pleistocene fossil soils on the Russian Plain. *Transactions (Doklady) of the Russian Academy of Science, Earth Science Section*, 209, 426–427.
- Dreimanis, A., Hütt, G., Raukas, A., Whippey, P.W. (1978). Dating methods of Pleistocene deposits: I. Thermoluminescence dating. *Geoscience Canada*, 5, 55–60.
- Ehlers, J., Kozarski, S., Gibbard, P. (1995) Glacial deposits of North-East Europe: general overview, In Ehlers, J., Kozarski, S., Gibbard, P. (Eds.), *Glacial deposits of north-east Europe: general overview* (pp. 547–552). Balkema Press, Netherlands.

- Faustov, S. S., Il'ichev, V. A., Bol'shakov, V. A. (1974). Paleomagnetic and thermoluminescence analysis of the Likhvin Section. *Transactions (Doklady) of the Russian Academy of Science, Earth Science Section*, 214, 123–125.
- Galbraith, R. F., Roberts, R. G., Laslett, G. M., Yoshida, H., Olley, J. M. (1999). Optical dating of single and multiple grains of quartz from Jinmium rock shelter, northern Australia. Part I: experimental design and statistical models. *Archaeometry*, 41, 339 – 364.
- Gerasimov, I. P., Velichko, A. A., Markov, A. K., et al. (1980). Prirodna-klimaticheskiye etapi v lednikovoi periglatsialnoi i premoskoi oblasti v vostochno-evropeiskovo sektora (Natural climatic stages in the glacial, periglacial and coastal regions of the east-European sector). In B. Gerbova, G., Krasnov, I. I. (Eds), *Kratkii istoricheskii obzor izucheniya stratigrafi chetvertichnoi sistemi (Brief historical review of the study of the stratigraphy of the Quaternary system)*, (pp. 34–37). Vcecoyuzni nayuchno-issledivatyelski geologichski institut (All-union Scientific-Research Geologic Institute).
- Gerbova, B. G., Krasnov, I. I. (1982). Kratkii istoricheskii obzor izucheniya stratigrafi chetvertichnoi sistemi (Brief historical review of the study of the stratigraphy of the Quaternary System). In E. V. Shantser (Ed.), *Chetverichnaya sistema. Stratigrafiya (Quaternary system stratigraphy) SSSR*, (pp. 9–44). Vcecoyuzni nayuchno-issledivatyelski geologichski institut (All-union Scientific-Research Geologic Institute), Moscow.
- Grichuk, V. P. (1984). Late Pleistocene Vegetation History. In A. A. Velichko (Ed.) *Late Quaternary environments of the Soviet Union*, (pp. 155–178). University of Minnesota Press, Minneapolis.
- Harry, D. G., Gozdzik, J. S. (1988). Ice wedges: growth, thaw, transformation, and paleoenvironmental significance. *Journal of Quaternary Science* 3, 39-55.
- Huntley, D. J., Clague, J. J. (1996). Optical dating of tsunami-laid sands. *Quaternary Research*, 46, 127–140.
- Huntley, D.J., Lamothe, M. (2001). Ubiquity of anomalous fading in K-feldspars, and the measurement and correction for it in optical dating. *Canadian Journal of Earth Sciences*, 38, 1093–1106.

- Huntley, D. J., Lian, O. B. (1999). Determining when a sediment was last exposed to sunlight using optical dating. In D.S. Lemmen, R.E. Vance (Eds.), *Holocene climate and environmental changes in the Palliser Triangle, southern Canadian prairies*, (pp. 211–222). Geological Survey of Canada Bulletin 534.
- Huntley, D. J., Berger, G. W. Bowman, S. G. E. (1988). Thermoluminescence responses to alpha and beta irradiations, and age determination when the high dose response is nonlinear. *Radiation Effects*, 105, 279–284.
- Huntley, D. J., Hutton, J. T., Prescott, J. R. (1993a). The stranded beach-dune sequence of south-east South Australia: a test of thermoluminescence dating, 0 – 800 ka. *Quaternary Science Reviews*, 12, 1–20.
- Huntley, D. J., Hutton, J. T., Prescott, J. R. (1993b). Optical dating using inclusions within quartz grains. *Geology*, 21, 1087–1090.
- Huntley, D. J., Nissen, M. K., Thompson, J., Calvert, S. E. (1986). An improved alpha scintillation counting method for determination of Th, U, Ra-226, Th-230 excess, and Pa-231 excess in marine sediments. *Canadian Journal of Earth Sciences*, 23, 959–966.
- Imbrie, J., Hays, J. D., Martinson, D. G., McIntyre, A., Mix, A. C., Morley, J. J., Pisias, N. G., Prell, W. L., and Shackleton, N. J. (1984). The orbital theory of Pleistocene climate: Support from a revised chronology of the marine $d^{18}O$ record. In "Milankovitch and Climate, Understanding the Response to Astronomical Forcing." (A. Berger, J. Imbrie, J. Hays, G. Kukla, and B. Saltzman, Eds.), pp. 269-305. NATA ASI Series C: Mathematical and Physical Sciences. Reidel publishing Company, Boston and Lancaster.
- Kitagawa, H., van der Plicht, J. (1998). Atmospheric radiocarbon calibration to 45,000 yr B.P.; late glacial fluctuations and cosmogenic isotope production. *Science*, 279, 1187–1190.
- Krasnov, I. I., Shantser, E. V. (1982). Klassifikantsiya i terminologiya stratigraficheskikh podrazdeleni chetvertichnoi [antropogenovoi] systemi (Classification and Terminology for stratigraphic subdivisions of the Quaternary [Anthropogenic] System). In E. V. Shantser (Ed.), *Chetverichnaya sistema (Quaternary system)*, (pp. 110–119). Stratigraphiya SSSR. Vcecoyuzni nayuchno-issledivatyelski geologichski institut (All-union Scientific-Research Geologic Institute), Moscow.

- Lian, O. B., Huntley, D. J. (1999). Optical dating studies of post-glacial aeolian deposits from the south-central interior of British Columbia, Canada. *Quaternary Science Reviews*, 18, 1453–1466.
- Lian, O. B., Huntley, D. J. (2001). Luminescence dating. In W. M. Last, John P. Smol (Eds.), *Tracking Environmental Change Using Lake Sediments: Physical and Chemical Techniques*, Kluwer Academic Publishers, The Netherlands. In press.
- Lian, O. B., Shane, P. A. (2000). Optical dating of palaeosols bracketing the widespread Rotoehu tephra, North Island, New Zealand. *Quaternary Science Reviews*, 19, 1649–1662.
- Lian, O. B., Hu, J., Huntley, D. J., Hicock, S. R. (1995). Optical dating studies of Quaternary organic-rich sediments from southwestern British Columbia and northwestern Washington State. *Canadian Journal of Earth Sciences*, 32, 1194–1207.
- Lowe, J. J., Walker, M. J. C. (1997). *Reconstructing Quaternary Environments*. Addison Wesley Longman Press, Essex.
- Lysenko, M. P. (1971). *Loessial Rocks of the European USSR*. Leningrad (St. Petersburg) University Press, Leningrad (St. Petersburg).
- Markova, A. K. (1975). Fossil rodents from Pleistocene buried soils of the Russian Plain. *Transactions (Doklady) of the Russian Academy of Science, Earth Science Section*, 222, 913–916 .
- Martinson, D. G., Pisias, N. G., Hays, J. D., Imbrie, J., Moore, T. C. J., Shackleton, N. J. (1987). Age dating and the orbital theory of the ice ages; development of a high-resolution 0 to 300,000-year chronostratigraphy: *Quaternary Research*, 27, 1–29.
- Morozova, T.D. (1981). Evolution of soils in Europe during the Pleistocene. Nauka, Moscow 281 p.
- Morozova, T. D. (1995). Identification of palaeosol types and their applicability for paleoclimate reconstructions. *GeoJournal*, 36, 199–205.
- Nalivkin, D. V. (1960). *The Geology of the USSR: A Short Outline*. Pergamon Press, Oxford.
- Nalivkin, D. V. (1973). *Geology of the USSR*. Oliver and Boyd Press, Edinburgh.

- Nikitin, S.N. (1885). Limits of glaciation traces in Central Russia and the Urals. *Proceedings of the Geology Committee*, 4, 8. (in Russian).
- Okulitch, A. V. (1999). Geological time scale, 1999. Geological Survey of Canada, Ottawa.
- Poore, R. Z., Burckle, L., Droxler, A., and McNulty, W. E. (1998). Marine Isotope Stage 11 and associated Terrestrial Records: *Workshop Report*. USGS Open File 99-312, <http://chht-ntsrv.er.usgs.gov/warmclimates/products>, pp. 6.
- Pospelova, G. A., Semenov, V. V., Sharonova, Z. V., Mironov, T. V. (1997). An Early Pleistocene Excursion of the Geomagnetic Field in the Upper Don Subaerial Deposits. *Transactions (Doklady) of the Russian Academy of Science, Earth Science Section*, 355, 778–782.
- Pravoslavlev, P.A., (1907). Korrelyatsii morskekh Kaspiskikh otlozheni i lednikovikh obrazovani severa evropeiskoi chasti SSSR (Correlation of Caspian Sea Sediments and Glaciogenic Deposits of the North European region of the USSR). As presented in Gerbova, B. G., Krasnov, I. I. (1982). *Kratkii istoricheskii obzor izucheniya stratigrafi chetvertichnoi sistemi (Brief historical review of the study of the stratigraphy of the Quaternary System)*. In E. V. Shantser (Ed.), *chetverichnaya sistema (Quaternary System). stratigrafiya SSSR* (p. 21), Vcecoyuzni nayuchno-issledivatyelski geologichski institut (All-union Scientific-Research Geologic Institute, Moscow.
- Prescott, J. R., Hutton, J. T. (1994). Cosmic ray contributions to dose rates for luminescence and ESR dating: large depths and long-term time variations. *Radiation Measurements*, 23, 497–500.
- Prescott, J. R., Robertson, G. B. (1997). Sediment Dating by Luminescence. *Radiation Measurements*, 27, 893–922.
- Roberts, R. G., Galbraith, R. F., Olley, J. M., Yoshida, H., Laslett, G. M. (1999). Optical dating of single and multiple grains of quartz from Jinmium rock shelter, northern Australia. Part II: Results and implications. *Archaeometry*, 41, 365 – 395.
- Soil Classification Working Group (1998). *The Canadian System of Soil Classification, Third Edition* (p. 187). Agriculture and Agricultural Foods Canada, Ottawa.

- Sudakova, N. G., Faustova, M. A. (1995). Glacial History of the Russian Plain. In J. Ehlers, S. Kozarski, and P. Gibbard (Eds.) *Glacial Deposits in North-East Europe*. A.A. Balkema, Rotterdam. pp. 151-156.
- Tsatskin, A. (1997). A History of Soviet Paleopedological Studies and Their Relation to Soil Science and Quaternary Geology. In D. H. Yaalon, S. Berkowicz (Eds.), *History of Soil Science*, (pp. 277–291). Advances in GeoEcology. Catena Verlag, Reiskirchen, Germany.
- Turner, C. (1996). A brief survey of the early Middle Pleistocene in Europe. In Turner, C. (Ed.) *The Early and Middle Pleistocene in Europe* (pp. 295-318). A.A. Balkema, Rotterdam.
- Van Kolfschoten, T., Roebroeks, W., and Vandenberghe, J. (1993). The Middle and Late Pleistocene sedimentary and climatic sequence at the Maastricht-Belvédère Interglacial. In Vandenberghe, J. Roebroeks, C., and Van Kolfschoten, T. (Eds.) *Maastricht-Belvédère: stratigraphy, palaeoenvironment and archaeology of the Middle and Late Pleistocene deposits; Part II* (pp. 81-91). Mededelingen Rijks Geologische Dienst.
- Velichko, A. A. (1990). Loess-Palaeosol Formation on the Russian Plain. *Quaternary International*, 7/8, 103–114.
- Velichko, A. A. (1995). Climatic rhythms in Europe during two last glacial-interglacial cycles and the Holocene. In Velichko, A.A. (Ed.), *Climate and environmental changes of east Europe during the Holocene and Late-Middle Pleistocene*, (pp. 4–13). Russian Academy of Science, Institute of Geography, Moscow.
- Velichko A.A., Nechayev, V. P. (1984). Late Pleistocene permafrost in European USSR. In A.A. Velichko, H.E. Wright, Jr., C.W. Barnosky (eds.), *Late Quaternary Environments of the Soviet Union*, (pp. 79-86). University of Minnesota Press, Minneapolis.
- Velichko A.A., Morozova T.D. (1972). Bryansk fossil soil, its stratigraphic significance and environments. In: Loess, fossil soils and cryogenic phenomena on the Russian Plain. *Nauka*, Moscow. Pp. 5-25. (In Russian).
- Velichko, A. A., Morozova, T. D. (1987). The role of loess-palaeosol formation in the study of the regularities of pedogenesis. *Catena*, 9, 55–66.

- Velichko, A. A., Shik, S. M. (1992). Stratigrafiya i paleogeografiya chetvertichnovo perioda vostochnoi evropi (Stratigraphy and Paleogeography of the Quaternary Period of Eastern Europe). In *Evolyutsiya pripodnoi sreda (Earth environmental evolution)*, (p. 245). Russian Academy of Sciences, Institute of Geography, Moscow.
- Velichko, A. A., Svetlitskaya. (1987). Paleomagnetic reference intervals of the Late Pleistocene in the central area of the Russian Plain. *Transactions (Doklady) of the Russian Academy of Science, Earth Science Section*, 300, 444–448.
- Velichko, A. A., Goortovaya, E. E., Drenova, A. H. (1994). Korotkoperiodniye i rezkiye landshaftno - klimaticheskiye izmeneniya za posledniye 15 000 let (Short periods and abrupt landscape - climate change during the last 15 000 years). Russian Academy of Sciences, Moscow. p. 219.
- Velichko A.A., Devirts A.A., Dobkina E.I., Markova A.K., Morozova T.D. (1964a). First absolute ages of fossil soils in the loess sequences of the Russian Plain. *Transactions (Doklady) of the Russian Academy of Science, Earth Science Section*, 155, 555-558 (In Russian).
- Velichko A.A., Gubonina Z.P., Morozova T.D. (1964b). On the age of periglacial loesses and fossil soils inferred from studies of lacustrine and bog deposits at the Mezin village. *Transactions (Doklady) of the Russian Academy of Science, Earth Science Section*, 150, 3. (In Russian).
- Velichko, A. A., Morozova, T. D., Nechayev, V. P. (1992). Soil formation and cryogenesis on the Russian Plain during the last 125 000 years. In *Joint Russian-American seminar on cryopedology and global change*, (pp. 122–131). Russian Academy of Sciences, Pushchino, Russia.
- Velichko, A. A., Morozova, T. D., Udartsev, V. P. (1986). Stratigraphy of loesses and of fossil soils within the Russian Plain and their correlation with the rhythms of oceanic bottom deposits. *Annales Universitatis Mariae Curie-Sklodowska Lublin-Polona*, 41, 87–109.

- Velichko, A. A., Akhlestina, E. F., Borisova, O. K., Gribchenko, Y. N., Zhidovinov, N. Y., Zelikson, et al. (1999). Glava 3: Bostochno-Evropeiskaya Ravnina (Chapter 3: East European Plain). In A. A. Velichko, V. P. Nechayev (Eds.), *Izmeneniye klimata i landshaftov za posledniye 65 millionov let [Kainozoi: ot paleotsena do golotsena] (Climate and environmental changes during the last 65 million years [Cenozoic: from Paleocene to Holocene])*, (pp. 43–83). GEOS, Moscow.
- Velichko, A. A., Bogucki, A. B., Morozova, T. D., Udartsev, V. P., Khalcheva, T. A., Tsatskin, A. I. (1984). Periglacial landscape of the East European Plain. In A. A. Velichko (Ed.) *Late Quaternary environments of the Soviet Union*, (pp. 95–118). University of Minneapolis Press, Minneapolis.
- Velichko, A. A., Gribchenko, Y. N., Gubonina, Z. P., Morozova, T. D., Nechayev, B. P., Cicheva, C. A., Timireva, C. N., Udartsev, B. P., Khalcheva, T. A., Tsatskin, A. I., Chikolini, N. I. (1997). Osnovnie cherti stroeneiya Lessovo-Pochvennoi Formatsii (Basic structural characteristics of loess-palaeosol formations). In A. A. Velichko (Ed.), *Lessovo-Pochvennaya Formatsiya Vostochno-Yevropaiskoi Ravnini (Loess-Palaeosol formation on the East-European Plain)*, (pp. 5–24). Russian Academy of Science, Institute of Geography, Moscow.
- Velichko, A.A., Dlussky, C.G., Morozova, T.D., Nechaev, V.P., Semenov, V.V., Rutter, N., and Little, E., (2000). The Gololobovo section: Loess-soil-cryogenic formation of the Moskva-Oka plain. In A.O. Makeev, and A.A. Velichko, (Eds.), *Paleosols and Modern Soils as Stages of Continuous Soil Formation: Abstracts and Field Excursion Guidebook of V International Symposium on Paleopedology: July 10-16, 2000, Suzdal*, Soil Science Society of the Russian Academy of Sciences, p. 67-87.
- Wagner, G.A., (1998). *Age Determination of Young Rocks and Artifacts*. Springer-Verlag, New York.
- Wintle, A. G. (1997). Luminescence dating: laboratory procedures and protocols. *Radiation Measurements*, 27, 769–817.
- Wintle, A. G., Huntley, D.J. (1982). Thermoluminescence dating of sediments. *Quaternary Science Reviews*, 1, 31–53.
- Yakimenko, E. Y. (1995). Pleistocene palaeosols in the loess and loess-like sediments of the central part of the Russian Plain. *Quaternary Science Reviews*, 14, 747–753.

- Zagwijn, W. H. (1992). The beginning of the ice age in Europe and its major subdivisions. *Quaternary Science Reviews*, 11, 583–591.
- Zagwijn, W. H. (1996). The Cromerian Complex Stage of the Netherlands and correlation with other areas of Europe. In Turner, C. (Ed.) *The Early and Middle Pleistocene in Europe* (pp. 145-172). A.A. Balkema, Rotterdam.
- Zhou, L. P., Dodonov, A .E., Shackleton, N. J. (1995). Thermoluminescence dating of the Orkutsay loess section in Tashkent region, Uzbekistan, Central Asia. *Quaternary Science reviews*, 14, 721–730.
- Zubakov, V. A. (1974). Predvaritelnaya klimatokhronologicheskaya shkala pleistotsena [vosrast po TL v tis. lyet] (Preliminary Climato-chronological scale of the Pleistocene [Age from TL in thousands of years]). In B. G. Gerbova, and I. I. Krasnov (Eds.), *Kratkii istoricheskii obzor izucheniya stratigrafi chetvertichnoi sistemi (Brief historical review of the study of the stratigraphy of the Quaternary system)*, (pp. 44). Vcecoyuzni nayuchno-issledivatyelski geologichski institut (All-union Scientific-Research Geologic Institute, Vcecoyuzni nayuchno-issledivatyelski geologichski institut).

Figure Captions

Fig. 1. Location maps showing (A) the extent of the east European Plain (modified after Velichko, 1990), (B) location of the study area and vicinity, and (C) location of the study sites in relation to prominent geomorphic features (modified after Anderson and Buckton, 1999).

Fig. 2. Comparison of contemporary Russian Plain stratigraphic schemes. Each scheme shown here is a summary of the original with the original absolute time associations for Russian divisions, zones, and litho- and pedo-complexes. In each of these schemes, the Brunhes/Matuyama boundary is presented (incorrectly) at 730 ka (black bar), as it does in each of the original schemes; for reference, we show the accepted age of the boundary (dark grey bar) at 780 ka (e.g., Cande and Kent, 1995). The SPECMAP curve has been corrected as per Bassinot et al. (1994) to account for the Brunhes/Matuyama boundary within OIS 19. Medium-grey zones within the sub-zone category of the 1982 scheme are un-named time intervals. * = North American Usage (Okulitch, 1999); H = Holocene. Unlike the 1982 and 1997 schemes, the originally published 1990 scheme did not include an absolute time scale. However, it is clear that the same absolute time scale was used in the 1990 scheme when comparisons are made between the 1987 and 1990 $^{16}\text{O}/^{18}\text{O}$ curves.

Fig. 3. Composite lithostratigraphic section logs illustrating sediment-palaeosol sequences, sample locations, and optical ages at the Likhvin and Gololobovo sites. The vertical extent of the individual sections that make up each composite are shown by black bars labelled LS1, LS2 for the Likhvin section, and GS1, GS2, GS3, and GS4 for the Gololobovo section. Units A to F are (palaeo)soils, whereas units LC-1 to LC-12, and GC-1 to GC-10, are intervening sediments. The optical ages shown have been corrected for anomalous fading; see text for discussion.

Fig. 4. A. The Mezin palaeosol complex at Likhvin which consists of the Krutitsy pedogenic phase (superscripted “kru”), the Salyn pedogenic phase (superscripted “sal”) and the lower portion of the Bryansk palaeosol (superscripted “bsk”). The Krutitsy phase is represented by Ah- and B-horizons most likely associated with a cool steppe environ-

ment; the Salyn phase is represented by Ah-, Ae- and Bt-horizons that suggest a warmer forest to forest-steppe environment (close to modern-day conditions). These inferred bio-climatic conditions suggest a scenario that encompasses a climatic optimum, the Salyn phase – OISS 5e, with subsequent climatic deterioration to the Krutitsy phase (OISS 5a, or perhaps 5c) where climate briefly stabilizes. This is then followed by a re-initiation of climatic deterioration into the early last glacial (OIS 4) which manifests itself through pervasive cryoturbation and permafrost features that overprint both soils. **B.** Texture triangle illustrating the grain size of the sediments in which the Mezin Pelaeosol complex had developed. Definitions of boundaries and grain sizes are based on Canadian Soil Science Classification system (Soil Classification Working Group, 1998).

Fig. 5. Luminescence decay as a result of infrared excitation as a function of time for samples GCSL1 and 2, LCSL1 and 2. The insets show the procedure used to find the equivalent dose using the ADTT method: the dose intercept is taken as the dose where the curve fitted to the additive-dose data (solid circle points) intersects the curve fitted to the thermal-transfer correction data (open circle points). The curves shown were constructed using the luminescence integrated over the first 10 s of excitation time; the equivalent dose was taken as the dose-intercept calculated using the luminescence integrated over the entire excitation time (100 s), after a correction for the luminescence decay that resulted from normalisation. N_{np} and B_{np} indicate the luminescence intensity from a “natural” and “bleached” aliquot that have not been preheated.

Fig. 6. Luminescence decay as a result of infrared excitation as a function of time for samples GCSL3 and 4, LCSL3 and 4. The inset for sample GCSL3 illustrates the procedure used to find the equivalent dose using the regeneration method: the additive-dose data (solid circle points) are shifted along the dose axis until they coincide with the regeneration data (open square points), a curve is fitted to both sets of data, the dose-axis shift being a parameter in the fit. The curves shown were constructed using the luminescence integrated over the first 10 s of excitation time; the equivalent dose was taken as the dose-axis shift

calculated using the luminescence integrated over the entire excitation time (100 s), after a correction for incomplete laboratory bleaching and the luminescence decay that resulted from normalisation. Nnp and Bnp are as in Fig. 5. Nnp points that are off the scale are not shown.

Fig. 7. Dose-intercept versus excitation time for all the samples as found using the ADTT method. Some of the points have been shifted slightly for clarity.

Table 1. K, U, and Th concentrations determined from laboratory analyses

Sample	K ^a (%)	Th ^b ($\mu\text{g g}^{-1}$)	U ^c ($\mu\text{g g}^{-1}$)
LCSL1	1.75 \pm 0.09	10.1 \pm 0.3	2.54 \pm 0.08
LCSL2	1.80 \pm 0.09	10.4 \pm 0.3	2.46 \pm 0.08
LCSL3	1.36 \pm 0.07	8.7 \pm 0.2	2.46 \pm 0.08
LCSL4	1.76 \pm 0.09	9.5 \pm 0.2	2.32 \pm 0.08
GCSL1	1.78 \pm 0.09	9.0 \pm 0.3	2.53 \pm 0.08
GCSL2	1.83 \pm 0.09	11.1 \pm 0.2	2.42 \pm 0.08
GCSL3	1.78 \pm 0.09	11.4 \pm 0.3	2.94 \pm 0.08
GCSL4	1.80 \pm 0.09	10.8 \pm 0.3	2.66 \pm 0.08

^a From inductively coupled plasma atomic emission spectrometry (ICP-AES).

^b From neutron activation analysis (NAA).

^c From delayed neutron counting (DNC).

Note: all analyses were done on dried and milled subsamples of the untreated sediment used for dating

Table 2. Thick-source α count (TSAC) rates^a, equivalent U and Th concentrations (U_e and Th_e), and water contents.

Sample	TSAC				organics and water ^b			
	Total count rate ($\text{cm}^{-2} \text{ks}^{-1}$)	Th count rate ($\text{cm}^{-2} \text{ks}^{-1}$)	Th_e ($\mu\text{g g}^{-1}$)	U_e ($\mu\text{g g}^{-1}$)	Δ^w	Δ_{ac}^w	Δ_{sat}^w	Δ^w
LCSL1	0.636 \pm 0.008	0.326 \pm 0.031	8.75 \pm 0.83	2.43 \pm 0.25	0.034	0.080	0.504	0.292 \pm 0.106
LCSL2	0.657 \pm 0.008	0.344 \pm 0.029	9.24 \pm 0.79	2.45 \pm 0.24	0.045	0.116	0.372	0.244 \pm 0.064
LCSL3	0.641 \pm 0.008	0.340 \pm 0.029	9.14 \pm 0.79	2.35 \pm 0.24	0.025	0.140	0.312	0.226 \pm 0.043
LCSL4	0.652 \pm 0.008	0.309 \pm 0.028	8.31 \pm 0.76	2.68 \pm 0.23	0.025	0.171	0.331	0.251 \pm 0.040
GCSL1	0.643 \pm 0.008	0.357 \pm 0.032	9.60 \pm 0.86	2.23 \pm 0.26	0.029	0.212	0.266	0.239 \pm 0.014
GCSL2	0.687 \pm 0.008	0.346 \pm 0.030	9.31 \pm 0.80	2.66 \pm 0.24	0.043	0.326	0.368	0.347 \pm 0.011
GCSL3	0.737 \pm 0.008	0.379 \pm 0.031	10.18 \pm 0.84	2.80 \pm 0.25	0.019	0.146	0.317	0.231 \pm 0.043
GCSL4	0.696 \pm 0.006	0.412 \pm 0.025	11.07 \pm 0.67	2.22 \pm 0.20	0.032	0.180	0.299	0.240 \pm 0.030

^a See Huntley et al. (1986).

^b Δ_{ac}^w and Δ_{sat}^w are the *as collected* and *saturated* water contents, respectively; Δ^w is the water content used for the

dose rate calculation. For each sample Δ^p is negligible, and was therefore not allowed for in the dose rate

calculation. Water and organic contents are defined as: Δ^w = mass of water / dry mass of minerals; Δ^o = mass of organics / dry mass of minerals.

Table 3. Equivalent doses (D_{eq}), b values, dose rates, and calculated optical ages.

Sample ^a	D_{eq} (Gy)		b value (Gy μm^2) ^b	\dot{D}_c ^c (Gy ka ⁻¹)	\dot{D}_T ^d (Gy ka ⁻¹)	Optical age (ka)		
	ADTT	Regeneration				ADTT	Regeneration ^e	Corrected ^f
LCSL1	71 \pm 6	85 \pm 3	1.02 \pm 0.04	0.09	3.15 \pm 0.29	22 \pm 3	27 \pm 3 (24 \pm 2)	29 \pm 3
LCSL1a	68 \pm 2	65 \pm 1	1.02 \pm 0.04	0.09	-	22 \pm 2	21 \pm 2 (21 \pm 1)	26 \pm 2
LCSL2	214 \pm 20	162 \pm 6	0.80 \pm 0.04	0.08	3.11 \pm 0.19	69 \pm 8	52 \pm 4 (55 \pm 4)	>70 \pm 7
LCSL3	444 \pm 34	423 \pm 25	-	0.02	2.77 \pm 0.14	-	153 \pm 12	>204 \pm 14
LCSL4	379 \pm 41	319 \pm 26	-	0.01	3.05 \pm 0.14	-	105 \pm 10	>136 \pm 17
GCSL1	76 \pm 2	73 \pm 2	0.89 \pm 0.04	0.16	3.20 \pm 0.09	24 \pm 1	23 \pm 1 (23 \pm 1)	28 \pm 2
GCSL1a	75 \pm 2	72 \pm 2	0.89 \pm 0.04	0.16	-	23 \pm 1	22 \pm 1 (23 \pm 1)	28 \pm 2
GCSL2	89 \pm 3	83 \pm 2	1.02 \pm 0.04	0.11	3.14 \pm 0.07	28 \pm 1	26 \pm 1 (27 \pm 1)	34 \pm 3
GCSL3	317 \pm 34	338 \pm 27	0.91 \pm 0.09	0.08	3.61 \pm 0.18	-	94 \pm 9	>122 \pm 15
GCSL4	430 \pm 90	306 \pm 45	-	0.08	3.41 \pm 0.14	-	90 \pm 14	>117 \pm 21

^a Aliquots used to construct the dose response of samples LCSL1a and GCSL1a were a subset of those used for samples LCSL1 and GCSL1, respectively. Samples LCSL1a and GCSL1a were preheated at 175 °C for 4 hours, whereas samples LCSL1–4 and GCSL1–4 were preheated at 140 °C for 7 days.

^b b value as defined by Huntley et al. (1988). Estimates of 1.0 \pm 0.1 Gy μm^2 were used for samples LCSL3, 4, GCSL4.

^c \dot{D}_c : dose rate due to cosmic rays, estimated from the formula of Prescott and Hutton (1994); see the text for a discussion.

^d \dot{D}_T : total dose rate (that due to cosmic rays plus that due to γ , β , and α radiation).

^e Ages in parenthesis are the weighted means of the ages calculated using the additive-dose with thermal transfer correction (ADTT) method and the regeneration method.

^f Ages were corrected for anomalous fading using the most precise fading ratio (that measured for sample GCSL3; see note below) and the model of Huntley and Lamotte (2001). The calculated fading rate, based on a starting time of 2 days after irradiation, is 4.1 \pm 1.1 % per decade, a decade being a factor of ten in time. Where appropriate, corrected ages were calculated using the weighted mean ages calculated from equivalent doses found using regeneration and ADTT. Lower age limits are given for samples for which the dose-response is significantly non-linear.

Note: fading ratios for samples LCSL1, LCSL2, GCSL1, and GCSL3 are 0.953 \pm 0.022, 1.009 \pm 0.014, 0.998 \pm 0.016, 0.976 \pm 0.006 respectively. Fading ratios were calculated from two luminescence measurements as follows: twenty-four hours after irradiation the samples were preheated at 140 °C for 7 days; the first measurement was made 24 hours after the preheat, and the second measurement was made 30 days later. See Iain and Shane (2000) for a more detailed explanation of the method used.

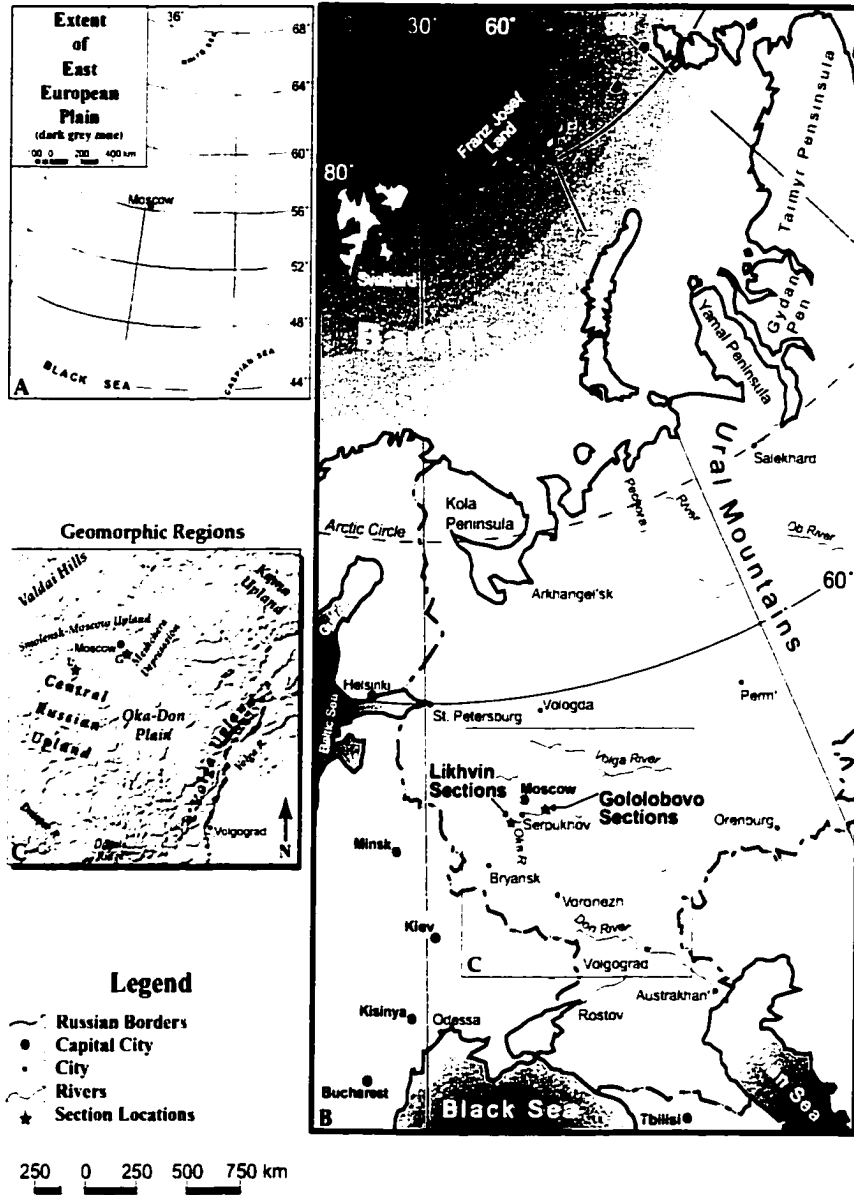


Fig. 1. (Little et al.)

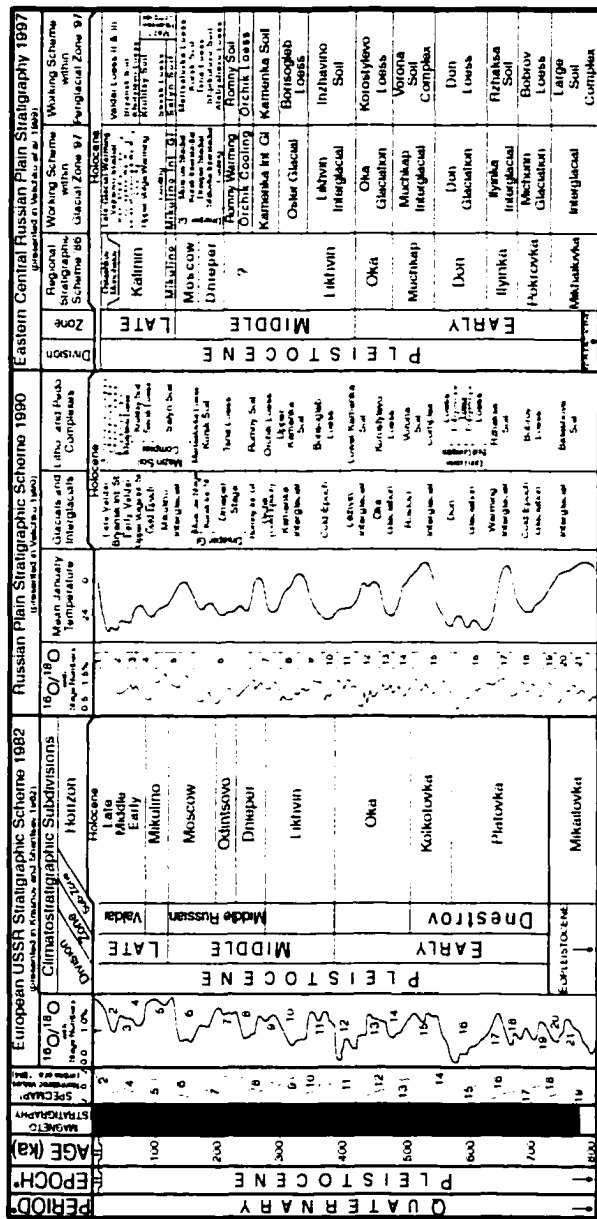


Fig. 2. (Little et al.)

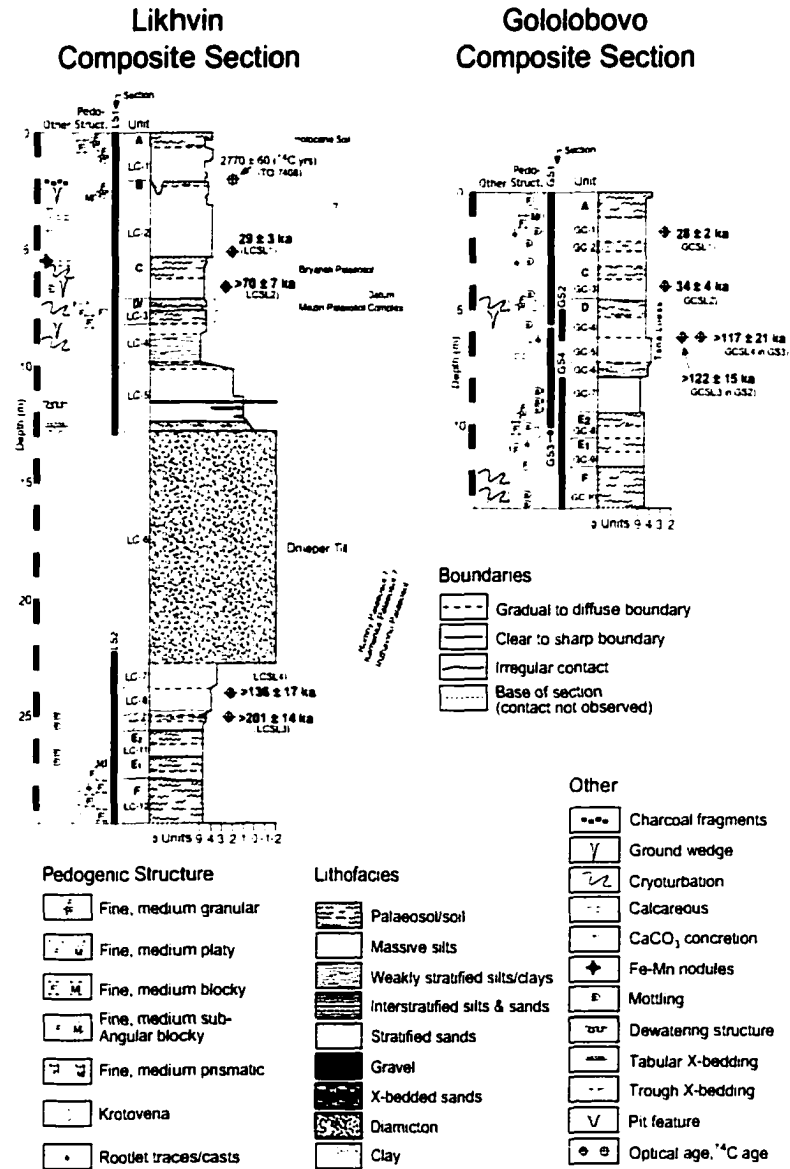


Fig. 3. (Little et al.)

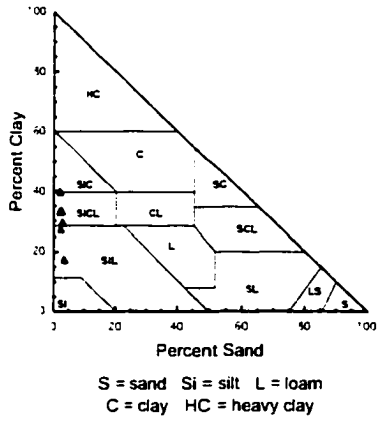
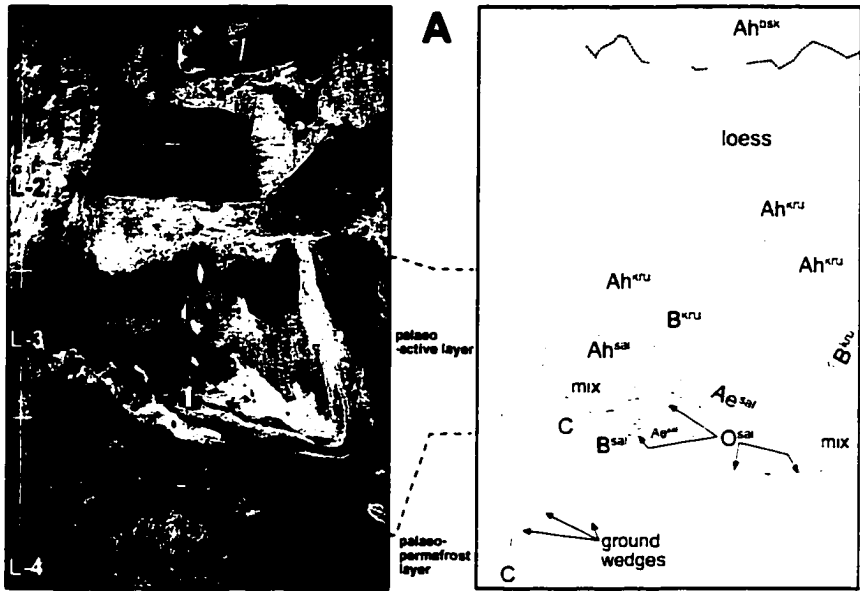


Fig. 4A,B. (Little et al.)

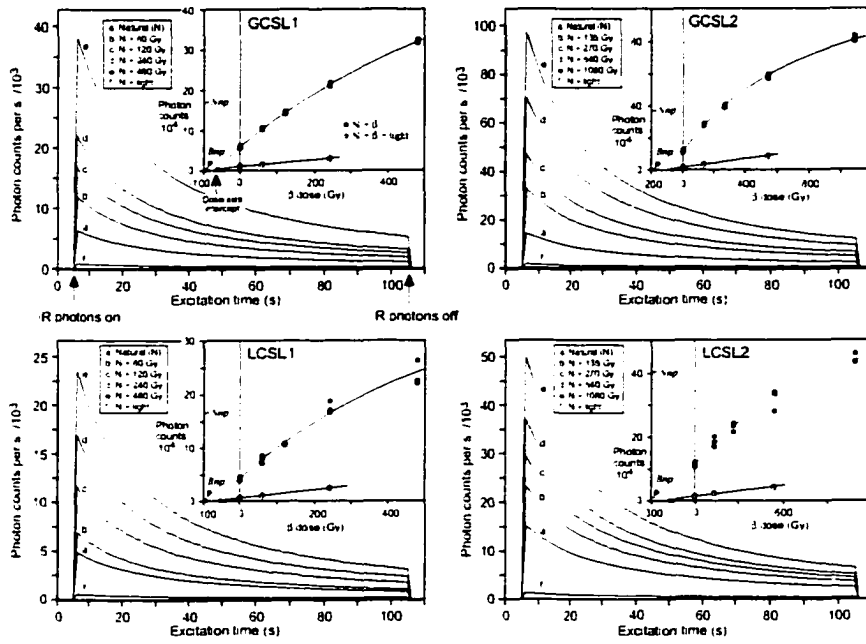


Fig. 5. (Little et al.)

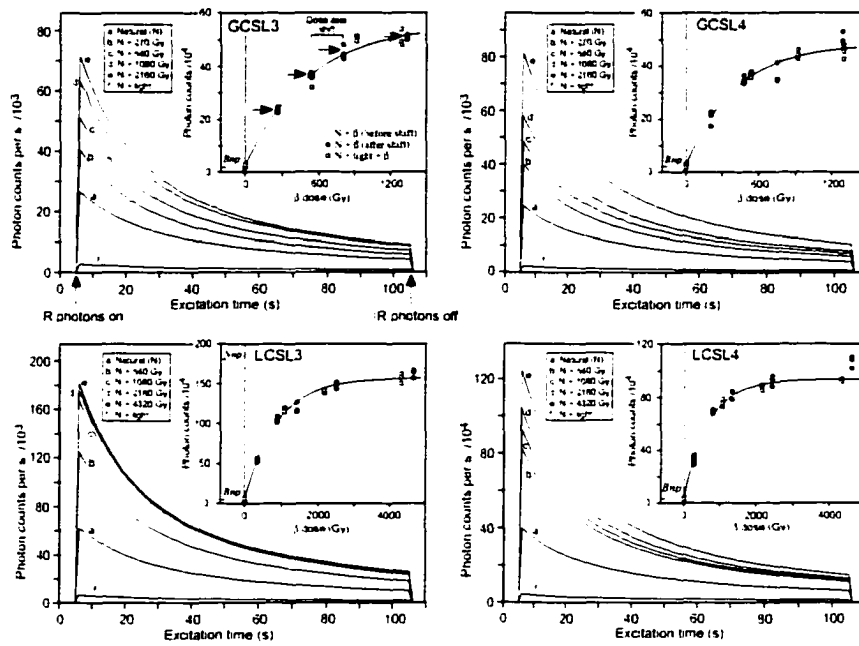


Fig. 6. (Little et al.)

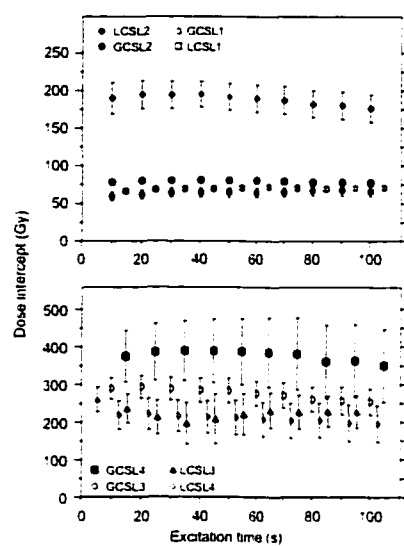


Fig. 7. (Little et al.)

Korostylievo and Mikhailovka Optical Dating Table

These data can be found in digital format on the accompanying CD-ROM, in the "Optical Dating data folder".

APPENDIX C - STRATIGRAPHIC METHODS

Introduction

Stratigraphy and sedimentology are two of the most fundamental geologic fields of study, and thus form the basis for all geologic observations and interpretations that deal with clastic sediments. The intent of Chapter 3 - Stratigraphy was to present field and laboratory data in an organized, logical manner based on sound stratigraphic and sedimentological principles. The final goal was to establish a *ca.* 700 km long, correlated, north-south transect that is tied to a temporally constrained stratigraphic framework.

Due to the large distances between study sites (Table 1.1), and the various sedimentary units observed -- lithostratigraphy alone can not be relied upon to correlate between the 4 key localities. Therefore pedostratigraphy and allostratigraphy (North American Commission on Stratigraphic Nomenclature 1983) were introduced to help interpret and properly correlate packages of lithological units over extended distances (*e.g.*, >180 km). However, the development of such a stratigraphic framework could only be achieved through a multi-criteria approach that involved several developmental phases: 1) presentation of field descriptions and lithostratigraphic units; 2) presentation of field pedologic descriptions for paleosol units at each section, the identification of marker paleosols horizons, and the recognition of major (traceable) bounding discontinuities; 3) local (intra-site) section correlations and the construction of composite sections for each site; 4) interpretations of the depositional environment for lithostratigraphic and pedostratigraphic units, and lithofacies (where applicable) within each composite section; and, 5) compilation of data from phases 1 through 4 in order to define discrete lithologic-pedologic packages, and develop an allostratigraphic framework. Only when phase 5 was completed, were these discrete lithologic-pedologic packages (*i.e.*, allostratigraphic units) correlated over the entire *ca.* 700 km long north-south transect.

This appendix briefly reviews the three different types of stratigraphies that are used to develop the stratigraphic framework along the *ca.* 700 km north-south transect.

Types of Stratigraphy - a review

Three types of stratigraphy were used to develop a final stratigraphic framework permitting correlation between sections that are separated by more than 180 km. These include lithostratigraphy, pedostratigraphy and allostratigraphy. Because the defining characteristics of both lithostratigraphic and pedostratigraphic units change along the length of the north-south transect they are not suitable for inter-site correlations. These types of stratigraphies, however, can be used in conjunction with optical ages, paleomagnetic chron identification and correlation to the marine isotope stages (SPECMAP; Imbrie *et al.* 1984) to develop an allostratigraphic framework. Below are brief discussions of each of the stratigraphies used in Chapter 3 - Stratigraphy.

Lithostratigraphy

Lithostratigraphy is the classification of rocks or unconsolidated sedimentary units based on lithic characteristics and stratigraphic position. A lithostratigraphic unit usually conforms to the Law of Superposition and is tabular in form. The basic unit is recognized and defined by observable rock/sediment characteristics. Suitable lithic characteristics for such units include: chemical and mineralogical composition, texture, and such supplemental features as colour, primary sedimentary structures, fossils (as rock-forming constituents), organic content and any other physical properties (North American Commission on Stratigraphic Nomenclature 1983). These characteristics should be used in conjunction, as alone they do not sufficiently describe the lithic character of a given unit. Boundaries may be made at distinct contacts, or can be drawn arbitrarily within a gradational zone that occurs between units that exhibit a lithological change (Figure C.1) (North American Commission on Stratigraphic Nomenclature 1983). Lithostratigraphic units are independent from inferred time-spans as they frequently transgress time horizons; inferred time-spans are not used to differentiate or delimit lithostratigraphic units (North American Commission on Stratigraphic Nomenclature 1983).

Pedostratigraphy

Pedostratigraphy is the classification of distinct (pedostratigraphic) units of rock or unconsolidated sediments that exhibit one or more

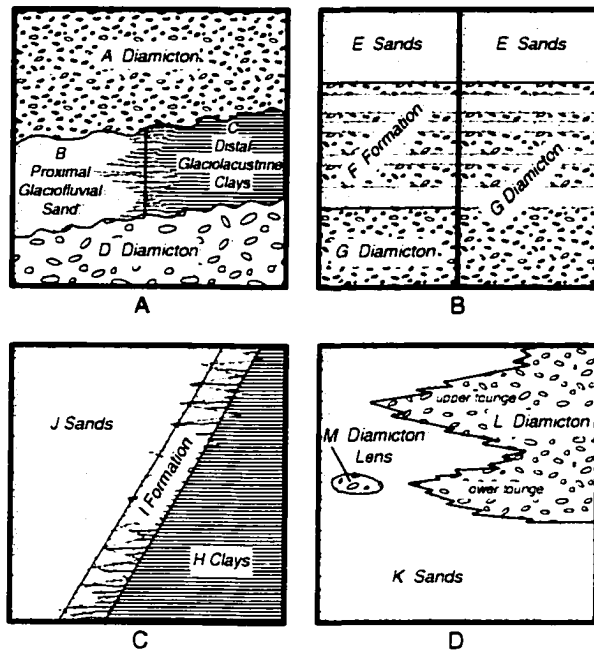


Figure C.1. Diagrammatic examples of lithostratigraphic boundaries and classification. A) Boundaries along sharp lithologic contacts and within a lateral gradation (silts). B) Two different lithostratification classifications on an identical vertical gradational or interbedded sequence. C) One possible lithostratigraphic interpretation for a laterally interfingering sequence. D) One possible lithostratigraphic classification for parts of an interfingering sequence. Figure modified after North American Commission on Stratigraphic Nomenclature (1983).

pedogenic horizons. Collectively, these horizons are referred to as a 'geosol'; geosols are developed within one or more lithostratigraphic (*vide ante*) and/or allostratigraphic (*vide post*) units, and are overlain by one or more lithostratigraphic and/or allostratigraphic units. They are distinguished on the recognition of products or characteristics produced through pedogenic processes subsequent to the formation of the parent unit. Pedostratigraphic units may be characterized by diagnostic features such as: colour, soil structure, organic-matter accumulation, texture, clay coatings, stains, or concretions. These characteristics may be identified in the field, and refined or initially described in the laboratory through techniques such as: micromorphology, particle size analysis, and/or clay mineralogy and magnetic susceptibility (North American Commission on Stratigraphic Nomenclature 1983). Boundaries of pedostratigraphic units are based on the uppermost and lowermost pedologic horizon identified within the buried soil profile. The stratigraphic position is based on the unit's relation to overlying and underlying stratigraphic units (North American Commission on Stratigraphic Nomenclature 1983). Concepts of time are not used in defining the boundaries of pedostratigraphic units, however, evidence of age may be important in distinguishing or identifying pedostratigraphic units (North American Commission on Stratigraphic Nomenclature 1983).

Pedostratigraphy, as strictly defined in the North American Stratigraphic Code is, however, restricted in its applicability, and therefore requires some modification. Morrison (1998) outlined some reasonable revisions that factored in circumstances that the original pedostratigraphic definition failed to address. In his discussion, he noted that there was no way to address pedocomplexes (two or more paleosols separated by a thin horizon of non-soil sediment) that merge into a "composite/amalgamated paleosol" (Morrison 1998, p. 31). Where a composite paleosol/geosol laterally grades into a pedocomplex, then the term 'geosol' should be used for the amalgamated paleosol, while the term 'pedomember' be used for the individual paleosols of the pedocomplex. It is also interesting to note that the 1983 Code states that "the physical and chemical properties of a pedostratigraphic unit commonly vary vertically and laterally" and therefore the Code inherently recognizes paleosol catenas. Morrison (1998) recommends the use of the term "pedofacies" of a geosol with a type location; all type location geosols should be defined along with their pedofacies variants.

The above recommendations by Morrison (1998) are extremely important to consider in this dissertation as some pedocomplexes observed along the north-south transect amalgamate at local and regional scales. In addition, because the north-south transect crosses modern bio-climatic zones, one can expect that past climates and soils also exhibited a latitudinal zonation. In this regard, lateral changes in the physical character of the paleosols are expected and thus, pedofacies should be evident within pedogenic horizons formed during coeval time-spans.

Pedostratigraphy presented in this dissertation is based on the North American Stratigraphic Code (1983) but also follows the recommendations of Morrison (1998). Pedo-units presented in this chapter were first recognized in the field based on preliminary observations (*vide* Chapter 2). Subsequent laboratory analyses such as: micromorphological analysis (of selected samples and soil horizons - *vide* Chapter 4), textural analysis, loss-on-ignition (for bulk organic and carbonate contents), and magnetic susceptibility were used to refine field descriptions and supplied complementary lines of evidence for pedogenesis. For simplicity,

only the organic enriched horizons of each paleosol are highlighted in the stratigraphic columns. A detailed discussion of selected paleosols and associated pedo-facies and -members is presented in the ensuing chapter.

Allostratigraphy

Allostratigraphy is the classification of mappable stratiform bodies of sedimentary rock or unconsolidated sediment that are delimited by bounding discontinuities (North American Commission on Stratigraphic Nomenclature 1983). The purpose of such a stratigraphic classification is to distinguish between any of the following: 1) superimposed deposits of similar lithologies that are bound by discontinuities; 2) contiguous deposits of similar lithology bound by discontinuities; 3) geographically separated units of similar lithology bounded by discontinuities; or, 4) to distinguish a single allostratigraphic unit comprised of superimposed, contiguous and/or geographically separated non-allostratigraphic units that exhibit lithologic heterogeneity, and that are bounded by corresponding discontinuities (North American Commission on Stratigraphic Nomenclature 1983). There are no fixed internal characteristics, as these may vary laterally and vertically throughout the allostratigraphic unit (Figure C.2). The boundaries of an allostratigraphic unit must be laterally traceable discontinuities. These discontinuities may be represented by erosive contacts, the upper boundary of a buried soil, geomorphic surfaces, or any other manifestation of non-deposition or erosion. In some instances, bounding discontinuities can not be traced; in these circumstances, they may be geographically extended based on the objective correlation of intra-unit properties (excluding lithic character) such as fossil assemblages, characteristic tephra or other marker beds within the unit, topographic position; numerical ages, or relative-age criteria (North American Commission on Stratigraphic Nomenclature 1983; p. 867). Inferred time-spans are not used to define an allostratigraphic unit (with exceptions previously noted), however, age relationships may aid in choosing allostratigraphic unit boundaries (North American Commission on Stratigraphic Nomenclature 1983).

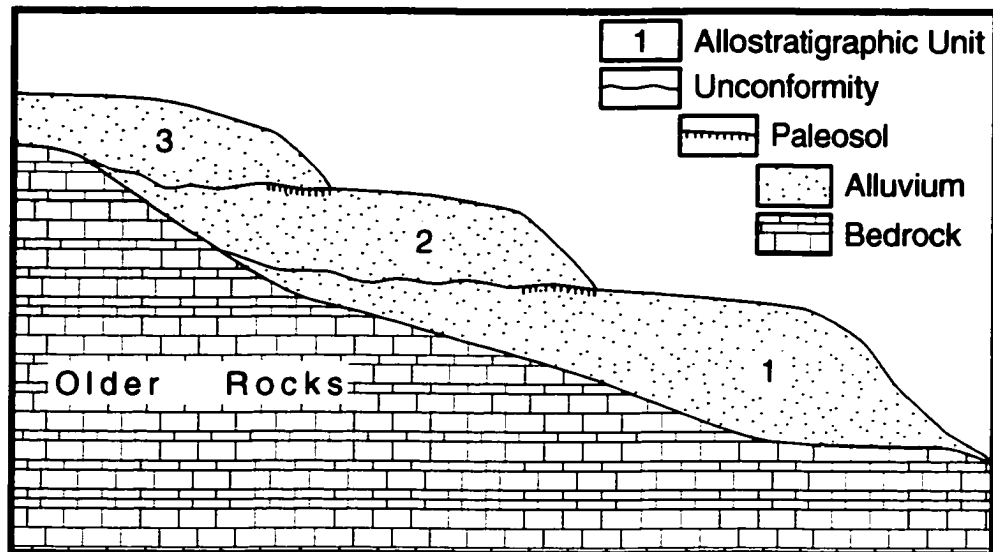


Figure C.2. Diagrammatic example of an allostratigraphic classification applied to contiguous deposits of similar lithology. Allostratigraphic units 1, 2, and 3 are the physical (geologic) record of three glaciations. These allostratigraphic units are all composed of alluvium that can not be subdivided on the basis of lithostratigraphy, and therefore constitute a single lithostratigraphic unit. Only using allostratigraphy can the different glacial depositional episodes be differentiated. Although this example depicts alluvial deposits, a similar scenario can be applied to loess-paleosol sequences. Figure modified after North American Commission on Stratigraphic Nomenclature (1983).

Allostratigraphic units in Chapter 3 are defined only after intra-site correlations and composite sections (based on litho- and pedostratigraphy) construction.

Technique used to construct New Russian Plain Allostratigraphy

Every pedogenic Ah-horizon that was identifiable in the field was initially considered to be a boundary between allounits. The crucial factor that determined the status of the boundary was whether the horizon (*i.e.*, the boundary) could be mapped between sections; dashed lines are used below the diamicton units at Mikhailovka because exposure limitations neither support nor refute the possible existence of allounits A-4 through A-7. Allounit designation was determined by examining the position and development of the paleosol in question relative to the observable sequences of paleosols/soils, internal and external to the section in question. The best example would be the uppermost

bounding discontinuity of the entire framework (*i.e.*, upper A-1 boundary; Figure 3.33). Clearly, this surface and the paleosol underneath it represent an observable discontinuity in depositional processes. It is this surface and the underlying soil that serve as an analogue that can be used to compare and contrast underlying paleosols for allunit boundary status classification.

Status classification of each boundary was accomplished by evaluating the respective bounding discontinuity, and comparing the characteristics of the associated paleosols. This comparison was done relative to other bounding discontinuities / paleosols within and between sites. For instance, paleosol-E is a relatively weakly developed soil that exhibits 2 related soil-forming intervals in the northern and mid-position sites, but only one at the southern-most site. Based on its relatively weak development, it is given a member status and the subdivision between E_1 and E_2 is not considered in the stratigraphic scheme because it can not be mapped in all of the studied regions (*i.e.*, it would be a sub-member, if the presented allostratigraphic framework considered such subdivisions). Another example is paleosol G: at Korostylievo, the associated paleosol horizons exhibit characteristics that are radically different from paleosols above it, and therefore a major boundary status is applied to this bounding discontinuity.

In addition to the recognition and classification of allostratigraphic units, a datum for the correlation was required. Two possibilities existed: paleosol A and its corresponding discontinuity, or paleosol-D and its corresponding discontinuity. Paleosol-D (D_1 where it was confidently identified) was chosen based on its association with surrounding units, the ease of recognition, and the corroboration of its placement in the stratigraphic record by optical luminescence dating methods. Paleosol-A was not chosen because placing the datum confidently within the stratigraphy at the top of A-2 (rather than at the uppermost stratigraphic position) allows other geologic relationships that exist between the study sites to be easily identified (*e.g.*, differences in accumulation during the last glacial cycle).

APPENDIX D: TEXTURAL DATA

Appendix D presents sand, silt and clay data plotted on texture triangles based on the Canadian System of Soil Classification (Soil Classification Work Group 1998). The data are grouped first by section and second by composite section unit number. The order of the sections follows the order in which they are described in Chapter 3 (*i.e.*, Likhvin, Gololobovo, Korostylievo, Mikhailovka). Sedigraph test examples are also presented in the later portions of this appendix.

For detailed Russian Plain grain size data that includes raw data tables and histograms, see the appropriate files in the supplied CD-ROM database (Table D.1).

Table D.1. Grain-size data: File reference table.

Section	Samples	Directory
LS1	1-54.2	L-1-96#1-54.2 sedigrph data.xl
	56-73	L-1-96#56-73 sedigrph data.xl
LS2	1-31	L-2-96 sedigrph data.xl
GS1	1-27*	G-1to4 all grain size data.xl
GS2	1-8*	G-1to4 all grain size data.xl
GS3	1-8*	G-1to4 all grain size data.xl
GS4	5-15*	G-1to4 all grain size data.xl
KS1	1-37	K-1-98 sedigraph data.xl
KS2	1-20	K-2-98 sedigraph data.xl
MS1	1-20	M-1&2-98 sedigrph data.xl
MS2	1-20	M-1&2-98 sedigrph data.xl
MS3	1-9	M-3-98 sedigrph data.xl
MS5	1-17	M-5-98 sedigrph data.xl

* not continuous sample sets

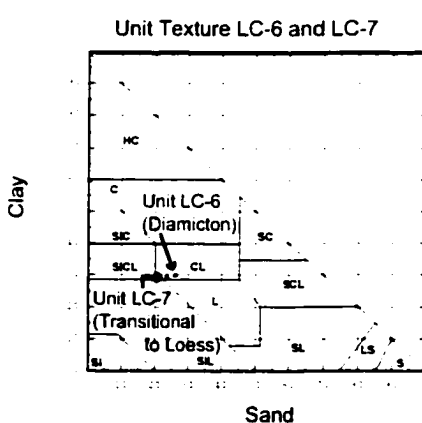
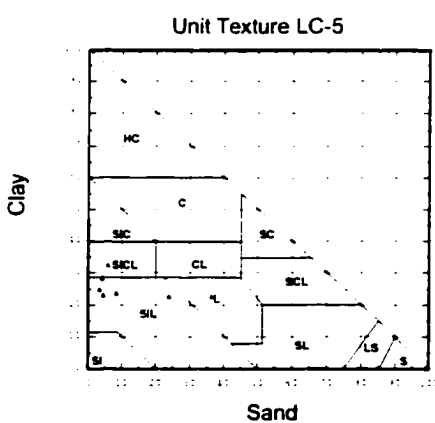
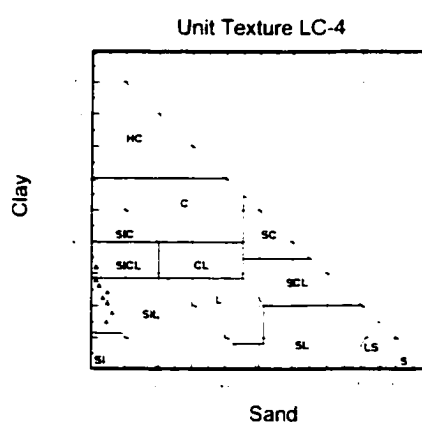
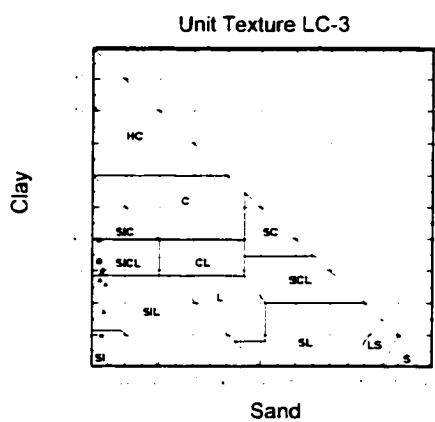
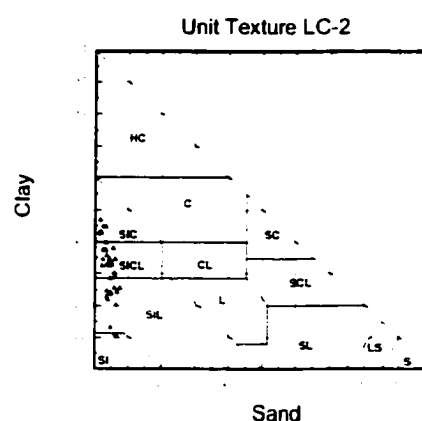
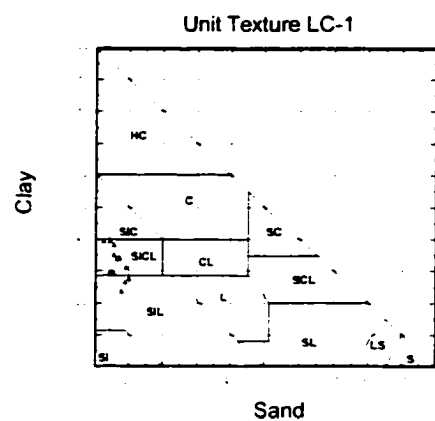
For other grain size data used as tests to ensure quality and aid in the interpretation of Russian Plain data sets, see the appropriate files in the supplied CD-ROM databases (Table D.2)

Table D.2. Non-Russian-Plain grain-size data: File Reference Table

Place	Environment	Directory
Greenland, Dnmk	Modern aeolian	Greenland Sedigraph data.xl
	Modern alluvial	Greenland Sedigraph data.xl
Peyto Glacier, AB, Can.	Modern glaciofluvial suspension load	Peyto Glaciofluvial Data.xl
Chinese Loess Plateau	Loess	Chinese Sedigraph Data.xl

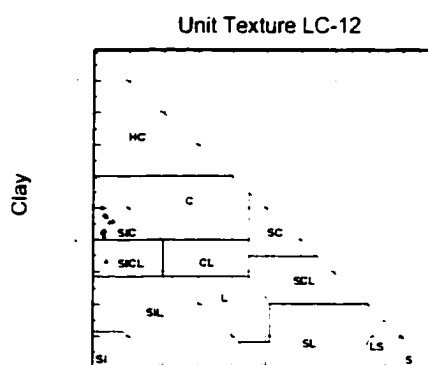
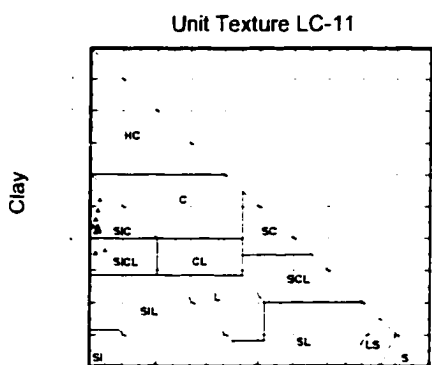
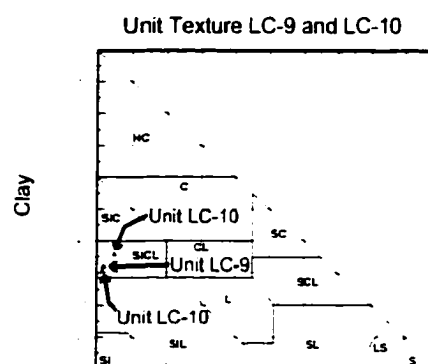
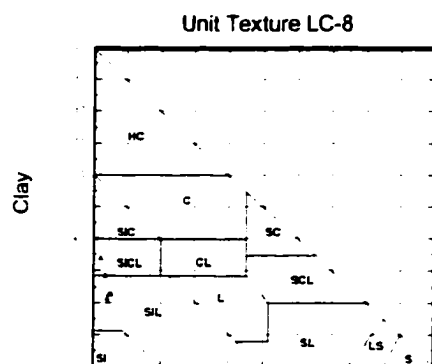
SAMPLE TEXTURES

Likhvin Composite Section Units 1 to 7



SAMPLE TEXTURES

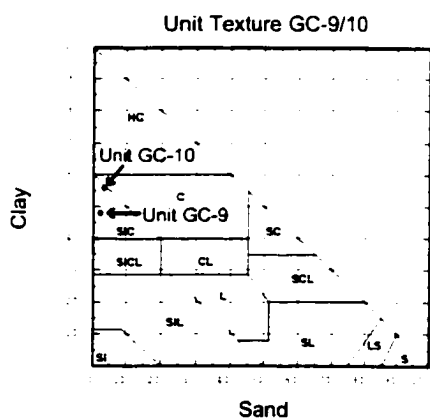
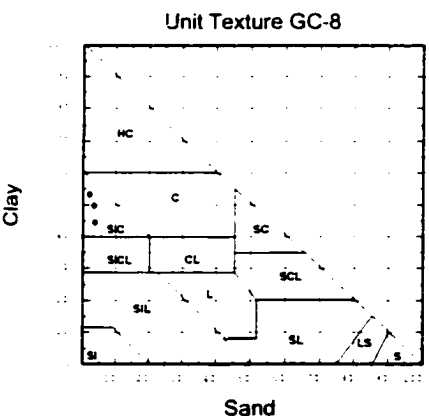
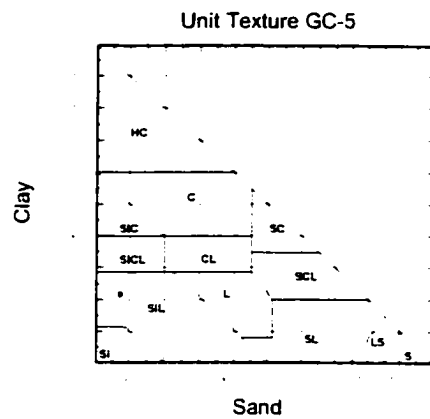
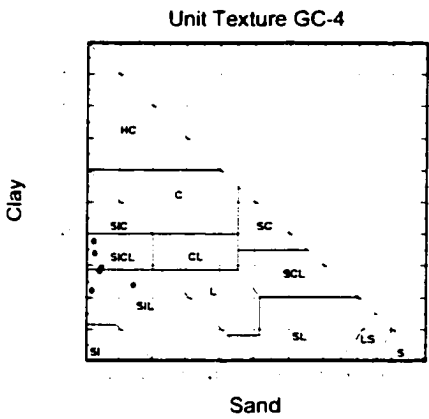
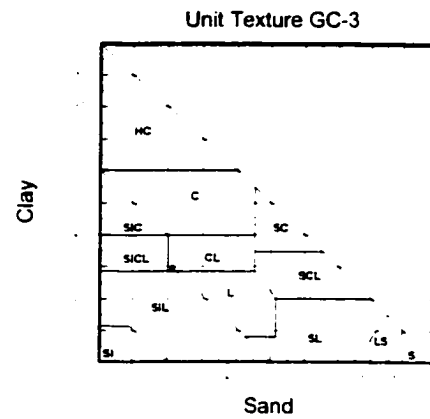
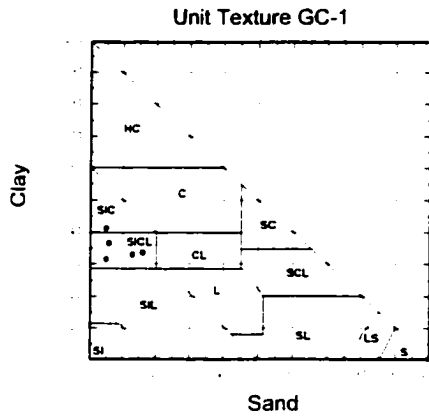
Likhvin Composite Section Units 8 to 12



Sand

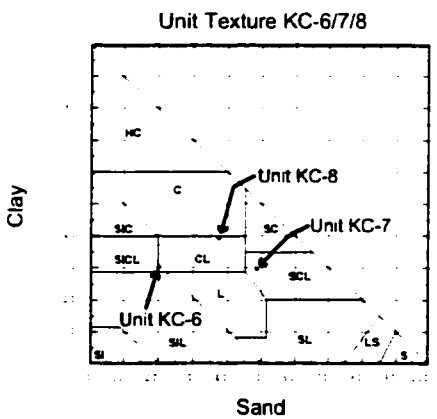
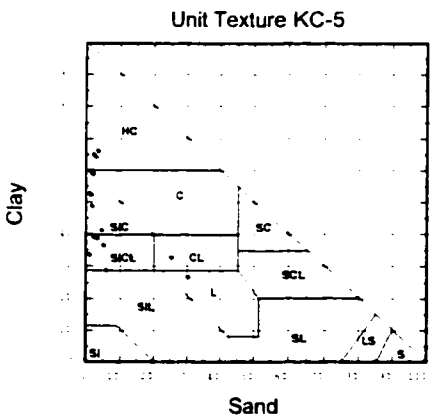
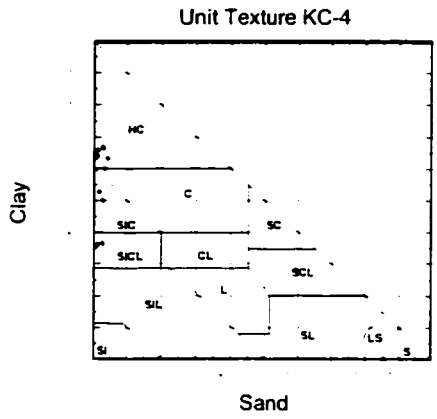
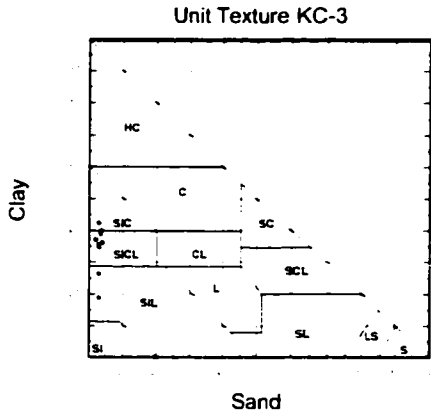
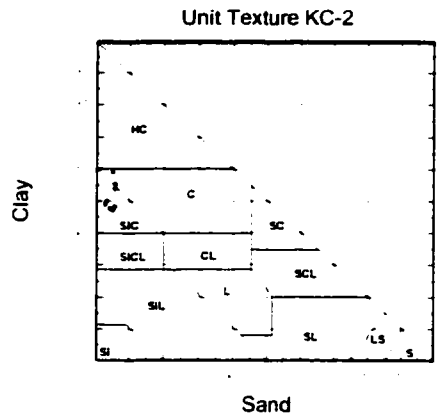
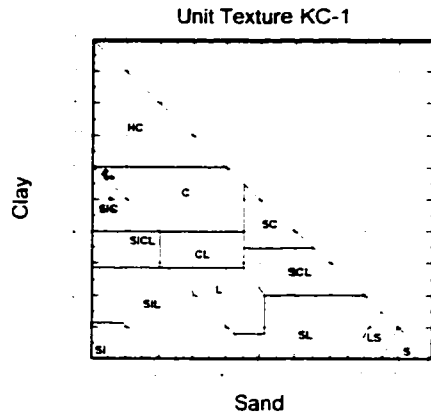
Sand

SAMPLE TEXTURES
Golobovo Composite Section Units 1 to 10
 (no data for units GC-3, -6 and -7)



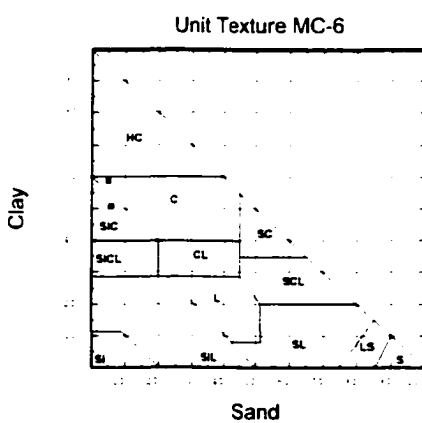
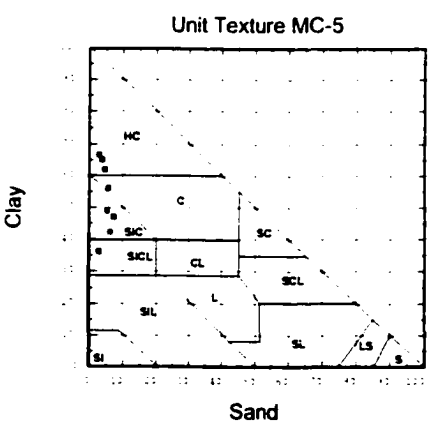
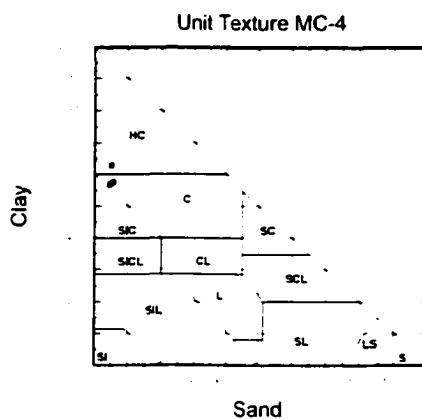
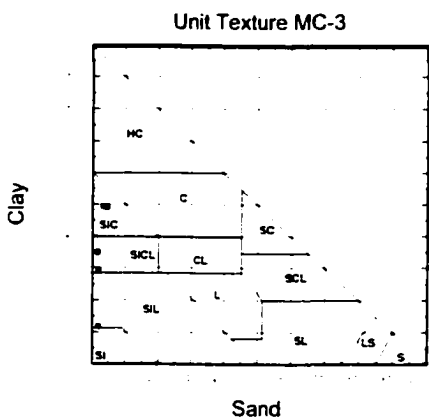
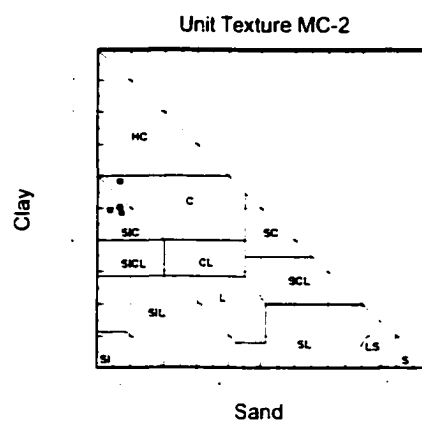
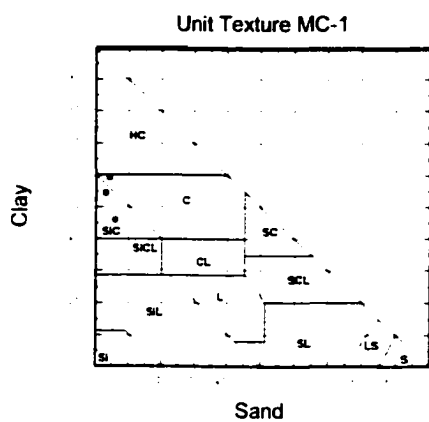
SAMPLE TEXTURES

Korostylievo Composite Section Units 1 to 8

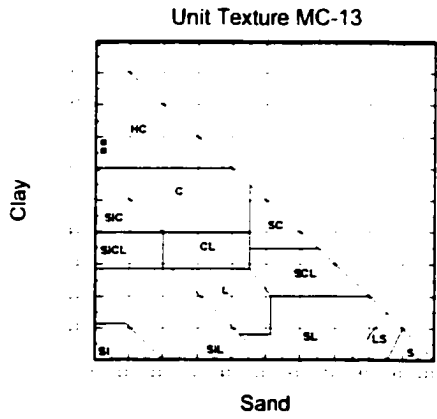
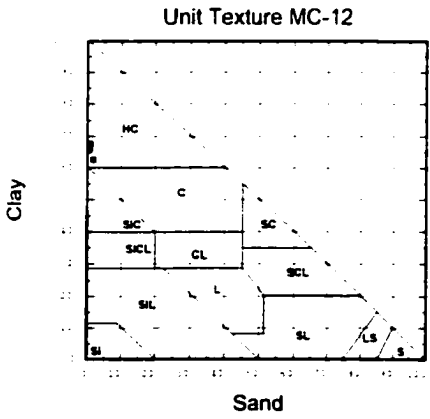
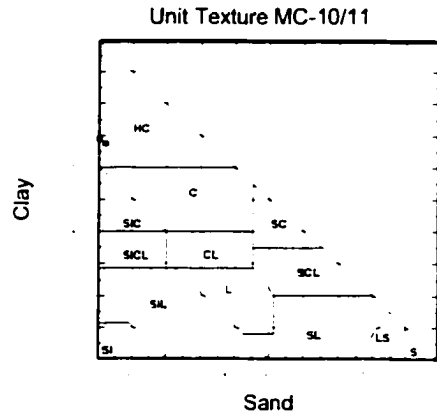
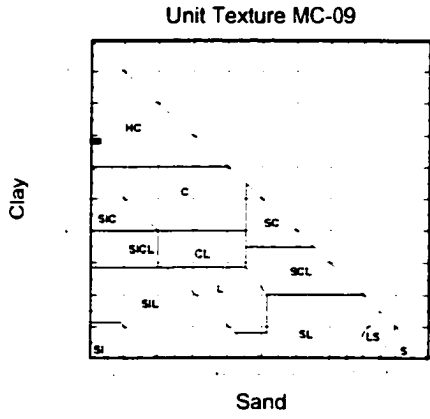
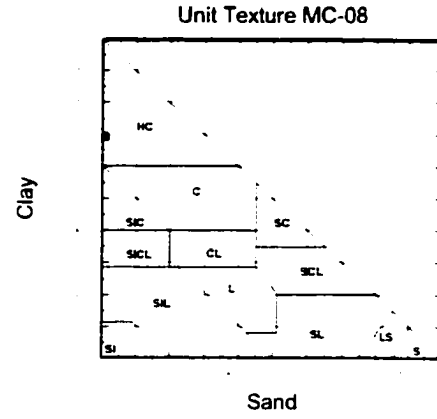
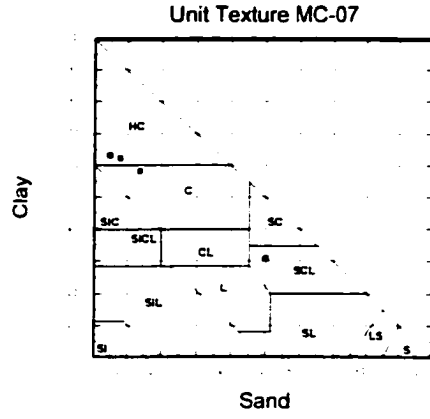


SAMPLE TEXTURES

Mikhailovka Composite Section Units 1 to 6

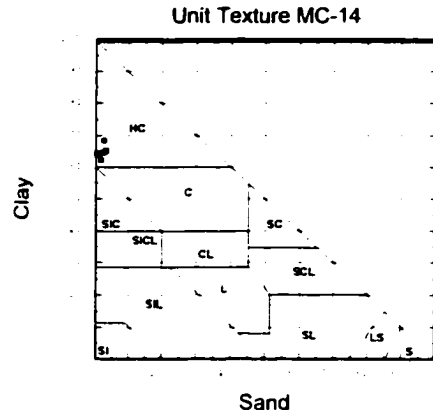


SAMPLE TEXTURES Mikhailovka Composite Section Units 7 to 13



SAMPLE TEXTURES

Mikhailovka Composite Section Unit 14



Sedigraph 5100 Specifications and Standard Run Results

This section presents the specifications and precision of the Sedigraph 5100 as well as samples run on the recommended "garnet standard". The results of the test run can be compared to the manufacturer's estimates of precision.

Product Bulletin

P/N: 5004/16810/00
 LOT NO: W20-65428-23

REFERENCE MATERIAL FOR INSTRUMENT PERFORMANCE EVALUATION

MATERIAL: Garnet

REFERENCE FOR: Particle Size Distribution

INSTRUMENT(S) TO WHICH APPLICABLE:

SediGraph 5000, 5000D, 5000E, 5000ET and 5100

RECOMMENDED QUANTITY PER TEST:

For SediGraphs 5000, 5000D, and 5000ET:

Disperse 0.5g in approximately 25ml of deionized water containing 0.05 weight percent sodium metaphosphate.

For SediGraph 5100:

Disperse 1.0g in approximately 50ml of deionized water containing 0.05 weight percent sodium metaphosphate.

PERTINENT TEST CONDITIONS:

For SediGraph 5000, 5000D, 5000ET, & 5100:

Material Density is 3.85 g/cm³
 Start Analysis at 50 microns

For SediGraph 5100 only:

Set Cell Pump Speed during full scale scan to 5
 Set Bubble Detection to Medium
 Use High Speed Run
 Set Ending Diameter to .18 microns
 Set Mixing Pump ON during analysis

 micromeritics[®] (continued over)

one micromeritics drive • norcross, georgia 30093 1877 • U.S.A. • telephone 404/662 3633

OTHER:

Mechanically stir dispersion while exposing to ultrasonic energy (75-100 W) for at least 30 sec.

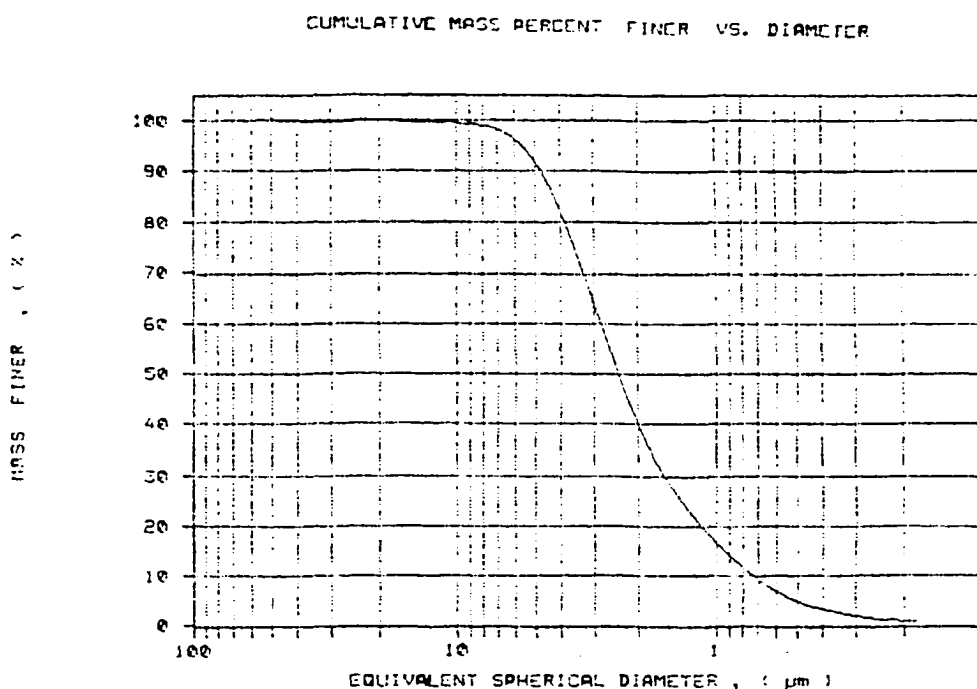
RESULTS:

Mass median equivalent spherical diameter = 2.40 ± 0.20 μM

10% > 4.75 = 0.50 μM

10% < 0.70 = 0.20 μM

A typical distribution of sizes is as below:



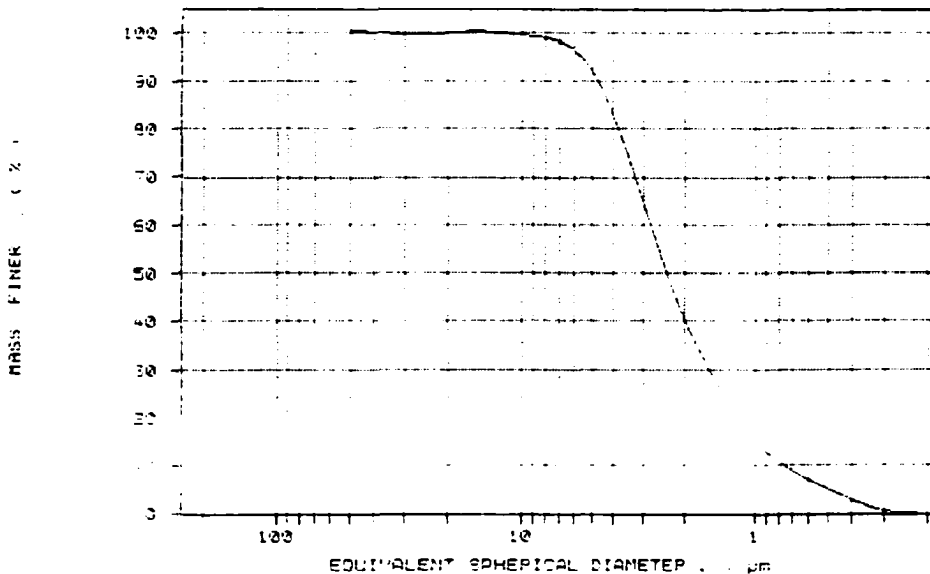
The lot from which this portion was extracted has been repeatedly analyzed using different instruments and various operators at a number of locations. We are confident the parameter(s) of interest is (are) represented within the limits stated and a satisfactorily performing instrument operated according to recommendations will reproduce it (them). We do not claim this to be a reference standard because the extensive blind testing utilizing independent laboratories that would enable us to make such an assertion has not been undertaken.

Russian Flain Project

SediGraph 5100 V3.01

SAMPLE DIRECTORY/NUMBER: TED 76 UNIT NUMBER: 1
 SAMPLE ID: Garnet Control (run 2) START 09:43:36 05/24/99
 SUBMITTER: E. Little REPT 00:16:28 05/24/99
 OPERATOR: E. Little TOT RUN TIME 0:19:24
 SAMPLE TYPE: Garnet SAM DENS: 3.8500 g/cc
 LIQUID TYPE: Water LIQ DENS: 0.9939 g/cc
 ANALYSIS TEMP: 75.5 deg C RUN TYPE: High Speed LIQ VISC: 0.7152 cp

CUMULATIVE MASS PERCENT FINER VS. DIAMETER



MASS DISTRIBUTION

MEDIAN DIAMETER: 2.39 μm MODAL DIAMETER: 3.09 μm

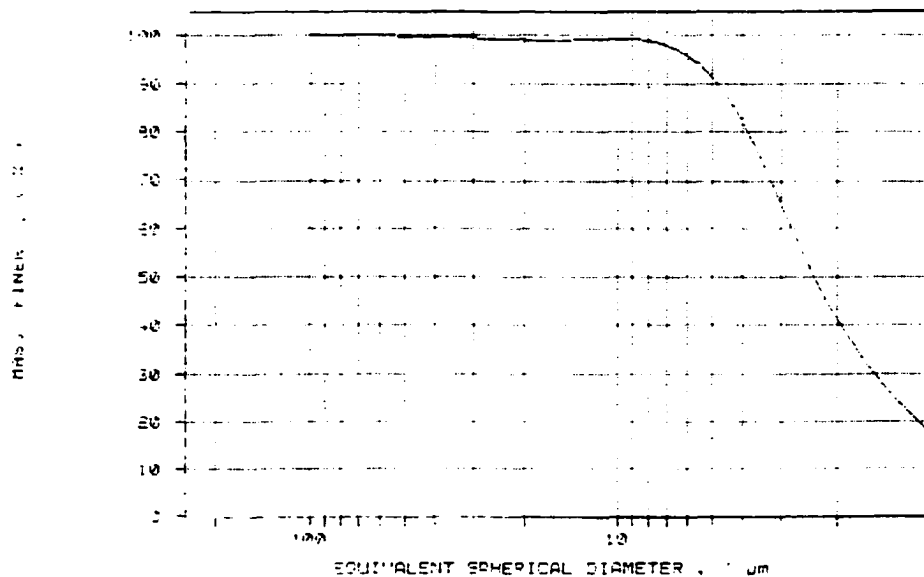
DIAMETER (μm)	CUMULATIVE MASS FINER (%)	MASS IN INTERVAL (%)
50.00	100.3	-0.3
44.00	100.1	0.2
31.00	99.5	0.6
22.10	99.6	-0.1
20.00	99.8	-0.2
15.60	100.1	-0.3
11.00	99.6	0.5
7.31	98.8	0.9
5.52	94.5	4.2
5.00	91.9	2.7
3.91	81.0	10.9
2.76	58.8	22.2
2.00	40.2	18.6
1.95	39.0	1.2
1.38	24.8	14.2
0.98	14.6	10.1

Russian Plain Project

SediGraph 5100 V3.01

SAMPLE DIRECTOR/NUMBER: TED /181 UNIT NUMBER: 1
 SAMPLE ID: Garnet CTRL 3 START 01:20:14 04/26/00
 SUBMITTER: E. Little REPT 01:40:21 04/26/00
 OPERATOR: E. Little TOT RUN TIME 0:20:02
 SAMPLE TYPE: Garnet SAM DENS: 3.8500 g/cc
 LIQUID TYPE: Water LIQ DENS: 0.9939 g/cc
 ANALYSIS TEMP: 35.5 deg C RUN TYPE: High Speed LIQ VISC: 0.7160 cp

CUMULATIVE MASS PERCENT FINER VS. DIAMETER



MASS DISTRIBUTION

MEDIAN DIAMETER: 2.36 μm MODAL DIAMETER: 2.95 μm

DIAMETER (μm)	CUMULATIVE MASS FINER (%)	MASS IN INTERVAL (%)
88.00	99.9	0.1
74.00	99.9	0.0
62.50	99.8	0.1
50.00	99.6	0.2
44.00	99.6	0.1
31.00	99.4	0.2
22.10	99.1	0.3
20.00	99.0	0.1
15.60	98.9	0.1
11.00	98.3	0.4
7.81	98.6	0.7
5.52	93.7	4.8
5.00	91.0	2.7
3.91	80.7	10.3
2.76	59.5	21.2
2.00	41.2	18.3
1.95	40.6	1.2
1.38	26.2	13.7
0.98	16.9	9.3